MECHANISTIC AND STRUCTURAL STUDIES OF A NOVEL L-PROLINE DEHYDROGENASE IDENTIFIED FROM THE HYPERTHERMOPHILE *PYROCOCCUS FURIOSUS* DSM 3638

By

PHILLIP JAMES MONAGHAN, BSc (UMIST)

Thesis submitted for the degree of Doctor of Philosophy

University of Leicester

Faculty of Medicine and Biological Sciences

University of Leicester

UNITED KINGDOM

August 2006

UMI Number: U489935

UMI

Dissertation Publishing

ProQuest

DECLARATION

I confirm that the work submitted in this thesis is my own research, carried out between
September 2002 and September 2005 at the University of Leicester, United Kingdom,
and that appropriate credit has been given where reference has been made to the work of
others.

August, 2006
University of Leicester

Phillip J. Monaghan

ABSTRACT

Mechanistic and Structural Studies of a Novel L-proline Dehydrogenase Identified from the Hyperthermophile *Pyrococcus furiosus* DSM 3638

Phillip J. Monaghan

The cloning of two open reading frames encoding a heterodimeric protein related in sequence to bacterial sarcosine oxidase and dimethylglycine oxidase from hyperthermophilic *Pyrococcus furiosus* DSM 3638 is described. The protein was overexpressed in *E. coli*, purified to homogeneity and identified as a flavoprotein by virtue of the enzymes UV-visible absorption spectrum showing characteristic λ_{max} at 367 and 450 nm. The physiological substrate was identified as L-proline ($t_{\frac{1}{2}}$ = ~105 s^{-1} for bleaching of flavoprotein spectrum at 450 nm). Additionally, the enzyme oxidises L-pipecolic acid ($t_{\frac{1}{2}}$ = ~110.5 s^{-1}) and, to a lesser extent sarcosine ($t_{\frac{1}{2}}$ = ~654 s^{-1}). No reactivity with sodium sulfite was detected, consistent with the enzyme belonging to the flavoprotein dehydrogenase class. These data classified the enzyme as a novel hyperthermophilic L-proline dehydrogenase.

The crystal structure of PRODH at 3.3 Å resolution shows the enzyme is a heterooctamer $(\alpha\beta)_4$. The holoenzyme contains one mol each of FAD, FMN and ATP per mol of $\alpha\beta$ complex. Isolation of monoflavinylated enzyme containing a single FAD cofactor permitted detailed redox potentiometry and pH-dependence studies of the reaction with L-proline. A bell-shaped dependence for k_{cat}/K_m as a function of pH was observed with macroscopic pK_a values (7.0 ± 0.2 and 7.6 ± 0.2) attributed to residue ionisations in the free enzyme. The pH dependence of k_{cat} is sigmoidal, with maximum activity realised in the alkaline region; the dependence is described by a macroscopic pK_a value of 7.7 ± 0.1 and by analogy with other flavoenzymes is tentatively attributed to the ionisation of L-proline in the Michaelis complex. Studies with H225A, H225Q and Y251F mutants ruled out the participation of these residues as catalytic bases, with neither essential for activity. These data are consistent with a concerted polar nucleophilic mechanism of amine oxidation, although a radical-based mechanism cannot be refuted.

ACKNOWLEDGEMENTS

UNITS AND ABBREVIATIONS

UNITS:

°C	Degrees Celsius
μg	Microgram
μl	Microlitre
μm	Micrometre
μM	Micromolar
μM^{-1} s^{-1}	Micromolar per second
Å	Angstrom
bp	Base pair
cm	Centimetre
Da	Dalton
g	Gram
g (rcf)	Relative centrifugal force, $= 1.12 \times 10^{-5}$
	$\times$ r $\times$ rpm^2, where r = rotor radius in cm
Hz	Hertz
K	Degrees Kelvin
Kb	Kilo base
KDa	Kilo Dalton
Lb/sq.in	Pounds per square inch.
M	Molar
M^{-1} cm^{-1}	Molar per centimetre
M^{-1} s^{-1}	Molar per second
mA	Milliampere
MHz	Mega Hertz
ml	Millilitre
mM	Millimolar
mV	Millivolts

Units And Abbreviations

nm	Nanometer
ppm	Parts per million
psi	Pounds per square inch
rpm	Revolutions per minute
s^{-1}	Per second
V	Volts

TEXTUAL ABBREVIATIONS:

λ_{max}	Absorbance maxima
Amp	Ampicillin
APS	Ammonium persulfate
ATP	Adenosine triphosphate
BSA	Bovine serum albumin
Cam	Chloramphenicol
DAAO	D-amino acid oxidase
DIP	di-*myo*-inositol 1, 1'-phosphate
DMGDH	Dimethylglycine dehydrogenase
DNase I	Deoxyribonuclease I
dNTP	Deoxynucleotides triphosphate.
E_m	Redox midpoint potential
E'_0	Standard reduction potential
EDTA	Ethylenediaminetetraacetic acid
F	Faraday constant
FAD	Flavin adenine dinucleotide
FMN	Flavin mononucleotide
FPLC	Fast protein liquid chromatography
HPLC	High performance liquid chromatography
IPTG	Isopropyl-β-*D*-thiogalactopyranoside
Kan	Kanamycin

k_{cat}	Catalytic turnover number
K_m	Michaelis-Menten constant
MG	α-mannosylglycerate
MSOX	Monomeric sarcosine oxidase
MTOX	*N*-methyltryptophan oxidase
NAD˙	Nicotinamide adenine dinucleotide
NADH	Reduced nicotinamide adenine dinucleotide
NADPH	Reduced nicotinamide adenine dinucleotide phosphate
P5C	Δ^1-pyrroline-5-carboxylate
P5CDH	P5C dehydrogenase
PEDANT	Protein extraction, description and analysis tool
PFAM	Protein families' alignment database
PIPOX	Pipecolate oxidase
PRODH	Proline dehydrogenase
SDH	Sarcosine dehydrogenase
SDS-PAGE	Sodium dodecyl sulfate-polyacrylamide gel electrophoresis
TEMED	*N,N,N',N'*-tetramethylethylenediamine
T_m	Primer melting temperature
Tris	Tris [hydroxymethyl]aminomethane
TSOX	Heterotetrameric sarcosine oxidase
UV	Ultraviolet
v	Initial velocity
v/v	Volume to volume
V_{max}	Steady-state maximal velocity
w/v	Weight to volume

TABLE SHOWING THE PROPERTIES OF THE 20 α-AMINO ACIDS FOUND IN PROTEINS:

Name	One-letter code	pK_a of α-carboxyl group	pK_a of α-amino group	pK_a of ionising side chain	Residues mass (Da)	Relative occurance in proteins (mol %)
Alanine	A	2.3	9.7	/	71.08	9.0
Arginine	R	2.2	9.0	12.5	156.20	4.7
Asparagine	N	2.0	8.8	/	114.11	4.4
Aspartic acid	D	2.1	9.8	3.9	115.09	5.5
Cysteine	C	1.8	10.8	8.3	103.14	2.8
Glutamine	Q	2.2	9.1	/	128.14	3.9
Glutamic acid	E	2.2	9.7	4.2	129.12	6.2
Glycine	G	2.3	9.6	/	57.06	7.5
Histidine	H	1.8	9.2	6.0	137.15	2.1
Isoleucine	I	2.4	9.7	/	113.17	4.6
Leucine	L	2.4	9.6	/	113.17	7.5
Lysine	K	2.2	9.0	10.0	128.18	7.0
Methionine	M	2.3	9.2	/	131.21	1.7
Phenylalanine	F	1.8	9.1	/	147.18	3.5
Proline	P	2.0	10.6	/	97.12	4.6
Serine	S	2.2	9.2	/	87.08	7.1
Threonine	T	2.6	10.4	/	101.11	6.0
Tryptophan	W	2.4	9.4	/	186.21	1.1
Tyrosine	Y	2.2	9.1	10.1	163.18	3.5
Valine	V	2.3	9.6	/	99.14	6.9

THE PURINE AND PYRIMIDINE BASES FOUND IN DNA AND RNA:

PURINES:

A (DNA/RNA)　　　　　　　　　Adenine

G (DNA/RNA)　　　　　　　　　Guanine

PYRIMIDINES:

C (DNA/RNA)　　　　　　　　　Cytosine

T (DNA)   Thymine

U (RNA)   Uracil

TABLE OF THE GENETIC CODE:

		SECOND POSITION				
		U	**C**	**A**	**G**	
FIRST POSITION	**U**	UUU (Phe)	UCU (Ser)	UAU (Tyr)	UGU (Cys)	**U**
		UUC (Phe)	UCC (Ser)	UAC (Tyr)	UGC (Cys)	**C**
		UUA (Leu)	UCA (Ser)	UAA (Stop)	UGA (Stop)	**A**
		UUG (Leu)	UCG (Ser)	UAG (Stop)	UGG (Trp)	**G**
	C	CUU (Leu)	CCU (Pro)	CAU (His)	CGU (Arg)	**U**
		CUC (Leu)	CCC (Pro)	CAC (His)	CGC (Arg)	**C**
		CUA (Leu)	CCA (Pro)	CAA (Gln)	CGA (Arg)	**A**
		CUG (Leu)	CCG (Pro)	CAG (Gln)	CGG (Arg)	**G**
	A	AUU (Ile)	ACU (Thr)	AAU (Asn)	AGU (Ser)	**U**
		AUC (Ile)	ACC (Thr)	AAC (Asn)	AGC (Ser)	**C**
		AUA (Ile)	ACA (Thr)	AAA (Lys)	AGA (Arg)	**A**
		AUG (Met)	ACG (Thr)	AAG (Lys)	AGG (Arg)	**G**
	G	GUU (Val)	GCU (Ala)	GAU (Asp)	GGU (Gly)	**U**
		GUC (Val)	GCC (Ala)	GAC (Asp)	GGC (Gly)	**C**
		GUA (Val)	GCA (Ala)	GAA (Glu)	GGA (Gly)	**A**
		GUG (Val)	GCG (Ala)	GAG (Glu)	GGG (Gly)	**G**

THIRD POSITION

TABLE OF PHYSICAL CONSTANTS:

Name	Symbol	SI Units
Avogadro' number	N	6.022137×10^{23}/mol
Boltzmann constant	k	1.38066×10^{-23} J/K
Curie	Ci	3.7×10^{10} d/s
Electron charge	e	1.602177×10^{-19} coulomb
Faraday constant	F	96485 J/V·mol
Gas constant	R	8.31451 J/K·mol
Light speed (vacuum)	c	2.99792×10^{8} m/s
Planck's constant	h	6.626075×10^{-34} J·s

MUTANT ENZYMES

Mutant enzymes are named by the following convention: the one letter code for the wild-type amino acid, followed by the amino acid position, followed by the one letter code for the amino acid in the mutant protein. *e.g.*, H225A is histidine at amino acid position 225 mutated to alanine.

CONTENTS

CHAPTER ONE

INTRODUCTION

CHAPTER TWO
METHODS

CHAPTER THREE

CLONING, RECOMBINANT EXPRESSION, PURIFICATION AND INITIAL CHARACTERISATION OF HYPERTHERMOPHILIC L-PROLINE DEHYDROGENASE (PRODH)

CHAPTER FOUR

A COMPREHENSIVE DESCRIPTION OF STEADY-STATE KINETIC PROPERTIES AND THERMODYNAMIC ANALYSIS OF PRODH REDOX CHEMISTRY

CHAPTER FIVE

MECHANISTIC ASPECTS OF PRODH-CATALYSED AMINE OXIDATION: STRUCTURAL BIOLOGY AND ASSIGNMENT OF SUBSTRATE IONISATION STABILISED IN THE MICHAELIS COMPLEX

CHAPTER SIX

DISCUSSION AND FUTURE DIRECTION

APPENDIX

CHAPTER ONE

INTRODUCTION

CHAPTER ONE

INTRODUCTION

1.1. INTRODUCTION

The research described in this thesis concerns the molecular cloning of open reading frames (ORF's) from the genome of the sulfur-reducing hyperthermophilic marine archaea *Pyrococcus furiosus* DSM 3638. Preliminary bioinformatics data regarding the amino acid sequence identity of the hypothetical proteins encoded by the identified ORF's highlights homology to flavoprotein amine oxidoreductases. The research detailed examines the cloning, recombinant expression, purification and structural/biophysical characterisation of the target protein. This introductory chapter presents an overview of the role of enzymes and their cofactors followed by a broad review concerning the molecular enzymology of the flavoproteins and their classification. A section highlighting the array of physiological roles played by amine compounds in nature is linked with an insight into the amine-oxidoreductase family of flavoproteins approached from a mechanistic perspective. A commentary of the catalytic and structural aspects of the multifunctional protein 'PutA' of enteric bacteria is proceeded by a description of the hyperthermophilic source organism *Pyrococcus furiosus*. An assessment of metabolic thermostability and a structural perspective regarding enzyme thermostability conclude this introductory chapter along with a description of the main aims of the research performed and documented in the thesis. This chapter is essentially constructed to place the research described in this thesis into the context of the field of flavoprotein enzymology research.

1.2. NATURES CATALYSTS: ENZYMES AND THEIR COFACTORS

Enzymes are a vast and diverse class of biomacromolecules that catalyse most of the reactions that occur in biological systems. Enzymes are globular proteins that work as catalysts by increasing the rate of intermolecular reactions by up to ~21 orders of magnitude over the uncatalysed reaction rate (Lad *et al.*, 2003) without their own structures suffering any overall chemical changes as a result of the catalysed reaction.

Enzymes also manifest incredible specificity highlighted by the fact that each reaction occurring in a biological system is catalysed by a different enzyme or enzyme sub-domain. Enzyme-catalysed reactions are also stereo-selective with a given enzyme-catalysed reaction leading to the formation of only a single stereoisomer as a result of the enzymes chiral binding site. This chiral binding site allows enzymes to differentiate between stereoisomeric substrates. The immense selectivity of enzyme catalysed reactions was first recognised in 1894 by Emil Fischer who discovered that the enzyme "invertin" responsible for the hydrolysis of sucrose utilises only the α-*D*-glucosides as substrate whilst β-*D*-glucosides are hydrolysed by the enzyme "emulsin". Fischer stipulated that these two enzymes constituted "asymmetrically built molecules". It was these early studies that led to Fischer's famous "Lock and Key" hypothesis of enzyme-substrate recognition and catalysis (Fischer, 1894).

Certain classes of enzymes utilise cofactors to assist in enzyme catalysis. Cofactors are a non-protein component whose presence is essential for the normal catalytic activity of an enzyme. Cofactors may be organic molecules (coenzymes) or inorganic ions. Certain enzymes bind cofactors very tightly so that they are very difficult to remove, in which case the cofactor is known as a prosthetic group (Harden, 1932). They may work so as to activate the enzyme by altering its three-dimensional structure or they may actually participate in the enzyme-substrate reaction by donating or accepting certain chemical groups. Many vitamins are precursors of coenzymes and the existence of coenzymes was first proposed by Arthur Harden who identified a small organic molecule that he named "co-zymase" involved in biological fermentation that was later identified as nicotinamide adenine dinucleotide (NAD^+) by Hans von Euler. When a cofactor is absent, resulting in an inactive enzyme form, the given protein component of the enzyme is called the 'apoenzyme'. This compares to the fully functional form known as the 'holoenzyme' applying to the active enzyme state when the cofactor(s) is in full occupancy. Cofactors are utilised in enzyme-catalysed redox reactions by acting as a conduit to transfer electrons from substrate to product (Duine, 2001). The cofactors perform an essential task since the catalytically relevant amino acid residues of an enzyme active site are not well suited to catalyse redox reactions alone since they are unable to store electrons that are released during catalysis, for example, during the oxidation of substrate.

1.3. THE FLAVOPROTEIN FAMILY OF ENZYMES

The flavoproteins are a family of ubiquitous proteins that possess one or more flavin molecules as a prosthetic group. These flavin-containing enzymes are present in all organisms and perform an array of biochemical functions (Palfey and Massey, 1998). Flavin is chemically defined as 7, 8-dimethyl-10-R-isoalloxazine, with R denoting an alkyl substituent (Edmondson and Ghisla, 1999). Flavins are derivatives of riboflavin (vitamin B_2) consisting of a tricyclic isoalloxazine ring moiety connected to a ribityl side-chain at the central N-10 position of the pyrazine moiety (Figure 1.1). The word 'flavin', derived from the Latin word for yellow (*flavus*) describes the colour of the fully oxidised form of the cofactor, the isoalloxazine ring of which is responsible for the light absorption in the UV-visible spectral range, resulting in a distinct yellow colouring diagnostic of a flavoprotein. Flavin mononucleotide (FMN) forming from the phosphorylation of riboflavin at the ribityl 5-OH by flavokinase, in addition to flavin adenine dinucleotide (FAD) which is formed from the phosphoryladenylation of the phosphate moiety of FMN in an ATP-dependent reaction catalysed by FAD-pyrophosphorylase, constitute the two common active flavin cofactors found in flavoproteins (Figure 1.1). The isoalloxazine ring system is the mechanistically relevant moiety acting as a reversible reduction-oxidation catalyst during biological redox events. The majority of flavoproteins have a strong propensity for either FMN or FAD binding due to the side-chain serving a key role in binding of the flavin ring system to the apoenzyme (Macheroux, 1999).

Most commonly, the flavin prosthetic group is non-covalent, but very tightly bound to the enzyme and does not dissociate during catalysis, with dissociation constants (K_d) for the flavin often in the nanomolar range. Covalent flavoproteins form the minor subgroup of the flavoproteins family and themselves can be divided into two subgroups, those in which the flavin is covalently bound to the protein at the C-6 position of the flavin isoalloxazine ring moiety, and those whereby the flavin-protein linkage is via the 8-α-methyl group (Decker, 1992). The majority of covalent flavinylation occurs via the 8-α-methyl group of the isoalloxazine ring with only two known enzymes possessing a linkage at the C-6 position, namely di and trimethylamine dehydrogenase that each harbours a C6-thioester linkage (Scrutton,
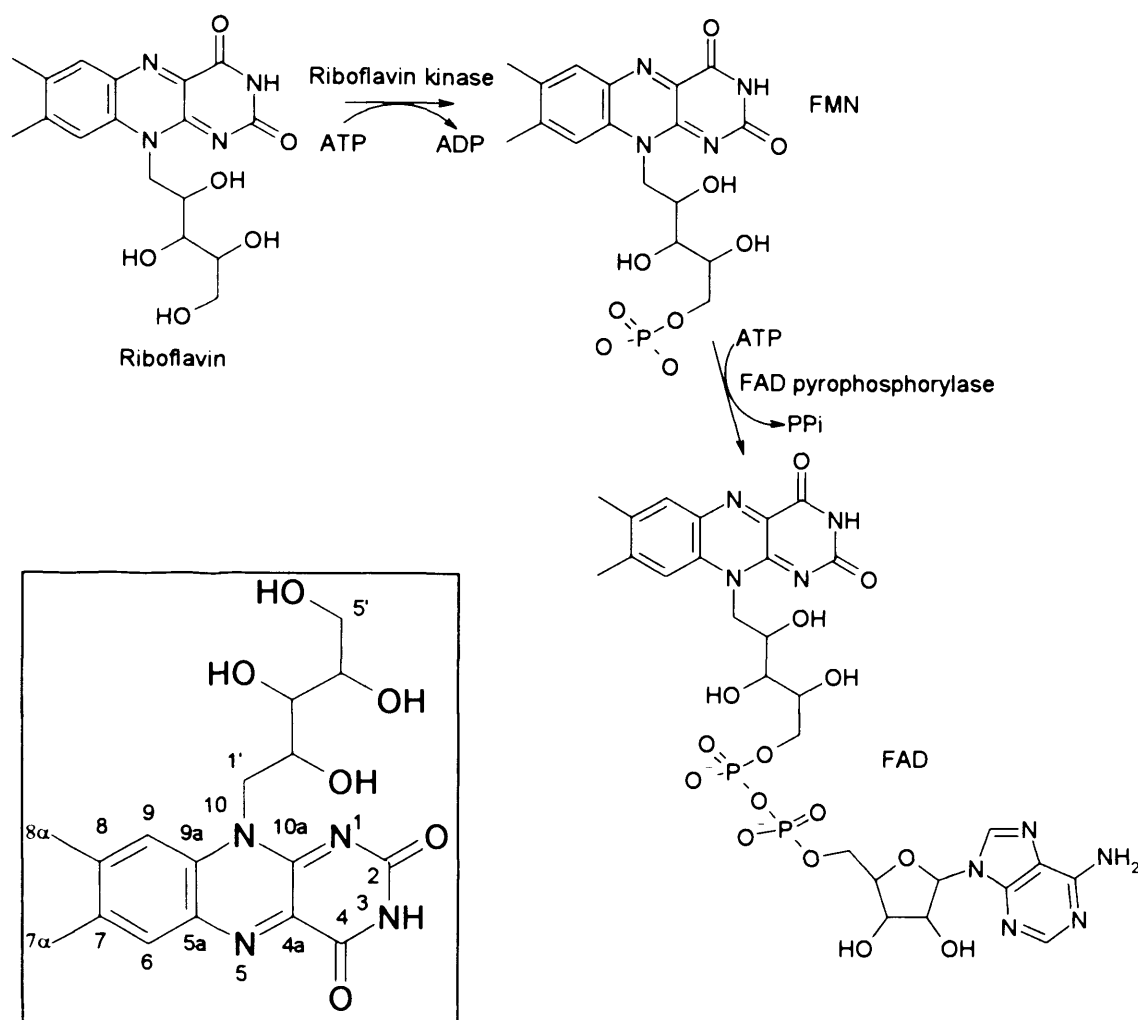
Figure 1. 1. The chemical structure of riboflavin (vitamin B₂) and biosynthesis of flavin cofactors flavin mononucleotide (FMN) and flavin adenine dinucleotide (FAD). *Main panel*, Riboflavin is the precursor compound for FMN and FAD biosynthesis in the cell. Phosphorylation at the ribityl 5-OH of riboflavin by flavokinase (riboflavin kinase) forms FMN. Subsequent phosphoryladenylation of the phosphate moiety of FMN by the enzyme FAD pyrophosphorylase gives FAD product. Both of the enzyme-catalysed reactions are ATP-dependent. *Boxed*, the chemical structure of riboflavin consisting of a tricyclic isoalloxazine moiety connected to a ribityl side chain via the central N10 position of the pyrazine function. Atomic numbering of the isoalloxazine and ribityl side chain is shown.

1999). The protein amino acid residues where covalent attachments with the flavin isoalloxazine 8α-methyl group are typically observed include histidine at either of the imidazole nitrogens, cysteine at the sulfur atom and tyrosine at the phenolic oxygen. The recent X-ray crystal structure determination of glucooligosaccharide oxidase from *Acremonium strictum* has revealed the first example of a double covalent flavinylation with FAD cofactor cross-linked via both a 6-*S*-cysteinyl and 8α-*N*1-histidyl attachment to residues Cys-130 and His-70, respectively (Figure 1.2; Huang *et al.*, 2005). Additionally, berberine bridge enzyme (BBE) involved in the transformation of (*S*)-reticuline to (*S*)-scoulerine during benzophenanthridine alkaloid biosynthesis in plants has recently been identified as containing a di-covalently bound FAD cofactor via the 8α-methyl and C6 positions of the FAD isoalloxazine ring moiety to residues His-104 and Cys-166, respectively (Winkler *et al.*, 2006), with derivatisation of the isoalloxazine ring system via the 6-*S*-cysteinyl residue acting to increase the midpoint redox potential of the covalent flavin cofactor by chemical modification in BBE and BBE-like proteins (Ghisla *et al.*, 1980). The NqrC subunit of the NQR respiratory Na$^+$-pump of *Vibrio cholerae* contains an FMN prosthetic group covalently attached to a threonine residue (Barquera *et al.*, 2001). Concerning the 8-α-histidyl derivatives, nucleophilic attack of the protein amino acid residue on the quinine methide tautomer leads to protein-flavin bond formation. A covalent enzyme-reduced flavin adduct is formed which is then oxidised in an apparently self-catalytic process (Brandsch and Bichler, 1991). Knowledge of the other nucleophilic amino acid residues that are known to form flavin adducts allows analogous mechanisms to be postulated from the chemistry of the side-chains. Mutagenesis studies on covalent flavoproteins have pinpointed key residues required for flavinylation reaction to occur (Kim *et al.*, 1995; Packman *et al.*, 1995). Biochemical factors necessitating the evolution of covalently bound flavins in the context of enzymological mechanisms of redox systems has lead to a variety of hypotheses. Covalent linkage at the C-6 position of the isoalloxazine ring of the flavin component of trimethylamine dehydrogenase has been proposed to be an evolutionary selection to inhibit hydroxylation of the isoalloxazine ring at this position with the effect of keeping the redox centre of the enzyme in an active chemistry (Mewies *et al.*, 1997). Additional roles proposed for covalent flavinylation include, enhancement of electronic coupling between cofactors as to improve electron transfer rates to downstream redox acceptors (Kim *et al.*, 1995) and modulation of flavin redox poise

8α-(*N*1)-histidyl

8α-*S*-cysteinyl

8α-(*N*3)-histidyl

6-*S*-cysteinyl

8α-*O*-tyrosyl

His-70

Cys-130

6-*S*-cysteinyl + 8α-(*N*1)-histidyl dicovalent linkage
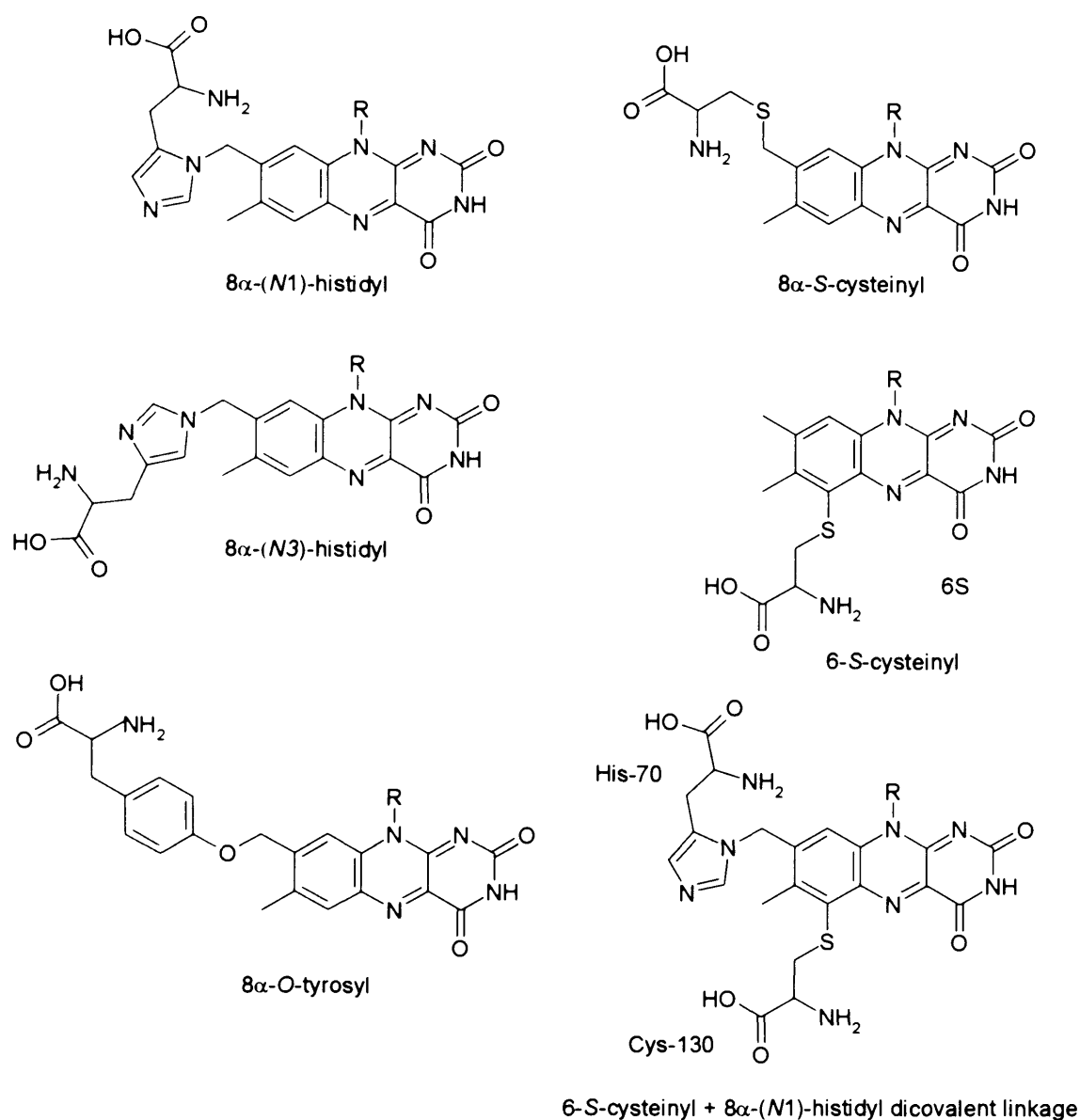
Figure 1. 2. Structures of the flavin amino acids discovered in covalent flavoproteins. Covalent attachment is via the 8α-methyl or C6 positions of the flavin isoalloxazine moiety and the amino acid side chain. Covalent attachment to a histidine residue is via the *N*1 or *N*3 atom of the side chain imidazole ring. Attachment to a cysteine or tyrosine residue occurs via the side chain sulfur and oxygen atoms, respectively. The FAD cofactor of glucooligosaccharide oxidase of *Acremonium strictum* is crosslinked by covalent binding via 6-*S*-cysteinyl and 8α-(*N*1)-histidyl linkages, providing the first known double attachment flavinylation observed in a flavoprotein (Huang *et al.*, 2005).

(Edmondson and De Francisco, 1992; Williamson and Edmondson, 1985; Fraije *et al.*, 1999). Covalent or tight non-covalent binding of flavin cofactors is essential for the redox activity of the flavoproteins. The cofactor cannot be released in an altered oxidation state during catalysis but must instead be returned to the original redox species to complete the catalytic cycle of the enzyme and to allow multiple substrate turnover to proceed (Ghisla and Massey, 1989). The only known example of a flavoprotein that does not tightly bind flavin is bacterial luciferase. In this unique case, luciferase actually utilises reduced FMN as substrate during the oxidation of long-chain aldehyde before releasing the oxidised form of the flavin (Baldwin and Zeigler 1992).

In addition to the flavoproteins that contain FAD and FMN prosthetic groups, cofactors harbouring modified isoalloxazine rings or ribityl side-chains have also been observed. F_{420}, a prosthetic group named because of its noticeable absorption at 420 nm contains an FMN moiety with an 8-hydroxy-5-deaza-5-carbaisoalloxazine modified ring bonded to an L-lactyl moiety and two glutamyl residues (Eirich *et al.*, 1978; Ashton *et al.*, 1979). F_{420} has been isolated from a variety of *Methanobacterium* species and is used by several redox enzymes including formate dehyrogenase and methyltetrahydrofolate dehydrogenase of *Methanococcus ruminantium* (Tzeng *et al.*, 1975 a, b), pyruvate dehydrogenase and α-ketoglutarate dehydrogenase of *Methanobacterium thermoautotrophicum*, (Zeikus *et al.*, 1977; Fuchs *et al.*, 1978), glucose-6-phosphate dehydrogenase from *Mycobacterium smegmatis* and alcohol dehydrogenase from *Methanoculleus thermophilicus* (Klein *et al.*, 1996), formate dehydrogenase of *Methanospirillium hungatii* (Ferry and Wolf, 1977) and an $NADP^+$ oxidoreductase from *Methanococcus vannielii* (Jones and Stadtman, 1980; Yamazaki and Tsai, 1980). F_{420} has a lower redox potential than both FMN and FAD of -373 mV with an unstable semiquinone state (Palfey and Massey, 1998), therefore, F_{420} only seems to participate in hydride transfer reactions (Figure 1.3).

Studies on modified ribityl side-chains in flavoproteins have shown that the presence and stereochemistry of the ribityl C-2' substituent is very important for normal catalysis. An example is found in peroxisomal methanol oxidase from yeast that

7
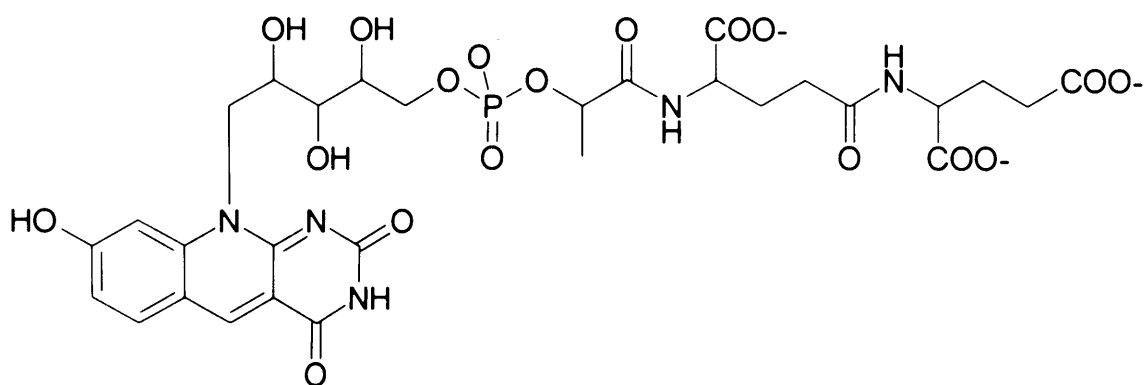
Figure 1. 3. The chemical structure of the prosthetic group F$_{420}$. This redox-active cofactor is related to flavins and consists of an FMN moiety with a modified isoalloxazine (8-hydroxy-5-deaza-5-carbaisoalloxazine). The molecule has λ_{max} at 420 nm and holds a redox midpoint potential of $-$ 373 mV with the semiquinone species being particularly unstable. Therefore, this cofactor only seems to function in reactions involving hydride transfer.

binds a flavin prosthetic group with a modified ribityl side-chain whereby the C-2'
chiral centre is inverted to the *arabino* configuration (Van Berkel, *et al*, 1994).

1.3.1. FLAVIN COFACTOR REDOX CHEMISTRY

The flavin nucleus can exist in three redox states; 1) the oxidised form, 2) a one-
electron reduced (semiquinone) form and 3) a two-electron reduced hydroquinone
form (also known as dihydroflavin). The one-electron reduced semiquinone can exist
in two radical states depending on electronic structure localisation in the flavin ring
function; the neutral/protonated semiquinone form also known as the blue
semiquinone, and the anionic mono-deprotonated semiquinone form also known as
the red semiquinone. This redox chemistry manifests on the heterocyclic
isoalloxazine ring moiety of the flavin cofactor, the structural chemistry of which
consists of a central diimine functionality, conjugated to electron-withdrawing
carbonyl groups, thus, the pyrimidine nucleus of the isoalloxazine ring is electron
deficient creating an 'electron sink' to permit electron transfer events as well as attack
by nucleophiles at either N5 or C4a positions (Figure 1.4, A). The electron-rich
phenylenediamine ring fused to the negatively charged (4,5-diamino)uracil function
comprises the reduced flavin. The number of electrons taken up by a flavin as well as
its ionisation state can be readily determined spectrophotometrically. The visible
absorption spectra for most flavoenzymes show λ_{max} at approximately 360 and 450
nm in the fully oxidised form whereas the one-electron reduced semiquinone forms
show λ_{max} at approximately 370 and 480 nm for the red anionic form and λ_{max} at
approximately 360 and 580 nm for the neutral blue semiquinone form, these spectral
signatures are again easily differentiated from the two-electron reduced flavin
spectrum that illustrates bleaching of the flavin chromophore with loss of the two λ_{max}
peaks in the UV-visible absorbance range (Figure 1.4, B).

The redox nature of the chemically active isoalloxazine moiety of a bound flavin
prosthetic group is precisely controlled by the flavoprotein through specific
interactions between amino acid residues and the flavin nucleus that, depending on
the nature of the reaction being catalysed, enhance or inhibit the flavin reactive
modes, i.e. the accessibility of the semiquinone (one-electron reduced) and

Oxidised

1e⁻-reduced semiquinone

1e⁻-reduced semiquinone

Neutral (Blue)
λ_{max} ~ 570 nm

Anionic (Red)
λ_{max} ~ 480 nm

pK_a ~ 8.4

Two-electron reduced hydroquinone
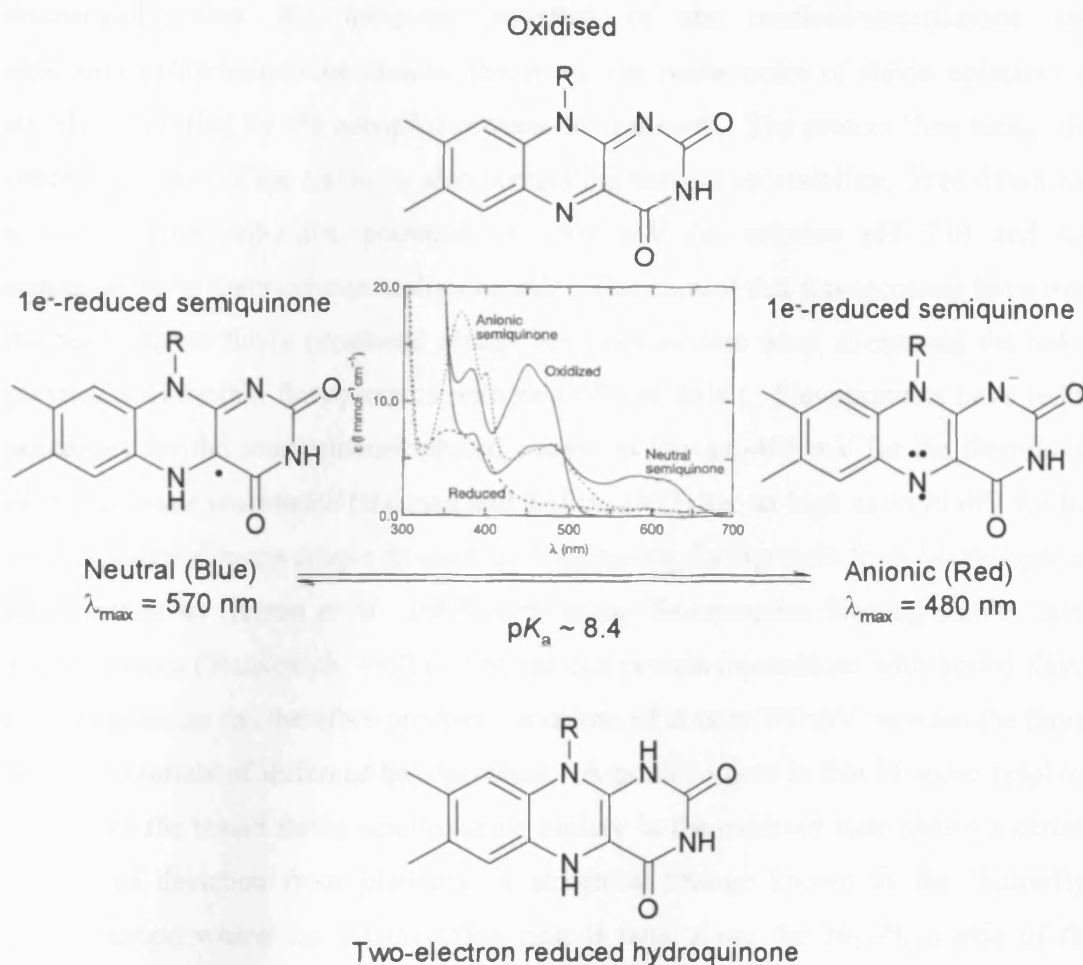
Figure 1. 4. The different redox states of the flavin isoalloxazine nucleus during one and two-electron transfer events and corresponding UV-visible spectral signatures for each species. The redox chemistry takes place on the heterocyclic isoalloxazine moiety of the flavin cofactor in an array of reactions including one and two electron transfers and attack at the electrophilic N5 or C4a sites by nucleophiles. *Centre panel*, the UV-visible absorption spectra for the oxidised, one-electron reduced anionic and neutral semiquinone states and the two-electron reduced hydroquinone species. The centre panel is taken from Palfey and Massey, 1998.

hydroquinone (two-electron reduced) form. Thermodynamic stabilisation through charge-charge/hydrophobic interactions between the flavin cofactor and protein can dramatically alter the midpoint potential of the oxidised/semiquinone and semiquinone/hydroquinone couple, therefore, the redox poise of flavin cofactors is strictly controlled by the occupied protein environment. The protein 'fine tunes' the redox chemistry of the flavin by also controlling solvent accessibility. Free flavin has a two-electron reduction potential of -207 mV (at solution pH 7.0) and the semiquinone is thermodynamically unstable. The control that flavoproteins have over the reactivity of flavin prosthetic groups becomes evident when comparing the redox potentials of certain flavoproteins with that of free flavin. Flavoproteins have redox potentials for the semiquinone/reduced couple as low as -495 mV for the flavodoxin of *Azotobacter vinelandeii* (Barman and Tollin, 1972) and as high as +190 mV for the oxidised/semiquinone couple of electron transferring flavoprotein from *Methylophilus methylotrophus* (Byron *et al.*, 1989) with many flavoproteins forming stable flavin semiquinones (Stankovich, 1991). The various protein interactions with bound flavin in flavoproteins can therefore produce variations of almost 700 mV between the flavin redox potentials of different flavoproteins. A point to note is that in some resolved structures the bound flavin isoalloxazine moiety in the oxidised state shows a certain degree of deviation from planarity, a structural change known as the 'butterfly' conformation where the isoalloxazine ring is bent along the $N_{(5)}$-$N_{(10)}$ axis of the central ring that is a result of protein-flavin interactions and provides further control of flavin redox behaviour (Figure 1.5). X-ray crystallography and nuclear magnetic resonance (NMR) spectroscopy techniques have permitted detailed structural insights into the flavin cofactor environments of flavoproteins. Primary sequence homologies and structural motifs have been identified and have shown that FAD is bound to a β-α-β secondary structural element known as a Rossmann fold (Rossmann *et al.*, 1974) with the signature sequence 'Gly-x-Gly-x-x-Gly' characteristic of nucleotide binding proteins. FMN is typically bound to β_8-α_8 barrels related to that of triose-phosphate isomerase (Palfey and Massey, 1998), although methylenetetrahydrofolate reductase (Guenther *et al.*, 1999) and the L-proline dehydrogenase domain of the multifunctional PutA protein from *Escherichia coli* (Lee *et al.*, 2003) are both examples of proteins containing FAD bound to a β_8-α_8 barrel structure.
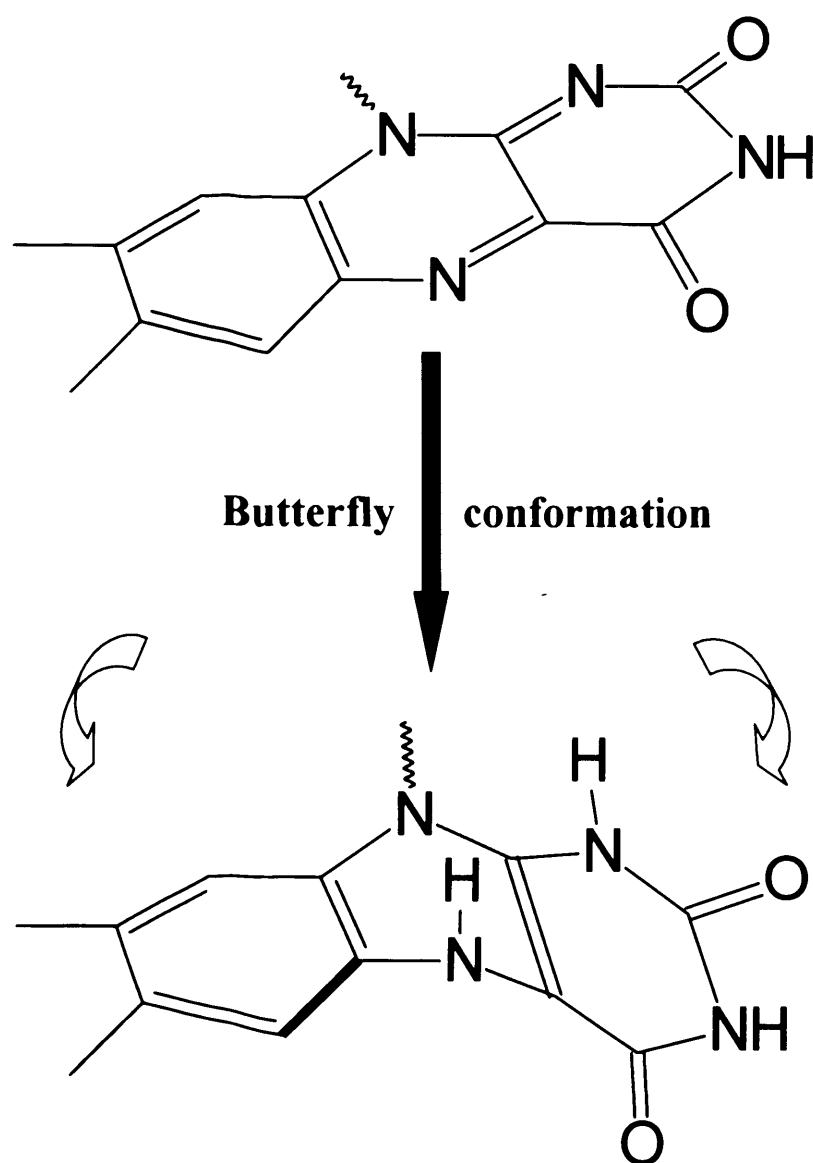
Figure 1. 5. The 'butterfly' conformation of the isoalloxazine ring of bound flavin cofactor. The isoalloxazine moiety is bent along the $N_{(5)}$-$N_{(10)}$ axis of the central ring as a result of protein-flavin interactions. This adopted conformation provides further control of the cofactor redox properties in certain flavoproteins by fine-tuning the redox midpoint potential and stabilising the redox state(s) of the flavin cofactor necessary for catalysis.

The isoalloxazine moiety of flavin prosthetic groups can undergo both one-electron and two-electron reductions via several mechanisms. Direct single electron transfer (SET) without the formation of covalent intermediates is known to occur between flavins and other redox active centres (i.e. hemes or iron-sulfur clusters). Examples of the closest orientation between the isoalloxazine ring moiety and the redox partner include the 8-methyl group and the N5 or N3 positions but no orientation between the isoalloxazine moiety and the redox partner is known to be optimal for electron transfer through space. Reduction of flavins by a single electron can occur by long-range electron transfer. Hydride transfer to flavins occurs by attack at the flavin N5 position which can be a relatively electrophilic site in many flavoproteins. The flavin prosthetic group can also be reduced resulting in covalent intermediates and flavin reduction by thiols entails nucleophilic attack of the thiolate at the C4a atom to form a transient adduct, proceeded by nucleophilic attack of a second thiolate on the adduct sulfur atom, the dihydroflavin acting as the leaving group (Ghisla and Massey, 1989; Palfey and Massey, 1998). Two electrons can be transferred to or from flavin in a concerted or sequential manner and either the *re* or *si* face of the isoalloxazine ring moiety can be involved in the stereoselective flavin-substrate reaction (Figure 1.6).

The redox cycle of flavoproteins always involves a 'reductive half-reaction' in which the flavin is reduced through organic substrate-hydrogen bond breakage (substrate oxidation) with concomitant transfer of two electrons to the flavin, and an 'oxidative half-reaction' whereby the two-electron reduced flavin cofactor is re-oxidised by transfer of electrons to molecular oxygen (as for the oxidase class) or to downstream electron acceptor redox centres such as a second flavin cofactor, heme group or iron-sulfur cluster or even pass the electrons to a second substrate to complete the enzymes catalytic cycle (Walsh, 1980; Ghisla and Massey, 1989). Ping-pong mechanisms are observed in the catalytic cycles of many flavoproteins during steady-state kinetic analysis (Palfey and Massey 1998) and through the advent of rapid reaction stopped-flow technologies, it is now possible to isolate and study in detail the individual oxidative and reductive half-reactions of flavoprotein enzymes towards the detailed description of catalytic events during a flavoenzymes redox cycle.
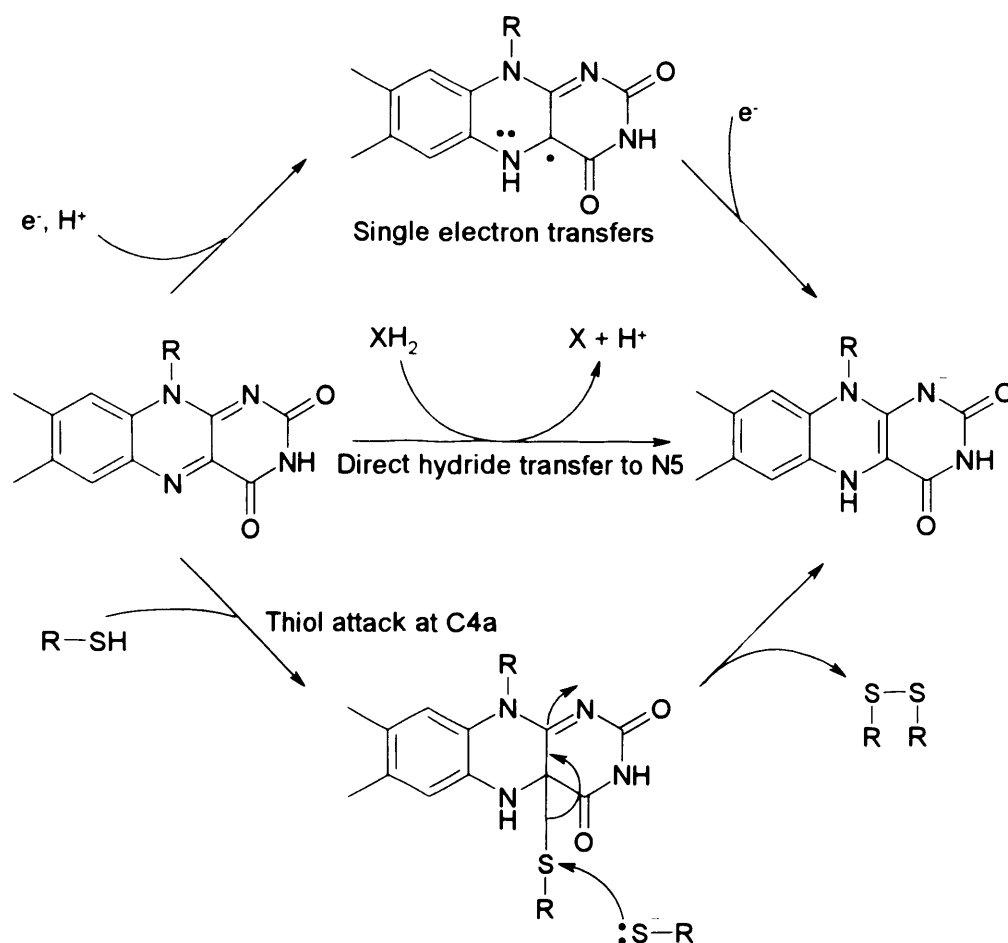
Figure 1. 6. Mechanisms of flavin cofactor reduction observed during flavoprotein-catalysed reactions. The isoalloxazine moiety of the flavin cofactor can undergo one-electron and two-electron reductions via several mechanisms. Direct single electron transfer (SET) without the formation of covalent intermediates occurs between flavins and other redox active centres. Hydride transfer to flavin occurs by attack at the N5 position. Flavin reduction by thiols involves nucleophilic attack of the thiolate at the C4a atom to form a covalent adduct, proceeded by the nucleophilic attack of a second thiolate on the adduct sulfur atom with dihydroflavin acting as the leaving group. The figure is adapted from Palfey and Massey, 1998.

1.3.2. BIOLOGICAL IMPORTANCE OF FLAVINS AND FLAVOENZYMES

The ability of flavins to mediate one and two-electron transfer reactions, whether through sequential one-electron steps or through concerted two-electron reductions as well as their susceptibility to nucleophilic attack to allow such mechanisms as hydride transfer to occur is what makes flavoproteins key components in cell biology. Energy metabolism requires the redox capabilities of flavoproteins to perform the oxidation of numerous organic substrates and pyridine nucleotides, proceeded with electron transfer events from the reduced flavin to downstream metal redox centre components in the respiratory chain (Figure 1.7). Redox transformation of both organic and inorganic substrates is the major employment of flavoproteins in the cell, although in certain cases the flavoprotein acts as redox catalyst in the formation of enzyme-bound intermediates that undergo a second non-redox catalytic process, the primary activating redox reaction is then reversed and the flavin reverts back to the original redox state ready for a subsequent catalytic cycle (Palfey and Massey, 1998). Certain systems investigated contain flavoproteins in which the bound flavin appears to have no catalytic role, for instance, DNA photolyase (Jorns *et al.*, 1987), *N*-methylglutamate synthase (Pollock and Hersh 1973), chorismate synthase (Macheroux *et al.*, 1996 a, b), oxynitrilase (Jorns, 1979), acetolactate synthase (Abell and Schloss, 1991; Tse and Schloss, 1993), glyoxylate carbo-ligase (Chung *et al.*, 1971) and hydroxyacyl-Co A dehydratase (Scherf and Buckel, 1993; Müller and Buckel, 1995). These apparently non-reactive flavin prosthetic groups may play a subtle structural role in the enzymes catalytic function or may just be relics of evolution.

The broad array of biological phenomena that the flavoproteins catalyse is quite remarkable. Ranging from the oxidation of amino acids and amine groups of many biologically relevant substrates including alkaloids, to energy generation in photosynthesis (Zanetti and Aliverti, 1991) and plant phototropism as blue-light receptors (Briggs, *et al.*, 1999; Briggs and Christie, 2002). Flavoproteins are also involved in major events in cell biology such as signal transduction for the initiation of apoptosis (Susin *et al.*, 1999; Daugas *et al.*, 2000), light-dependent DNA damage repair mechanisms (Jorns *et al.*, 1987) and light emission (Ghisla and Massey, 1989).
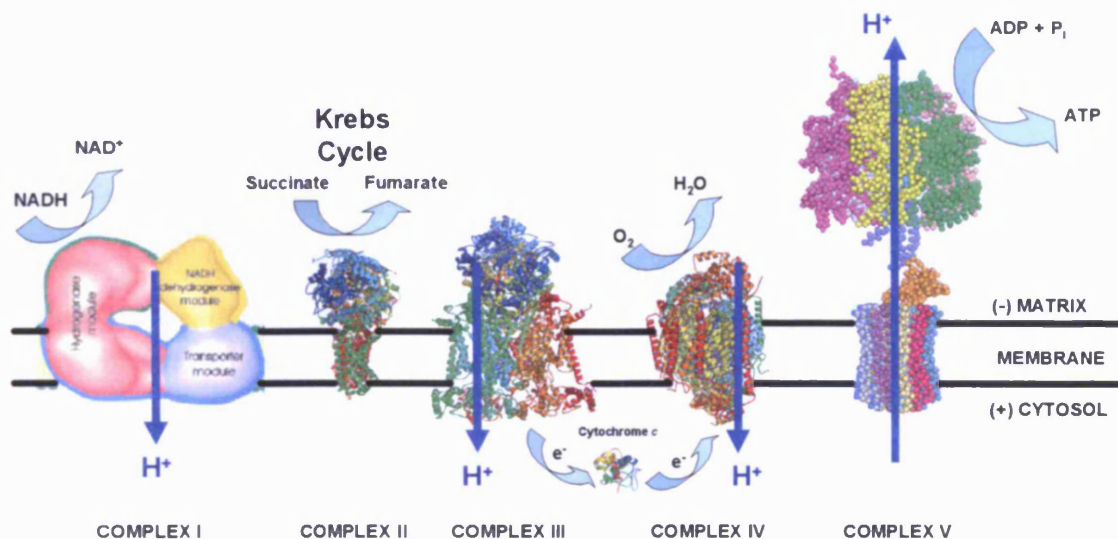
Figure 1. 7. Schematic representation of the respiratory enzyme complexes of the mitochondrial membrane. The model for the low ionic strength conformation of NADH:ubiquinone oxidase (complex I) resolved by electron microscopy is taken from Böttcher *et al.*, 2002. The three-dimensional X-ray crystal structures of complex II (fumarate reductase), III (*bc*₁ complex), cytochrome *c*, complex IV (cytochrome *c* oxidase) and V (ATP-synthase) were constructed using PyMOL v.0.99 (DeLano, 2002; http://www.pymol.org), from the respective PDB accession codes, 1LOV, 1BGY, 1CXA, 1OCC and 1QO1.

A riboflavin-binding protein has also been shown to be required in developmental biology, necessary for the correct development of chicken and mammalian fetus' (Murty and Adiga, 1982). Flavoproteins have also been shown to be involved in the detoxification of aromatic pollutants in soil (Dagley, 1987).

1.3.3.   FLAVOPROTEIN TAXONOMY

The large number of flavoproteins that have been discovered along with the diversity of the reactions that they catalyse makes classification of the enzymes within the flavoprotein family into smaller groups a substantial task. Several hundred members of the flavoprotein family have now been discovered (Massey, 2000) spanning a wide range of molecular weights, and the number of redox centres that these flavoproteins contain are varied. The sizes of these flavoproteins range from the relatively small flavodoxin family with members that have molecular weights as low as 14 KDa and only possess a single flavin redox centre (Mayhew and Tollin 1992), to the larger multi-redox centre enzymes such as cytochrome P-450$_{BM-3}$ at 119 KDa, binding two flavins and a heme (Narhi and Fulco 1986). Trimethylamine dehydrogenase (TMADH) is another example of a complex flavoprotein. This enzyme is a homodimer with a subunit molecular weight of approximately 83 KDa and catalyses the oxidative demethylation of trimethylamine to dimethylamine and formaldehyde (Steenkamp and Mallinson, 1976). The enzyme is present in many obligate and restricted facultative methylotrophic bacteria and allows the organisms to grow on trimethylamine by utilising the tertiary amine as sole carbon source (Steenkamp and Mallinson, 1976). Each subunit of TMADH possesses three prosthetic groups, a covalent FMN (6-S-cysteinyl-FMN; Steenkamp *et al.*, 1978) a 4Fe-4S cluster (Hill *et al.*, 1977) and a tightly bound adenosine diphosphate (Lim *et al.*, 1988).

Seven subgroups of the flavoprotein family have been proposed (Walsh, 1979) with groups classed as dehydrogenases, oxidases, oxidase-decarboxylases, monooxygenases, dioxygenases, metalloenzymes and flavodoxins. Five major lineations within the flavoprotein family recognised as Class I: the transhydrogenases, which are further subdivided into three types of transhydrogenase: carbon-carbon, carbon-sulfur and carbon-nitrogen transhydrogenases, Class II: the dehydrogenases/oxidases, Class III: the dehydrogenases/oxygenases, ClassIV: the

dehydrogenases/electron transferases and Class V: the pure electron transferases (Massey and Hammerich, 1980) has been the widely accepted classification scheme over the last 26 years. A further taxonomy has been proposed (Palfey and Massey, 1998) to update the ageing classification scheme proposed by Massey and Hammerich in 1980. This modern classification scheme divides flavoproteins into four 'simple' groups based on the reactions they catalyse, the flavoprotein reactivity towards certain reagents, the ability to stabilise semiquinone states and the experimental observations based on artificial flavin analogue substitutions. The reaction mechanisms of a given group that catalyse similar types of reaction often leads to members of that group reacting in the same way to a certain reagent, i.e. oxidases react with sulfite to stabilise a flavin N5-sulfite adduct. Some enzymes even catalyse reactions other than that common to their group, a trait which therefore makes them more difficult to assign to a class. The four groups of this scheme to classify the 'simple' flavoproteins are: disulfide oxidoreductases, oxidases, monooxygenases and a group comprising reductases, dehydrogenases and the electron transferases (Figure 1.8).

The similarity that a lot of the more 'complex' multi-redox centre flavoproteins have with the 'simple' flavoproteins makes classification of these enzymes in terms of their functional properties somewhat more logical. Some flavoproteins however still cannot be assigned to a group within the parameters of this classification scheme, these include the enzymes previously discussed within which the flavin prosthetic groups appear to have no discernible catalytic redox function. Additionally, the flavoproteins which carry only flavin as the prosthetic group but manifest multiple properties that span more than one of the four subgroups of the scheme, therefore making them difficult to assign.

1.4.   AMINES IN BIOLOGY

Enzyme-catalysed amine oxidation reactions are a common process in biology, attributable to the numerous diverse and key events modulated by amine compounds in nature. Amines are organic compounds that contain nitrogen as the central atom in the amine functional group in which one or more of the hydrogen atoms have been replaced by an alkyl substituent. They can be looked upon as structural relatives of ammonia in the same way that alcohols and ethers are related to water. If any of the

I XH + O_2 $\longrightarrow$ X + H_2O_2

Oxidases

II $R^{S}\diagdown_{S}^{R}$ + NAD(P)H + H^+ $\longrightarrow$ 2 R^{SH} + NAD(P)$^+$

Disulfide oxidoreductases

III Substrate + O_2 + NAD(P)H + H^+ $\longrightarrow$ Substrate-OH + H_2O + NAD(P)H + H^+

Monooxygenases

IV AH_2 + B $\longrightarrow$ A + BH_2

Reductases, Dehydrogenases and electron transferases
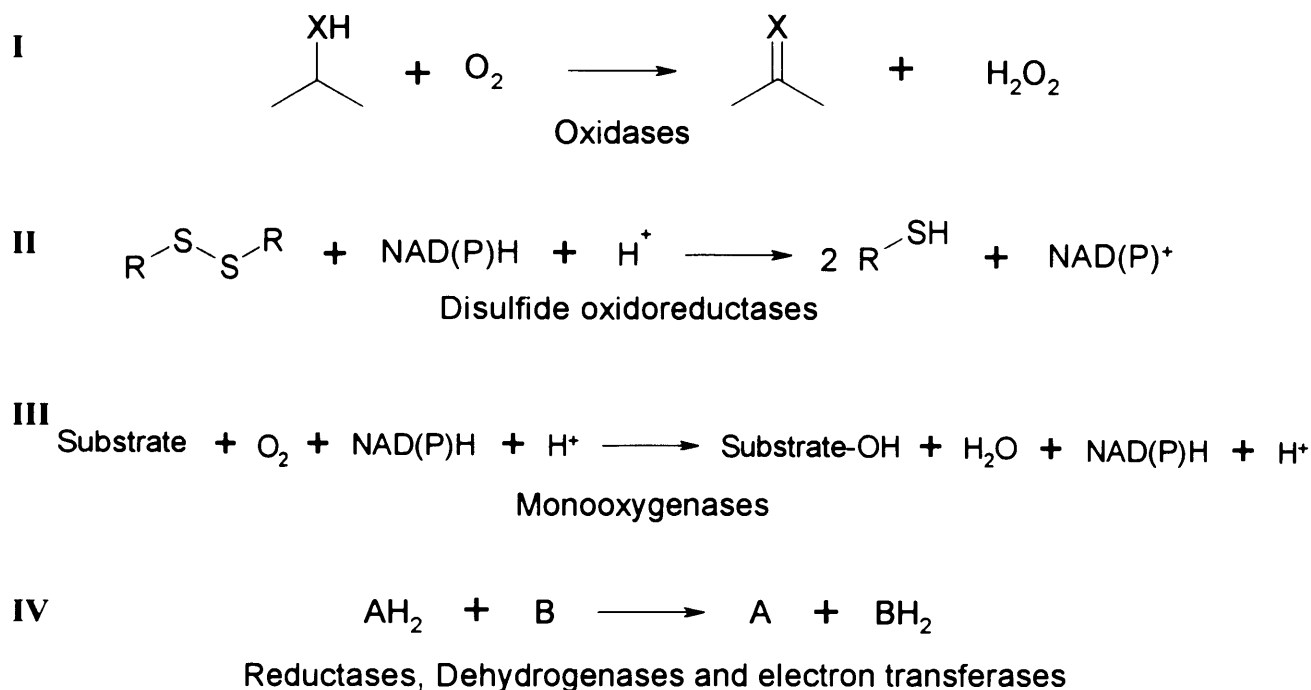
Figure 1. 8. A summary of the generic reactions catalysed by the simple flavoproteins based on the classification scheme devised by Palfey and Massey, 1998. The schemes depict the reactions catalysed by I) the oxidases)II the disulfide oxidoreductases, III) the monooxygenases, and IV) a group comprising of the reductases, dehydrogenases and electron transferases. X represents the electron-withdrawing atom, AH_2 is the reduced pyridine nucleus and B is the electron-acceptor atom. The figure is adapted from Palfey and Massey, 1998.

carbons bonded to the nitrogen are part of a carbonyl group, then the molecule is an amide rather than an amine (Streitwieser *et al.*, 1992). Amines are classified as primary (1°), secondary (2°) and tertiary (3°) amines or quaternary ammonium ions depending on the number of alkyl or aryl groups bonded to the central nitrogen. If one carbon-based group is bonded to the nitrogen the molecule is a primary amine, if two carbon-based groups are bonded to the nitrogen, then the molecule is a secondary amine, if three carbon-based groups are bonded to the nitrogen, then the molecule is a tertiary amine and if four carbon-based substituents are bonded to the nitrogen and the nitrogen becomes positively charged as a result, the compound is named a quaternary ammonium salt (Figure 1.9, A).

Amines have a pyramidal geometry. The nitrogen-hydrogen bond length for the primary amine methylamine is 1.011 Å and the carbon-nitrogen bond length is 1.474 Å with hydrogen-nitrogen-hydrogen (H-N-H) and hydrogen-nitrogen-carbon (H-N-C) bond angles of 105.9 ° and 112.9 ° respectively. Amines that have an aryl group attached to nitrogen are characterised by larger H-N-H and H-N-C bond angles, i.e. the nitrogen atom is nearly planar compared to alkylamines. The nitrogen is sp^3 hybridised in aliphatic amines and the non-bonding lone pair of electrons held by the nitrogen are important in the reaction chemistry of the amines, being responsible for the typical basic and nucleophilic properties of amine molecules. Examples of aliphatic amines are shown in figure 1.9, B. Amines in which at least one of the carbon atoms attached to the central nitrogen is sp^2-hybridised are illustrated in figure 1.9, C.

As a result of the pyramidal geometry of amine compounds, if three different chemical groups are attached to the central nitrogen atom, then the amine is chiral. Additionally, the stereochemistry of these molecules is important in terms of enzyme-substrate recognition. The two enantiomers of a chiral amine molecule are also readily interconvertible by the process of 'nitrogen inversion', therefore making separation of amine enantiomers less straight forward. The activation energy required for nitrogen inversion of simple amines is small on the order of 6 kcal/mol^{-1}. The planar transition state holds the central nitrogen in sp^2-hybridisation with the lone pair of electrons in the p_z-orbital (Figure 1.10). Nitrogen inversion is not possible for

A

| | | | | R4 |
| Ammonia | Primary amines | Secondary amines | Tertiary amines | Quaternary ammonium ions |

B

| | | | | CH₃ |
| Methylamine | Benzylamine | Pyrrolidine | Triethylamine | Benzyl trimethyl ammonium ion |

C

| Aniline | Pyrrole | Imidazole | Pyrimidine | Purine |
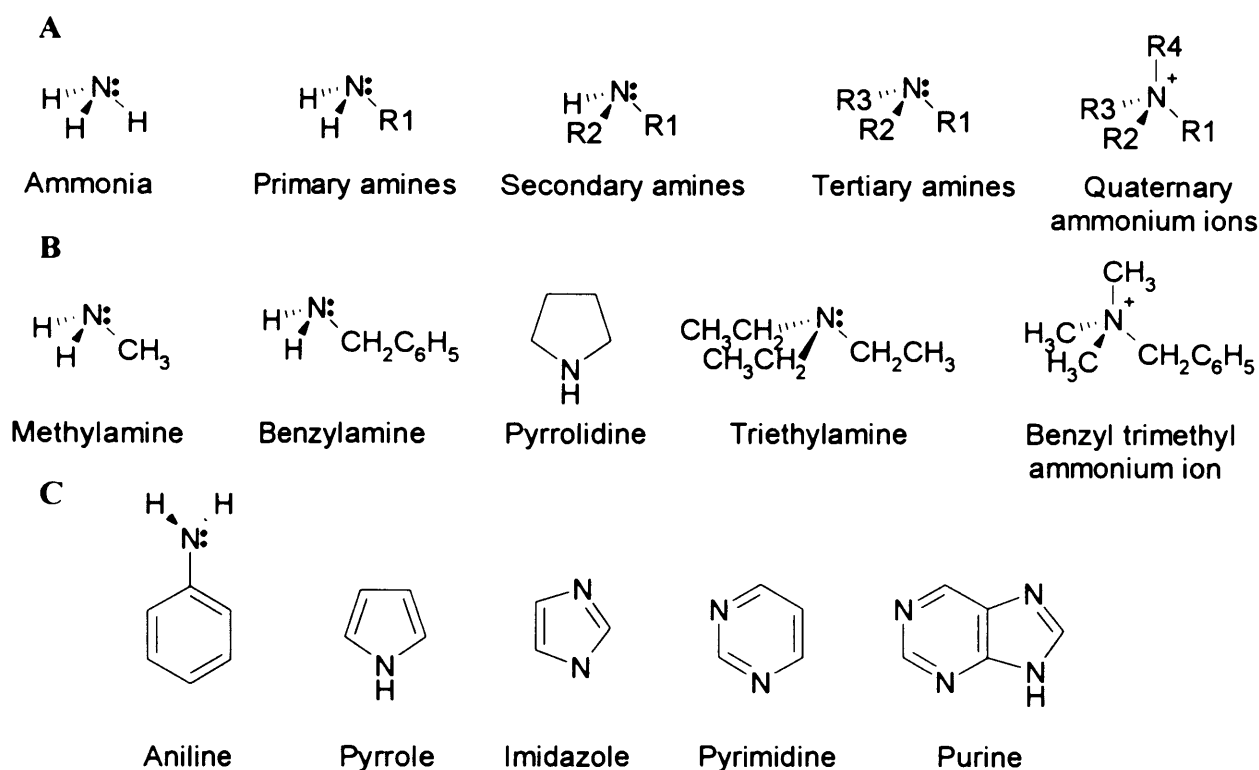
Figure 1. 9. The structural classification of amines and examples of aliphatic and conjugated amine compounds. *Panel A*, The structural relationship of ammonia and the four classes of amine compound, the R-group represents a carbon-based substituent and the number of R-groups attached to the central nitrogen atom dictates the class of the amine compound. Primary amines contain one R-group, secondary amines contain two R-groups, tertiary amines contain three R-groups and a quaternary ammonium ion has four R-groups bonded to the central nitrogen atom. *Panel B*, examples of aliphatic amine compounds. In these amines the carbon atoms bonded to the central nitrogen atom are saturated (sp^3-hybridised). *Panel C*, examples of conjugated amine compounds. In these amines at least one of the carbon atoms bonded to the central nitrogen atom is sp^2-hybridised. A lone pair of electrons on the central nitrogen interacts with (is conjugated to) the *pi* system of the adjacent double bond(s).
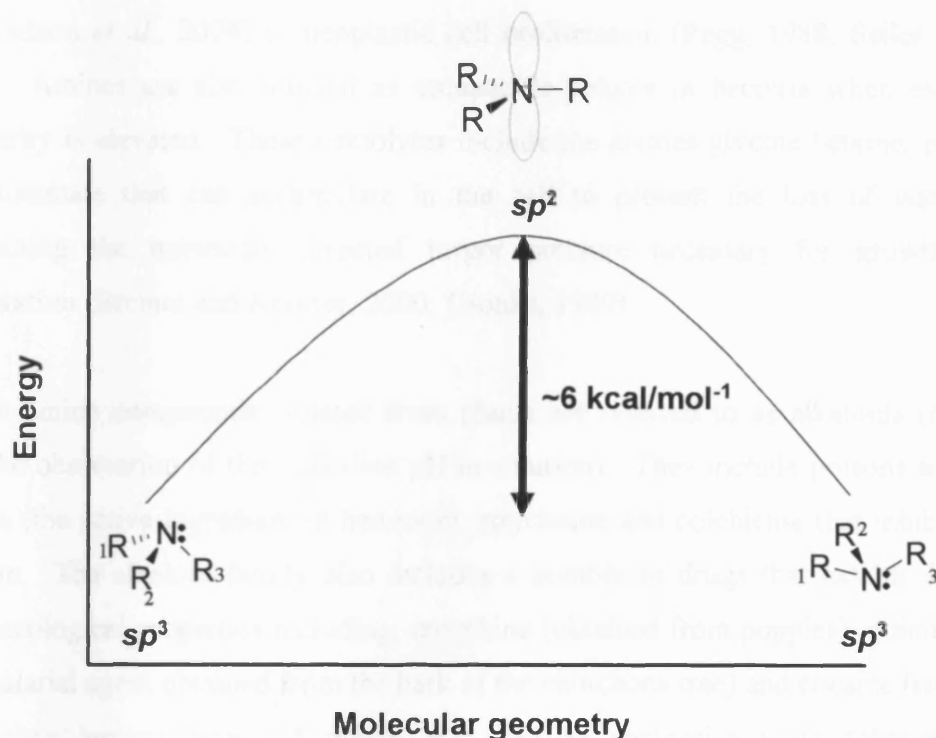
Figure 1. 10. Graphical representation of 'nitrogen inversion' in amine compounds. The two enantiomers of the tertiary amine molecule are readily interconvertible through the process of 'nitrogen inversion'. The activation energy required for nitrogen inversion of simple amines is ~6 kcal/mol[-1]. The planar transition state holds the central nitrogen atom in sp^2-hybridisation with the lone pair of electrons in the p_z-orbital.

quaternary ammonium salts and therefore, these enantiomers can be separated in a stable form.

Amine substrates play key roles in such diverse events from neurotransmission (Edmondson *et al.*, 2004) to neoplastic cell proliferation (Pegg, 1988; Seiler *et al.*, 1998). Amines are also utilised as compatible solutes in bacteria when external osmolarity is elevated. These osmolytes include the amines glycine betaine, proline and glutamate that can accumulate in the cell to prevent the loss of water by maintaining the outwardly directed turgor pressure necessary for growth and proliferation (Bremer and Kramer, 2000; Csonka, 1989).

Certain amine compounds isolated from plants are referred to as alkaloids (named after the observation of their alkaline pH in solution). They include poisons such as coniine (the active ingredient in hemlock), strychnine and colchicine that inhibit cell division. The alkaloid family also includes a number of drugs that exhibit diverse pharmacological properties including, morphine (obtained from poppies), quinine (an anti-malarial agent obtained from the bark of the chinchona tree) and cocaine (isolated from coca leaves) many of which are used as analgesics (pain relievers) or anaesthetics. This family of compounds also includes synthetic analogues such as heroin and lysergic acid diethylamide (LSD).

The organic polycations known as biogenic amines are derived from cationic or aromatic amino acids (Medina *et al.*, 2003). They each have a hydrophobic skeleton and one or more positive charges on a protonated amino group or a permanently charged ammonium moiety. Each biogenic amine has a similar metabolic and intracellular handling pattern but the physiological roles played by these biogenic amines in mammals is varied playing key roles in neurotransmission and other signaling functions. Biogenic amines acting as neurotransmitters are synthesised in nerve cells from amino acids (Figure 1.11, A) and are released into the synaptic cleft from vesicles localised in presynaptic terminals, once in the synaptic cleft these biogenic amine neurotransmitters bind to receptors at the postsynaptic terminals. Re-uptake transporters located at the presynaptic terminal act to clear the synaptic cleft of surplus neurotransmitter molecules in conjunction with enzymes that degrade these bioactive molecules. A selection of biogenic amines and alkaloids are given in figure

A

Dopa

Dopamine

5-hydroxytryptophan

Serotonin

B

piperidine

Coniine
poison hemlock

indole

Serotonin
an important neurochemical

Caffeine

pyrrolidine

Nicotine
tobacco

pyridine

Muscarine
from Amanita muscaria

pyrrolidine

piperidine Atropine

pyrimidine

Thiamine
vitamin B₁

piperidine

Morphine (opium)
analgesic

piperidine

quinoline

Quinine
pyridine antimalarial

Figure 1. 11. The chemical structures of neurotransmitters synthesised from amino acid precursors and a selection of biogenic amines and alkaloids with basic structural group and cyclic moieties highlighted. *Panel A*, dopa is converted to the biogenic amine dopamine and 5-hydroxytryptophan is the precursor of the biogenic amine serotonin. Both dopamine and serotonin are important neurotransmitters and are synthesized in nerve cells. *Panel B*, Serotonin and thiamine are primary amines, coniine is a secondary amine, atropine, morphine and quinine are tertiary amines and muscarine is a quaternary ammonium salt. Indole, imidazole, piperidine, pyridine, pyrimidine and pyrrolidine moieties are also found in these structures.

1.11, B, with basic structural elements highlighted within the more complex structural formulae of these selected compounds, therefore showing that serotonin and thiamine are primary amines, coniine is a secondary amine, atropine, morphine and quinine are tertiary amines and muscarine is a quaternary ammonium salt. Indole, imidazole, piperidine, pyridine, pyrimidine and pyrrolidine moieties are also evident in these structures.

As a direct result of the essential roles played by the polycationic alkylamines known as polyamines in cell growth, including transcription/translation processes and cell proliferation, polyamine homeostasis is key to cell survival, and diseases such as cancer (Cohen, 1998), psoriasis (Pietila *et al.*, 2005) and neurodegenerative disorders (Lesort *et al.*, 2000; Esposito and Caputo, 2005) are the severe manifestation of polyamine homeostasis deregulation (Rodriguez-Caso *et al.*, 2006). The positively charged amine groups of polyamines interact with negatively charged macromolecules such as nucleic acids (Ruiz-Chica *et al.*, 2001), as well as certain proteins (Brandes *et al.*, 1998; Seiler, 2005) and phospholipids (Wallace *et al.*, 2003). The degree of non-covalent polyamine-macromolecule interactions in living cells predicts that only 10 % of total polyamines are free in mammalian cells (Igarashi and Kashiwagi, 2000). Increased polyamine biosynthesis has been linked to rapid tumor growth (Russell, 1983; Huang *et al.*, 2005) with increased polyamine levels implicated in aggressive forms of breast tumors (Manni, 1994; Leveque *et al.*, 2000; Manni, 2002). In light of findings that demonstrate the deregulation of polyamine homeostasis in breast tumor cells, breast cancer therapies have been developed by rational targeting of polyamine metabolism through the design polyamine analogues that mimic certain self-regulatory functions of natural polyamines but do not imitate growth stimulating functions (Marton and Pegg, 1995). Recent findings regarding polyamine analogues called oligoamines have shown that specific oligoamine compounds reduce the activity of the enzyme ornithine decarboxylase (ODC) and induce activity of spermidine/spermine N^1-acetyltransferase (SSAT), a polyamine catabolic enzyme resulting in a decrease in the polyamine pools in a number of human breast cancer cell lines (Huang *et al.*, 2003; Huang *et al.*, 2004). Rodriguez-Caso and co-workers (Rodriguez-Caso *et al.*, 2006) have taken a systems biology approach in the construction of a mathematical model for polyamine metabolism in mammals with the preliminary model pointing to relevant roles for *S*-adensoyl methionine and

acetyl-CoA availability in polyamine homeostasis, the model does not however account for polyamine and cationic amino acid compartmentalisation, transport and gene expression regulation (Childs *et al.*, 2003).

1.4.1. THE AMINE-OXIDOREDUCTASE FLAVOPROTEINS: A CASE STUDY OF PROPOSED MECHANISMS OF FLAVOPROTEIN-CATALYSED AMINE OXIDATION

Mechanisms of amine oxidation catalysed by the quinoprotein amine dehydrogenase/oxidases are well established. Oxidation occurs through the formation of enzyme–substrate covalent adducts with topaquinone (TPQ), tryptophan tryptophylquinone (TTQ), cysteine tryptophylquinone (CTQ) or lysine tyrosyl quinone (LTQ) redox centres (Figure 1.12; Mure *et al.*, 2002; Datta *et al.*, 2001; Satoh *et al.*, 2002; Davidson 2000; Wang *et al.*, 1996) and H-transfer by quantum mechanical tunnelling has been demonstrated for some quinoprotein enzymes (Masgrau *et al.*, 2004; Masgrau *et al.*, 2006). However, the mechanistic basis that underlies flavoprotein-catalysed amine oxidation, despite intense research interest in this area of enzymology, still remains contentious and to date, four basic and contrasting mechanisms have been considered (Scrutton, 2004). These mechanisms include i) A carbanion mechanism in which a general active site base abstracts an α-proton to form a substrate carbanion, first proposed for TMADH (Rohlfs and Hille, 1994), ii) an aminium cation radical species (Silverman, 1995) based on the receptivity of amine substrates to sustain single electron transfer (SET) chemistry, therefore permitting SET from the substrate nitrogen lone pair yielding a flavin semiquinone and substrate radical species, iii) H-atom abstraction by an active site radical species (Edmondson, 1995), with the first direct EPR spectroscopic evidence in support of a SET mechanism for monoamine oxidase A, recently being published documenting the detection of a stable tyrosyl radical species (Rigby *et al.*, 2005), and finally iv) a polar nucleophilic mechanism involving nucleophilic attack by the substrate nitrogen on the flavin C4a atom, proceeded by proton abstraction by an active site base (Kim *et al.*, 1993) or in a later alternative, proton abstraction by the flavin N5 atom (Miller and Edmondson, 1999) coined the 'concerted' polar nucleophilic mechanism. The reformulation of the polar nucleophilic mechanism
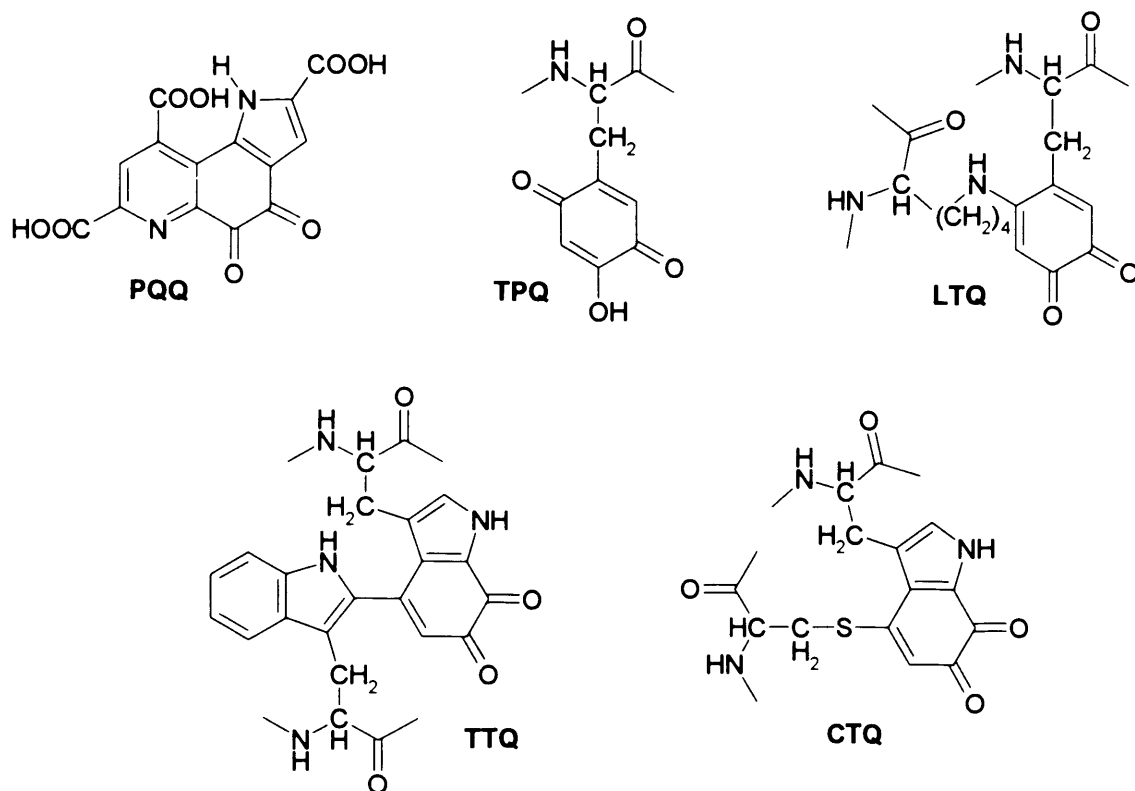
Figure 1. 12. The chemical structures of the various *O*-quinone prosthetic groups found in quinoenzymes. The tyrosine and tryptophan-derived prosthetic groups include lysine tyrosylquinone (LTQ; cofactor of lysyl oxidase), tryptophan tryptophylquinone (TTQ; cofactor of methylamine dehydrogenase) and topaquinone (TPQ; cofactor of diamine oxidase). The cofactor pyrroloquinone quinone (PQQ; cofactor of alcohol dehydrogenases) is formed from the annulation of peptidyl glutamic acid and tyrosine residues. Cysteine tryptophylquinone (CTQ) was recently identified in quinohemoprotein amine dehydrogenase of *Pseudomonas putida* encaged by multiple thioether cross-bridges (Satoh *et al.*, 2002). These quinone cofactors are involved in key catalytic processes in biology, including free-radical redox events and oxidative deaminations.

(Miller and Edmondson, 1999) is based on the chemistry of the 4a-alkylated isoalloxazine ring adduct that harbours a very strong base at the N5 position of the flavin ring that holds a pK_a value of ~30, characteristic of aniline compounds (Chan and Bruice, 1978).

It is now generally considered that both the carbanion and H-atom abstraction mechanisms unlikely represent the true catalytic scenario for flavoprotein-catalysed amine oxidation. The process for the carbanion mechanism (Rohlfs and Hille, 1994) involving the formation of a carbanion species through the abstraction of an α-proton by an active site base residue is unfavourable on the basis that this ionisation is represented by a pK_a value of ~30 for the α-H$^+$ and is therefore not acidic enough to permit deprotonation (Erdem *et al.*, 2006). Likewise, the H-atom abstraction mechanism of substrate α-C-H bond breakage by a non-flavin protein-based radical species first proposed for MAO-B (Edmondson, 1995) has been dismissed for the two isozymic forms of MAO through a lack of supporting evidence for the presence of a stable resting-state protein-based radical species, with EPR spectroscopic studies on resting-state MAO-A and MAO-B confirming the absence of such a protein radical (Li and Hubalek, 2002; Newton-Vinson *et al.*, 2000).

Towards the formulation of the polar nucleophilic mechanism (Kim *et al.*, 1993; Miller and Edmondson, 1999) early flavin model reactions by Brown and Hamilton using 10-phenylisoalloxazine in reaction with methyl phenylglycine inspired a polar nucleophilic mechanism with the participating deprotonated amine reactant undergoing attack at the isoalloxazine C4a position resulting in an isoalloxazine-amine reactant adduct (Figure 1.13, A), proceeded by H-atom abstraction at the adduct α-carbon by a general active site base (Brown and Hamilton, 1970). Additional support for this mechanism came from chemical model studies concerning lumiflavin reactivity with amine compounds. Oxidation of benzylamine substrate by N^5-ethyl-3-methyllumiflavinium perchlorate, a stable non-acidic analogue salt of N^5-protonated 3-methyllumiflavin (3MLF) produced key evidence for the presence of a stable C4a lumiflavin-amine substrate adduct (Figure 1.13, B; Kim *et al.*, 1993), with oxidation of substrate benzylamine by 3MLF occurring by a proposed mechanism of reversible N5 protonation of the isoalloxazine function of 3MLF in conjunction with

A

10-phenylisoalloxazine

Substrate-flavin C4a adduct

B

N^5-ethyl-3-methyllumiflavinium perchlorate

Stable C4a-adduct analog

C
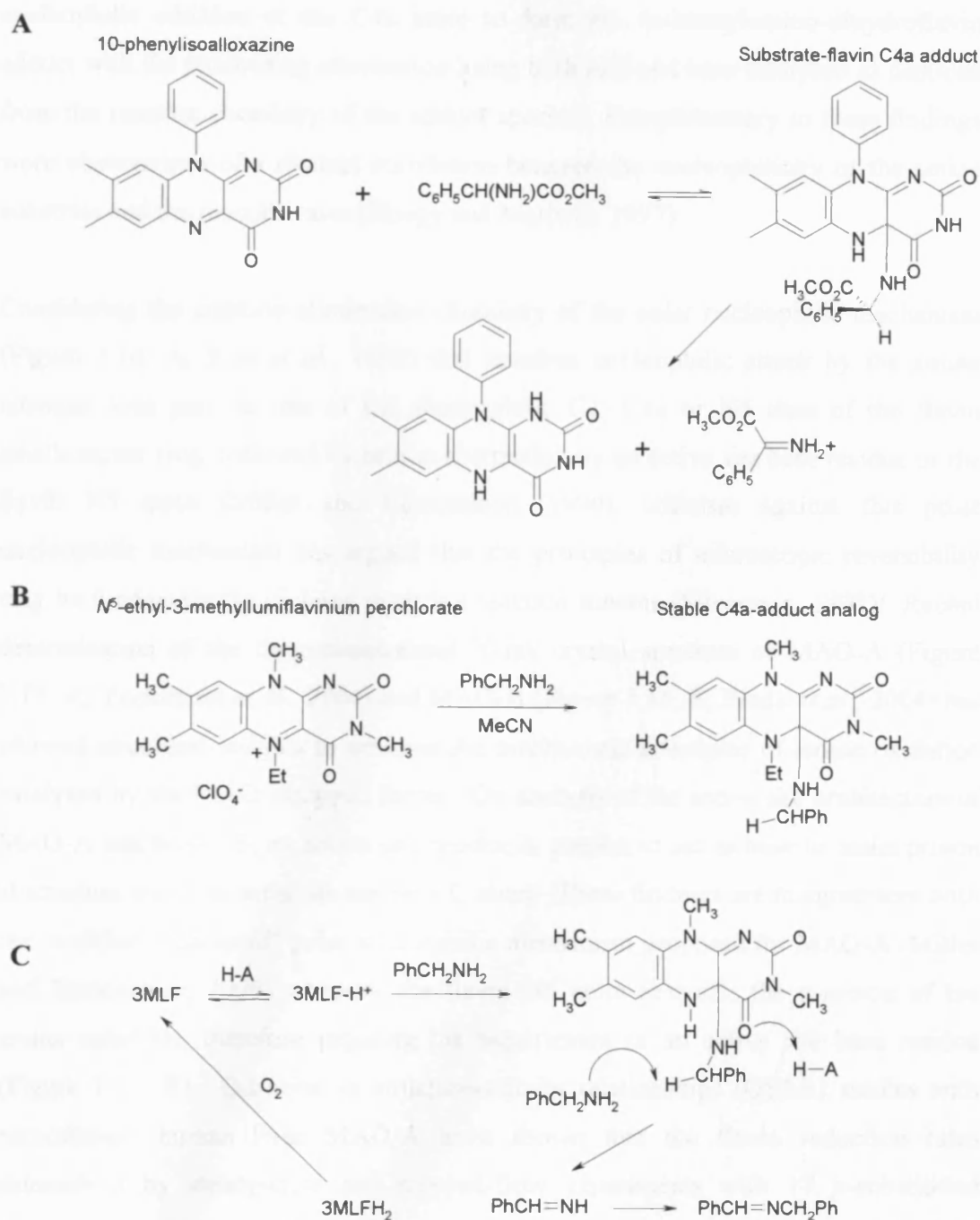
Figure 1. 13. Early flavin model reactions of 10-phenylisoalloxazine with methyl phenylglycine and later chemical model studies of the reaction of lumiflavin with benzylamine providing support for the polar nucleophilic mechanism. *Panel A*, the proposed mechanism for 10-phenylisoalloxazine-catalysed amine oxidation via a substrate-flavin C4a adduct. *Panel B*, the proposed mechanism for the oxidation of benzylamine by N^5-ethyl-3-methyllumiflavinium perchlorate, a stable non-acidic analogue salt of N^5-protonated 3-methyllumiflavin (3MLF). A stable C4a-benzylamino-dihydroflavin adduct is formed during the reaction in MeCN at a solution temperature of 25 °C. This reaction provided supporting evidence that the acid-catalysed oxidative deamination reaction of 3MLF with benzylamine (*Panel C*) proceeds via an intermediate C4a-adduct.

nucleophilic addition at the C4a atom to form the 4a-benzylamino-dihydroflavin adduct with the proceeding elimination being both acid and base catalysed as deduced from the reaction chemistry of the adduct species. Complimentary to these findings were observations of a distinct correlation between the nucleophilicity of the amine substrate and the reaction rates (Hoegy and Mariano, 1997).

Considering the addition-elimination chemistry of the polar nucleophilic mechanism (Figure 1.14, A; Kim *et al.*, 1993) that involves nucleophilic attack by the amine nitrogen lone pair on one of the electrophilic C2, C4a or N5 sites of the flavin isoalloxazine ring, followed by proton abstraction by an active site base residue or the flavin N5 atom (Miller and Edmondson, 1999), criticism against this polar nucleophilic mechanism has argued that the principles of microscopic reversibility may be fundamentally violated in such a reaction scheme (Silverman, 1992). Recent determination of the three-dimensional X-ray crystal structure of MAO-A (Figure 1.15, A; Yoshimura *et al.*, 2004) and MAO-B (Figure 1.15, B; Binda *et al.*, 2004) has allowed structural insights to advance the mechanistic principles of amine oxidation catalysed by the MAO isozymic forms. On analysis of the active site architecture of MAO-A and MAO-B, no active site residue is present to act as base to assist proton abstraction from the substrate amine α-C atom. These findings are in agreement with the modified 'concerted' polar nucleophilic mechanism proposed for MAO-A (Miller and Edmondson, 1999) whereby the flavin N5 atom abstracts the α-proton of the amine substrate, therefore negating the requirement of an active site base residue (Figure 1.14, B). Quantitative structure-activity relationships (QSAR) studies with recombinant human liver MAO-A have shown that the flavin reduction rates determined by steady-state and stopped-flow experiments with 17 *p*-substituted benzylamine analogues showed a strong correlation with electronic effects (σ) of the substituent, with increased rates of flavin reduction with a large positive *p*-value (2.0) apparent from reactions with electron-withdrawing substituents, consistent with a proton abstraction mechanism (Miller and Edmondson, 1999). Large deuterium isotope effects were also observed consistent with the mechanistic proposal. Additional evidence corroborating the concerted polar nucleophilic mechanism comes from the failure to detect an EPR spectral signature corresponding to a protein-based radical species in the resting state of the protein (Li *et al.*, 2002). Further studies with mitochondrial bovine liver MAO-B in reactions with various *para* and *meta*

A: Kim *et al.*, 1993 (Polar nucleophilic)
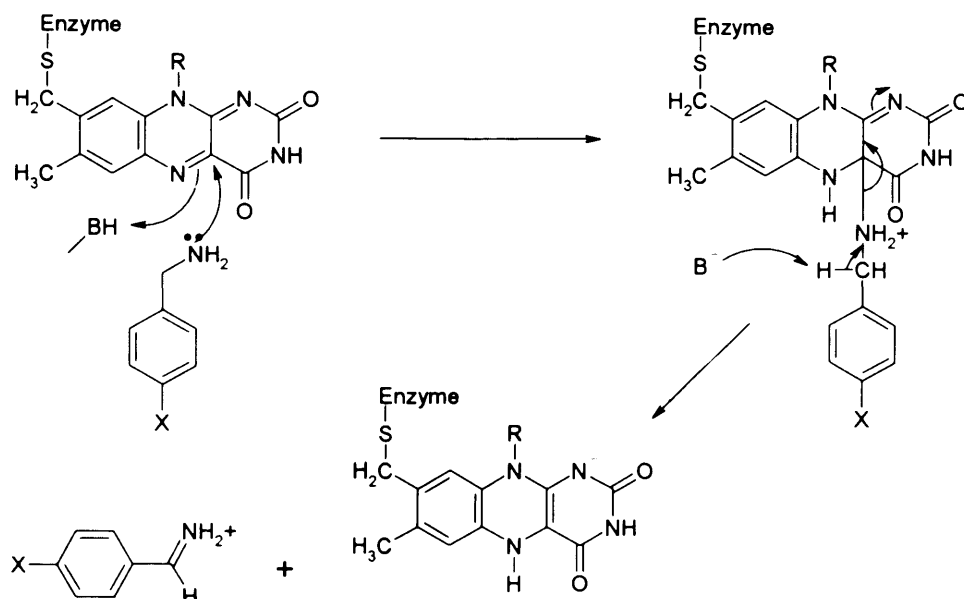
B: Miller and Edmondson, 1999 (Concerted polar nucleophilic)
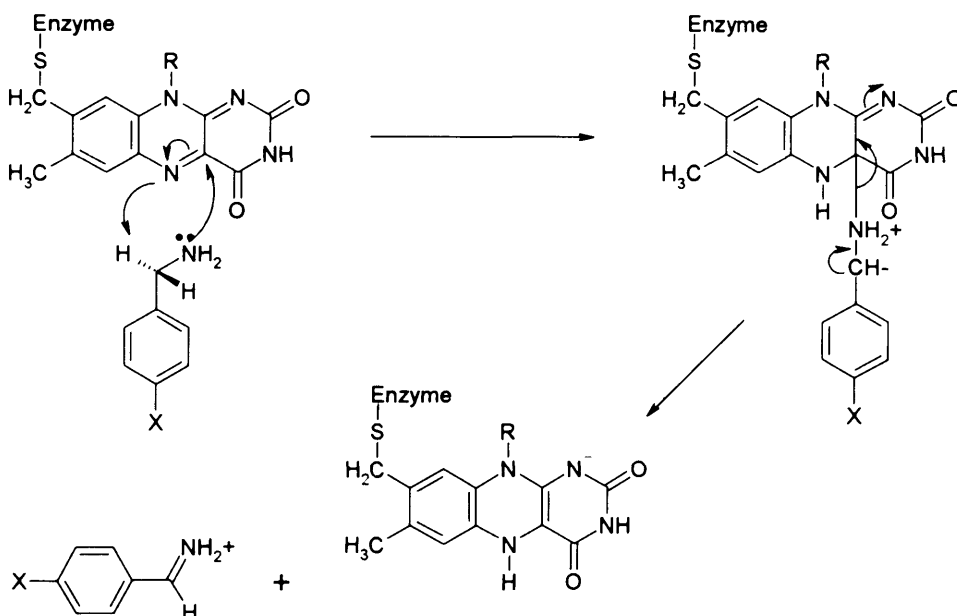
Figure 1. 14. The proposed polar nucleophilic mechanism of MAO catalysis, and the later concerted polar nucleophilic mechanism advanced for MAO-A. *Panel A*, the polar nucleophilic mechanism involves initial nucleophilic attack of deprotonated amine substrate at the flavin C4a position forming the substrate-flavin C4a-adduct, followed by proton abstraction from the adduct α-carbon by an active site base. *Panel B*, elucidation of the X-ray crystal structure of MAO-A highlighted the absence of an active site base required for the polar nucleophilic mechanism. Miller and Edmondson therefore proposed that the strong base at the flavin N5 of the 4a-alkylated isoalloxazine ring (pK_a ~30) permits concerted transfer of the benzyl proton to the N5 atom proceeded by an elimination to produce the protonated imine product and reduced flavin cofactor.

Human MAO-A
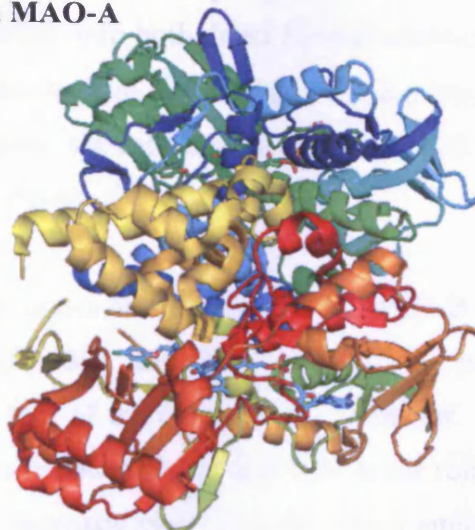
Human MAO-B
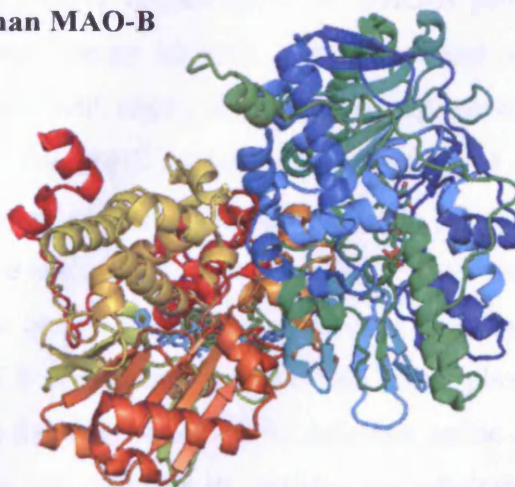
Figure 1. 15. The three-dimensional X-ray crystal structures of the human monoamine oxidase isozymic forms, hMAO-A and hMAO-B. The structure of hMAO-A was solved at 3.0 Å resolution by molecular replacement using the hMAO-B coordinates. The structure revealed a monomeric form exhibiting an active site consisting of a 550 Å^3 hydrophobic cavity (Colibus *et al.*, 2005). The structure of hMAO-B was solved at 3.0 Å resolution in dimeric form that is proposed to be the native quaternary form *in vivo*. The structure reveals an active site characterised by a 420 Å^3 hydrophobic substrate cavity interconnected to a 290 Å^3 entrance cavity (Binda *et al.*, 2002). The structure figures were constructed using PyMOL v.0.99 (DeLano, 2002; http://www.pymol.org) using the PDB accession codes 2BXR and 1GOS for hMAO-A and hMAO-B, respectively. The active site figure is taken from Colibus *et al.*, 2005.

benzylamine substituents showed no dependence of the limiting rate of flavin reduction on the substituents electronic properties (Walker and Edmondson, 1994). These data are incompatible with both direct H-atom abstraction and hydride transfer mechanism, the later mechanism also being a high-energy process and therefore unlikely to occur. However, the data are also consistent with the aminyl radical cation mechanism (Silverman, 1995).

An interesting structural aspect of the active site of MAO-B concerns the presence of two tyrosyl residues (Tyr-398 and Tyr-435) that are positioned approximately perpendicular to the *re* face of the covalent FAD cofactor. Li and co-workers have proposed that these two residues play a key functional role during the catalysis of MAO-B in forming an 'aromatic cage' through which amine substrate must pass to gain access to the flavin (Li *et al.*, 2006). Structural elucidation of the Y435F, Y435L, Y435H and Y435W mutant forms of MAO-B permitted the calculation of dipole-dipole coupling energy between the amino acid 435 side chain and the substrate amine moiety, with results showing a strong correlation between the dipole coupling energy and the $\Delta(\Delta G)$ calculated from ratios of k_{cat}/K_m measurements in addition to a correlation of dipole strength with the pK_a values of para-substituted benzylamine substrate analogues (Li, *et al.*, 2006). Mechanistic conclusions based on these analyses centre on the dipole environment of the 'aromatic cage' of MAO-B with a distance of 7.8 Å between the two side chain phenolic rings rendering an environment suitable for polarisation of the substrate amine lone pair as the substrate passes between these two residues to increase the substrates nucleophilicity in the activated state (Figure 1.16; Li *et al.*, 2006). This functional proposal for an 'aromatic cage' in MAO-B is consistent with the concerted polar nucleophilic mechanism of MAO-catalysed amine oxidation proposed for MAO-A (Miller and Edmondson, 1999), with the dipole environment mediated by the 'aromatic cage' resulting in deprotonation of the amine substrate prior to nucleophilic attack on the flavin C4a atom during the reductive phase of catalysis. Therefore, it is suggested that both MAO-A and MAO-B isozymic forms follow similar mechanisms for amine oxidation (Li *et al.*, 2006). Recent quantum chemical calculations of amine oxidation by MAO using the semi-empirical PM3 method and single-point B3LYP/6-31G* calculations showed a good correlation between the log of the calculated rate constants and the electronic parameter (σ) of the *p*-substituent (Erdem *et al.*, 2006) that are in
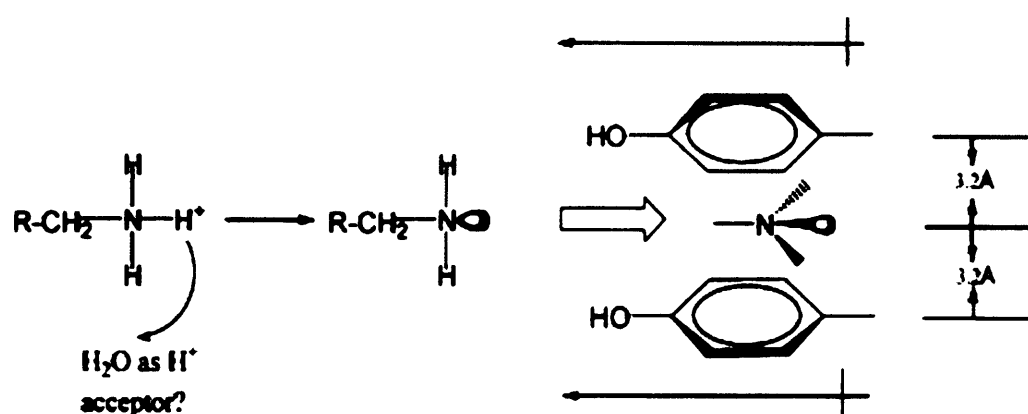
Figure 1. 16. Schematic representation describing the proposed function for the 'aromatic cage' during MAO-B-catalysed amine oxidation. The aromatic cage formed by residues Tyr-398 and Tyr-435 establish an environment agreeable for polarisation of the amine nitrogen lone pair, therefore increasing substrate nucleophilicity with the effect of elevating the population of 'activated' substrate molecules for catalysis. Figure taken from Li *et al.*, 2006.

agreement with experimental QSAR studies (Miller and Edmondson, 1999) in support of the polar nucleophilic mechanism for MAO-A.

Elucidation of the X-ray crystal structure of the flavoprotein dimethylglycine oxidase (DMGO) at 1.6 Å resolution (Figure 1.17, A; Leys *et al.*, 2003) has led to the proposal of a polar nucleophilic-based mechanism for the enzyme-catalysed oxidative demethylation of dimethylglycine substrate as based on the enzymes active site architecture. DMGO contains an FAD cofactor covalently bound via the 8α methyl of the FAD and residue His-48 at the NE2 atom, with the cofactor held butterfly bent so as to modulate the midpoint reduction potential of the cofactor to thermodynamically favour substrate amine oxidation (Leys *et al.*, 2003). The conserved active site residues His-225 and Tyr-259 form a catalytic dyad in close proximity to the N5 atom of the FAD isoalloxazine moiety and form a proton shuttle enabling proton abstraction from the amine substrate prior to nucleophilic attack of the deprotonated substrate at the flavin C4a atom. Consequently, the highly basic N5 position (pK_a ~30) abstracts a proton from the methyl group of complexed substrate (Figure 1.17, B; Leys *et al.*, 2003), a mechanism of C-H bond cleavage advanced for MAO-A (Miller and Edmondson, 1999). Mechanistic investigations with mutant forms of DMGO have advanced the mechanistic details. Steady-state turnover of the DMGO Y259F mutant is compromised ~200-fold in comparison with the wild-type enzyme. Likewise, stopped-flow studies revealed that FAD reduction in the Y259F mutant is diminished by a factor of ~1500 in comparison to wild-type. Thus, a key role for Tyr-259 in substrate deprotonation prior to FAD reduction has been inferred (Basran *et al.*, 2006). Crystallographic analyses of the H225Q mutant highlighted that this enzyme adopts different conformational states. It has been proposed that His-225 likely modulates the acid-base properties of Tyr-259 by perturbing the pK_a of this residue, permitting the 'fine-tuning' of the reaction chemistry of DMGO so that under physiological conditions, proton abstraction is facilitated (Basran *et al.*, 2006). Further experiments based on magnetic field effects are required to resolve the current argument of whether a polar nucleophilic or radical-based mechanism is applicable in DMGO catalysis.

Kinetic studies of other amine oxidising flavoproteins including trimethylamine dehydrogenase (TMADH; Basran *et al.*, 2001a), have identified a kinetically
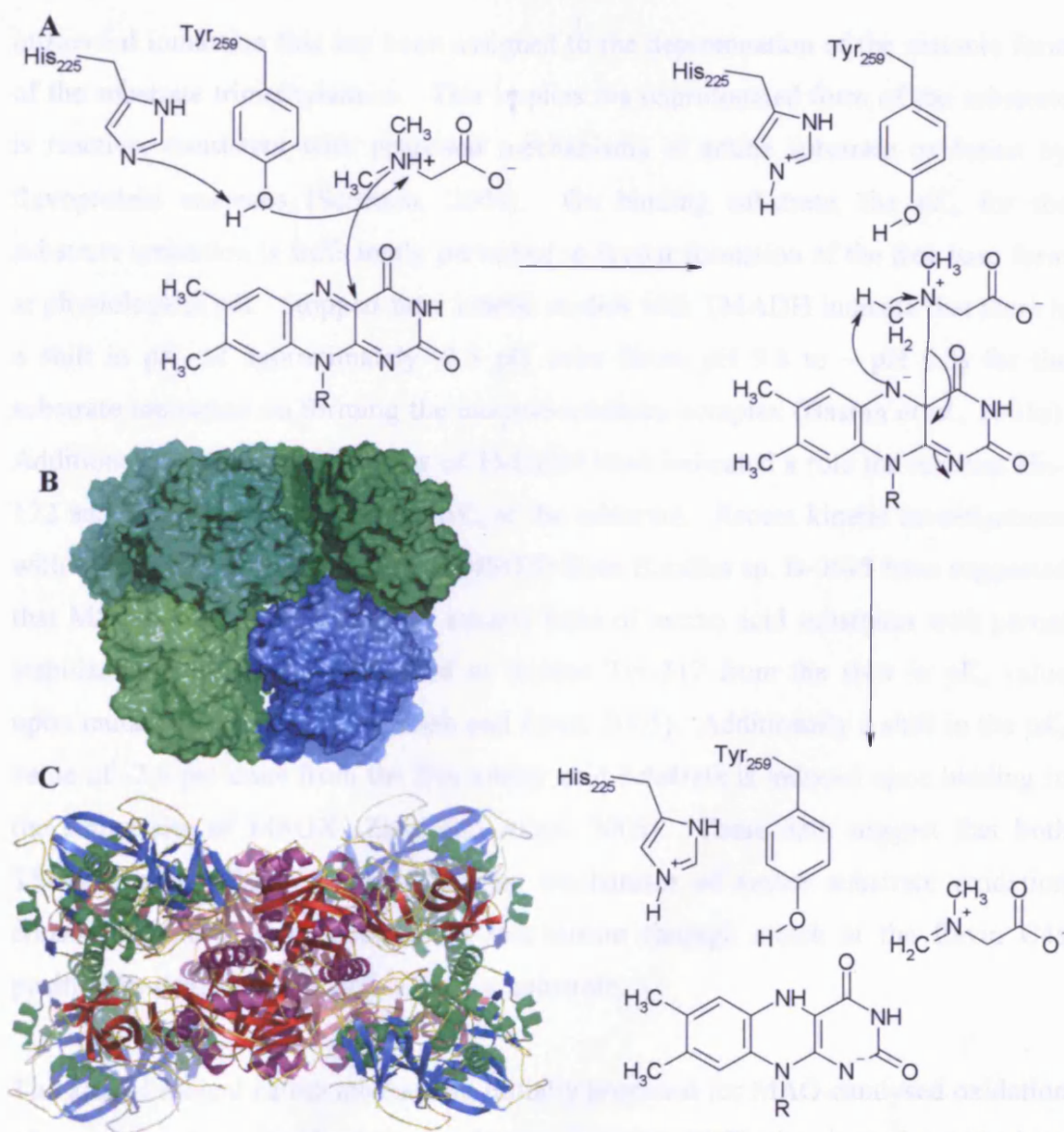
Figure 1. 17. The X-ray crystal structure of the dimethylglycine oxidase (DMGO) tetramer of *Arthrobacter globiformis* and the proposed mechanism of amine oxidation by this enzyme. *Panel A*, The proposed mechanism of DMGO-catalysed oxidative demethylation of dimethylglycine involving deprotonation of substrate amine by the His225-Tyr259 catalytic dyad. This initial deprotonation is followed by nucleophilic attack of the substrate at the flavin C4a atom and proton abstraction from the covalent adduct by the basic N5 position of the flavin ring with concomitant reduction of the isoalloxazine moiety and release of intermediate dimethylglycine iminium ion. *Panel B*, Molecular surface view of the DMGO tetramer with monomers defined by individual colouring. *Panel C*, as for panel B, but the DMGO tetramer backbone is displayed in ribbons with monomers colour coded as in panel B. The crystal structure was solved at 1.6 Å resolution by the method of MIRAS. Panel A is adapted from Leys *et al.*, 2003, and both of the DMGO structure figures in Panels B and C are also taken from this article.

influential ionisation that has been assigned to the deprotonation of the cationic form of the substrate trimethylamine. This implies the unprotonated form of the substrate is reactive, consistent with proposed mechanisms of amine substrate oxidation by flavoprotein enzymes (Scrutton, 2004). On binding substrate, the pK_a for the substrate ionisation is sufficiently perturbed to favour formation of the free base form at physiological pH. Stopped-flow kinetic studies with TMADH indicate that there is a shift in pK_a of approximately -3.5 pH units (from pH 9.8 to ~ pH 6.5) for the substrate ionisation on forming the enzyme-substrate complex (Basran *et al.*, 2001a). Additionally, mutagenesis studies of TMADH have indicated a role for residues His-172 and Tyr-60 in perturbing the pK_a of the substrate. Recent kinetic investigations with monomeric sarcosine oxidase (MSOX) from *Bacillus* sp. B-0618 have suggested that MSOX stabilises the reactive anionic form of amino acid substrates with partial stabilization of substrate attributed to residue Tyr-317 from the shift in pK_a value upon mutation of this residue (Zhao and Jorns, 2005). Additionally a shift in the pK_a value of -2.6 pH units from the free amino acid substrate is induced upon binding in the active site of MSOX (Zhao and Jorns, 2005). These data suggest that both TMADH and MSOX follow a similar mechanism of amine substrate oxidation consistent with a polar nucleophilc mechanism through attack at the flavin C4a position by deprotonated 'active' amine substrate.

The aminyl radical cation mechanism initially proposed for MAO-catalysed oxidation of amine substrate involves single electron transfer (SET) chemistry from the lone pair of the substrate amine nitrogen atom to yield a substrate aminyl radical cation and flavin semiquinone (Silverman *et al.*, 1980), followed by H˙ abstraction or deprotonation of the amine radical α-proton (pK_a ~10) and subsequent radical transfer generating reduced flavin and product iminium ion (Figure 1.18, A). This proposal is consistent with mechanism-based inhibitor studies on MAO-B using various cyclopropyl inhibitors that form the cyclopropylaminyl radical species through rapid ring opening and SET chemistry (Figure 1.18, B; Silverman, 1995). Analogous studies with the inhibitor aminomethanecubane gave support for the deprotonation/radical transfer step in the aminyl radical cation mechanism inferred from destruction of the cubane nucleus on reaction with MAO indicating formation of the α-carbon radical that is not produced in the alternate H˙ abstraction route (Silverman *et al.*, 1993). Subsequent mechanism-based inhibitor studies with MAO

Figure 1. 18. Schematic representation of the aminyl radical cation mechanism proposed for MAO-catalysed amine oxidation and mechanism-based inhibitor studies with MAO using 1-phenylcyclopropylamine. *Panel A*, the aminyl radical cation mechanism proposed by Silverman, (1980), for MAO catalysis that involves single electron transfer (SET) chemistry from the substrate amine nitrogen lone pair to yield the substrate aminyl radical cation and flavin semiquinone. This is proceeded with H˙ abstraction (route *d*) or deprotonation of the amine radical α-proton and subsequent radical transfer (route *a, b*) generating reduced flavin and product iminium ion. This later route is consistent with QSAR studies that identified a strong correlation between reaction rates and electronic effects (σ) of the substituent. Route *c* depicts a protein-based radical also consistent with QSAR data. *Panel B*, the proposed mechanism of MAO inactivation by 1-phenylcyclopropylamine. Rapid ring opening of the 'reporter' cyclopropyl group generates a primary radical that reacts with the flavin semiquinone (route *a*) or amino acid radical species (route *b*). Figures adapted from Scrutton, 2004.

using cinnamylamine 2,3-oxide gave benzaldehyde and glycoaldehyde, congruous with the formation of an α-carbon radical species as opposed to an α-carbanion that would be expected to break the C-O bond of the inhibitor molecule to yield cinnamaldehyde product (Silverman *et al.*, 1994). However, until recently, direct detection of the one-electron oxidant necessary for aminyl radical cation formation was the critical 'missing piece' of evidence in the mechanisms puzzle.

The Silverman aminyl radical cation mechanism generates a radical pair consisting of the flavin semiquinone and aminyl radical cation that rearranges to form a carbon-centered radical, thus generating dihydroflavin and product iminium cation, or sustains reverse electron transfer to form amine reactant and oxidised flavin. In an effort to detect a radical species to ratify this mechanism, magnetic field effect (MFE) studies were initiated for the MAO-catalysed oxidation of amine substrates by rapid-scan stopped-flow spectrophotometry (Miller *et al.*, 1995) to detect the generation of spin-correlated radicals weakly coupled to permit intersystem crossing between triplet and singlet states, for example, via hyperfine coupling (Grissom, 1995). This study failed to observe MFE's in the reaction of MAO-B, although the stringent chemical and experimental criteria required for MFE investigations on enzyme systems could potentially contribute to this negative experimental result, and precise optimisation of MFE parameters may lead to this result being falsified.

The first direct evidence of a radical species during MAO-catalysed oxidation of amines has come from EPR and ENDOR studies on partially reduced MAO-A that have detected the presence of a stable tyrosyl radical in the enzyme (Rigby *et al.*, 2004), therefore necessitating a revision of the SET radical mechanism by inclusion of a Tyr˙ during catalysis. Subtraction of the EPR spectrum of the anionic non-covalent flavosemiquinone radical of electron transferring flavoprotein (ETF) from the EPR spectrum of the anionic covalent flavin radical of partially reduced MAO-A gave a residual spectrum presenting a g_{av} of 2.0042 (Figure 1.19, A; Rigby *et al.*, 2004), a value in agreement with the assignment of a tyrosyl radical (Mezzetti *et al.*, 1999) that is greater than the value of 2.0032 expected from a flavosemiquinone radical (Edmondson, 1985). Redox equilibrium between the flavosemiquinone and an active site tyrosine radical in MAO-A must exist to facilitate oxidation of amine substrate (Figure 1.19, B). Enzyme reduction by single electron transfer (SET) from

A
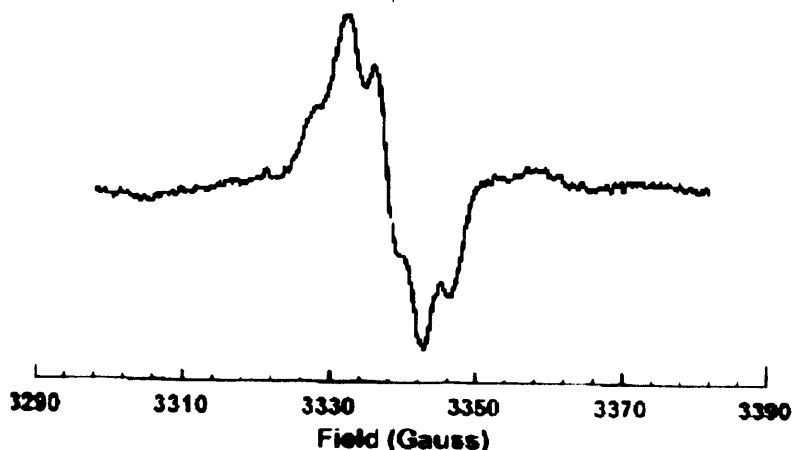
B
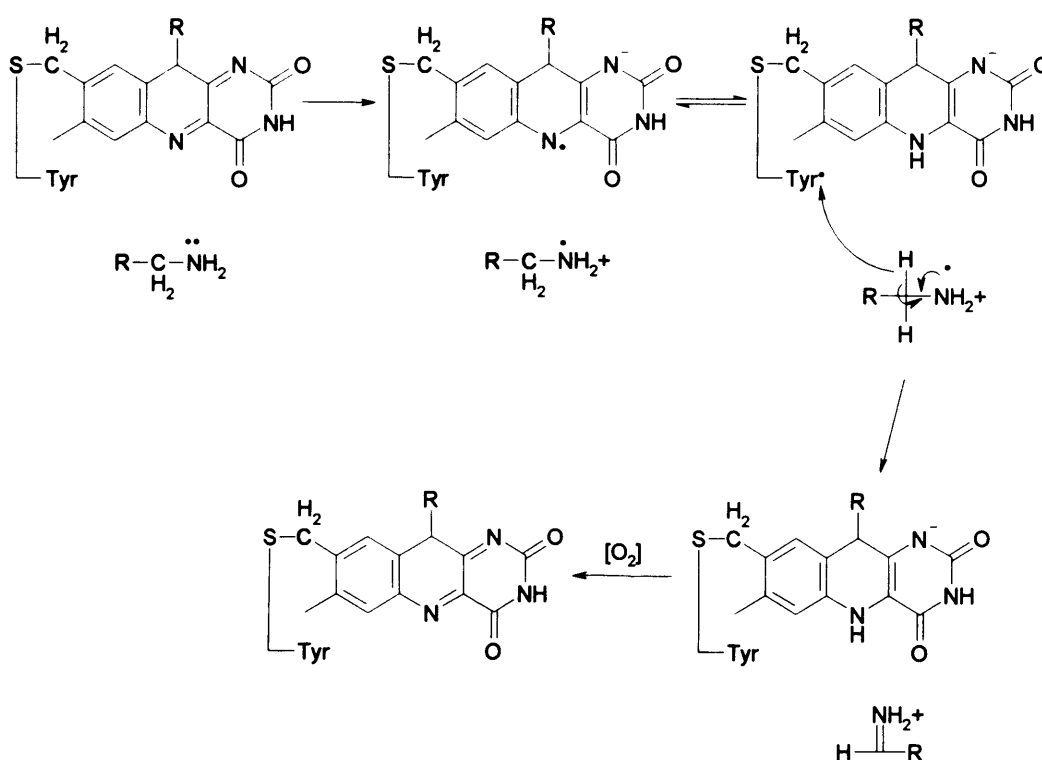
Figure 1. 19. The difference EPR spectrum of partially reduced MAO-A assigned to the formation of a tyrosyl radical species and, a possible mechanism proposed for substrate amine oxidation by radical catalysis. *Panel A*, the difference EPR spectral signature resulting from subtraction of the EPR spectrum of the anionic non-covalent flavosemiquinone radical of electron transferring flavoprotein (ETF) of *Methylophilus methylotrophus* from the EPR spectrum of dithionite-reduced MAO-A, presenting a g_{av} of 2.0042 consistent with the presence of a stable tyrosyl radical species. *Panel B*, a proposed mechanism for radical mediated amine substrate oxidation. Single electron transfer (SET) from substrate to flavin establishes a tyrosyl radical species, permitting a subsequent direct H-transfer mechanism. Figures adapted from Rigby *et al.*, 2004 (*Panel A*) and Scrutton, 2004 (*Panel B*).

substrate to flavin during catalytic turnover generates the proposed redox equilibrium with formation of both a tyrosyl radical and aminyl radical cation species.

The use of difference EPR spectra for the detection of organic radical species should be approached with caution according to Ramsay and co-workers who argue that non-covalent and covalent anionic flavin radicals have differing EPR spectral properties. Additionally, this group also highlight that a one-electron oxidation of tyrosine (Tyr˙/Tyr couple $E_m = \sim +1$ V) by a flavin radical (Fl˙/FlH˙ couple $E_m = \sim -0.2$ V for free flavin) as depicted in Scheme 1.1 is energetically unfavourable (~ 20 kcal/mol^{-1}; Stubbe *et al.*, 2003).

$$FAD˙ + Tyr \longleftrightarrow FADH˙ + Tyr˙ \qquad \textbf{Scheme 1. 1}$$
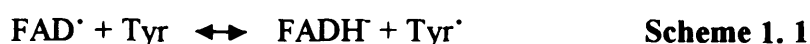
Resonance Raman data on MAO-B flavin anionic semiquinone shows no 1500 cm^{-1} band that would be diagnostic of a phenoxy radical (Yue *et al.*, 1993; Tripathi and Schuler, 1984) and recent optical and EPR data point to the flavin anionic semiquinone as the only radical species formed during catalytic turnover of MAO isozymic forms and they suggest that observation by Rigby and co-workers of a Tyr˙ is likely an artifact of spectral subtraction and that assignment of a tyrosyl radical species from the difference EPR spectra alone is presumptive (Ramsay *et al.*, 2005).

The current mechanisms debate taking into account all relevant scientific literature concerning this topic highlights that further structural elucidation of flavoprotein amine dehydrogenase/oxidases coupled to additional detailed spectroscopic and kinetic studies are required to advance the mechanistic details of amine oxidation by this class of enzymes.

1.5. MULTIFUNCTIONAL PutA PROTEIN OF ENTERIC BACTERIA: STRUCTURE AND FUNCTION IN L-PROLINE METABOLISM

As a secondary amine, L-proline can be utilised as a source of reducing equivalents through its oxidation by FAD-containing oxidases. Dye-linked L-proline dehydrogenase activity has been recently observed in a number of hyperthermophilic archaea (Kawakami *et al.*, 2004), yet a search of these genomes does not reveal the presence of hypothetical proteins homologous to the well characterised

multifunctional L-proline-oxidising enzyme 'PutA' of enteric bacteria and PRODH enzymes of eukaryotes. PutA (EC 1.5.99.8) flavoprotein was first identified and isolated from *E. coli* (Scarapulla and Soffer, 1978) and *S. typhimurium* (Menzel and Roth, 1981) and has been demonstrated to play multiple roles in L-proline catabolism by acting as both a membrane associated L-proline dehydrogenase/Δ^1-pyrroline-5-carboxylate (P5C) dehydrogenase (Menzel and Roth, 1981) and an autogeneous transcriptional repressor of the proline utilisation (*put*) regulon (Wood, 1981; Menzel and Roth, 1981; Brown and Wood, 1992; Vilchez *et al.*, 2000). The *E. coli* PutA is a single polypeptide containing 1320 amino acid residues and when purified reveals a native homodimeric state with a molecular weight of 293 KDa containing one mol of noncovalent FAD cofactor per mol of PutA monomer (Brown and Wood, 1992). The membrane associated L-proline dehydrogenase domain catalyses the two-step oxidation of L-proline to glutamate (Menzel and Roth, 1981). PutA in conjunction with the high affinity Na^+/proline transporter protein 'PutP' enables enteric bacteria to utilise L-proline as a source of carbon, nitrogen and electrons (Chen *et al.*, 1985). PutA accumulates in the cytoplasm when L-proline substrate is absent and binds to promoter sites in the intergenic DNA region of the *put* regulon between *putP* and *putA* to repress transcription. When L-proline becomes available, PutA associates peripherally with the plasma membrane with concomitant activation of *put* transcription (Wood, 1987; Muro-Pastor *et al.*, 1997; Surber and Maloy, 1999).

Proline is oxidised to Δ^1-pyrroline-5-carboxylate (P5C) by the proline dehydrogenase (PRODH) domain of PutA in a redox reaction that is coupled to a two-electron reduction of the non-covalently bound FAD of PutA to the dihydroflavin state. These electrons are then transferred to an acceptor in the electron transport chain (Abrahamson *et al.*, 1983; Surber and Maloy, 1999). PutA association with the membrane is regulated by the redox state of the PRODH domain FAD (Surber and Maloy, 1999). Zhu and Becker have shown that PutA of *E. coli* undergoes a substrate L-proline-induced conformational change leading to peripheral association with the plasma membrane (Zhu and Becker, 2003) where the PRODH domain mediates the transfer of reducing equivalents from reduced FAD cofactor to the electron transport chain (Abrahamson *et al.*, 1983). The redox state of FAD has been shown to have negligible influence on the PutA-DNA interaction (Becker and Thomas, 2001), although recent studies of PutA protein using tryptophan fluorescence spectroscopy

have demonstrated that residue W211 in a flexible region close of the PRODH active site is a primary molecular marker of the conformational change upon proline binding and FAD reduction (Zhu and Becker, 2006). Studies with the *E. coli* protein have also demonstrated that oxidised PutA does not bind to polar lipid bilayers although a strong PutA-membrane complex (K_d < 0.01 nM) is assumed upon reduction of the PutA FAD cofactor (Zhang *et al.*, 2004). This provides strong evidence that FAD reduction initiates the formation of an *E. coli* PutA conformer harbouring high affinity for the plasma membrane where it binds peripherally resulting in the de-repression of *put* regulon transcription during L-proline metabolism.

The intermediate labile product P5C is hydrolysed to γ-glutamic semialdehyde in what is thought to be a spontaneous hydrolysis, although Schiff base hydrolysis catalysed by PutA has not yet been conclusively ruled out (Vinod *et al.*, 2002). γ-glutamic semialdehyde is subsequently oxidised to glutamate by the P5C dehydrogenase domain (P5CDH; EC 1.5.1.12) of PutA, coupled to the reduction of soluble NAD^+ to NADH. The crystal structure of a truncated form of PutA from *E. coli* (Lee *et al.*, 2003) suggests that this hydrolysis reaction may take place in the active site. Counter-clockwise rotation of P5C in the active site relative to the position of L-proline would be necessary to bring C5 close to a local water molecule (Wat1) to promote a hydrolysis reaction. The increase in molecular volume and conformational entropy as a result of conversion of P5C to γ-glutamic semialdehyde in the active site could present a catalytic advantage by facilitating product release (Lee *et al.*, 2003). Channelling of substrate between the discrete PRODH and P5CDH active sites of PutA has also been proposed in studies with PutA from *S. typhimurium* whereby intermediate P5C may be transferred directly between the two PRODH/P5CDH active sites of PutA via a 'leaky channel' mechanism (Surber and Maloy, 1998), with channelling suggested to play a potential role in the regulation of L-proline utilisation.

In addition to multifunctional PutA protein characterised from *E. coli*, *S. typhimurium*, and the soil microbe *Pseudomonas putida*, all possessing autogeneous transcriptional regulator activity (Brown and Wood, 1992; Menzel and Roth, 1981; Vilchez *et al.*, 2000), a bifunctional PutA has recently been cloned and characterised from the soil microbe *Bradyrhizobium japonicum*. Interestingly, the protein lacks the

autogeneous transcriptional regulator activity described for other PutA proteins (Krishnana and Becker, 2005), whilst retaining similar catalytic and membrane-binding functions. The membrane-binding activity of *B. japonicum* PutA has been shown to vary significantly from the respective binding by *E. coli* PutA, with the later enzyme having no noticeable electrostatic dependence on the type of lipid required for membrane-binding which is in stark contrast to the PutA protein of *B. japonicum* that exhibits marked binding to 1-palmitoyl-2-oleoyl-*sn*-glycero-3[phosphor-*rac*-(glycerol)] (POPG) lipids in comparison to zwitterionic 1,2-dioleoyl-*sn*-glycero-3-phosphocholine (DOPC) lipids where binding was undetectable. Additionally, isothermal titration calorimetry (ITC) demonstrated that the endothermic binding reaction of *B. japonicum* PutA lipid-association is entropically driven (Zhang *et al.*, 2006).

In most Gram-positive bacteria and eukaryotes, the two reactions carried out by PutA are catalysed by distinct enzymes. Human proline oxidase hsPRODH2/PIG6 (for p53-induced genes) has been well characterised with molecular genetic studies revealing that genetic variations, mainly in the form of missense mutations greatly increase susceptibility to schizophrenia (Liu *et al.*, 2002). Structural analyses of PutA669 in complex with competitive inhibitors including acetate, L-lactate and tetrahydro-2-furoic acid (THFA) suggest that elevated plasma L-proline concentrations in patients with schizophrenia that carry the L441P missense mutation is a direct result of the decreased stability of the human PRODH2 isoform that expresses in the brain, heart pancreas, kidneys and liver (Zhang *et al.*, 2004). The inactive PRODH leads to elevated levels of cytoplasmic L-proline in neuronal cells that may act as a direct modulator of glutamatergic transmission, therefore contributing to the presentation of schizophrenia (Liu *et al.*, 2002; Chakravarti, 2002). The enzyme is mitochondrial in humans and has also been shown to play a role in p53-mediated apoptosis (Polyak *et al.*, 1997) and is involved in the proline dependent production of reactive oxygen species (Donald *et al.*, 2001).

The X-ray crystal structure of truncated PutA consisting of the first 669 amino acid residues (PutA669), and containing the PRODH domain has been solved at 2.0 Å resolution (Figure 1.20) by the technique of multiple isomorphous replacement with anomalous scattering (MIRAS; Lee *et al.*, 2003). The N-terminal 669 residues of the
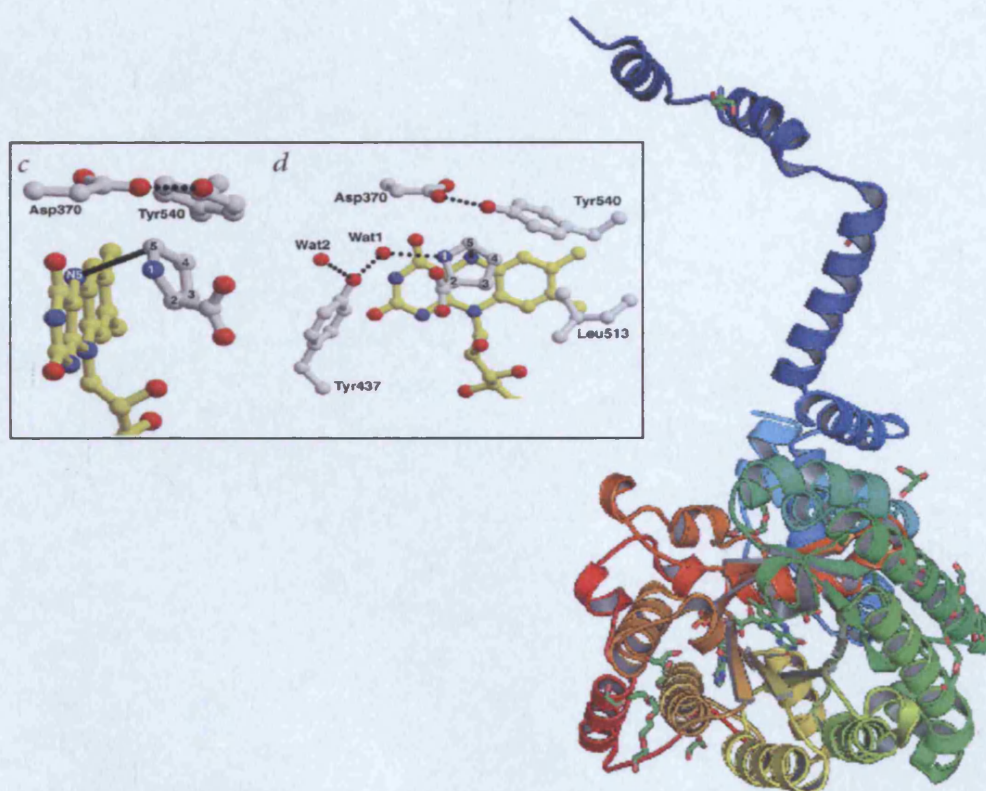
Figure 1. 20. The three-dimensional X-ray crystal structure of the *E. coli* PutA669 monomer. The structure was resolved at 2.0 Å resolution by the method of MIRAS. The 669-residue truncated form of *E. coli* PutA formed a domain-swapped dimer via a helical dimerisation arm in each subunit. The truncated PutA possessed both L-proline dehydrogenase (PRODH) activity and DNA-binding activity, but did not show Δ^1-pyrroline-5-carboxylate dehydrogenase (P5CDH) activity (mapped to residues 650-1,130 from sequence alignment data). *Boxed*, orthogonal views of L-proline modeled into the active site of the PRODH domain of PutA. L-proline and the flavin isoalloxazine are coloured white and yellow, respectively, with H-bonds represented by the dotted lines. A distance of 3.2 Å between the hydride transfer partners C5 and N5 is represented by a solid line. The PutA figure was constructed using PyMOL v.0.99 (DeLano, 2002; http://www.pymol.org) using PDB accession number 1K87. The active site figure is taken from Lee *et al.*, 2003.

full length 1320 residue PutA protein contains one mol FAD per mol of enzyme monomer and displays PRODH activity. PutA669 also exhibits DNA recognition by specifically binding to *put* intergenic DNA with a dissociation constant of 15 nM (Vinod *et al.*, 2002). The truncated enzyme does not contain the P5CDH domain, this being located within the residues 650-1130 (deduced from sequence alignment data). Also, the enzyme does not possess the membrane association activity of PutA. The PutA669 native oligomeric structure is of a homodimer of interlocking subunits with dimensions: 97 Å × 57 Å × 50 Å. A large interfacial buried surface area of 9,002 Å^2 led to the identification of the mode of dimerisation with crystallographic two-fold rotation around the *c*-axis in the asymmetric unit. Three structurally distinct domains have been identified within the PutA669 subunit. Residues 87-139 constitute 'domain I' that comprises three α-helices responsible for the three-dimensional domain swapped dimer (Bennett *et al.*, 1995). These helices create an arm to bind the other subunit. 'Domain II' within residues 140-260 is a six α-helices cluster and 'domain III' within residues 261-612 presents a $\beta_8\alpha_8$-barrel and is responsible for FAD-binding. This third domain is responsible for the PRODH activity of PutA669. The pyrimidine carbonyls of the FAD prosthetic group are orientated towards strand β3 and the isoalloxazine dimethyl benzene edge points towards strand β7. The *re* face of the isoalloxazine moiety is supported by strands β4-6 of the barrel and the adenine group is positioned above the barrel wedged between α-helices α5a and α5. The ribityl side-chain and pyrophosphate group are inserted between strands β5 and β6. L-lactate has been shown experimentally to act as a competitive inhibitor of L-proline for PRODH active sight occupancy and inhibitor binding has identified key active sight residues in the crystal structure (Lee *et al.*, 2003). L-lactate binds close of the pyrimidine function of the *si* face of the isoalloxazine moiety of FAD cofactor. The basic residues Lys-329, Arg-555 and Arg-556 bind the inhibitor carboxylate group with these residues being stabilised by an ion-pair network comprising residues Glu-559, Glu-289, Asp-370 and Arg-431. Arg-431 acts as hydrogen-bond donor to the N5 position of the FAD isoalloxazine ring and residues Arg-556 and Glu-559 form hydrogen-bonds with the ribityl side-chain. Asp-370, Tyr-540 and a water molecule (Wat1) take part in hydrogen-bonding with the inhibitor hydroxyl group, with the water molecule additionally hydrogen-bonded to residue Tyr-437. Van der Waals interactions are also apparent between residue Leu-513 and the methyl group of the

inhibitor molecule. Modelling of the substrate L-proline into the active site of PutA669 suggests that several features of the L-lactate complex are evident in the L-proline complex (Baban *et al.*, 2004).

The catalytic mechanism of L-proline oxidation by *E. coli* PutA669 has been postulated to be via a direct hydride-transfer mechanism analogous to the catalytic mechanism of D-amino acid oxidase (DAAO) that catalyses the oxidation of D-amino acid enantiomers to imino acids (Mattevi *et al.*, 1996; Umhau *et al.*, 2000). The L-proline C5-H bond in the PutA669-L-proline model complex is directed towards the flavin N5 atom at a C5-N5 distance of 3.2 Å, a similar ligand-FAD geometry being evident in DAAO. These results from the substrate-bound PutA model are therefore consistent with the proposed hydride transfer mechanism of DAAO (Pollegioni *et al.*, 1997; Kurtz *et al.*, 2000).

Active site residues from PutA669 are highly conserved between bacterial PutA and eukaryotic PRODH enzymes. A high active site sequence homology is particularly evident in hsPRODH2 that shares 47 % identity and 62 % similarity with PutA669, therefore giving rise to the possibility that these two enzymes share a common active site or even a common fold. The archaeal thermophilic and hyperthermophilic Dye-linked L-proline dehydrogenase sequences that have undergone sequence alignment analysis against bacterial and eukaryotic PutA and PRODH sequences show little or no homology at active site residues, although sequence motifs are conserved between archaeal strains (Kawakami *et al*, 2004). A heterotetrameric enzyme showing a bifunctional L-proline/NADH dehydrogenase activity has been cloned and characterised from the hyperthermophilic archaeon *Thermococcus profundus* (Kawakami *et al*, 2004), with similar gene clusters identified in the genomes of *Pyrococcus horikoshii*, *Pyrococcus abyssi*, *Pyrococcus furiosus* and *Archaeoglobus fulgidus*, indicating that a bifunctional L-proline/NADH dehydrogenase complex may be widely distributed in hyperthermophilic archaeal strains. More recently, a second Dye-linked L-proline dehydrogenase has been identified from the hyperthermophile *Pyrococcus horikoshii* OT-3 (Kawakami *et al.*, 2005) and the X-ray crystal structure determined at 2.86 Å resolution (Tsuge *et al.*, 2005), presenting a heterooctameric ($\alpha\beta_4$) native structure. The crystallisation of a monofunctional L-proline dehydrogenase from the thermophile *Thermus thermophilus* that possesses 24 %

sequence identity with *E. coli* PutA protein but lacks P5CDH activity has recently been documented (White and Tanner, 2005). Analysis of these monofunctional L-proline catabolising enzymes from bacteria will provide further advances into the functional aspects of related human PRODH enzymes. Future studies on hyperthermophilic L-proline dehydrogenase systems should also address the pertinent questions regarding the delineation of the physiological roles played by the two types of L-proline dehydrogenase isolated from hyperthermophilic sources and additionally, probe the mechanisms of substrate oxidation and electron transfer by these archaeal amine oxidoreductase enzymes.

1.6.   *PYROCOCCUS FURIOSUS* DSM 3638

P. furiosus DSM 3638 is an archaeal species within the order of Thermococcales. This sulfur-reducing ($S^\circ \rightarrow H_2S$) heterotrophic, hyperthermophilic marine archaea is an obligate anaerobe that was first isolated from solfataric mud off the coast of Vulcano island, Italy (Fiala and Stetter, 1986). The organism inhabits shallow and deep-sea sulfurous volcanic environments (Stetter, 1996; Stetter *et al.*, 1990) and is capable of growing at temperatures ranging from 70-103 °C with an optimal growth temperature of 100 °C within a pH range of 5-9 by the fermentation of carbohydrates and peptides to organic acids, CO_2 and H_2. Cells of this microorganism are motile cocci that possess ~50 polar flagella.

The *P. furiosus* genome is 1.908 Mbp in length with a GC content of 41 %. The complete genomic sequence is now available (Robb *et al.*, 2001) along with the other related hyperthermophilic genomic sequences for *P. horikoshii* (Kawarabayasi *et al.*, 1998) with a genome of 1.738 Mbp and *P. abyssi* (Genoscope: Heilig *et al.*, unpublished, direct submission to GenBank, 2001), therefore permitting scientists to begin to elucidate the biochemistry of these archaeal species. The sequence identity between these microorganisms is very high, with the average nucleotide identity between the genomic sequences of *P. furiosus* and *P. horikoshii* being 70-75 % within ORFs.

All species of the genera *Pyrococcus* and *Thermococcus*, except for *Tc. zilligii*, have been isolated from marine geothermal areas and are therefore slightly halophilic. These microorganisms therefore require osmoadaptivity mechanisms in adjusting to osmotic upshock that leads to a loss of cytoplasmic water. To adjust to higher environmental osmolarities, these microorganisms may accumulate intracellular osmolytes to re-establish cellular turgor pressure and cell volume and also to protect intracellular enzymes and other macromolecules, including DNA, from dehydration. Failure to adjust to environmental osmolarities causes growth cessation and cell death (Brown, 1990). In relation to stress responses in *P. furiosus*, the organism resorts exclusively to the *de novo* synthesis of the compatible solute α-mannosylglycerate (MG), and the level of MG increases concomitantly with NaCl concentration. The absence of glycine betaine and ectoine in hyperthermophiles is likely due to these compatible solutes being unstable at hyperthermophilic physiological growth temperatures (80 °C – 113 °C).

1.7. PRINCIPLES OF METABOLIC THERMOSTABILITY

Concerning temperature, it is generally assumed that the upper limit for life is dictated by molecular instability. *In vitro*, certain small metabolites are shown to be unstable at temperatures corresponding to the optimal growth temperatures of the hyperthermophiles within which they are present (Daniel and Cowan, 2000). For example, nicotinamide adenine dinucleotide (NAD^+) and nicotinamide adenine dinucleotide phosphate ($NADP^+$) each have a half-life ($t_{1/2}$) < 2 minutes at a solution temperature of 95 °C (Walsh *et al.*, 1983). Likewise, NADH has a $t_{1/2}$ ~2 minutes at 95 °C/solution pH 7.0, although at a higher pH this coenzyme gains increased thermostability (Lowry *et al.*, 1961; Hudson *et al.*, 1993). An array of mechanisms *in vivo* are employed to counteract thermal instability. These include rapid turnover, metabolic channelling of intermediate substrates between physically juxtaposed enzymes in a metabolic pathway (Alhabori, 1995) and local stabilisation. Physical association of carbamoyl phosphate synthetase with the enzyme ornithine carbamoyl transferase of *P. furiosus* has been proposed as a mechanism of evading the thermal degradation of the labile intermediate carbamoyl phosphate that is synthesised by the former enzyme and channelled to the later enzyme for consumption (Legrain *et al.*,

1995; Van de Casteele *et al.*, 1997; Massant and Glansdorff, 2004). DNA duplex stability in hyperthermophiles is assisted by higher salt concentrations, cationic proteins (Sandman *et al.*, 1990; Pereira *et al.*, 1997), polyamines (Friedman, 1986) and positive supercoiling by ATP-dependent topoisomerases (Slesarev *et al.*, 1991) as opposed to increased GC content (Grogan, 1998). The role of reverse gyrase in the thermostability of DNA has been critically assessed by Marguet and Forterre with findings arguing against the importance of these topoisomerases in thermostability (Marguet and Forterre, 1994). *P. furiosus* also synthesises di-*myo*-inositol 1, 1'-phosphate (DIP) for thermal protection at growth temperatures above the optimum (Martins and Santos, 1995).

Analysis of the biochemical behaviour of redox systems at high temperatures is an interesting area of enzymology requiring closer attention and the effects of the optimal growth temperature for *P. furiosus* (100 °C) on equilibrium electron transfer potentials (E'_0) demands closer investigation. A notable characteristic of redox centres in hyperthermophilic enzymes reveals these centres often utilise tungsten as opposed to molybdenum. Both metals are redox-active under physiological conditions between oxidation states VI and IV, also acting as transducers between obligatory two-electron and one-electron redox systems due to the V valence state accessibility (Pilato and Stiefel, 1999). In attempting to unravel the logic behind the use of tungsten over molybdenum within redox centres in hyperthermophiles, taking into account the extreme hot and anaerobic conditions that *P. furiosus* inhabits and in which life may have first evolved some 3.8 billion years ago, tungsten may have been the first of these metal elements to be acquired. Tungsten-sulfur bonds in tungsto-enzymes are more stable when compared to molybdenum-sulfur bonding. The low valent tungsten sulfides are more soluble in aqueous environments and may therefore have been more readily available to the organisms in these aqueous reducing environments. The probable low intracellular redox state of early life will have also suited the lower reduction potentials of tungsten containing systems (Hille, 2002).

1.7.1. ENZYME THERMOSTABILITY: A STRUCTURAL PERSPECTIVE

Studies into the structural basis of enzyme thermostability have primarily relied on the elucidation of high resolution X-ray crystal structures of selected hyperthermophilic enzymes to enable structural comparisons to be drawn with regard to homologous mesophilic and psychrophilic counterparts through the observations of potential differences in structural motifs and/or bonding elements that may contribute to enhanced thermostability (Danson and Hough, 1998). Thermophilic proteins heterologously expressed in mesophilic hosts often retain thermostability suggesting that this property is intrinsic of the macromolecule (Li *et al.*, 2005). No novel amino acids, covalent modifications or structural motifs have been discovered in thermophilic proteins to account for this enhanced thermostability (Field, 2001). Structural studies with glutamate dehydrogenase (Yip *et al.*, 1998) and citrate synthase (Russell *et al.*, 1997) have highlighted the important contributions of extensive ion-pair networks toward enzyme thermostability, with ion-pair interactions being more prevalent in hyperthermophilic proteins in comparison to homologous mesophilic enzyme structural data. In particular, intersubunit ion-pair interactions have been found to be important structural requirements for thermostability in the case of citrate synthase from *P. furiosus* (Russell *et al.*, 1997). This enzyme also displays greater compactness and further inter-subunit interactions via amino acid residues near the C-terminus, all contributing to enhanced thermostability.

With the wealth of scientific information now available concerning the thermostability of enzymes in terms of both the available three-dimensional coordinates and thermodynamic studies of thermozymes, no consensus rule dictating enzyme thermostability has become apparent due to the varied and conflicting data collected. For example, the crystal structure of glutamate dehydrogenase from hyperthermophilic bacterium *Thermotoga maritima* (Knapp *et al.*, 1997) highlights increased numbers of hydrophobic interactions at the subunit interface instead of the inter-subunit ion-pair networks observed in the respective enzyme from *P. furiosus* (Danson and Hough, 1998). These data suggest that molecular mechanisms to enhance thermostability may differ between archaeal and bacterial thermozymes (Knapp *et al.*, 1997). Additionally, the structure of a thermostable β-glycosidase from

Sulfolobus solfataricus exhibits a solvent-filled hydrophilic cavity in its core. This observation is also inconsistent with the view that thermostability is accompanied by increased rigidity (Aguilar *et al.*, 1997). Overall, it appears that the thermostability of proteins isolated from thermophilic and hyperthermophilic origin arises from a combination of different physical factors, with each factor differing in its level of influence from one enzyme to the next, or between homologous enzymes of different organisms (Petsko, 2001). Modulation of the canonical physico-chemical principles that contribute to enzyme thermostability, including hydrogen-bonds, electrostatic/hydrophobic interactions, disulfide bonds, packing efficiency and reduced entropy of unfolding is necessary to achieve enzyme thermostability. A description of the major physical factors that contribute to protein thermostability is delivered in the proceeding section.

1.7.2. PROTEIN COMPOSITION AT THE AMINO ACID LEVEL

As more and more experimental data regarding proteins of thermophilic and hyperthermophilic origin becomes available, these data allow comparisons of amino acid composition relative to enzyme stability. Studies by Böhm and Jaenicke on the relevance of sequence statistics in describing the properties of hyperthemophilic proteins found only minor trends when comparing the genomic sequences of eight mesophilic and seven hyperthermophilic organisms (Böhm and Jaenicke, 1994). These minor sequence characteristics included, i) a +3.24 % increase in charged residue content in hyperthermophilic proteins compared to mesophilic proteins predominantly at the expense of uncharged polar residues (-4.98 %) including glutamine (-2.21 %). Slightly more hydrophobic and aromatic residues were present in the hyperthermophilic protein category (Table 1.1).

1.7.3. DISULFIDE BRIDGES

The presence of disulfide bridges in proteins are thought to have an entropically favourable effect in protein stability by decreasing the entropy of the proteins unfolded state (Matsumura *et al.*, 1989). Evidence in favour of this notion came later in the form of mutagenesis studies with subtilisin E that targeted residues Gly-61 and Ser-98 for cysteine substitution. The mutant enzyme had a melting temperature (T_m)

Residues	Amino acid composition (%) of:		Variation of composition in hyperthermophilic relative to mesophilic proteins
	Mesophilic proteins	Hyperthermophilic proteins	
A	8.09 ± 1.54	6.82 ± 1.42	- 1.27
C	1.10 ± 0.18	0.86 ± 0.27	- 0.24
D	5.06 ± 0.18	4.63 ± 0.54	- 0.43
E	6.45 ± 0.54	8.55 ± 0.95	+ 2.10
F	4.61 ± 0.78	4.40 ± 0.82	- 0.21
G	6.70 ± 0.96	7.16 ± 0.68	+ 0.46
H	2.04 ± 0.21	1.57 ± 0.16	- 0.47
I	7.40 ± 1.69	7.82 ± 1.64	+ 0.42
K	6.81 ± 2.00	7.61 ± 2.16	+ 0.80
L	10.43 ± 0.55	10.21 ± 0.68	- 0.22
M	2.42 ± 0.28	2.29 ± 0.25	- 0.13
N	4.90 ± 1.20	3.52 ± 0.94	- 1.38
P	3.77 ± 0.77	4.36 ± 0.99	+ 0.59
Q	3.99 ± 0.75	1.78 ± 0.22	- 2.21
R	4.33 ± 0.98	5.57 ± 1.16	+ 1.24
S	6.08 ± 0.57	5.54 ± 1.01	- 0.54
T	5.09 ± 0.57	4.34 ± 0.23	- 0.75
V	6.35 ± 0.75	8.05 ± 0.68	+ 1.70
W	1.02 ± 0.31	1.06 ± 0.20	+ 0.04
Y	3.30 ± 0.43	3.82 ± 0.33	+ 0.52
A, G	14.79	13.98	- 0.81
D, E	11.51	13.18	+ 1.67
K, R, H	13.18	14.75	+ 1.57
S, T	11.17	9.88	- 1.29
N, Q	8.99	5.3	- 3.69
I, L, M, V	26.60	28.37	+ 1.77
F, W, Y	8.93	9.28	+ 0.35

Table 1. 1. Table of the relative amino acid composition of mesophilic and hyperthermophilic proteins. Of the sequences studied, only minor trends were observed upon comparison of the genome sequences of eight mesophiles and seven hyperthermophiles. Hyperthermophilic proteins were shown to contain more charged residues at the expense of uncharged polar residues. Also, hyperthermophilic proteins contained slightly more hydrophobic and aromatic residues in comparison to the mesophilic proteins. The table is adapted from Vieille and Zeikus, 2001.

that was 4.5 °C higher in comparison to wild-type and a corresponding $t_{\frac{1}{2}}$ 2-3-fold longer than the wild-type enzyme (Takag *et al.*, 1990).

In conflict with the known susceptibility of cysteines and disulfides to destruction at high temperatures, the presence of disulfide bridges in enzymes that are optimally stable and active above 100 °C suggests that these disulfide bonds are protected by the conformational environment of the protein to reduce solvent accessibility. The $t_{\frac{1}{2}}$ of serine protease of *Aquifex pyrophilus* is six hours at 105 °C/pH 9.0 that is far longer than the $t_{\frac{1}{2}}$ calculated for disulfide bridges in unfolded proteins (one hour). These results therefore suggest that the disulfide bridges in the enzyme are protected in the protein environment through inaccessibility (Choi *et al.*, 1999).

1.7.4. HYDROPHOBIC INTERACTIONS

The hydrophobicity of a protein molecule is defined as the ratio of buried non-polar surface area relative to the total non-polar surface area of the protein. Hydrophobic interactions have also been found to be a key mechanism in thermostabilisation of proteins of thermophilc origin (Goodenough and Jenkins, 1991), with the calculation that each buried methyl group in a folded protein contributes to an increase in stability equating to 1.3 ± 0.5 kcal/mol^{-1} (Pace, 1992). Studies on the adenylate kinase of *M. jannaschii* have proposed that a larger and more hydrophobic enzyme core resulting from high aliphatic residue content and residue side chain volume is accountable for the thermostability properties of adenylate kinase from this methanogen.

1.7.5. AROMATIC INTERACTIONS

Like hydrogen-bonds, aromatic interactions are strongly distance-dependent and are as such defined by a distance of < 7.0 Å between phenyl ring centroids (Vieille and Zeikus, 2001). From a structural investigation of thirty-four high resolution X-ray crystal structures of mesophilic proteins, key traits regarding the stabilising effects of aromatic interactions were extracted. This analysis noted 272 aromatic pairs with the majority of these partaking in a network. Most of the aromatic pairs are involved in non-local interactions by linking secondary structural elements, with most interactions taking place between buried or partially buried residues (Burley and Petsko, 1985).

1.7.6. HYDROGEN BONDS

Hydrogen-bonds are an abundant intermolecular interaction in aqueous protein environments that occur both between neighbouring peptide domains and also with the surrounding aqueous solvent. H-bonds typically form within a H-donor-to-H-acceptor distance of within 3 Å accommodated by a donor-acceptor angle < 90° (Vieille and Zeikus, 2001). An internal intra-molecular H-bond buried within a protein macromolecule contributes a net stabilisation energy of ~ 0.6 kcal/mol^{-1}. A structural comparison of α-amylase from *Bacillus licheniformis* (BLA) and *Bacillus stearothermophilus* (BSTA) found that a major contributing factor towards the stability of BSTA relative to the more thermostable BLA was the nine fewer H-bonds within the structures of BSTA in comparison to the three-dimensional structure of BLA at a resulting thermodynamic cost of ~ 12 kcal/mol^{-1} in BSTA (Suvd *et al.*, 2001).

The number of charged-neutral H-bonds evident in the structure of *D*-glyceraldehyde-3-phosphate dehydrogenase (GAPDH) has been observed to correlate strongly with the enzymes thermostability (Tanner *et al.*, 1996). Reasoning for the thermodynamic stabilising contribution of H-bonds include, i) the lower desolvation penalty associated with burying a H-bond compared to burying an ion-pair interaction between two charged residues, and ii) the charge-dipole interaction in a charged-neutral H-bond results in a greater enthalpic reward in comparison to a neutral-neutral H-bond (Tanner *et al.*, 1996). The study of H-bond contributions to the thermostability of enzymes is largely dependent on the availability of high resolution structural data for hyperthermophilic proteins. Only sufficiently resolved three-dimensional structures will enable the distance-dependent H-bond interactions to be assigned and subsequent thermostability correlations drawn (Vieille and Zeikus, 2001).

1.7.7. ELECTROSTATIC INTERACTIONS

Electrostatic interactions are mainly of three force types: charge-charge, charge-dipole and dipole-dipole. As stated, the desolvation contribution [ΔΔG(desolvation)] to the free energy of folding as a result of the structural aspects of bringing oppositely

charged residue side chains together is unfavorable and large in comparison to the H-bond desolvation penalty. However, at higher solution temperatures, this $\Delta\Delta G$(desolvation) is lowered, partly as a result of the decrease in the water dielectric constant (Vieille and Zeikus, 2001). At these higher temperatures, the water molecules at the protein surface are less ordered, therefore allowing charged residues at the surface to rearrange in conformation to optimize side chain-side chain electrostatic interactions. This gain in interaction energy approximately compensates for the loss in salvation free energy (de Bakker *et al.*, 1999; Elcock, 1998).

Ion-pairs represent a major stabilising mechanism in hyperthermophilic proteins as illustrated by glutamate dehydrogenase (GDH) of *P. furiosus* that contains forty-five ion-pair interactions per subunit. 90 % of the arginine residues in GDH of *P. furiosus* form ion-pairs with networks of these interactions apparent between the individual subunits. The largest of these ion-pair networks in GDH consists of twenty-four residues on four different subunits forming eighteen ion-pairs. The formation of ion-pair networks makes energetic sense, since with each new pair in the ion-pair network, only one additional residue needs to be desolvated and immobilised, therefore the burial cost of a new ion-pair in a network is half in comparison to an individual ion-pair (Yip *et al.*, 1995).

1.7.8. INTERSUBUNIT INTERACTIONS AND HIGHER ORDER OLIGOMERISATION

Structural analyses of hyperthermophilic enzymes and mesophilic homologues has in many cases revealed a higher degree of subunit oligomerisation in hyperthermophilic proteins (Table 1.2). Subunit interactions logically play a key role in stabilising the hyperthermophilic proteins into higher oligomeric native structures, but no unique subunit interaction is singularly responsible for the observed stabilisation.

Glyceraldehyde-3-phosphate dehydrogenase (GAPDH) of *B. subtilis* has a $t_{\frac{1}{2}}$ of 19 minutes at 50 °C. The mutation Gly281Arg in GAPDH of *B. subtilis* that matches the sequence of the more stable GAPDH of thermophile *B. stearothermophilus* showed an increased $t_{\frac{1}{2}}$ of 198 minutes at 75 °C resulting from the formation of a stabilising intersubunit ion-pair (Mrabet *et al.*, 1992). Hydrophobic interactions at the subunit

Source	Enzyme	Number of subunits in:	
		Hyperthermophilic enzyme	Mesophilic enzyme
Pyrococcus woesei	PGK	2	1
Methanothermus fervidus	PGK	2	/
Pyrococcus furiosus	β-Glucosidase	4	1
Sulfolobus solfataricus	β-Glucosidase	4	/
Thermotoga maritima	β-Glucosidase	2	/
T. maritima	Anthranilate synthase	2	1
T. maritima	Dihydrofolate reductase	1 or 2	1
T. maritima	Phosphoribosyl-anthranilate isomerase	2	1
S. solfataricus	β-Glycosidase	4	2
Thermosphaera aggregans	β-Glycosidase	4	/
Methanopyrus kandleri	MkCH	3	2

Table 1. 2. Table showing the comparison of the number of subunits in hyperthermophilic proteins relative to mesophilic homologues. The increasing number of hyperthermophilic protein structures being solved has highlighted that subunit oligomerisation is a major structural strategy employed to enhance enzyme thermostability. The table is adapted from Vieille and Zeikus, 2001.

57

interface in 3-isopropyl dehydrogenase of *T. thermophilus* have been probed by site-directed mutagenesis studies and were found to be a central aspect in making the protein dimer more resistant to dissociation (Kirino *et al.*, 1994; Moriyama *et al.*, 1995). Monomeric variants of phosphoribosylanthranilate isomerase of *T. maritima* produced by site-directed mutagenesis have been shown to retain activity comparable to the dimeric wild-type enzyme form. However, the $t_{1/2}$ of the monomeric variants at a solution temperature of 85 °C was 3-5 minutes in comparison to 310 minutes for wild-type, therefore showing that the dimerisation of this enzyme is a major stabilizing factor (Thoma *et al.*, 2000).

1.7.9. HELIX STABILISATION

Put simply, α-helix stabilisation is achievable at the amino acid level by substituting resides that have a lower α-helical propensity, such as the β-branched residues (Val, Ile and Thr) with residues that harbour a high α-helical propensity. A comparative study of thirteen thermophilic proteins relative to mesophilic homologues highlighted that the only consistent disparity between the X-ray crystal structures of protein homologues was the significant lack of β-branched residues evident in the α-helices of the thermophilic protein category (Facchiano *et al.*, 1998).

Additional stabilisation of α-helices in protein structures occurs by stabilisation of the α-helix dipole through the presence of negatively charged residues at the α-helix N-terminal and positively charged residues at the α-helix C-terminal. The α-helix dipoles in pig phosphoglycerate kinase (PGK) are stabilised by nine N-terminal residues and twelve C-terminal residues, whereas the corresponding thermophilic PGK of *T. maritime* has seventeen N-terminal and fourteen C-terminal residues to stabilise the proteins α-helix dipoles (Auerbach *et al.*, 1997).

1.7.10. PACKING EFFICIENCY

The packing efficiency of a given protein is represented by its degree of compactness defined as the ratio of accessible surface area of the protein to the surface area of a sphere that has the same volume as the protein molecule (Li *et al.*, 2005). Strategies to achieve enhanced compactness include the shortening of loop regions, increasing

the amount of buried atoms as to shield a higher percentage of the macromolecule from solvent, conformational optimisation of side chain packing in the interior of the macromolecule and also, reduce or eliminate internal cavities (Russell *et al.*, 1997).

Thermodynamic stabilisation of proteins by greater packing efficiency has been experimentally demonstrated through mutant studies with histone proteins of the mesophile *M. formicicum* (HFoB) and hyperthermophile *M. fervidus* (HMfB). A solvent-accessible cavity in the histone protein of *M. formicicum* is partially filled in the corresponding *M. fervidus* protein by the bulky side chains of hydrophobic residues (Zhu *et al.*, 1998). The HFoB of *M. formicicum* gained an increase in melting temperature (T_m) of 11 and 14 °C as a consequence of mutations Ala31Ile and Lys35Met, respectively. Conversely, mutations Ile31Ala and Met35Lys in HMfB of *M. fervidus* decreased the proteins T_m by 4 and 17 °C, respectively (Li *et al.*, 1998).

In conflict with the proposal of increased compactness and reduced internal cavity volume as a structural strategy towards enhanced molecular stability, mutant studies with isopropylmalate dehydrogenase of *T. thermophilus* showed that a mutation creating an internal cavity of 32 Å^3 in volume had no detrimental effect on the enzymes thermostability (Wallon *et al.*, 1997).

1.8. THESIS AIMS

From the outset, the research documented in this thesis was primarily aimed at the structural and biophysical characterization of a novel flavoprotein amine oxidoreductase system from *Pyrococcus furiosus* DSM 3638 with the intention of advancing current knowledge of the mechanism of flavoprotein-catalysed amine oxidation (Scrutton, 2004). The recombinant enzyme cloned from *P. furiosus* genomic DNA was purified to homogeneity and found to be a flavoprotein L-proline dehydrogenase with activity also displayed towards other secondary amine compounds sarcosine and L-pipecolic acid. Through a combination of both kinetic/redox potentiometric studies with wild-type and mutant forms of the enzyme and the timely elucidation of the three-dimensional X-ray crystal structure of the enzyme by the method of molecular replacement, a polar nucleophilic mechanism of L-proline substrate oxidation has been proposed for this enzyme analogous to the

mechanism previously proposed for MAO (Kim *et al.*, 1993) and advanced for MAO-A (Miller and Edmondson, 1999). In addition to the mechanistic advances made during the research, fundamental questions regarding amine metabolism by *P. furiosus* have been raised. The new PRODH cloned from this hyperthermophile is not a 'classical' L-proline oxidase like the multifunctional PutA protein found in enteric bacteria that possess both PRODH and P5CDH activity in addition to DNA-binding ability for autogeneous transcriptional regulation (Wood, 1981; Menzel and Roth, 1981; Brown and Wood, 1992; Vilchez *et al.*, 2000). This work also demonstrates the structural diversity amongst L-proline dehydrogenase/oxidase enzymes. Identification of a second PRODH system in *P. furiosus* also necessitates future work in delineating the role of the two types of L-proline dehydrogenase.

Chapter three documents the initial cloning of two ORFs from the genome of *P. furiosus* and the subsequent recombinant expression and purification of this new protein. The UV-visible Spectrum of the purified protein indicated the presence of flavin cofactor(s) that was later identified as non-covalently bound FAD in the mono-flavinylated form of the enzyme. Systematic compound screening under anaerobic conditions identified this hypothetical amine oxidoreductase as an L-proline dehydrogenase with steady-state kinetic experiments highlighting activity not only for the physiological substrate, but also for the secondary amines sarcosine and L-pipecolic acid.

Chapter four further documents the more detailed characterisation of wild-type PRODH by a combination of kinetic and redox thermodynamic investigations. Identification of the product of PRODH-catalysed oxidation of L-proline by MALDI-ToF and electrospray mass spectrometry is also described.

Chapter five combines both a structural description of PRODH by the elucidation of the X-ray crystal structure and solution studies of three active site mutants H225A, H225Q and Y251F. The data presented in this final results chapter culminates in a mechanistic proposal for the PRODH-catalysed oxidation of substrate L-proline.

CHAPTER TWO

MATERIALS AND METHODS

CHAPTER TWO

MATERIALS AND METHODS

2.1.   MATERIALS

2.1.1.   CHEMICALS AND REAGENTS

The chemicals listed were all of Analar purity (analytical grade) or equivalent apart from the glacial acetic acid and methanol used for staining of SDS-PAGE gels that were classified as laboratory grade reagents. Bovine serum albumen (BSA), N,N,N',N'-tetramethylethylenediamine (TEMED), 2-mercaptoethanol, ampicillin (D[-]-α-aminobenzyl penicillin; sodium salt), dithiothreitol, chloramphenicol, ethidium bromide (tablets), Tris-acetate, EDTA (TAE), bromophenol blue, sodium n-dodecyl sulfate (SDS), Coumassie Brilliant Blue R-250, mineral oil, sarcosine, dimethylglycine, glycine betaine, L-proline, D-proline, L-pipecolic acid, flavin mononucleotide (FMN), flavin adenine dinucleotide (FAD), adenosine triphosphate (ATP), adenosine diphosphate (ADP), adenosine monophosphate (AMP), β-nicotinamide adenine dinucleotide (phosphate) [β-NAD(P)$^+$], β-nicotinamide adenine dinucleotide (phosphate) reduced form; disodium salt [β-NAD(P)H], 2, 6-dichlorophenol indophenol; sodium salt (DCPIP), 1, 1'-dibenzyl-4, 4'-bipyridinium dichloride (benzyl viologen), 1, 1'-dimethyl-4, 4'-bipyridinium dichloride (methyl viologen), 2-hydroxy-1, 4-napthaquinone, phenazine methosulfate (PMS), diethanolamine, 2-(N-morpholino)ethanesulfonic acid (MES), 3-{[tris(hydroxymethyl)-methyl]amino}-2-hydroxypropane sulfonic acid (TAPSO), (3-[N-morpholino]propanesulfonic acid (MOPS), potassium ferricyanide ($K_3Fe(CN)_6$), sodium fumarate; dibasic ($NaOOCCH=CHCOONa$), sodium sulfite (Na_2SO_3) and pH reference standards (pH 4.0 ± 0.1, 7.0 ± 0.1 and 10.0 ± 0.1) were purchased from Sigma. Glycine, acetic acid, sodium chloride (NaCl), EDTA, hydrochloric acid (HCl), sodium hydroxide (NaOH), potassium chloride (KCl), potassium di-hydrogen orthophosphate anhydrous (KH_2PO_4), di-potassium hydrogen orthophosphate anhydrous (K_2HPO_4), magnesium

sulfate ($MgSO_4$), magnesium chloride ($MgCl_2$), phosphoric acid (H_3PO_4), glycerol, agarose, low-melting point agarose, butan-1-ol, methanol and ethanol were purchased from Fisher Chemicals. Deuterium oxide (D_2O) was purchased from Goss Scientific Instruments Ltd. Sodium hydrosulfite (sodium dithionite) was purchased from FSA Laboratory Supplies. Complete protease inhibitor cocktail tablets were purchased from Roche Diagnostics. 2-amino-2-(hydroxymethyl)-1,3-propanediol (Tris-Base) and isopropyl β-D-thiogalactopyranoside (IPTG) were purchased from Melford Laboratories. Bacto-yeast extract, bacto-tryptone and bacteriological agar for biological media were purchased from Oxoid. Bradford reagent and ammonium persulfate (APS) were purchased from Bio-rad. 30 % (w/v) acrylamide, 0.8 % (w/v) bis-acrylamide (Protogel) was purchased from National Diagnostics. Clear Strategy Screening kits I (MD 1-14) and II (MD 1-15) were purchased from Molecular Dimensions Ltd. Ferricenium hexafluorophosphate was synthesized as described (Lehman *et al.*, 1990), Oxygen-free nitrogen and Pureshield brand argon were purchased from the British Oxygen Company (BOC).

Water used for laboratory experimentation was distilled and deionised (ddH_2O) with an Elgastat Option 2 water purifying system. For molecular biology work this ddH_2O was further clarified by filtration through a sterile 0.22 μm Millex-GP Acrodisc filter purchased from Millipore.

2.1.2. MEDIA

For the preparation of glycerol stocks and the mini preparation of construct DNA for sequencing and storage, strains were grown in Luria-Bertani (LB) broth consisting of 10 g (1 % w/v) bacto-tryptone, 5 g (0.5 % w/v) bacto-yeast extract and 10 g (170 mM) NaCl dissolved in one litre of ddH_2O and adjusted to pH 7.5. For expression of recombinant protein, strains were grown in 2x Yeast Extract Tryptone (2xYT) media consisting of 16 g (1.6 % w/v) bacto-tryptone, 10 g (1 % w/v) bacto-yeast extract and 5 g (85 mM) NaCl dissolved in one litre of ddH_2O and adjusted to pH 7.5. Ampicillin was added to a final concentration of 50 μg/ml for selection of the pPRODH1, pPRODH2, pP2HA, pP2HQ

and pP2YF constructs. Chloramphenicol was added to a final concentration of 34 μg/ml for selection of the tRNA encoding pLysSRARE plasmid during the growth of Rosetta(DE3)pLysS cells. Prior to antibiotic supplementation, all media were autoclaved at 126 °C for 20 minutes at a pressure of 15 lb/sq. in. using a Denely autoclave. All antibiotics were filtered through a sterile 0.22 μm Millex-GP Acrodisc filter prior to use. For bacterial outgrowth during transformation procedures, SOC media was used. SOB media consisting of 20 g bacto-tryptone, 5 g bacto-yeast extract and 0.5 g NaCl dissolved in 990 ml of ddH$_2$O and supplemented with 10 ml of 250 mM KCl was prepared and autoclaved. 10 ml of a 2 M solution of MgCl$_2$:MgSO$_4$ (1 M each) was sterilised by filtration through a sterile 0.22 μm Millex-GP Acrodisc and added to one litre of autoclaved media to make SOB. 10 ml of a 2 M solution of glucose sterilised by filtration through a sterile 0.22 μm Millex-GP Acrodisc was then added to the SOB media prior to use to make SOC media.

2.1.3. BACTERIAL STRAINS AND GENOTYPES

Escherichia coli (*E. coli*) strain BL21(DE3), is a general purpose expression host with genotype: F$^-$ *ompT hsdS$_B$(r_B^- m_B^-) gal dcm* (DE3). *E. coli* strain BL21(DE3)pLysS is a high stringency expression host with genotype: F$^-$ *ompT hsdS$_B$(r_B^- m_B^-) gal dcm* (DE3) pLysS (Cm^R). The pLysS plasmid confers resistance to the antibiotic chloramphenicol. *E. coli* strain Rosetta(DE3)pLysS is a high stringency expression host used for the expression of genes containing rare *E. coli* codons. The genotype of this strain is: F$^-$ *ompT hsdS$_B$(r_B^- m_B^-) gal dcm lac* Y1 (DE3) pLysSRARE (Cm^R). The pLysSRARE plasmid confers resistance to the antibiotic chloramphenicol. The plasmid also carries genes encoding tRNAs that translate codons rare in *E. coli*, therefore allowing recombinant expression of archaeal and eukaryotic genes containing these rare codons in the Rosetta host strain. *E. coli* strain B834(DE3) is a methionine auxotroph and the parental strain of BL21. This strain is useful for the selenomethionine labelling of protein for crystallography (Leahy, 1992; Wood, 1966). The genotype of this strain is: F$^-$ *ompT hsdS$_B$(r_B^- m_B^-)gal dcm met* (DE3). *E. coli* strain Novablue is a host strain designed for initial transformation post ligation due to its high transformation efficiency. The

genotype of this strain is: *end*A1 *hsd*R17 ($r_{K12}^-m_{K12}^+$) *sup*E44 *thi*-1 *rec*A1 *gyr*A96 *rel*A1 *lac*F'[*pro*A⁺B⁺ *lac*I�q ZΔM15::Tn*10* (Tc^R)]. These five *E. coli* strains were purchased from Novagen in competent 'singles' form. *E. coli* strain XL1-blue is a host strain designed for optimal propagation of plasmid DNA with genotype: *rec*A1 *end*A1 *gyr*A96 *thi*-1 *hsd*R17 *sup*E44 *rel*A1 *lac* [F'*pro*AB *lac*Iq ZΔM15 Tn*10* (Tet^r)]. This *E. coli* strain was purchased in supercompetent form from Stratagene.

Glycerol stocks were made by the addition of 250 µl of 50 % (v/v) autoclaved glycerol to 500 µl of late exponential phase culture (glycerol at 16.7 % final concentration) in a 1.5 ml sterile cryovial followed by mixing the solution by inversion and flash freezing in liquid nitrogen. Glycerol stocks were stored at -80 °C.

2.1.4. MOLECULAR WEIGHT MARKERS FOR ELECTROPHORESIS

The GeneRuler 1 Kb DNA size maker ladder was used for analytical agarose gel electrophoresis of DNA, purchased from Fermentas. The DNA ladder consisted of linear DNA of sizes 10.0 Kb, 8.0 Kb, 6.0 Kb, 5.0 Kb, 4.0 Kb, 3.5 Kb, 3.0 Kb, 2.5 Kb, 2.0 Kb, 1.5 Kb, 1.0 Kb, 750 bp, 500 bp and 250 bp. A low molecular weight calibration kit was used for SDS-PAGE analysis of proteins, purchased from Amersham Pharmacia Biotech. The protein marker consisted of proteins with molecular weights of 97.0 KDa, 66.0 KDa, 45.0 KDa, 36.0 KDa, 20.1 KDa and 14.4 KDa.

2.1.5. COMPONENTS FOR MOLECULAR BIOLOGY

pET11d expression vector was purchased from Novagen. Oligonucleotides were synthesised on an ABI 394 synthesiser equipped with trityl monitoring. Oligonucleotides used during the course of the research described in this thesis were synthesised at the Protein and Nucleic Acid Chemistry Laboratory (PNACL), University of Leicester, UK. dNTP stock solutions were purchased from Qiagen. *P. furiosus* genomic DNA was from the American Type Culture Collection (ATCC 43587).

2.1.6.   DNA PURIFICATION SYSTEMS

PCR amplification products were gel purified from low melting point agarose (1 % w/v gel) using a PCR purification kit purchased from Promega. Plasmid purification was carried out using a Wizard *Plus* Minipreps DNA Purification System purchased from Promega. For the purpose of DNA sequencing, plasmid DNA was purified using a QIAprep Spin Miniprep Kit purchased from Qiagen.

2.1.7.   DNA AND PROTEIN MODIFYING ENZYMES

The enzymes *Xba* I, *Bam* HI, *Dpn* I, *Hind* III, calf intestinal alkaline phosphatase (CIAP) and T4 DNA ligase were all purchased from New England Biolabs. Restriction digests were performed as recommended by the supplier using the specific buffer solutions supplied with each restriction enzyme. The DNA-dependent DNA polymerase enzymes *Taq* polymerase, *TaqPlus* precision PCR polymerase and *Pfu Turbo* polymerase used for PCR cloning methodologies were purchased from Stratagene. KOD DNA polymerase used for site-directed mutagenesis was purchased from Novagen. Lysozyme and deoxyribonuclease I (DNase I) were purchased from Sigma.

2.1.8.   LABORATORY EQUIPMENT

Pipettes (Gilson Pipetman) of 1 μl, 20 μl, 200 μl, 1000 μl and 5 ml capacities were purchased from Gilson. Vortex-2 Genie vortex mixer was purchased from Scientific Industries. Hot plate/magnetic stirrer model HB 501 was purchased from Bibby. pH meter model 410 equipped with protein-resisting micro pH electrode was purchased from Thermo Orion. Microfuge model micro centaur was purchased from Sanyo MSE. SDS-PAGE hardware and the Econo-Pac 10 DG gel filtration columns were purchased from Bio-rad. Orbital incubators were purchased from New Brunswick Scientific. Petri dish incubator was purchased from LEEC. Sonicator model Soniprep 150 was purchased from MSE. French pressure cell was purchased from the American instrument company. Centrifuge model Avanti J-20 XP was purchased from Beckman. Centrifuge model RC-

genomic template DNA, 0.5 µM final concentration of each primer and the reaction mixture brought to a final reaction volume of 49 µl with PCR grade deionised water. 1 µl (5U) of *TaqPlus* Precision Polymerase was then added to the mixture immediately prior to PCR cycling and the solution gently mixed before being covered with 30 µl of mineral oil to prevent evaporation. Thermal cycling parameters started with an initial DNA denaturation phase at 94 °C for 5 minutes followed by a 45 second denaturation step at 94 °C, an annealing step at 58 °C for 1 minute 30 seconds and an elongation step at 72 °C for 2 minutes 45 seconds, this three step program being repeated for 35 cycles of exponential amplification followed by a 10 minute final elongation phase at 72 °C. Reactions were performed in sterile 0.5 ml Eppendorf tubes.

Name	Sequence (5' – 3')	Size (nt)	T_m (°C)	GC (%)
UP-SSOX	GTG AGA AAC TTG AGG CCA CTA GAC TTA ACG G	31-mer	63.0	48.4
DOWN-SSOX	TCA ACC CAT TTG AAG AGC AAC AGT TCT TAA TTC TCC C	37-mer	63.3	40.5

Table 2. 1. Primers used to PCR amplify target DNA from *Pyrococcus furiosus* genomic DNA. The table gives the names of the primers used to isolate and amplify the two ORF's (gi_18977617 and gi_18977618) with sarcosine oxidase homology and the primer sequences in the 5'-3' direction. The length of the primers, the melting temperature (T_m) and the GC content is also shown.

PCR reaction products were electrophoresed and gel purified from low melting point agarose gels (1%) and a purified sample run on a second 1% agarose gel to estimate the DNA yield (ng/µl). This DNA was then used as a template for a second PCR reaction using a new set of primers designed to engineer flanking restriction sites (5' *Xba* I site and a 3' *Bam* HI site) for directional cloning and also a 5' ribosome-binding site (RBS) to allow expression of the cloned ORF's (Table 2.2). This strategy of engineering an RBS 5' on the PCR product was decided because direct cloning into an *Nde* I site was hindered by an internal *Nde* I site in the target DNA sequence. PCR reaction parameters were

identical to the initial PCR protocol with the only modifications being 1) 10 ng of PCR product from the initial PCR reaction was used as template and 2) the new primers required an annealing temperature of 49 °C for a 30 second duration.

Name	Sequence (5' - 3')	Size (nt)	T_m (°C)	GC (%)
Forward-SSOX	GGG GGG TCT AGA **AAG GAG** ATA AAG AG**A TG**A GAA ACT TGA G	40-mer	54.0	45.0
Reverse-SSOX	GGG GGG GGA TCC TCA ACC CAT TTG AAG AGC A	31-mer	54.0	58.0

Table 2. 2. Primers designed to engineer flanking restriction sites (5' *Xba* I and 3' *Bam* HI) for directional cloning and a 5' ribosome-binding site (RBS) for recombinant expression of the cloned DNA. The table gives the names of the primers and the sequence in the 5'-3' direction. The length of the primers, the melting temperature (T_m) and the GC content is also shown. In primer 'Forward-SSOX', the engineered RBS is shown in bold and underlined proximal to the initiation codon of ORF1 that is shown in bold and double-underlined.

Six PCR reactions were performed and the products pooled and gel purified to remove contaminants. Purified DNA was run on a 1 % agarose gel to estimate DNA yield. Approximately 6 μg of target DNA was then prepared for the ligation reaction by performing a double restriction digest with the Type II restriction endonucleases *Xba* I and *Bam* HI using the protocol recommended by the supplier (New England Biolabs). After incubation, the whole reaction was run on a 1 % low melting temperature agarose gel and purified, the pure DNA being eluted in 30 μl of nuclease-free water to give a DNA concentration of approximately 50 ng/μl. This prepared insert DNA was then stored at -20 °C until the ligation procedure.

2.2.3. CLONING

The vector chosen for cloning of the target DNA insert was pET11d. This vector contains unique restriction sites for both *Xba* I (downstream of the T7 promotor and *lac* operator sequences) and *Bam* HI. A double restriction digest reaction was performed on 2 µg of pET11d DNA using identical reaction conditions to those employed for restriction of the insert DNA. After restriction, 1 U of calf intestinal alkaline phosphatase (CIAP) was added to the restriction mixture and the reaction incubated for a further 1 hour at 37 °C to dephosphorylate the 5' ends of the restricted vector to inhibit self-ligation, therefore reducing background non-recombinant colonies post-ligation. Vector DNA was gel purified and pure DNA eluted into 20 µl of nuclease-free water giving a DNA concentration of approximately 50 ng/µl. 1 µl of prepared vector and insert DNA were each run on a 1 % agarose gel to verify concentration. A ligation reaction was then formulated using a 1 : 6.67 molar ratio of vector : insert DNA. The ligation mixture consisted of 10x T4 DNA ligase buffer, 109 ng (0.03 pmol) of restricted pET11d DNA, 344 ng (0.2 pmol) of restricted target DNA, 0.4 Weiss units of T4 DNA ligase and the reaction mixture brought to 20 µl final volume with filter sterilized molecular biology grade deionised water. The reaction mixture was incubated overnight at 16 °C in a water bath. A vector only ligation mixture was formulated as a negative control to give an estimation of the level of non-recombinant transformant background.

2.2.4. TRANSFORMATION OF COMPETENT CELLS

A 50 µl aliquot of chemically competent cells was thawed on ice (Novablue, BL21(DE3), BL21(DE3)pLysS, Rosetta(DE3)pLysS, B834(DE3), B834(DE3)pLysS) for 5 minutes then 1 µl of DNA was added and the cells gently swirled. Cells were incubated on ice for 5 minutes then heat-shocked for exactly 30 seconds at 42 °C in a water bath followed by immediate incubation on ice for a further 2 minutes. 250 µl of room temperature SOC medium was then added to the cells and 50 µl of the resulting suspension was plated directly onto a selective LB agar plate. Non-Novablue host cell strains required a 1 hour outgrowth period at 37 °C/220 rpm in an orbital incubator. The plate was allowed to

stand on the bench for 15 minutes then was incubated inverted overnight at 37 °C. The pET11d vector carries a gene that encodes for β-lactamase that confers ampicillin resistance on the host cell, therefore allowing for selection of recombinants when transformed cells are grown in media containing ampicillin. pLysS and pLysSRARE plasmids carry a gene that confers chloramphenicol resistance (Cm^R) on the host cell through expression of a chloramphenicol acetyltransferase. Selection of host cells harbouring these plasmids is therefore achieved by growth in media supplemented with chloramphenicol.

Transformation of supercompetent XL1-Blue cells was performed by thawing 100 μl of supercompetent cells on ice in a 1.5 ml Eppendorf tube then adding 1.7 μl of 2-mercaptoethanol to the cells and incubating on ice for 10 minutes with stirring every 2 minutes. 1 μl of a 50-fold dilution of purified plasmid DNA (~1 ng/μl) was then added to the cells and the mixture gently swirled followed by incubation on ice for a further 30 minutes. Cells were heat-shocked in a water bath at 42 °C for precisely 45 seconds followed by immediate incubation on ice for 2 minutes. 900 μl of SOC media preheated to 42 °C was then added to the cells and the cell mixture incubated for a 1 hour outgrowth period at 37 °C/220 rpm in an orbital incubator. 200 μl of the resulting culture was plated directly onto an ampicillin (50 μg/ml) selective LB agar plate and allowed to stand on the bench for 15 minutes before being incubated inverted overnight at 37 °C.

2.2.5.   MINIPREPARATION AND RESTRICTION DIGEST ANALYSIS

Colonies were picked from the selective plate and streaked onto fresh selective LB agar plates and incubated overnight inverted at 37 °C. 5 ml of 2xYT media containing ampicillin (50 μg/ml) in a 25 ml sterilin tube was then inoculated with one fresh colony from each streak plate and incubated overnight at 37 °C/220 rpm in an orbital incubator. Plasmid minipreparation was performed on each culture and positive clones identified by restriction digest analysis. Small-scale plasmid purification was performed using the Wizard *Plus* Minipreps DNA Purification System according to the manufacturer's protocol. 5 ml of stationary-phase culture was centrifuged in a lab-top microfuge for 10

minutes at 13,000 rpm and the supernatant decanted. Cell pellet was resuspended in 300 μl of cell resuspension solution (50 mM Tris-HCl pH 7.5, 10 mM EDTA and 100 μg/ml RNase). 300 μl of cell lysis solution (1 % (w/v) SDS in 0.2 M NaOH) was added to the resuspension followed by continuous inversion until the solution became clear. 300 μl of neutralisation solution (1.32 M potassium acetate, pH 4.8) was added and the lysate immediately inverted five times to prevent localised precipitation. The lysate was centrifuged at 13,000 rpm for 10 minutes in a microfuge and the supernatant loaded onto a Wizard minicolumn prepared by attaching a 3 ml disposable syringe barrel (without plunger) to the Luer-Lok extension of the minicolumn. 1 ml of resuspended resin was then loaded into the barrel. Supernatant was then loaded onto the resin and a vacuum applied to draw solution through the minicolumn. 2 ml of column wash solution (95 % ethanol) was loaded into the barrel and the solution drawn through the minicolumn by vacuum. The vacuum was continued for an additional 30 seconds to dry the minicolumn resin. The minicolumn was then transferred to a fresh 1.5 ml Eppendorf tube and centrifuged at 13,000 rpm for 2 minutes to remove residual column wash solution. The minicolumn was then transferred to a fresh 1.5 ml Eppendorf tube and 50 μl of nuclease-free water (preheated to 65 °C) was added to the minicolumn in the centre of the resin. After incubation for 1 minute at room temperature the minicolumn-tube apparatus was centrifuged at 13,000 rpm for 1 minute to elute plasmid DNA. Purified plasmid DNA was stored at -20 °C.

Restriction digest analysis using the Type II restriction endonucleases *Bam* HI and *Xba* I in a double digest reaction was performed on 5 μl of each plasmid DNA minipreparation and digested DNA analysed on a 1 % agarose gel (Section 2.2.1) to visualise the two bands of DNA with the molecular weight of the insert and vector estimated from comparison with a 1 Kb DNA ladder. Positive clones were further analysed by a second restriction digest performed to verify the orientation of the insert DNA. This digest reaction employed *Hind* III that cuts once in the vector DNA sequence and once in the insert DNA sequence therefore giving a unique and predictable two band pattern to deduce the orientation of the ligated insert DNA. The new construct harbouring the *Pyrococcal* cloned DNA was designated pPRODH1.

2.2.6. DNA SEQUENCING

XL1-Blue competent cells were transformed with 1 µl of pPRODH1 as previously described (Section 2.2.4). A stab culture was then prepared from a single colony in a sterile 1.5 ml cryovial containing 1 ml of selective LB agar (ampicillin 50 µg/ml) and the stab culture incubated overnight at 37 °C. The stab culture was then sealed and encased in foil and sent along with sequencing primers (Table 2.3) to the DNA sequencing company, GRI-Genomics, Surrey, UK, for automated DNA sequencing. MJ BaseStation automated sequencers were employed utilising BigDye sequencing chemistry.

2.2.7. SITE-DIRECTED MUTAGENESIS

To eradicate a putative internal RBS in ORF1 of pPRODH1, site-directed mutagenesis was employed. Sense and antisense primers were designed (Table 2.4) to incorporate a silent mutation in the region of the gene-internal RBS to diminish the sequence affinity of this site with the 16S rRNA of translating ribosomes without altering the native amino acid sequence of the recombinant enzyme. The QuikChange mutagenesis kit was used following the protocol recommended by the supplier (Stratagene). DNA-dependent DNA polymerase used for PCR cycling was KOD DNA polymerase (Novagen). The pPRODH1 plasmid was used as template DNA during the PCR reaction. The PCR reaction mixture was formulated on ice in a 0.5 ml sterile Eppendorf tube and comprised of 10x KOD polymerase buffer (1.2 M Tris-HCl, 100 mM KCl, 60 mM $(NH_4)_2SO_4$, 1 % Triton X-100, 0.01 % BSA, pH 8.0), 200 µM final concentration of each dNTP, 20 pmol each of both the forward primer 'Mut1' and reverse primer 'Mut2', 10 ng of pPRODH1 template DNA, $MgCl_2$ to 1 mM final concentration and PCR grade ddH_2O (filtered through a 0.22 µm sterile Millex-GP Acrodisc) to bring the final reaction volume to 49.6 µl. The reaction solution was gently mixed and briefly pulse centrifuged before being returned to ice. 0.4 µl of KOD DNA polymerase (1 U) was then added to the mixture immediately prior to PCR cycling and the solution gently mixed before being covered

Name	Sequence (5' - 3') and position (bp)	Size (nt)	T_m (°C)	GC (%)
T7 prom	TAA TAC GAC TCA CTA TAG GG*	20-mer	56.0	40.0
FORp11SS	GAC TCA CTA TAG GGG AAT TGT GAG CGG*	27-mer	61.1	52.0
F2	+ 205 GGA GTA AAG GGT GTC GAT GC + 224	20-mer	53.7	55.0
F2.1	+ 732 GGA AGT AGC TCC AGG TTG G +750	19-mer	53.1	57.9
F3	+ 1042 GCA GGC AGT GCA GTG ACG ATA AA +1064	23-mer	56.9	52.2
F3.1	+ 1472 GGA GGT GAG AGG GAT GAT TCC + 1492	21-mer	56.2	57.1
F4	+ 1566 GGA ACG GGA ATT AGA CAG CA + 1585	20-mer	51.7	50.0
F4.1	+ 1898 GGC AAA GGA GTA TGG TGC + 1915	18-mer	50.2	55.6
F4.2	+ 2191 CGC ATG GAG GGA TTA TAG G + 2209	19-mer	51.0	52.6
F5	+ 2331 ACC TGG GCA GGT TAT TAC GC + 2350	20-mer	53.7	55.0

Table 2. 3. Table of the primers used for sequencing the cloned region of the pPRODH1 construct. The table gives the name and position of each individual primer and the sequence of each primer in the 5'-3' direction. The length of the primers, the melting temperature (T_m) and the GC content is also shown. * Primers T7 prom and FORp11SS are upstream of the insert DNA sequence.

Name	Sequence (5' – 3') and position (bp)	Size (nt)	T_m (°C)	GC (%)
Mut1	+ 214 GGT GTC GAT GCT AGG AAA ACA AA**A** GTT AAA GAT GGA ATG AAA GTA C + 259	46-mer	65.4	37.0
Mut2	- 259 GTA CTT TCA TTC CAT CTT TAA C**T**T TTG TTT TCC TAG CAT CGA CAC C - 214	46-mer	65.4	37.0

Table 2. 4. Primers designed for site-directed mutagenesis of pPRODH1 ORF1 to eradicate a gene-internal RBS. The table gives the name and position of each primer and the sequence of each primer in the 5'-3' direction. The length of the primers, the melting temperature (T_m) and the GC content is also shown. Letters shown in bold and underlined indicate the mismatch with the template DNA.

with 30 μl of mineral oil. Thermal cycling parameters for the PCR program were as follows: initial denaturation at 94 °C for 1 minute followed by 12 cycles of 94 °C/30 seconds (denaturation), 60 °C/30 seconds (annealing, T_m – 5.4 °C) and 72 °C/78 seconds (elongation) followed by a final elongation step at 72 °C for 10 minutes. Following the PCR reaction, 20 μl of the PCR product was placed into a fresh sterile 0.5 ml Eppendorf tube. 1 μl of the restriction endonuclease _Dpn_ I was then added to this aliquot and the solution gently mixed followed by incubation at 37 °C for 2 hours to digest _Dam_ methylated template DNA. Chemically competent XL1-Blue cells were then transformed as previously described (Section 2.2.4) with 1 μl of the restriction reaction, plated and incubated inverted overnight on selective LB agar (ampicillin 50 μg/ml) at 37 °C. As a control experiment for _Dpn_ I activity, XL1-Blue cells were also transformed with 1 μl of un-restricted PCR product (if _Dpn_ I is active, there should be a significantly larger number of colonies on the control plate). Colonies were picked from the plate and fresh streak plates were made and incubated inverted overnight at 37 °C. 10 ml of 2xYT autoclaved media supplemented with 50 μg/ml ampicillin for selection of recombinants was inoculated for each streak colony and incubated in 50 ml sterile falcon tubes overnight at 37 °C/220 rpm. 5 ml of each culture was centrifuged at 7,000 rpm for 15

minutes in a bench top centrifuge and the pellets sent for Level 1 sequencing to the PNACL along with the sequencing primer (Table 2.5) designed to sequence the region targeted for mutagenesis.

Name	Sequence (5' – 3') and position (bp)	Size (nt)	T_m (°C)	GC (%)
Seq1	+ 169 GCA TTT ACC TTT GGT CCA GTC C + 190	22-mer	54.7	50.0

Table 2. 5. Primer designed for the sequencing of the region targeted for site-directed mutagenesis. The table gives the name and position of the primer and the sequence in the 5'-3' direction. The length of the primer, the melting temperature (T_m) and the GC content is also shown.

Once successful mutagenesis was verified, sequencing of the entire insert was repeated to ensure spurious changes had not occurred during the mutagenesis reaction. Plasmid construct DNA was stored at -20 °C. The new construct with the silent mutation was designated pPRODH2.

The H225A, H225Q and Y251F mutant forms were also isolated using the QuikChange mutagenesis kit following the protocol recommended by the supplier (Stratagene). The pPRODH2 construct was used as template in PCR reactions using the primers detailed in Table 2.6. Each PCR reaction mixture was formulated on ice in 0.5 ml sterile Eppendorf tubes and comprised of 10x KOD polymerase buffer, 200 μM final concentration of each dNTP, 20 pmol of each relevant primer, 10 ng of pPRODH2 template DNA, $MgCl_2$ to 1 mM final concentration and PCR grade ddH_2O (filtered through a 0.22 μm sterile Millex-GP Acrodisc) to bring the final reaction volume to 49.6 μl. The reaction solution was gently mixed and briefly pulse centrifuged before being returned to ice. 0.4 μl of KOD DNA polymerase (1 U) was then added to the mixture immediately prior to PCR cycling and the solution gently mixed before being covered with 30 μl of mineral oil. Thermal

Name	Mutation	Sequence (5' – 3') and position (bp)	Size (nt)	T_m (°C)	GC (%)
H225Afor	H225A	+ 2079 CCA ATT GAG CCC TAC AAG **GC**T CAA GCA GTG ATA ACC +2114	36-mer	66.7	50.0
H225Arev	H225A	- 2114 GGT TAT CAC TGC TTG A**GC** CTT GTA GGG CTC AAT TGG – 2079	36-mer	66.7	50.0
H225Qfor	H225Q	+ 2079 CCA ATT GAG CCC TAC AAG CA**G** CAA GCA GTG ATA ACC + 2114	36-mer	66.7	50.0
H225Qrev	H225Q	- 2114 GGT TAT CAC TGC TTG **C**TG CTT GTA GGG CTC AAT TGG – 2079	36-mer	66.7	50.0
Y251Ffor	Y251F	+ 2159 CAA GTA TGG TCA CGC TT**T** TTT AAC ACA AAC TGC GC +2193	35-mer	63.2	42.9
Y251Frev	Y251F	- 2193 GCG CAG TTT GTG TTA AA**A** AAG CGT GAC CAT ACT TG – 2159	35-mer	63.2	42.9

Table 2. 6. Primers designed for site-directed mutagenesis of construct pPRODH2. Table shows the primers used for the production of PRODH mutants H225A (pP2HA), H225Q (pP2HQ) and Y251F (pP2YF). The name and position of each primer, the sequence of each primer in the 5'-3' direction, the length of each primer, the melting temperature (T_m) and the GC content of each primer is shown. Letters shown in bold and underlined indicate the mismatch with the template DNA.

cycling parameters for the generation of H225A and H225Q mutant constructs were as follows: initial denaturation at 94 °C for 1 minute followed by 12 cycles of 94 °C/30 seconds (denaturation), 61 °C/30 seconds (annealing, T_m – 5.7 °C) and 72 °C/78 seconds (elongation) followed by a final elongation step at 72 °C for 10 minutes. Thermal cycling parameters for the generation of the Y251F mutant construct were identical to those employed for the generation of the His-225 substituted mutants with the exception of an annealing temperature of 58 °C/30 seconds (T_m – 5.2 °C). PCR products were digested with *Dpn* I and XL1-Blue chemically competent cells were transformed with 1 μl of each reaction product as previously described (Section 2.2.4). Pellets of XL1-Blue cells containing the putative mutant constructs were sent for Level 1 DNA sequencing to the PNACL using the sequencing primer F4.1 (Table 2.3). Once successful mutagenesis was verified, sequencing of the entire insert for each mutant construct was performed to ensure spurious changes had not occurred during the mutagenesis reaction. Plasmid construct DNA was stored at -20 °C. The new mutant constructs were designated pP2HA (H225A), pP2HQ (H225Q) and pP2YF (Y251F).

2.3.   ANAEROBIC CONDITIONS

Several experiments were performed under anaerobic conditions. Buffers were made anaerobic by bubbling humidified oxygen-free argon gas at 5 psi through solutions for ~2 hours with stirring. Solutions were then transferred to an anaerobic glovebox and left opened overnight to remove residual traces of oxygen. Samples of PRODH were made anaerobic by passing through a 10-DG gel filtration column (Bio-rad) equilibrated with anaerobic buffer in an anaerobic glovebox. Solutions of substrates, dithionite, potassium ferricyanide and mediator dyes were made by dissolving the appropriate solid in anaerobic buffer. All anaerobic experiments were performed in a Belle Technology glovebox under a positive pressure atmosphere of nitrogen with residual oxygen levels maintained at <0.05 ppm by a BASF R3-11 oxygen-scavenging catalyst. The oxygen level inside the glove box was measured with a Type 02M-1 Belle Technology oxygen meter.

2.4. PROTEIN PRODUCTION AND PURIFICATION METHODS

2.4.1. SDS-POLYACRYLAMIDE GEL ELECTROPHORESIS

SDS-polyacrylamide gel electrophoresis (SDS-PAGE) was performed following the protocol of Laemmli (1970) to assess protein expression and purity during stages of purification. 12 % acrylamide gels with 100 mm x 85 mm dimensions were cast and run using a Mini-PROTEAN II electrophoresis cell system (Bio-rad) according to the supplier's instruction manual. Reagents in order of addition are given in Table 2.7.

Reagent	Resolving gel	Stacking gel
ddH$_2$O	3.35 ml	6.1 ml
Tris-HCl	2.5 ml (1.5 M, pH 8.8)	2.5 ml (0.5 M, pH 6.8)
Protogel	4.0 ml	1.33 ml
SDS (10 % w/v)	100 µl	100 µl
APS (10 % w/v)	50 µl	50 µl
TEMED	5 µl	10 µl

Table 2. 7. Table showing the composition of gels for SDS-PAGE of protein samples. Reagents and their volumes are given in the order that they are assembled. Note, the molarity and pH of Tris-HCl buffer is different in the two gel tiers.

The resolving gel was overlaid with water-saturated isobutanol and allowed to set at room temperature for 45 minutes. Isobutanol was then decanted and the stacking gel was pipetted onto the top of the resolving gel and a comb submerged into the gel solution to form wells for the samples to be loaded. Protein samples of 5-50 µg were mixed with an equal amount of 2x sample buffer, vortex mixed in Eppendorf tubes and pulse centrifuged. The caps of the Eppendorf tubes were pierced with a clean hypodermic needle and the samples boiled at 100 °C in a water bath for 5 minutes to denature sample proteins. 5-20 µl of sample was loaded into the gel wells. Cell pellet samples for SDS-

PAGE analysis were firstly dissolved in 8 M Urea then mixed with an equal volume of 10 % (w/v) SDS and vortex mixed before being mixed again with an equal volume of 2x sample buffer and boiled for 5 minutes prior to loading. Gels were run at a constant current of 35 mA and a voltage of 180 V until the dye front had migrated to the base of the gel (approximately one hour).

2.4.2. EXPRESSION STRAIN SCREENING

Laboratory strains of *E. coli* were screened for recombinant expression from construct pPRODH1. Candidate host cells carried the T7 RNA polymerase gene (λDE3 lysogen) to induce recombinant gene expression from the T7 promoter in the construct. BL21(DE3), BL21(DE3)pLysS and Rosetta(DE3)pLysS strains were assessed for expression levels. Cells were transformed as previously described (Section 2.2.4) with 1 μl of pPRODH1 DNA (1 ng/μl). All expression strains transformed required a 1 hour outgrowth period at 37 °C/220 rpm in an orbital incubator after heat-shock and media addition steps. 50 μl of each transformation mixture was plated onto selective LB agar plates (ampicillin 50 μg/ml) and incubated overnight inverted at 37 °C. Isolated colonies were then used to individually inoculate 10 ml of selective 2xYT media (ampicillin 50 μg/ml; chloramphenicol 34 μg/ml for pLysS strains) in 25 ml sterilin tubes. These inoculums were then grown at 37 °C/220 rpm in an orbital incubator to an optical density (OD $_{600\,nm}$) of ~0.8 measured using a Cary Varian 300 Bio UV-visible spectrophotometer blanked with an aliquot of 2xYT fresh media. 1 ml samples were taken of the uninduced cultures before each was chemically induced with isopropyl β-*D*-thiogalactopyranoside (IPTG) to a final concentration of 1 mM and returned to incubation at 37 °C/220 rpm. 1 ml samples were then taken four hours post-induction. Uninduced and induced 1 ml samples (normalised to OD $_{600\,nm}$ ~0.8) were centrifuged for 5 minutes at 13,000 rpm in a microfuge and cell pellets prepared for SDS-PAGE analysis as previously described (Section 2.4.1). 10 μl samples were run on SDS-PAGE gels to visualise expression of recombinant protein.

2.4.3. OVEREXPRESSION AND PURIFICATION OF PRODH

Rosetta(DE3)pLysS competent cells were transformed with pPRODH1/pPRODH2 and incubated overnight as previously described (Section 2.2.4). 5ml autoclaved 2xYT selective media (ampicillin 50 µg/ml and chloramphenicol 34 µg/ml) in a sterilin tube was inoculated with a single colony and grown overnight at 37 °C/220 rpm in an orbital incubator. This subculture was used to inoculate 240 ml of fresh autoclaved selective 2xYT media (ampicillin 50 µg/ml and chloramphenicol 34 µg/ml) in a 1 L flask and grown overnight at 37 °C/220 rpm in an orbital incubator. 12 L of autoclaved 2xYT media (1 L media in a 2 L flask for aeration) containing the selective antibiotics was then inoculated with the overnight subculture to an initial optical density of OD $_{600\ nm}$ ~0.1 (~20 ml of subculture per 1 L of fresh selective media) and incubated at 37 °C/220 rpm in an orbital incubator. Cultures were grown to an OD $_{600\ nm}$ ~0.8 and chemically induced with IPTG to a final concentration of 1 mM and incubated for a further 8 hours at 37 °C/220 rpm in an orbital incubator. Cells were harvested by centrifugation at 7,000 rpm for 20 minutes in a Beckman Avanti J-20 XP centrifuge using a JLA 8.1 rotor. Cell pellet was resuspended in ice-cold 50 mM potassium phosphate buffer, pH 8.0 and frozen at -20 °C for storage. Cells were thawed at room temperature following the addition of a Complete Protease Inhibitor Cocktail tablet (Roche). A cycle of freezing and thawing was utilised to efficiently lyse the resuspended cells owing to internal expression of T7 lysozyme from the pLysSRARE plasmid harboured by the Rosetta(DE3)pLysS expression host. This 'autolysis' property rules out the need for a french press disruption procedure. Lysozyme (100 µg/ml final concentration) was added and the resuspension sonicated on ice at a power level of 5 with 50 % duty for 5 x 10 second bursts with 30 second intervals to promote complete cell lysis. DNA was hydrolysed by addition of DNase I (~10 µg) in the presence of 20 mM $MgCl_2$ and the lysate incubated at 4 °C with swirling for 30 minutes. Lysate was centrifuged at 10,000 rpm for 50 minutes to remove cellular debris in a Sorvall RC-5B centrifuge using a Fas20c rotor. The supernatant was decanted and heated in a water bath at 80 °C for 1 hour and denatured host proteins removed by centrifugation at 15,000 rpm for 30 minutes in a Sorvall RC-5B centrifuge using a Fas20c rotor. The yellow coloured supernatant was dialysed exhaustively against

8 litres of 50 mM Tris-HCl pH 8.0 at 4 °C. The sample was then clarified by filtration through a 0.22 μm Millex-GP Acrodisc and applied using a peristaltic pump to a HiLoad 26/10 MonoQ anion-exchange column (75 ml bed volume) equilibrated with 50 mM Tris-HCl pH 8.0. Protein was eluted on a 0.23 – 0.4 M salt gradient using a fast protein liquid chromatography (FPLC) system at a flow rate of 5.0 ml/min. Eluted fractions (7 ml fraction size) were analysed by SDS-PAGE and UV-visible absorbance spectrums (280-600 nm) were recorded for each fraction. Fractions containing PRODH were pooled and concentrated using a YM-30 Centriprep filtration unit. The concentrated protein sample (~1.5 – 2.0 ml) was then applied using a peristaltic pump to a HiLoad 26/60 Superdex 75 size-exclusion column (330 ml bed volume) equilibrated with 50 mM Tris-HCl, pH 8.0, 0.15 M NaCl and eluted at a flow rate of 0.75 ml/min using an FPLC system. Eluted fractions (3 ml fraction size) were analysed by SDS-PAGE and UV-visible absorbance spectrums (280-600 nm) were recorded for each fraction. Fractions containing pure PRODH were pooled and buffer exchanged extensively against 100 mM potassium phosphate buffer, pH 7.5 to render PRODH in monoflavinylated (FAD-bound) form for kinetics studies. H225A, H225Q and Y251F mutant forms of PRODH expressed from constructs pP2HA, pP2HQ and pP2YF, respectively, were isolated in the monoflavinylated form using the purification protocol described for wild-type enzyme. Purified protein was stored at -20 °C. PRODH for crystallogenesis trials was purified as previously described (Monaghan *et al.*, 2005) in order to retain FMN cofactor non-covalently bound at the αβ subunit interface. PRODH for crystallogenesis trials was concentrated to 12.2 mg/ml^{-1}, sterilised by filtration through a 0.22 μm Millex-GP Acrodisc and stored on ice at 4 °C. Purity of PRODH expressed from construct pPRODH2 was >95 % as judged by SDS-PAGE.

2.4.4. ANAEROBIC EXPRESSION AND PARTIAL PURIFICATION OF WILD-TYPE PRODH

10L of 2xYT media containing 20 mM sodium fumarate (used by the cells as a terminal electron acceptor in place of oxygen) was made sterile and anaerobic by autoclaving in 1L duran bottles. Ampicillin (50 μg/ml) and chloramphenicol (34 μg/ml) were added to

the media under anaerobic conditions and the media inoculated with Rosetta(DE3)pLysS cells transformed with plasmid pPRODH2. Cells were grown at 37 °C in a standing incubator until the optical density (OD $_{600\ nm}$) reached ~0.8. Cells were induced with IPTG to 1 mM final concentration and grown for a further 48 hours at 37 °C. Cells were contained anaerobic during cell harvest by transferring duran bottles into an anaerobic glovebox under a positive nitrogen atmosphere for transfer of cell culture into air-tight centrifuge tubes. Cell pellet was resuspended in 50 mM anaerobic MOPS buffer pH 7.9 and sealed in an air tight centrifuge tube. Cells were lysed anaerobically by three cycles of freezing and thawing and cell debris removed by centrifugation following DNA hydrolysis with DNase I in the presence of 20 mM $MgCl_2$. The supernatant was transferred to an air tight tube inside the glovebox and the solution subjected to a heat denaturation step at 80 °C for 1 hour and denatured protein removed by centrifugation. The supernatant was then transferred back into the glovebox and loaded onto a DE52 anion-exchange column equilibrated with anaerobic 50 mM MOPS buffer pH 7.9 and anaerobic wild-type PRODH eluted on a 0 – 0.5 M NaCl gradient. Fractions containing PRODH were pooled and sealed in airtight cryovials and stored at -20 °C.

2.4.5.   PRODUCTION OF SELENOMETHIONINE-SUBSTITUTED PRODH

For the purpose of Multiwavelength Anomalous Diffraction experimentation, selenomethionine-substituted (Smet) PRODH was produced by recombinant expression in the methionine auxotroph host cell strain B834(DE3). Recombinant expression of PRODH from _P. furiosus_ requires the host cell to express the tRNAs expressed from the compatible pLysSRARE plasmid that is harboured in Rosetta(DE3)pLysS cells. B834(DE3) does not contain this plasmid essential for PRODH expression, therefore, plasmid pLysSRARE was miniprepared from a fresh batch of Rosetta(DE3)pLysS cells using the method previously described (Section 2.2.5). Chemically competent B834(DE3) cells were then transformed with pLysSRARE plasmid using the method previously described (Section 2.2.4) and grown on a selective LB agar plate (chloramphenicol 34 μg/ml) inverted at 37 °C overnight. Chemically competent stocks of the new cell strain B834(DE3)pLysS were prepared using the method of Inoue _et al._,

(1990). B834(DE3)pLysS cells were then transformed with the pPRODH2 construct and incubated overnight as previously described (Section 2.2.4) on a selective LB agar plate (ampicillin 50 µg/ml, chloramphenicol 34 µg/ml). B834(DE3)pLysS-pPRODH2 recombinants were grown and purified using the methods described previously for wild-type recombinant PRODH (Section 2.4.3) with the only modifications being: 1) a four hour post-IPTG chemical induction growth period, and 2) the growth media was 'SelenoMet' minimal media mix consisting of a commercial blend of 'SelenoMet Medium Base' and 'SelenoMet Nutrient Mix' (Athena Enzyme Systems). 1 L of minimal media was supplemented with ampicillin (50 µg/ml), chloramphenicol (34 µg/ml) and DL-selenomethionine (10 mg/ml) that was added upon induction. All work with selenomethionine was performed in a fume cupboard and the appropriate protective clothing (nitrile gloves, lab coat, particulate respirator) was worn throughout the procedure. Quality control experiments for the production of Smet-substituted PRODH enzyme was performed by electrospray mass spectrometry analysis against non-substituted enzyme as described (Section 2.5.2).

2.4.6. DETERMINATION OF PRODH SOLUTION CONCENTRATION

The concentration of PRODH was determined by following the method of Bradford (1976). 20 µl of PRODH and standard protein solutions (bovine serum albumin) of 0.125 − 1.0 mg/ml concentration were each mixed with 1 ml of Bradford reagent (Bio-rad) in disposable 1 ml cuvettes and incubated at room temperature for 5 minutes. A blank sample containing 1 ml Bradford reagent and 20 µl buffer was also made and incubated along with the protein solutions. A Cary Varian 300 Bio UV-visible spectrophotometer was used to measure the absorbance of the PRODH and protein standard samples against the blank sample at 595 nm and a calibration curve for the protein standards was plotted of absorbance (595 nm) as a function of protein concentration. The concentration of PRODH was then determined from the calibration curve.

2.5.   METHODS OF PROTEIN ANALYSIS

2.5.1.   N-TERMINAL SEQUENCING

Purified PRODH expressed from the pPRODH1 construct was electrophoresed on an SDS-PAGE gel as previously described (Section 2.4.1). The unstained gel was then electroblotted onto polyvinylidene difluoride (PVDF) sequencing-compatible membrane. Electroblotting was performed using a minigel blotting system (Bio-rad). Blotter's Scotch pads and 2 pieces of 3 mm paper were soaked in transfer buffer (48 mM Tris-HCl, pH 6.8, 39 mM glycine, 10 % methanol and 0.03 % (w/v) SDS). A gel-sized piece of PVDF was then cut and saturated in methanol followed by soaking in transfer buffer until required. A gel sandwich was then constructed in a blotting cassette. A pre-soaked Scotch pad was placed in the cassette followed by a piece of pre-soaked 3 mm paper on top. The unstained gel was placed in the centre of the paper and any trapped air bubbles were removed from between the two surfaces. The PVDF membrane was then placed on top of the gel, again removing any trapped air bubbles. A second piece of pre-soaked 3 mm paper was placed on top of the PVDF membrane and any trapped air bubbles were removed by gently rolling a clean test tube over the surface of the sandwich. A second pre-soaked Scotch pad was then placed on top of the 3 mm paper to complete the sandwich and the cassette closed. This cassette was submerged in the blotter tank filled with transfer buffer orientated so that the gel was facing the cathode and the PVDF facing the anode. The lid was placed on the tank and the blot run for 2 hours at a constant current of 125 mA. Once the blotting was complete, the PVDF was removed from the sandwich and stained/destained. The membrane was then rinsed with ddH$_2$O and left to dry. N-terminal sequencing analysis of excised bands was performed using a ABI 476 Protein Sequencer identifying the first six amino acid residues of the amino-terminal of each protein band.

2.5.2. MASS SPECTROMETRY ANALYSIS OF PRODH

To accurately measure the molecular weight of the PRODH subunits, MALDI-ToF and electrospray mass spectrometric analyses were performed on pure samples of PRODH. The enzyme was exchanged into ddH$_2$O and concentrated to 1 mg/ml. MALDI-ToF mass spectrometry was performed using a Kratos Kompact MALDI-ToF III mass spectrometer utilising sinapinic acid as the matrix. The spectrometer was calibrated with a combination of peptides of known mass. MALDI-ToF mass spectrometry experiments with PRODH were performed with the assistance of Dr. Sharad Mistry at the PNACL. Electrospray mass spectrometry experiments with PRODH and selenomethionine-substituted PRODH were performed using a Waters Micromass LCT ToF mass spectrometer with the assistance of Mr Peter Ashton of the School of Chemistry, University of Birmingham, UK.

2.5.3. THE NATURE OF COFACTOR BINDING IN PRODH

The nature of the covalent/non-covalent binding of flavin cofactor(s) in PRODH was determined by the method of Mewies *et al.*, 1998. Three samples of pure PRODH were electrophoresed on an SDS-PAGE gel as previously described (Section 2.4.1). After electrophoresis, sample lanes were separated using a clean scalpel blade. One lane was stained/destained according to standard SDS-PAGE protocol, the second lane was soaked in 7 % acetic acid for 15 minutes and the third lane was sprayed with performic acid to convert potential 8α-*S*-cysteinyl linked flavins from the thioester to the corresponding sulfone in order to remove internal fluorescence quenching, followed by soaking in 7 % acetic acid for 15 minutes. The two non-stained sample lanes were then illuminated under UV-light to detect intrinsic fluorescence of any covalent flavin, the stained gel being used as a positional marker to identify which subunit carries the covalent flavin attachment site. Tetrameric sarcosine oxidase (TSOX) from *Arthrobacter* sp. 1-IN was used as a positive control for the experiment as this enzyme has covalently bound FMN attached to the β subunit (Harris *et al.*, 2000).

2.5.4. QUANTITATIVE TITRATION OF PRODH WITH SODIUM DITHIONITE

Anaerobic titrations of PRODH with the potent reducing agent sodium dithionite were performed to calculate the number of electrons required to reduce the flavin cofactor(s) of PRODH from the fully oxidised to hydroquinone forms, therefore allowing quantitation of the number of redox-active flavin cofactors that PRODH binds. 200 ml of 50 mM potassium phosphate buffer pH 7.5 was made anaerobic in a duran bottle as previously described (Section 2.3). A 2 ml stock solution of FAD was made in an opaque 1.5 ml Eppendorf tube (photo sensitive compound) by dissolving the appropriate solid in anaerobic buffer in a glovebox and the solution passed through a 10-DG size exclusion column equilibrated with anaerobic buffer. This FAD stock solution was required to calibrate the reducing power of the sodium dithionite solution used for quantitative titration of PRODH. A stock solution of PRODH was placed in the glovebox via the purge port and made anaerobic as previously described (Section 2.3). The Jasco V-530 UV-visible spectrophotometer situated inside the glovebox was blanked with two quartz cuvettes each containing 1 ml of 50 mM potassium phosphate buffer pH 7.5 and the Spectra Manager program (PC) was set up in the 'spectrum measurement' mode to collect the absorbance spectrum of a given sample between 300-600 nm. Both the FAD and PRODH stock solutions were diluted with anaerobic buffer to an absorption reading at 450 nm of ~0.2. The FAD stock solution was quantified using the Beer-Lambert law by its absorption reading at 450 nm using an extinction coefficient ($\varepsilon_{450\,nm}$) of 11,300 M^{-1} cm^{-1} in a 1 cm light path. All titrations were carried out at 25 °C by the use of a HMC-358 rectangular water jacketed cuvette holder (Jasco) attached to a water bath with an internal thermostat and water pump (Grant). 1 ml of FAD solution was placed in the spectrophotometer and the oxidised absorption spectrum recorded. A small amount of solid sodium dithionite stored inside the glove box was then dissolved in 15 ml of anaerobic buffer in a clean sterilin tube. The sodium dithionite stock solution was prepared immediately before use because the compound slowly oxidises during the time course of the experiment. Oxidised FAD solution was titrated with µl additions of sodium dithionite and the absorbance spectrum of the FAD solution recorded after each

addition of the reducing agent. Spectra were allowed to equilibrate after each addition of sodium dithionite (1-5 minutes). The titration was considered complete when no further spectral changes occurred upon addition of the reducing agent. Titration of 1 ml of PRODH (9 μM) with the sodium dithionite stock solution was then performed, immediately followed by a second titration of 1 ml of the FAD stock solution. The time scale of the whole experiment and the specific times at which each titration was performed was recorded. The reducing power of the sodium dithionite stock solution over the course of the experiment was quantified from the two FAD titrations that flanked the titration of PRODH. The reducing power of the sodium dithionite stock (electrons/μl dithionite) at the beginning and end of the experiment was determined and this data plotted as a function of time and interpolated to the time-point at which the titration of PRODH was performed, therefore giving a more accurate calculation of the number of electrons PRODH was reduced by during titration. The experiment was repeated four times on different days and the number of electrons calculated to fully reduce PRODH averaged. Spectral data was plotted and analysed using the GraFit software package, Version 5.0.

2.5.5. MALDI-ToF MASS SPECTROMETRY ANALYSIS OF PRODH COFACTOR

Identification of the non-covalently bound flavin cofactor of PRODH (isolated in monoflavinylated form for kinetic studies) was determined by MALDI-ToF mass spectrometry analysis of the released cofactor. A sample of monoflavinylated wild-type PRODH was exchanged into ddH$_2$O and concentrated using Centriprep and Centricon centrifugal membrane filter units with YM-30 membranes. PRODH was placed into an opaque 1.5 ml Eppendorf tube and heated at 100 °C in a water bath for 10 minutes to denature the protein. Denatured protein was immediately removed by centrifugation at 13,000 rpm for 10 minutes at 4 °C. Supernatant containing the released flavin cofactor was carefully decanted and transferred to a fresh opaque 1.5 ml Eppendorf tube and flash frozen in liquid nitrogen prior to storage at -80 °C. Standard solutions of authentic FAD, FMN, ATP, ADP and AMP were prepared as 1 mg/ml stock solutions in ddH$_2$O and

treated in the same way as PRODH through subsequent heating and centrifugation steps. These standard solutions were also flash frozen in liquid nitrogen and stored at -80 °C. MALDI-ToF mass spectrometry was performed with each of the standard solutions and the released PRODH cofactor solution using dihydroxybenzoic acid as the matrix on a Bruker Biflex mass spectrometer in positive-ion mode. The spectrometer was calibrated externally with a combination of peptides of known concentration.

2.5.6. OPTICAL TITRATIONS AND IDENTIFICATION OF REDUCING SUBSTRATES

Reducing substrates were identified by anaerobic titration of PRODH with amine compounds. Experiments were performed at 80 °C in 100 mM potassium phosphate buffer pH 7.5 utilising the buffers low temperature coefficient $[d(\text{p}K_a)/dT = -0.0028]$ (Stevens, 1992; Beynon and Easterby, 1996). Titrations were performed anaerobically to preclude potential oxidase chemistry. 200 ml of 100 mM potassium phosphate buffer pH 7.5 was made anaerobic and transferred to an anaerobic glovebox as previously described (Section 2.3). 1 ml stock solutions of dimethylglycine (2 M), sarcosine (2 M), glycine (1 M), L-proline (1 M), D-proline (1 M), L-pipecolic acid (1 M), glycine betaine (1 M) and sodium sulfite (1 M) were prepared by dissolving the appropriate amount of solid in anaerobic buffer in an anaerobic glovebox and pH corrected to pH 7.5. Samples of purified PRODH expressed from the pPRODH1 construct were made anaerobic by passing through a 10 DG size-exclusion column pre-equilibrated with four column volumes of anaerobic buffer in an anaerobic glovebox and brought to 13 μM. The UV-visible spectrophotometer situated in the anaerobic glovebox was temperature controlled by using a HMC-358 rectangular water jacketed cuvette holder attached to a thermostated waterbath and heated to a reaction temperature of 80 °C. Reaction temperatures were recorded by direct measurement inside the cuvette using a Cole-Palmer Digi-thermo thermocouple thermometer accurate to 0.1 °C. Quartz cuvettes containing buffer were placed in the spectrophotometer in a 1 cm light path and equilibrated to reaction temperature for 10 minutes before the baseline was measured. The Spectra Manager program (PC) was used during the collection of absorption spectra. 13 μM of PRODH

was placed into a clean quartz cuvette that was sealed to prevent solution evaporation and the enzyme solution equilibrated to reaction temperature for 10 minutes. Amine compounds were tested sequentially for reactivity with fresh batches of enzyme by mixing with equilibrated enzyme in a quartz cuvette to a final concentration of 20 mM in a reaction volume of 800 μl. The oxidised spectrum of PRODH was recorded prior to the addition of compounds and enzyme reduction was then monitored by time-dependent spectral acquisition in the 300-600 nm region. Spectral data was analysed using the GraFit software package, Version 5.0.

2.6. KINETIC STUDIES

2.6.1. STEADY-STATE KINETIC ANALYSIS

Steady-state kinetic measurements with identified substrates were performed spectrophotometrically in a 1 cm light path in 100 mM potassium phosphate buffer, pH 7.5, at 80 °C in a final reaction cell volume of 800 μl. Purified wild-type PRODH expressed from construct pPRODH2 (not expressing truncated α subunit) was utilised for steady-state characterisation of wild-type enzyme. The presence of oxygen on steady-state assay measurements was assessed by performing identical spectrophotometric enzyme assays in an aerobic and anaerobic environment. Ferricenium hexafluorophosphate, a potent oxidising agent (E'_0 = + 380 mV) was used as electron acceptor. Initial reaction rates were measured by following the reduction of ferricenium ion to ferrocene at 300 nm over a 1-5 minutes time course, depending on substrate concentrations and assay temperature. Buffer and substrate were equilibrated at the assay temperature for 10 minutes prior to the addition of ferricenium (200 μM) followed by the addition of enzyme to initiate the reaction. Initial velocities were measured by following reduction of ferricenium ($\Delta\varepsilon_{300}$ = 4,300 M^{-1} cm^{-1}) (Lehman *et al.*, 1990) and expressed as the concentration of ferricenium reduced in unit time ($\mu M/min^{-1}$). To establish that initial velocity recordings were actually a result of enzyme activity, control assays were performed at various PRODH concentrations with fixed concentrations of ferricenium and substrate. The initial velocities of these assays were then plotted as a function of

enzyme concentration to assess if a linear trend was evident. Initial velocities as a function of amine substrate concentration using a fixed concentration of enzyme (75 nM with L-proline as substrate, 200 nM with L-pipecolic acid as substrate) were analyzed by fitting to the standard Michaelis-Menten rate equation (Equation 2.1).

$$v = \frac{V_{max}[S]}{K_m + [S]}$$

Equation 2. 1

Where K_m is the Michaelis constant (substrate concentration at half V_{max}), $[S]$ is the substrate concentration and V_{max} is the maximum rate. Baseline controls were performed with each assay component in the absence of enzyme.

Similar reaction conditions were employed when studying the activity of PRODH in FMN-reconstituted diflavinylated form during assays with *P. furiosus* 4Fe-4S ferredoxin. The ferredoxin was supplied by Professor W. Hagan (Delft University) in the reduced form. The protein was oxidised in air for 2 hours with gentle agitation (oxidation followed at 390 nm) and reduction of the 4Fe-4S ferredoxin was monitored at 390 nm in an anaerobic glove box as described previously for aldehyde ferredoxin oxidoreductase activity (Mukund and Adams, 1991), but using L-proline as substrate.

The apparent kinetic constants of the Y251F mutant form of PRODH for L-proline as substrate were derived by fitting data to a steady-state rate expression that incorporates substrate inhibition (Tipton, 1996; Equation 2.2).

$$v = \frac{V_{max}}{1 + \frac{K_m}{[S]} + \frac{[S]}{K_i}}$$

Equation 2. 2

Where K_m is the Michaelis constant (substrate concentration at half V_{max}), $[S]$ is the substrate concentration, V_{max} is the maximum rate and K_i is the equilibrium constant for inhibitor binding.

For the acquisition of temperature dependent steady-state data, enzyme activity was measured in a continuous assay using the ferricenium ion as an artificial electron acceptor. During temperature dependence assays, substrate concentrations were maintained at 10 times K_m to provide pseudo-first order conditions. Reaction temperatures were recorded by direct measurement inside the cuvette using a Cole-Palmer Digi-thermo thermocouple thermometer accurate to 0.1 °C. The temperature was recorded during temperature equilibration prior to the reaction at both the top and bottom of the cuvette to detect for any temperature gradient in the assay mixture. Temperatures were also recorded immediately after assay completion and reactions were repeated if temperature fluctuations exceeded 0.1 °C. Assays were performed over a temperature range of 40 to 90 °C. Assays were initiated by addition of microlitre volumes of enzyme to ensure no significant effect on the overall reaction temperature. Kinetic parameters for hyperbolic plots of reaction velocity as a function of substrate (L-proline) concentration were calculated by fitting to the Michaelis-Menten expression (Equation 2.1). Thermodynamic parameters for the temperature dependence of the PRODH-catalysed reaction at saturating substrate concentration (200 mM L-proline) were obtained by fitting data to the Eyring equation (Equation 2.3).

$$\ln(k/T) = \ln k_B/h + \Delta S^\ddagger/R - \Delta H^\ddagger/RT \qquad \textbf{Equation 2.3}$$

Where T is the temperature in K, k_B and h are the Boltzmann and Planck constants, respectively, R is the gas constant and k is the observed rate constant. The standard entropy of activation ($\Delta S^\ddagger$), is calculated by extrapolation to the ordinate axis and the enthalpy of activation ($\Delta H^\ddagger$), is calculated from the gradient of the slope. The Gibbs free energy of activation ($\Delta G^\ddagger$) is calculated directly from the Gibbs free energy relationship (Equation 2.4).

$$\Delta G^\ddagger = \Delta H^\ddagger - T\Delta S^\ddagger \qquad \textbf{Equation 2.4}$$

Initial velocity data were plotted as a complete data set of rate *versus* time *versus* temperature analogous to the studies performed on thermophilic enzymes by Peterson *et*

al., (2004) describing an equilibrium model to determine the thermal parameter T_{eq} that represents a sub-millisecond timescale-reversible temperature-dependent equilibrium between active enzyme and inactive (or less active) forms. The effect of a decrease in enzyme activity above the optimal temperature that occurs due to a shift in T_{eq} is up to two orders of magnitude greater than the contribution of thermal denaturation. It is important to note, however, that the application of this proposed equilibrium model may be restricted to monomeric enzymes as the model does not take into account the complicating effects of thermally induced subunit dissociation of oligomeric enzymes. The function of time in the three-dimensional data set is necessary in these thermodynamic analyses to detect for the thermal inactivation/denaturation of enzyme at temperatures at and exceeding the source (evolved) temperature.

For pH dependent studies, steady-state assays were performed over the pH range of 5.5-10.0 in increments of 0.5 pH units at an assay temperature of 60 °C. To keep the ionic strength of the assay solutions constant over the experimental pH range, a three-component buffer system was employed comprising 2-(*N*-morpholino)ethanesulfonic acid (MES; pK_a 6.02), 3-{[tris(hydroxymethyl)-methyl]amino}-2-hydroxypropane sulfonic acid (TAPSO; pK_a 7.49) and diethanolamine (pK_a 8.88) at final concentrations of 0.052, 0.052 and 0.1 M, respectively (Ellis and Morrison, 1982). Kinetic parameters were calculated by fitting data to the Michaelis–Menten expression (Equation 2.1). pH profiles for the kinetic parameters k_{cat} and K_m were constructed and the data fitted to Equation 2.5 and 2.6, respectively, to obtain the relevant pK_a values.

$$k_{cat} = \frac{EH \times 10^{(-pH)} + E \times 10^{(-pK_a)}}{10^{(-pH)} + 10^{(-pK_a)}}$$

Equation 2. 5

$$\frac{k_{cat}}{K_m} = \frac{T_{max}}{1 + 10^{(pK_{a1} - pH)} + 10^{(pH - pK_{a2})}}$$

Equation 2. 6

Where *EH* and *E* are the catalytic activities of the protonated and unprotonated forms of the ionization group, respectively, and T_{max} is the theoretical maximal value of k_{cat}/K_m. All steady-state data were analysed using the GraFit software package, Version 5.0.

2.7.   PRODUCT IDENTIFICATION AND QUANTIFICATION

The product of the enzyme catalysed oxidation of L-proline was identified using a modified method described for the PutA protein of enteric bacteria (Wood, 1987). PRODH (75 nM) was used to oxidise a solution of L-proline (200 mM) in a final reaction volume of 800 µl using 200 µM ferricenium ion as the artificial electron acceptor in 100 mM potassium phosphate buffer, pH 7.5. Assays were performed at 60 °C and allowed to progress until complete reduction of ferricenium. The reduction of ferricenium was monitored spectrophotometrically at 300 nm. The assay mixture was then immediately incubated at 4 °C to maximise the stability of any product formed. A sample (100 µl) of chilled assay mixture was added to o-aminobenzaldehyde (0.5-4 mM) and formation of the o-aminobenzaldehyde-(product) chromophore was followed at 443 nm at 25 °C. o-aminobenzaldehyde was made as a 50 mM stock solution in 20 % ethanol and stored at -20 °C between assays to minimise polymerisation. The extinction coefficient used for quantifying the complex was $\varepsilon_{443} = 2.71$ mM^{-1} cm^{-1}. Baseline controls were performed with each assay component in the absence of enzyme. The product of the o-aminobenzaldehyde reaction was mass analysed by electrospray mass spectrometry using a Waters Micromass LCT ToF mass spectrometer in positive ion mode. 10 µl samples of the reaction were injected via a Rheodyne valve into a mobile phase of methanol flowing at 0.2 ml per minute into the electrospray source. The source temperature was maintained at 80 °C and the needle voltage was ~3.0 kV. The sample cone was operated at 20 V and the desolvation and sheath gas were nitrogen at 600 and 100 litres per hour, respectively. The spectrometer was calibrated with a solution of sodium iodide.

Direct analysis of the product of the enzyme catalysed reaction was also performed using MALDI-ToF mass spectrometry. Wild-type enzyme was reacted with 200 mM L-proline and limiting ferricenium ion (200 µM) as electron acceptor in ddH$_2$O and the reaction followed to completion at 300 nm. All assay components were filtered through a 0.22 µm Millex-GP Acrodisc filter prior to use. Following enzyme turnover, a 1 µl sample of the reaction mixture was plated for analysis on a Bruker Biflex mass spectrometer in positive ion mode using dihydroxybenzoic acid as matrix. A 1 mg/ml standard solution

of authentic L-proline was also prepared in ddH_2O and filtered through a 0.22 μm Millex-GP Acrodisc filter for MALDI-ToF mass spectrometric analysis. The spectrometer was externally calibrated using a combination of peptides of known mass.

2.8. REDOX POTENTIOMETRY

Anaerobic redox titrations were performed in an anaerobic glovebox (oxygen maintained at <5 ppm) under a positive nitrogen atmosphere between 5-31 °C in 100 mM potassium phosphate buffer, pH 7.0, using a 10 ml water-jacketed beaker attached to a thermostated water bath. Buffer was made anaerobic and transferred to the glovebox as previously described (Section 2.3). Concentrated stocks of enzyme were deoxygenated by passing through a 10-DG size-exclusion column equilibrated with anaerobic buffer inside the glovebox. Enzyme (5 ml; 16.3 mg/ml) was electrochemically titrated following the method of Dutton, (1978) using sodium dithionite as the reductant and potassium ferricyanide as oxidant. The mediator dyes, methyl viologen (0.3 μM), benzyl viologen (1 μM), 2-hydroxy-1,4-napthaquinone (7 μM) and phenazine methosulfate (2 μM) were added to enzyme immediately prior to titration to facilitate electrical communication between the enzyme and electrode across the range of +100 mV to -480 mV (Daff *et al.*, 1997; Munro *et al.*, 2001). Equilibration times after each microlitre addition of reductant were typically between 10-15 minutes, after which the potential was noted and the corresponding absorbance spectra measured between 280-800 nm. Absorption spectra were recorded on a Cary 50 Probe UV-visible scanning spectrophotometer, and the electrochemical potential was monitored using a CD 740 pH meter (WPA) coupled to a Russell Pt/calomel electrode. Calibration of the electrode was achieved using the Fe(II)/Fe(III)-EDTA couple (108 mV) as a standard. Complete titration curves typically consisted of ~40 different potential measurements. The observed potentials were those relative to the calomel electrode, and these were corrected (using calibration data for the Fe(II)/Fe(III)-EDTA couple) to values relative to the standard hydrogen electrode (SHE) by the addition of +244 mV to the observed data set recorded using the Pt/calomel electrode. Plots of absorbance at 450 nm ($λ_{max}$ for oxidised flavin) against redox

potential were fitted to Equation 2.7, which is derived by extension of the Nernst equation and the Beer-Lambert law as described previously (Munro *et al.*, 2001).

$$A_{obs} = \frac{(a + b10^{(E_{12}-E)/29.5})}{1 + 10^{(E_{12}-E)/29.5}}$$

Equation 2. 7

Where A_{obs} is the absorbance value at the peak for the oxidised flavin at the electrode potential E, and a, b are the absorbance values of the fully oxidised and reduced enzyme at this wavelength, respectively. E_{12} is the midpoint potential for the concerted two-electron reduction of the flavin. Data manipulation and analysis were performed using Origin software package, Version 6.0 (Microcal).

Thermodynamic parameters for the reduction of enzyme with sodium dithionite were calculated from the temperature dependence of the experimentally determined midpoint potential of the enzyme. Measurement of the standard reduction potential (E_0') of the enzyme redox-active flavin cofactor allows the standard free energy change ($\Delta G^{o'}$) of the reaction to be calculated directly using Equation 2.8, provided that the number of electrons (n) involved in the process is known.

$$\Delta G^{o'} = -nF\Delta E_0'$$

Equation 2. 8

Where $\Delta G^{o'}$ is the standard free energy change of the reaction, n is the number of electrons involved in the redox process, F is the Faraday constant and E_0' is the standard reduction potential. Determination of $\Delta G^{o'}$ enables the calculation of the equilibrium constant (K'_{eq}) for the redox reaction and thus reveals the direction of the reaction by implementing Equation 2.9.

$$\Delta G^{o'} = -RT \ln K'_{eq}$$

Equation 2. 9

Where R is the gas constant and T is the temperature in K. By experimental measurement of the PRODH flavin cofactor midpoint potential (E_m) value at various temperatures, the standard entropy change of the reaction ($\Delta S^{o'}$) can be calculated by using Equation 2.10.

$$\Delta S^{o'} = \frac{dE'_0}{dT} \times (nF)$$ **Equation 2.10**

The standard enthalpy change of the reaction ($\Delta H^{o'}$) is then calculated by rearrangement of Equation 2.4 as illustrated by Equation 2.11.

$$\Delta H^{o'} = \Delta G^{o'} + T\Delta S^{o'}$$ **Equation 2.11**

2.9. X-RAY CRYSTALLOGRAPHY WITH WILD-TYPE PRODH

For crystallogenesis trials, PRODH expressed from constructs pPRODH1 and pPRODH2 was purified as previously described (Monaghan _et al._, 2005; Section 2.4.3) and the enzyme concentration determined by the method of Bradford as previously described (Section 2.4.6). This concentrated sample was then centrifuged at 13,000 rpm in a microfuge for 20 minutes to clarify the solution of particulate contamination that may have adversely affected the crystallisation process. Two initial crystal screens were performed using the sitting drop vapour diffusion technique utilising the Clear Strategy Screens MD 1-14 and MD 1-15 (Molecular Dimensions) that each gave 24 potential crystallisation conditions. 180 μl of each crystallisation solution was pipetted into the designated tray wells along with 20 μl of 1 M Tris-HCl pH 7.5/pH 8.5 to control the pH of the screening conditions. These 'mother liquors' were allowed to equilibrate for 10 minutes at room temperature. 2.0 μl of enzyme was then pipetted into each 'well ledge' and immediately mixed with 2.0 μl of the relevant super-saturated mother liquor. The screen trays were sealed with transparent tape and incubated at 19 °C with minimal vibration. Trays were assessed for protein crystal formation on a daily basis under a light microscope. Screening conditions accommodating crystal and quasi-crystal structures were optimised by variation of the concentration of the salt and the concentration and

nature of the polyethylene glycol (PEG) that comprised the mother liquor. These subsequent screens were also composed at various solution pH values between pH 6.0 – 8.5 with increments of 0.5 pH units.

For the purpose of multiple isomorphous replacement (MIR) x-ray diffraction analysis, selected crystals were soaked in heavy metal solutions of lead (II) acetate trihydrate, trimethyl lead acetate, di-μ-iodobis (ethylene diamine) platinum (II) nitrate (PIP), potassium tetrabromoplatinate (II), platinum potassium cyanide, potassium hexabromoplatinate (IV), p-chloro mercury phenylsulfonic acid and mercury (II) acetate to produce heavy-atom derivatives to provide sufficient experimental phasing information. 10 μl of mother liquor was added to the crystal drop containing the relevant crystal before the crystal was transferred to a drop consisting of 90 % mother liquor containing a PEG concentration 1 % higher than that in the original mother liquor (to account for dilution) and 10 % of the relevant 100 mM heavy metal stock solution. The crystal was allowed to soak for 10 minutes before being placed into a drop consisting of 90 % original mother liquor and 10 % PEG 200 acting as a cryoprotectant. The crystal was soaked in this drop for 1 minute before being flash frozen and stored for transportation under liquid nitrogen.

Diffraction data were collected from cryocooled crystals (100 K) using a Quantum ADSC (Area Detector Systems Corporation) CCD detector on beamline ID 14-3 at the European Synchrotron Radiation Facility, Grenoble, France. Data were collected using 1° oscillations with the crystal-to-detector distance set to 230 mm. All data were indexed, integrated and scaled using the programs _DENZO_ and _SCALEPACK_ from the _HKL_ software package (Otwinowski and Minor, 1997). Using the program _MOLREP_ (Vagin and Teplyakov, 1997), a general self-rotation function was computed for a number of κ angles (60, 90, 120 and 180°) to test for the presence of non-crystallographic twofold, threefold, fourfold and sixfold axes.

Structure determination of wild-type recombinant PRODH was performed by the method of molecular replacement (Rossmann and Blow, 1962) using the protein PDH1 of _P._

horikoshii (Tsuge *et al.*, 2005) as the phasing model. Molecular replacement was performed using the AMoRe software package (Navaza, 1994). Improvement of the structure model was an iterative process. Atomic and B-factor refinement was performed using the Refmac5 program (Murshudov *et al.*, 1997) of the Collaborative Computational Project Number 4 (CCP4) suite for maximum-likelihood-based macromolecular refinement, alternated with manual rebuilding using the model-building/map-fitting program Coot (Emsley and Cowtan, 2004) of the CCP4 program suite. All aspects of the structure determination of PRODH were performed with Dr David Leys, University of Manchester, UK.

CHAPTER THREE

CLONING, RECOMBINANT EXPRESSION, PURIFICATION AND INITIAL CHARACTERISATION OF HYPERTHERMOPHILIC L-PROLINE DEHYDROGENASE (PRODH)

CHAPTER THREE

CLONING, RECOMBINANT EXPRESSION, PURIFICATION AND INITIAL CHARACTERISATION OF HYPERTHERMOPHILIC L-PROLINE DEHYDROGENASE (PRODH)

3.1. INTRODUCTION

The term 'Hyperthermophile' refers to an intriguing group of microorganisms with optimum growth temperatures above 80 °C. To date, around 70 species of bacteria and archaea growing at temperatures near and above 100 °C have been isolated from marine and continental volcanic environments (Adams, 1993). The underlying mechanistic phenomena that confer such extreme thermal stability on the cellular components of these microorganisms has piqued academic curiosity for the past two decades. The isolation of enzymes of hyperthermophilic origin, known as 'Extremozymes' has allowed a comparative approach to studying the structural biology of these proteins in conjunction with their mesophilic and in some cases psychrophilic counterparts (Danson and Hough, 1998). These studies have shed light on certain cooperative molecular interactions that may impart the intrinsic thermal stability of these extremozymes. Berezovsky and Shakhnovich (Berezovsky and Shakhnovich, 2005) propose that hyperthermophilic organisms have developed two diverse and fundamental physical mechanisms of thermostability, the evolutionary history of a given microorganism dictating which strategy manifests. Microorganisms that originate from an extreme environment (i.e. *Pyrococcus furiosus*) tend to harbor proteins that are more compact and hydrophobic when compared to their mesophilic homologues, whereas proteins isolated from microorganisms that evolved as mesophiles and later recolonised a hot environment (i.e. *Thermotoga maritima*) rely on a 'sequence-based' mechanism of thermostability. Aside from the fact that these heat-tolerant enzymes serve as excellent models for the study and understanding of protein thermostability, they also carry immense biotechnological potential. The need to perform biotechnologically related processes such as those

involving chemical reactions of organic solvents at high temperatures whereby the decrease in viscosity and increase in diffusion coefficient at elevated temperatures results in accelerated reaction rates (Krahe *et al.*, 1996; Becker *et al.*, 1997), the ability to exploit hydrophobic compounds that would otherwise be insoluble at ambient temperature for use in biodegradation and the obvious benefits of the decreased likelihood of bacterial contamination at high temperatures have all lent to a surge in applied interest in extremozyme research (Eichler, 2001).

Pyrococcus furiosus is the most extensively characterized extremophilic microorganism to date and is a hyperthermophilic archaeon first isolated by Fiala and Stetter (Fiala and Stetter, 1986) from geothermally heated marine sediments at the beach of Porto Levante, Vulcano Island, Italy. Electron microscopy reveals *P. furiosus* to hold a mostly regular cocci cell topology of 0.8 μm – 1.5 μm diameter with monopolar polytrichous flagellation. This microorganism is a strictly anaerobic heterotroph that grows between 70 – 103 °C with an optimal growth temperature of 100 °C and pH 7.0 by fermentation of carbohydrates giving acetate, alanine, CO_2 and H_2 by-products. On elevation of H_2 partial pressure, increased pyruvate is converted to alanine in preference of oxidation to acetate and production of ATP (Kengen *et al.*, 1994). Growth is inhibited at high partial pressure, but H_2S is readily formed instead of H_2 and growth is observed even at high partial pressure in the presence of elemental sulfur (Fiala and Stetter, 1986) and this finding has been postulated to be a mechanism of detoxification or an energy conservation process (Schicho *et al.*, 1993). *P. furiosus* accommodates a unique energy metabolism at the molecular level, core to which is the small iron-sulfur protein ferredoxin employed as a redox partner for an array of enzymes that transfer electrons to this protein. Reduced ferredoxin in turn transfers these electrons liberated from the primary metabolic pathways of carbohydrate and peptide fermentation to a membrane-bound hydrogenase complex and to an as yet unresolved sulfur-reducing system. Information regarding the detailed biochemical aspects of hyperthermophile metabolism is at present circumscribed and *P. furiosus* remains an enigmatic subject for extremophile metabolic research.

Early investigations showed only low activity in the glycolytic direction of key enzymes involved in conventional sugar metabolism and preliminary observations led to the postulation of glucose degradation to pyruvate occurring via a modified non-phosphorylating Entner-Doudoroff pathway (Mukund and Adams, 1991; Schaffer and Schonheit, 1992). This pathway demonstrated pyroglycolysis without the necessity of nucleotide-dependent enzymes, but with the tungsten-dependent aldehyde oxidoreductase (Mukund and Adams, 1991) playing a key role in the metabolic scheme. However, further studies highlighted major differences in key metabolic steps in the pathway of *P. furiosus*, including the phosphorylation of glucose and fructose-6-phosphate by ADP as opposed to ATP in the initial stages of the pathway (Kengen *et al.*, 1994). The primary explanation for this is based on ADP likely being more stable and resistant to hydrolysis than ATP at high temperature but the free energy change for the hydrolysis of the two nucleotides (31 kJ/mol^{-1}) is essentially equal (Mathews and van Holde, 1996). Another distinction in the pathway of *P. furiosus* was the finding by Mukund and Adams (Mukund and Adams, 1995) that glyceraldehyde-3-phosphate (GAP) is oxidised by glyceraldehyde-3-phosphate:ferredoxin oxidoreductase (GAPOR) to 3-phosphoglycerate (3-PG). In the conventional Embden-Meyerhoff pathway, GAP is oxidised to 3-PG in a two step process. The first oxidation is catalysed by glyceraldehyde-3-phosphate dehydrogenase whereby GAP is oxidised to 1,3-bisphosphoglycerate. The high energy phosphate of this molecule is later transferred to a molecule of ADP by a phosphoglycerate kinase yielding one molecule each of ATP and 3-PG as final products. Both glyceraldehyde-3-phosphate dehydrogenase and phosphoglycerate kinase in *P. furiosus* when assayed show low activity in the glycolytic direction (Kengen *et al.*, 1994) under physiological growth conditions, but have been shown to be likely involved in gluconeogenesis as suggested from growth on pyruvate where induction for both enzymes showed a 10-fold increase (Schaffer and Schonheit, 1993). Together, these observations highlighted the actual pathway of sugar fermentation in *P. furiosus* to be a modified Embden-Meyeroff pathway.

The thiamin pyrophosphate-containing iron-sulfur enzyme pyruvate:ferredoxin oxidoreductase (POR) (Blamey and Adams, 1993) and a novel acetyl-CoA synthetase

(Schaffer and Schonheit, 1991) utilize the pyruvate formed in the pathway for additional energy and reducing equivalents. The ADP-generating acetyl-CoA synthetase catalyses formation of acetate from acetyl-CoA with concomitant formation of one molecule of ATP. Therefore, during the oxidation of one molecule of glucose giving two molecules of both acetate and carbon dioxide in the modified Embden-Meyerhoff pathway in _P. furiosus_, a total of four molecules of ATP are generated along with the reduction of eight ferredoxin (Figure 3.1).

The 2-ketoacids derived from the transamination of amino acids are used by the two isoenzymes of acetyl-CoA synthetase isolated from _P. furiosus_, acetyl-CoA synthetase I uses acetyl-CoA and isobutyryl-CoA, form II utilizing indoleacetyl-CoA and phenylacetyl-CoA in addition to those used by isoenzyme I. A sundry of ferredoxin:oxidoreductases and aldehyde-oxidising enzymes, indolepyruvate (Mai and Adams, 1994), 2-ketoisovalerate (Heider, _et al._, 1996), 2-ketoglutarate (Adams, 1993) and formaldehyde (Mukund and Adams, 1993) believed to be involved in the fermentation of amino acids have been purified from _P. furiosus_ emphasizing that the primary carbon metabolism and energy production through peptide fermentation and glycolysis is focused on the small iron-sulfur containing ferredoxin that acts as redox-acceptor to a host of enzymes. Regeneration of oxidised ferredoxin is therefore essential for a sustained fermentative metabolism (Figure 3.2, A).

Under sulfur-limited conditions cytoplasmic ferredoxin enables energy to be conserved by hydrogen gas (H_2) production. In the absence of elemental sulfur, the anaerobic respiratory chain of _P. furiosus_ consists of a single enzyme, a membrane-bound multi-protein hydrogenase complex (MBH) that employs the low-potential electron donor, cytoplasmic ferredoxin to reduce protons to hydrogen gas, thus producing a proton motive force (pmf) for chemiosmotically driven ATP synthesis (Sapra _et al._, 2003) by coupling electron transfer to both proton reduction and proton translocation. This in turn regenerates oxidised ferredoxin for use in the glycolytic and peptidolytic pathways of _P. furiosus_ (Figure 3.2, B).
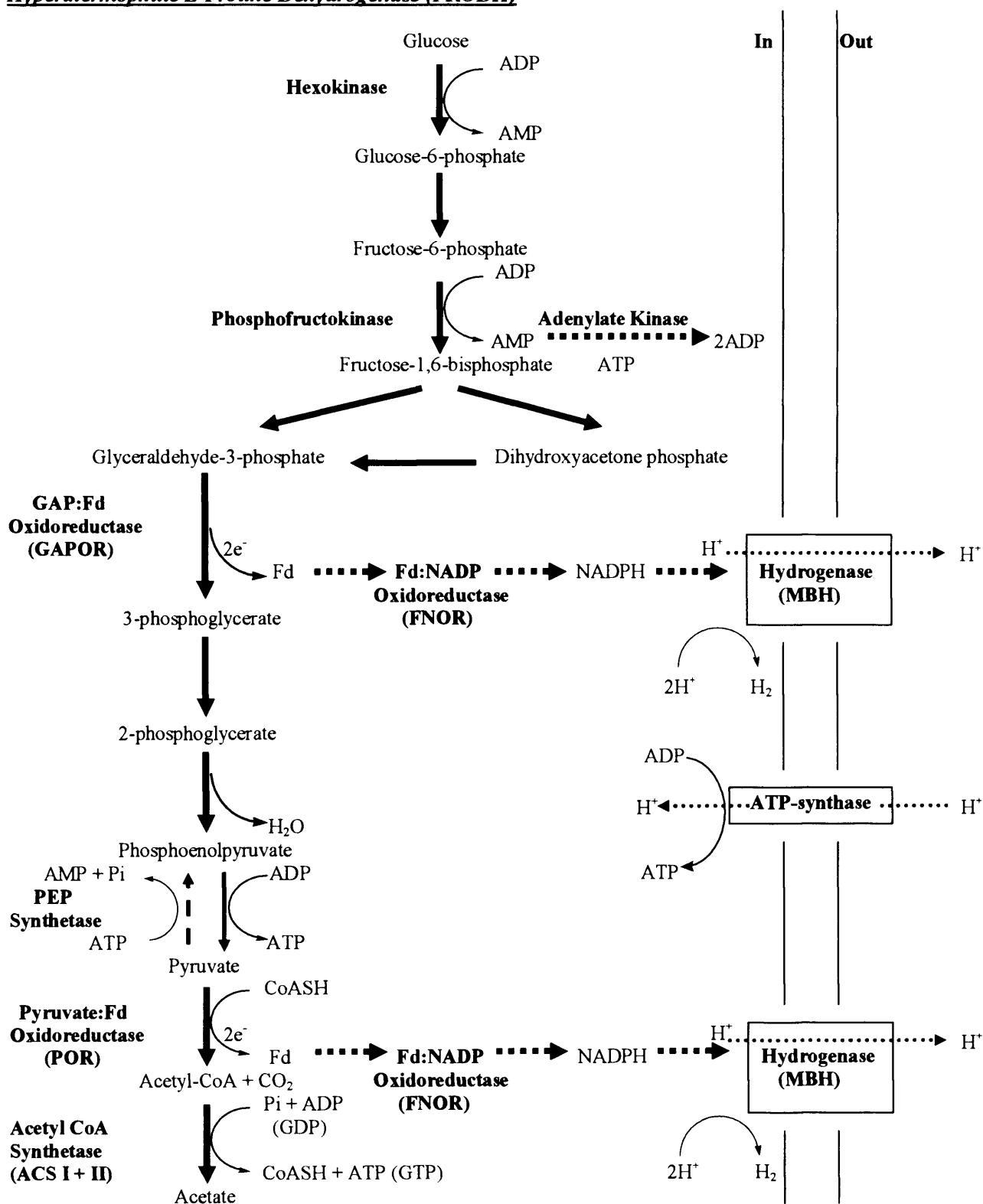
Figure 3.1. The modified Embden-Meyerhoff pathway proposed for glucose degradation in *P. furiosus*. Fd represents the electron carrier protein ferredoxin. Figure modified from, Adams *et al.*, 2001; Sapra *et al.*, 2003.

A

Peptides

N-acyl amino acids

In | Out

Prolidase

Formaldehyde:Fd Oxidoreductase (FOR)

Aminoacylase

Acyl CoAs? ← ─ ─ ─ ─ Amino acids

$NADP^+$

Fd ↓ $2e^-$

2-ketoglutarate

Glutamate Dehydrogenase (GDH)

Transaminase

Glutamate

NADPH

2-Keto acid

CoASH

POR VOR KGOR IOR

$2e^-$

Fd ▪▪▪ ▶ **Fd:NADP** ▪▶ NADPH ▪▪▪ ▶ **Hydrogenase (MBH)**

Aldehydes + CO_2

Acyl CoAs + CO_2

Oxidoreductase (FNOR)

H^+

Pi + ADP (GDP)

$2H^+$ H_2

Aldehyde:Fd Oxidoreductase (AOR)

Acyl CoA Synthetase (ACS I + II)

$2e^-$

Fd ◀

CoASH + ATP (GTP)

Acids

B

H^+

H^+

OUT

Hydrogenase (MBH)

ATP synthase

IN

FeS

H_2

Fd_{ox} Fd_{red}

$2H^+$

ADP + P_i

ATP

H^+

Amino acids Sugars

Organic Acids + CO_2

H^+

Figure 3.2. Peptide metabolism and chemiosmotic coupling in *P. furiosus*. *Panel A*, Proposed peptidolytic pathway in *P. furiosus*. *Panel B*, The proposed model of chemiosmotic coupling between the membrane-bound hydrogenase (MBH) and ATP synthase complex (ATPase) of *P. furiosus*. Fd_{red} and Fd_{ox} represent reduced and oxidised forms of the low-potential electron donor ferredoxin respectively. Fd, reduced by oxidative metabolism is reoxidised by the MBH that reduces protons to produce H_2. MBH also acts as a proton pump across the membrane accumulating a transmembrane proton gradient that is utilised by ATPase to produce energy in the form of ATP. Figures modified from, Adams *et al.*, 2001; Sapra *et al.*, 2003.

Concerning the fermentation of peptides by *P. furiosus*, the first stage of this process necessitates hydrolysis of the amide bonds of the peptide chain thus resulting in the individual amino acid residues, an action performed by several peptidases. The most extensively characterized peptidase of *P. furiosus* for which the crystal structure has also been recently determined is the Xaa-Pro metallopeptidase prolidase (Maher *et al.*, 2004). As one of the products of peptidase activity, L-proline, a secondary amine can be utilized by *P. furiosus*, its catabolism providing a source of carbon, nitrogen and electrons. Sakuraba and colleagues have assayed dye-linked L-proline dehydrogenase activity in several strains of *Thermococcales* (Sakuraba *et al.*, 2001), one of these strains being *P. furiosus* DSM 3638 with an observed specific activity of 2.0 mU/mg when coupled to the reduction of the artificial electron acceptor 2,6-dichloroindophenol. The 1.908 Mbp genome of *P. furiosus* with a GC content of 41 % has been fully sequenced and is now available (Maeder *et al.*, 1999) along with the other related hyperthermophilic genomic sequences of *P. horikoshii* (Kawarabayasi *et al.*, 1998) with a genome of 1.738 Mbp and *P. abyssi* (Genoscope: Heilig *et al.*, unpublished, direct submission to GenBank, 2001). The sequence identity between these microorganisms is very high, with the average nucleotide identity between the genomic sequences of *P. furiosus* and *P. horikoshii* being 70-75 % within the deduced open reading frames. The availability of the complete genome sequence for *P. furiosus* has enabled a search to identify putative oxidoreductases encoded within its genome with the aim of elucidating key stages in amino acid catabolism. Only by conducting such research will the metabolism of *P. furiosus* at a systems level be illustrated, and the components that enable this microorganism to survive and flourish in such an extreme environment be uncovered.

In addition to the requirements concerning oxidoreductase/dehydrogenase enzyme research to further understand the metabolism of *P. furiosus*, the nature of the catalytic mechanism at the atomic level in the flavoprotein family of such enzymes is still hotly debated by the scientific community. Amine oxidation is widespread in biology and the mechanisms of amine oxidation catalysed by the quinoprotein amine dehydrogenase/oxidases are well established. Oxidation occurs through the formation of enzyme–substrate covalent adducts with topaquinone (TPQ), tryptophan

tryptophylquinone (TTQ), cysteine tryptophylquinone (CTQ) and lysine tyrosyl quinone (LTQ) redox centres (Mure *et al.*, 2002; Datta *et al.*, 2001; Satoh *et al.*, 2002; Davidson, 2000; Wang *et al.*, 1996) and H-transfer by quantum mechanical tunnelling has been demonstrated for some quinoprotein enzymes (Masgrau *et al.*, 2004). The mechanism of amine oxidation by flavoproteins is not as well understood (Scrutton, 2004). These enzymes catalyse the two-electron oxidation of amine substrates to the corresponding iminium ion. Mechanisms involving (i) proton abstraction by an active site base to generate a carbanion species (Rohlfs and Hille, 1994), (ii) an aminium radical cation species (Silverman, 1995), (iii) H-atom abstraction by an active site radical species (Edmondson, 1995) and (iv) nucleophilic attack by the substrate nitrogen on the flavin C4a atom, followed by proton abstraction by an active site base or the flavin N5 atom (Kim *et al.*, 1993) have been considered over the years, but controversy remains in the field. Further structural elucidation of flavoprotein amine dehydrogenase/oxidases coupled with detailed spectroscopic and kinetic studies are required to unravel further the mechanistic details of amine oxidation by this class of enzyme.

This chapter reports on the identification, cloning and purification of a putative flavoprotein oxidoreductase from *P. furiosus* DSM 3638. Initial characterisation of the recombinant protein and its cofactors by MALDI-ToF and electrospray mass spectrometry are presented and discussed. This chapter also gives account of substrate profiling experiments leading to the identification of the physiological substrate as being the secondary amine L-proline. Robust, high temperature steady-state assay development and initial steady-state characterisation of the new L-proline oxidase/dehydrogenase with physiological substrate and the six-membered ring homologue L-pipecolic acid are detailed.

3.2.   RESULTS

3.2.1.   SEQUENCE ALIGNMENT OF GENE TRANSLATION PRODUCTS

To further address the pertinent topics of *P. furiosus* metabolism and the flavoenzyme mechanisms debate, two ORFs were identified from the genomic sequence of *P. furiosus* DSM 3638 (gi_18977617 and gi_18977618) using the online protein extraction description and analysis tool (PEDANT) genome analysis server (http://pedant.mips.biochem.mpg.de). Alignment of the translated amino acid sequences of these two ORFs against the primary structures of known enzymes suggested that the identified operon expression product may be an amine-specific oxidoreductase, the translation products of both ORF1 and ORF2 sharing primary structure sequence identity with the well characterised amine oxidase bacterial sarcosine oxidase. Further research intimating the nature of the target putative amine oxidoreductase was highlighted by a whole genome microarray study (Schut *et al.*, 2003) on the genome of *P. furiosus* monitoring the regulation at the transcript level of 2,065 annotated ORFs in cells grown in the presence of elemental sulphur at 95 °C in response to growth on carbohydrates (maltose) or peptides (hydrolysed casein) as the sole carbon source. This study quantitatively showed an up-regulation in the transcription levels of both target ORF1 (5.1-fold) and ORF2 (4.9-fold) in response to growth on peptides as the main carbon source. These results suggested that not only are the genes of this operon transcriptionally-coupled during expression and that the translated subunit products may complex to form a heterodimeric enzyme, but that this enzyme is also involved in peptide and/or amino acid catabolism (Schut *et al.*, 2003).

The target DNA sequence isolated and cloned is 2633bp in length. ORF1 (α subunit encoding) of the operon is 1476 bp in length, the corresponding translation product (492 residues) showing 18 % sequence identity (using BLASTP analysis) with the N-terminal region of the α subunit of tetrameric sarcosine oxidase (TSOX) from *Corynebacterium* sp. P-1 (Chlumsky *et al.*, 1995) and *Arthrobacter* sp. 1-IN (Meskys *et al.*, 2001). The PFAM (protein families alignment) database indicated the presence of a pyridine

nucleotide domain, comprising of a small NADH binding domain within a larger FAD binding domain to be present in the α subunit. ORF2 (β subunit encoding) is 1146 bp in length, the translation product (382 residues) showing 24 % identity with dimethylglycine oxidase (DMGO) from *Arthrobacter globiformis* (Meskys *et al.*, 2001) and 26 % sequence identity with dimethylglycine dehydrogenase from *Mus musculus* (Okazaki *et al.*, 2002). This sequence has a putative FAD-dependent oxidoreductase domain as speculated from the PFAM database. Both ORFs are in the same orientation further suggesting transcriptional-coupling with only five nucleotides separating the termination codon of ORF1 and the initiation codon of ORF2, therefore, translational-coupling is also probable. Translational coupling is a phenomenon that permits control of gene expression for the maintenance of an appropriate stoichiometry between one protein and another through the sequential expression of their genes in an operon. Three types of translational coupling mechanism have been identified that all differ by the origin of the ribosomes that translate the coupled distal gene. The first mechanism, termed 'reinitiation' describes that upon completing translation of the proximal gene, the same ribosome subsequently scans the region for a near-located translation initiation signal to initiate translation of the distal gene of the operon. This mechanism of translational coupling has been proposed for the controled expression of the overlapping coat and lysis genes of phage MS2 and fr (Adhin and van Duin, 1989, Adhin and van Duin, 1990). The other two mechanisms of translational coupling are in the form of 'facilitated binding' whereby the ribosome translating the proximal gene proceeds to melt the inhibitory mRNA secondary structure masking the ribosome-binding site of the distal gene. During one mechanism of facilitated binding the distal gene is then translated exclusively by free ribosomes from solution, but in the alternative mechanism the distal gene is translated both by free ribosomes and the ribosomes that translated the proximal gene. The mechanism of translational coupling that controls the expression of the α and β subunits from ORF1 and 2 respectively must be determined experimentally and is not an immediate concern for this project. However, for the reinitiation mechanism to occur, the termination codon of ORF1 and the initiation codon of ORF2 must be in very close proximity, usually overlapping or within two nucloetides of each other, although physical closeness can be achieved through a loop structure in the transcript (Inokuchi *et al.*,

2000). The proximal termination and distal gene initiation codons in the target sequence are five nucleotides apart and also evident is a putative ribosome-binding site for ORF2 with sequence 'AGGAGG' positioned eight nucleotides upstream of the initiation codon (Figure 3.3). Combined, these factors lend to the tentative postulation that the apparent translational coupling for controlled expression of the target operon may occur by a facilitated binding mechanism. Solution data in unison with computational analysis of possible mRNA secondary structures and corresponding ΔG_0 values for thermodynamically favourable folding around the region of the ribosome-binding site of ORF2 are required to accurately determine the given translational coupling mechanism employed.

Further analysis of the amino acid sequences for both the target α and β subunits of this putative enzyme revealed conserved binding motifs between the target hyperthermophilic sequences and those of related enzymes of mesophilic origin. The α subunit sequence exhibits an ADP-binding motif near the amino-terminus with the eleven participating residues satisfying the physico-chemical parameters for the consensus sequence (Wierenga et al., 1986). The sequence also contains a conserved GG doublet just five nucleotides downstream of the ADP-binding motif that is found in most flavoproteins with two dinucleotide-binding domains. When structural data is available on proteins containing the GG doublet, the two glycine residues appear to play an important role in binding FAD or ADP (Vallon, 2000). The glycine doublet seems to play a similar role to the first α-helix of the Rossmann fold where the first phosphate of the cofactor pyrophosphate is permitted close contact with the amino-terminal end of a structurally critical α-helix. H-bonding of the adjacent residue with O2A or O1A aids cofactor stabilisation in conjunction with favourable electrostatic interactions between the negatively charged phosphate and the helix dipole (Hol et al., 1978). An ATG peptide-motif is also present in the α subunit sequences. This motif is present in both FAD and NAD(P)H-binding proteins forming the fourth β-strand of the Rossmann fold and the connecting loop. In flavoproteins, the ATG-motif has a defined function because it is always present at the junction with the substrate-binding domain, and not within a domain as in NAD(P)H binding proteins (Vallon, 2000). The α subunit manifested the
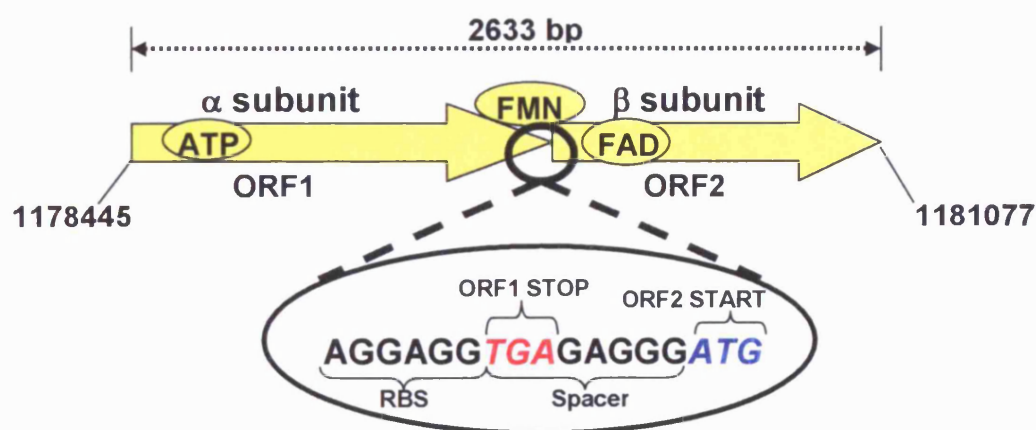
Figure 3.3. Schematic representation of the operon encoding PRODH cloned from the genomic DNA of *P. furiosus* DSM 3638. The cloned DNA fragment is 2633 bp in length and the α and β subunit translations are illustrated by the yellow arrows. The location of each cofactor is depicted in the schematic showing FAD situated on the β subunit, ATP on the α subunit and FMN bound at the subunit interface. The numbers 1178445-1181077 flanking the subunits represent the genome location of the cloned operon. The DNA sequence at the boundary of the two ORF's is highlighted and shows the ribosome-binding site (RBS) of the distal ORF that is separated from the corresponding start codon (blue) by an eight nucleotide spacer sequence that is made up in part by the termination codon of the proximal ORF (red).

highest sequence identity (76 %) with the amino terminal region of a putative sarcosine oxidase α subunit from _P. abyssi_. The α subunit also shared 22 % sequence identity with coenzyme $F_{420}H_2$ quinone oxidoreductase from _A. fulgidus_, 15 % sequence identity with the α subunit of opine oxidase from _S. meliloti_ and 16 % sequence identity with the hydrogen cyanide synthase (HCNB) from _P. fluorescens_. The sequence identity that the α subunit carries with HCNB may point to a downstream role for the α subunit after sarcosine oxidation, where glycine product is subsequently oxidised to iminoacetic acid in which the C-C bond is then split with a concomitant second dehydrogenase reaction to produce HCN and CO_2. The α subunit shares sequence identity with the amino-terminus of _Corynebacterial_ TSOX α subunit, but the C-terminus of this TSOX subunit contains a folate-binding motif that is also present in the C-terminal regions of dimethylglycine dehydrogenase (DMGDH) and sarcosine dehydrogenase (SDH) enzymes from various sources as well as being present in the tetrahydrofolate aminomethyltransferases (T-proteins) of the glycine cleavage system of various organisms that catalyse tetrahydrofolate-dependent reactions analogous to the reactions of DMGDH and SDH (Fujiwara _et al._, 1984). This folate-binding motif important for the binding of folate that acts as a C1-acceptor to sequester formaldehyde product during TSOX, DMGO, DMGDH and SDH catalysis, forming 5, 10-methylenetetrahydrofolate (Chlumsky _et al._, 1995; Wagner _et al._, 1997) is not present in monomeric sarcosine oxidase (MSOX) nor in the α subunit sequence of the pyrococcal cloned enzyme under investigation (Figure 3.4). Therefore, if formaldehyde is a product in the physiological reaction catalysed by the putative pyrococcal enzyme, _P. furiosus_ must hold a separate mechanism for its detoxification.

The β subunit of the putative enzyme also possesses a clear amino-terminal ADP-binding domain with all eleven residues conforming to the consensus sequence with the exception of the glutamate residue at position one, though this hydrophilic residue holds the correct physico-chemical requirements of this position. The β-subunit of various TSOX enzymes share sequence homology with MSOX and show conservation of active site residues implicated in the catalytic mechanism of MSOX. However, the target β subunit sequence does not share this active site homology and only one residue defined in MSOX

```
PRODHa          EEPLPQDG------------------------------------EVKQVVVDVLVIGGG 118
P.ABYSSI SoxA   EEPVIEGG------------------------------------EVKEVVVDVAVVGGG 120
P. fu. FeSoxA   PPANSNGS------------------------------------KAKTVKGDIIVIGGG 123
COENZYME F420H2 DKVFPHGSHYTKFTTSKKAREFMVKRMRKFTGFGNPPKAVFQGRAELEEIETDVLVIGGG 178
CORYN. TSOXa    GVLDPSTDP-----------------------------AYYDHVHVHTDVLVVGAG 139
                                                              *   *  *
```

```
PRODHa          PAGLGAVLEMQEH-LNVALVEEKGWLGGDMFLKTSTAEGFEESSR-------KVVDKLAK 170
P.ABYSSI SoxA   PAGIGALELQDD-LTVALIEEKGWLGGDMWLKSTKQEGFNKEAR-------KAVEELTK 172
P. fu. FeSoxA   PAGLMAAISAHDAGAKVVLIDENPILGGQLVKQTHKFFGKREQFAGIRGIKIAQILEEEI 183
COENZYME F420H2 PGGMSAAINAGKYGAKVLLVDENPFLGGQLVKQTHRFFGSAKERAGTRGIKIAGILEEEL 238
CORYN. TSOXa    PAGLAAAREASRSGARVLLLDERAEAGGSLRDAAGEQIDGQDAAAWIDATVAELAAAEET 199
                * *      * *     *  *  *    **
```

```
PRODHa          EVK--ANVYLGTVALGVFDKG-EYFLVPATKGN-----NLIEFLAKRVVLATGAVDNIML 222
P.ABYSSI SoxA   KIKDEVKVFLGASALGVFDKG-EYFLVPVVKEN-----SLIEILAKRVVLATGAVDSIML 226
P. fu. FeSoxA   R-KRNIETFLETSAVGIFQEGNEKIVVGVRKEK-----ELIEFRGKAIIVATGAMERAIP 237
COENZYME F420H2 NSIENVEVRRETRVFGIYNGEAGAYQRLNDDEG-----KLLRIKAKKIVVATGAYERTLI 293
CORYN. TSOXa    THLQRTTVLGSYDANYVVAVQRRTVHLDGPSGAGVSRERIWHIRANQVVLATGAHERPIV 259
                                                                  ****
```

Figure 3.4. Multiple sequence alignment against the amino acid sequence of the PRODH α subunit. The primary structure of the α subunit of PRODH of *P. furiosus* (PRODHa) was analysed for sequence identity with the amino-terminal sequence of the hypothetical protein SoxA from *P. abyssi* (P.ABYSSI SoxA), the α subunit of FeSOX (P. fu FeSoxA) also cloned from *P. furiosus* genomic DNA, coenzyme $F_{420}H_2$ quinone oxidoreductase from *A. fugidus* (COENZYME F420H2) and TSOX α-subunit from *Corynebacterium* sp. P-1 (CORYN. TSOXa). The residues that comprise the ADP-binding motif are shown in bold and highlighted in yellow where residues are conserved (note Thr-127 [shaded dark red] of *P. abyssi* SoxA does not comply with the consensus that a hydrophobic residue must occupy this position). The GG doublet five nucleotides downstream of the ADP-binding motif is highlighted in red and the ATG-motif is highlighted in green. Additional residue conservation across all five sequences analysed is indicated by an asterisk. Sequence alignment was performed using 'ClustalW' (http://www.ebi.ac.uk/clustalw/).

as an active site participant is conserved (Arg-52). This lack of active site conservation in the β subunit sequence indicates that sarcosine may not be the true physiological substrate and that other molecules with similar molecular structures to sarcosine must be probed experimentally to determine the physiological substrate, the results of such experiments intimating possible active site components. The β subunit sequence holds 27 % sequence identity with the β subunit of TSOX from both *Corynebacterium* sp. P-1 and the soil bacterium Arthrobacter sp. 1-IN, 26 % sequence identity with the amino-terminal half of human DMGDH, 24 % sequence identity with glycine oxidase from *Bacillus anthracis*, 25 % sequence identity with the amino-terminal half of human SDH, 23 % sequence identity with the amino-terminal half of T-protein from *Arthrobacter nicotinovorans* and 24 % sequence identity with hydrogen cyanide synthase from *Pseudomonas aeruginosa*. The high sequence identity that the β subunit carries with hydrogen cyanide synthase of *P. aeruginosa* (24 %) may again point to a downstream processing role for this subunit in terms of glycine oxidation. The β subunit possesses sequence identity with amino-terminal regions of DMGDH and SDH from various sources as well as the amino-terminal of T-protein form *Arthrobacter nicotinovorans* but again, the hyperthermophilic sequence does not carry a folate-binding domain motif (Figure 3.5).

Of particular note is the finding that the β subunit shows sequence conservation with active site residues His225, Tyr259 and Gly270 of DMGO from *Arthrobacter globiformis* and the cDNA translation product of DMGDH from mouse lung tissue (Figure 3.6). The structure of DMGO from *Arthrobacter globiformis* has been resolved to 1.6 Å resolution (Leys *et al.*, 2003). In DMGO the Try259-His225 dyad could form a proton shuttle that acts as to abstract a proton from the substrate amine (C-H bond breakage mechanism requires deprotonation of the substrate amine nitrogen) prior to nucleophilic attack of the substrate at the flavin C4a atom (Figure 1.17), the flavin N5 position would then abstract a proton from the methyl group of the substrate in a concerted reaction to yield dihydroFAD and iminium product (as in the reactions of TMADH and monoamine oxidase). Gly270 is sterically the only residue permitted at this position due to the relative positions of His225 and Tyr259. From these initial alignment results it can be

```
PRODHb           -MIPEKSEIVVIGGGIVGVTIAHELA-KRG-EEVILVEKRF-------------------  38
P.horikoshii SoxB -MLPEKSEIVVIGGGIVGVTIAHELA-KRG-EEVTVIEKRF-------------------  38
P. fu. FeSoxB    -MIG------IIGGGIIGVATAYELA-KLG-EEVVVFEKRY-------------------  32
Human N-ter SDH  RPLPSTAHVVVIGGGSLGCQTLYHLA-KLGMSGAVLLERER----------------- 100
A. nico. T-protein DPLPTHVRTVVVGGGIIGASIAYHLS-AAGENDTLLLESNV-------------------  59
Human N-ter DMGDH TQWKDRAETVIIGGGCVGVSLAYHLA-KAGMKDVVLLEKSE-------------------  83
Coryn. TSOXb     PEPKKSYDVVIVGGGGHGLATAYYLAKNHGITNVAVLEKGW------------------  56
Arthro. TSOXb    PEPKKSYDVVIVGGGGHGLATAYYLAKNHGITNVAVLEKGW------------------  56
B. anthracis Glyox ---MRHCDVLIIGGGIIGCSIAYYTS-KYG-RDVTIIEKGE------------------  36
P. aerug. HCNsyn --MNRTYDIVIAGGGVIGASCAYQLS-RRGNLRIAVVDDKRPGNATRASAGGLWAIGESV  57
                       ***  *                        *

PRODHb           -IGSGSTFRCGTGILQQFNDEANVQVMKRS-------------------VELWKKYSEE  77
P.horikoshii SoxB -IGSGSTFRCGTGILQQFNDEANVRVMKRS-------------------VELWKKYSEE  77
P. fu. FeSoxB    -FGSGSTFRCASGILAQFTDEANIKLMKYS-------------------IERWKTLSEE  71
Human N-ter SDH  -LTSGTTWHTAGLLWQLRPSDVEVELLAHTR------------------RVVSRELEEE 140
A. nico. T-protein -LGSGTSWHAAGLVTGARGTTTMTKLAKYGL------------------DFYS-RLEQM  98
Human N-ter DMGDH -LTAGSTWHAAGLTTYFHPG-INLKKIHYDS------------------IKLYEKLEEE 122
Coryn. TSOXb     -LAGGNMARNTTIIFSNYLWDESAGIYEKS-------------------LKLWEQLPEE  95
Arthro. TSOXb    -LAGGNMARNTTIIFSNYLWDESAGIYEKS-------------------LKLWEQLPEE  95
B. anthracis Glyox -FVSGTSSRCDGNILAIDKDPRFDSQMSLVS------------------QKLVTDLSEE  76
P. aerug. HCNsyn GLGCGVIFFRMMSSRNRREAQGAAVAVDASTPHILPPAFFDLALQSNALYPELHRELIER 117
                       *
```

Figure 3. 5. Multiple sequence alignment against the amino acid sequence of the PRODH β subunit. The primary structure of the β subunit of PRODH of *P. furiosus* (PRODHb) was analysed for sequence identity with the amino-terminal sequence of the hypothetical protein SoxB from *P. horikoshii* (P. horikoshii SoxB), the β subunit of FeSOX (P. fu FeSoxB) also cloned from *P. furiosus*, the amino-terminus of human SDH (Human N-ter SDH), the amino-terminus of T-protein from *Arthrobacter nicotinovorans* (A. nico. T-protein), the amino-terminus of human DMGDH (Human N-ter DMGDH), TSOX β-subunit from both *Corynebacterium* sp. P-1 (Coryn. TSOXb) and *Arthrobacter* sp. 1-IN (Arthro. TSOXb), glycine oxidase from *Bacillus anthracis* (B. anthracis Glyox) and hydrogen cyanide synthase from *Pseudomonas aeruginosa* (P. aerug. HCNsyn). The residues that comprise the ADP-binding domain are shown in bold and highlighted in yellow where residues are conserved. All eleven residues in each sequence that comprise the ADP-binding motif satisfy the consensus amino acid sequence fingerprint with the exception of the glutamate residue at position one in human DMGDH, though this hydrophilic residue holds the correct physico-chemical requirements of this position. The putative covalent flavin attachment site in human SDH (His-108) is highlighted in red and the conserved arginine residue implicated in the active site catalytic mechanism of MSOX is highlighted in green. In contrast to the α subunit, no GG-doublet or ATG-binding motifs are found in the PRODH β subunit amino acid sequence. Sequence alignment was performed using 'ClustalW' (http://www.ebi.ac.uk/clustalw/).

A

```
PRODHb    GVIKTGIVVNATNAWAKLINAMAGIKTSIPIEPYKHQAVITQPIKRG-------TIKPM  241
DMGDH     GSVRANRIVNAAGFWAREVGKMIGLDH--PLIPVQHQYVVTSTIPEVKALKR---ELFTP  292
DMGO      GVIPADIVVSCAGFWGAKIGAMIGMAV--PLLPLAHQYVKTTPVPAQQGRNDQPNGARLP  249
            *      *      *      * *     * *     * * **  *
```

```
PRODHb    VISFKYGHARLTQTAHGGIIG---------GVGYEVGPTYDLTPTYEFLREVSYYFS--  289
DMGDH     VLRDLEGSYRLRQERDGLLFGPYESQEKMKLQASWVTHGVPPGFGKELFESDLDRISD--  350
DMGO      ILRHQDQDLRYREHGDRYGIGSYAHR-PMPVDVDTLGAYAPETVSEHHMPSRLDFTLEDF  308
                     *           *
```

B
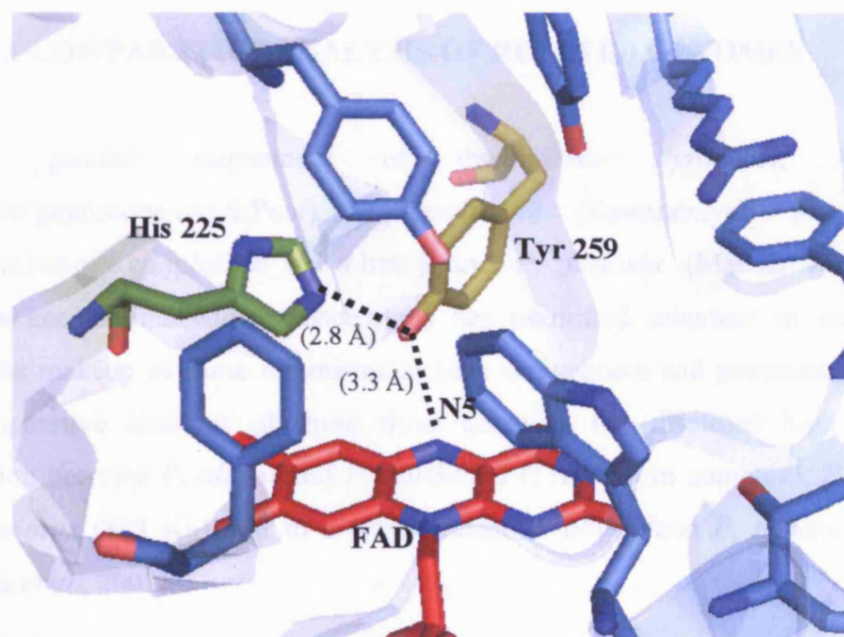
Figure 3. 6. Multiple sequence alignment deduced for the β-subunit of PRODH showing alignment with conserved active site residues in DMGO and DMGDH. *Panel A*, multiple sequence alignment data for the β subunit of PRODH of *P. furiosus* (PRODHb) showing 24 % sequence identity with dimethylglycine oxidase (DMGO) from *Arthrobacter globiformis* and 26 % sequence identity with the cDNA translation product of dimethylglycine dehydrogenase (DMGDH) from *Mus musculus* lung tissue. DMGO active site residues His225, Tyr259 and Gly270 identified from the crystal structure align with conserved residues in both DMGDH and PRODHb and are highlighted as bold and shaded. Additional conserved residues are marked with an asterisk. *Panel B*, structure of the flavin oxidase domain of DMGO from *Arthrobacter globiformis*. Residues lining the active site are illustrated in stick representation and coloured sky blue. The conserved residue His225 is coloured pea-green with the nitrogen atoms of the side chain imidazole ring coloured blue. The conserved residue Tyr259 is coloured olive-orange with the phenolic hydroxyl group coloured pale-red. The covalently bound FAD is depicted in stick representation and coloured red with the nitrogen atoms of the isoalloxazine ring coloured blue. Tyr259 is hydrogen bonded to both His225 and the FAD N5 atom at bond distances of 2.8 Å and 3.3 Å respectively, depicted by the dashed lines. Figure constructed using PyMOL v.0.99 (DeLano, 2002; http://www.pymol.org). The crystal structure of DMGO has been resolved to 1.6 Å (Protein Data Bank accession codes 1PJ5, 1PJ6 and 1PJ7 for the acetate, folic acid and folinic acid-bound forms, repectively.

postulated that the putative pyrococcal enzyme could utilise a similar mechanism for substrate oxidation (requiring deprotonated substrate) and that DMG could even be the physiological substrate. The data also points to the β subunit being the component of the putative enzyme where the active site is localised and therefore where the flavin prosthetic group participating in substrate oxidation is likely to be bound.

3.2.2. A COMPARATIVE ANALYSIS OF RELATED GENOMES

Complete genome sequencing of the three *Pyrococci*, *P. abyssi* (http://www.genoscope.cns.fr/Pab/), *P. horikoshii* (Kawarabayasi *et al.*, 1998; http://www.bio.nite.go.jp/ot3db_index.html) and *P. furiosus* (Maeder *et al.*, 1999; http://www.genome.utah.edu/sequence.html) has permitted scientists to compare and contrast the makeup of these organisms at both the genome and proteome level. Pair wise comparative analyses of these three genomes has disclosed high nucleotide conservation between *P. abyssi* and *P. horikoshii* (1122 Kb in common), *P. horikoshii* and *P. furiosus* (898 Kb) and to a lesser extent *P. abyssi* and *P. furiosus* (847 Kb) (Lecompte *et al.*, 2001).

Since the divergence of the three species, high differential gains and losses of genes appear to have occurred (Ettema *et al.*, 2001). Only two-thirds of the proteome of these species account for conserved proteins evident in the three *Pyrococci*, this emphasizing the genomic and metabolic plasticity of these archaea.

On comparing the proteome of these three species, the number of annotated ORFs with at least one homologue are 1723, 1651 and 1947 in *P. abyssi*, *P. horikoshii* and *P. furiosus* respectively. The closest homologues of *P. abyssi* and *P. horikoshii* share 77 % sequence identity at the amino acid level, 73 % sequence identity between *P. furiosus* and *P. horikoshii* homologues and 72 % sequence identity between *P. furiosus* and *P. abyssi* counterparts (Lecompte *et al.*, 2001). These results further corroborate earlier intimations that *P. abyssi* and *P. horikoshii* are more closely related than *P. furiosus* (Kalman *et al.*, 1999). The genome of *P. furiosus* also differs from the other two species of *Pyrococci* in

terms of its larger size and the existence of insertion sequences (ISs). These differences along with the appreciably larger content of paralogous proteins encoded for within the genome agree favourably with the ribosomal RNA phylogenetic analyses (Gonzalez *et al.*, 1998) that suggest *P. abyssi* and *P. horikoshii* diverged after the speciation of *P. furiosus*.

3.2.3. PCR CLONING OF TARGET ORF'S

The 2633 bp target DNA sequence identified in the genome of *P. furiosus* was isolated and amplified from purified genomic DNA using the polymerase chain reaction (PCR) protocol as described (Section 2.2.2). The resulting amplified target DNA was in turn subjected to a second round of PCR using primers designed to engineer a 5' *Xba* I site and a 3' *Bam* HI site for directional cloning. A computational search of the target DNA sequence for restriction sites using NEB cutter V.2.0 (http://tools.neb.com/NEBcutter2/index.php) indicated the presence of an *Nde* I site within the sequence. This hindered attempts to clone the target DNA directly in frame for expression in a pET vector. The 5' primer was therefore designed to engineer the consensus ribosome-binding site sequence used by the pET vector system 'AAGGAG' separated upstream from the initiation codon of ORF1 by an eight nucleotide spacer sequence. The engineered ribosome-binding site sequence possesses a high binding energy for the 3' end of the 16S rRNA of the translating ribosome allowing optimal and direct expression when cloned. The ORF1 initiation codon was also mutated during PCR from 'GTG' to the preferred initiation codon of *E. coli* 'ATG' that accounts for 94 % of start codons in the *E. coli* genome compared to 90.8 % of start codons in the genome of *P. furiosus* (Hannenhalli *et al.*, 1999). The distribution of start codons in the genomes of the Gram-negative bacterium *E. coli*, the archaebacterium *P. furiosus* and the gram-positive bacterium *B. subtilis* are given in Table 3.1. The amplified target DNA sequence was subsequently cloned directly into the expression vector pET11d by the protocol described (Section 2.2.3). The new expression construct designated pPRODH1 was 8252 bp in length and harbored a β-lactamase encoding gene to confer host ampicillin resistance to allow transformant selection on a selective agar plate (Figure 3.7, A).

Genome	_B. subtilis_	_E. coli_	_P. furiosus_
% ATG	79.9	94.0	90.8
% GTG	8.9	4.9	9.2
% TTG	11.2	1.1	0.0

Table 3. 1. Table of the percentage distribution of start codons in various genomes. The sequences for _E. coli_ (accession number U00096) and _B. subtilis_ (accession number AL009126) were taken from GenBank. The sequence for _P. furiosus_ was provided to the researchers by Bob Weiss at the Utah Genome Center (http://www.genome.utah.edu), and homology with _P. horikoshii_ (GenBank accession numbers AP000001-7) was used to extract start sites. The table is adapted from Hannenhalli _et al._, 1999.

A

B
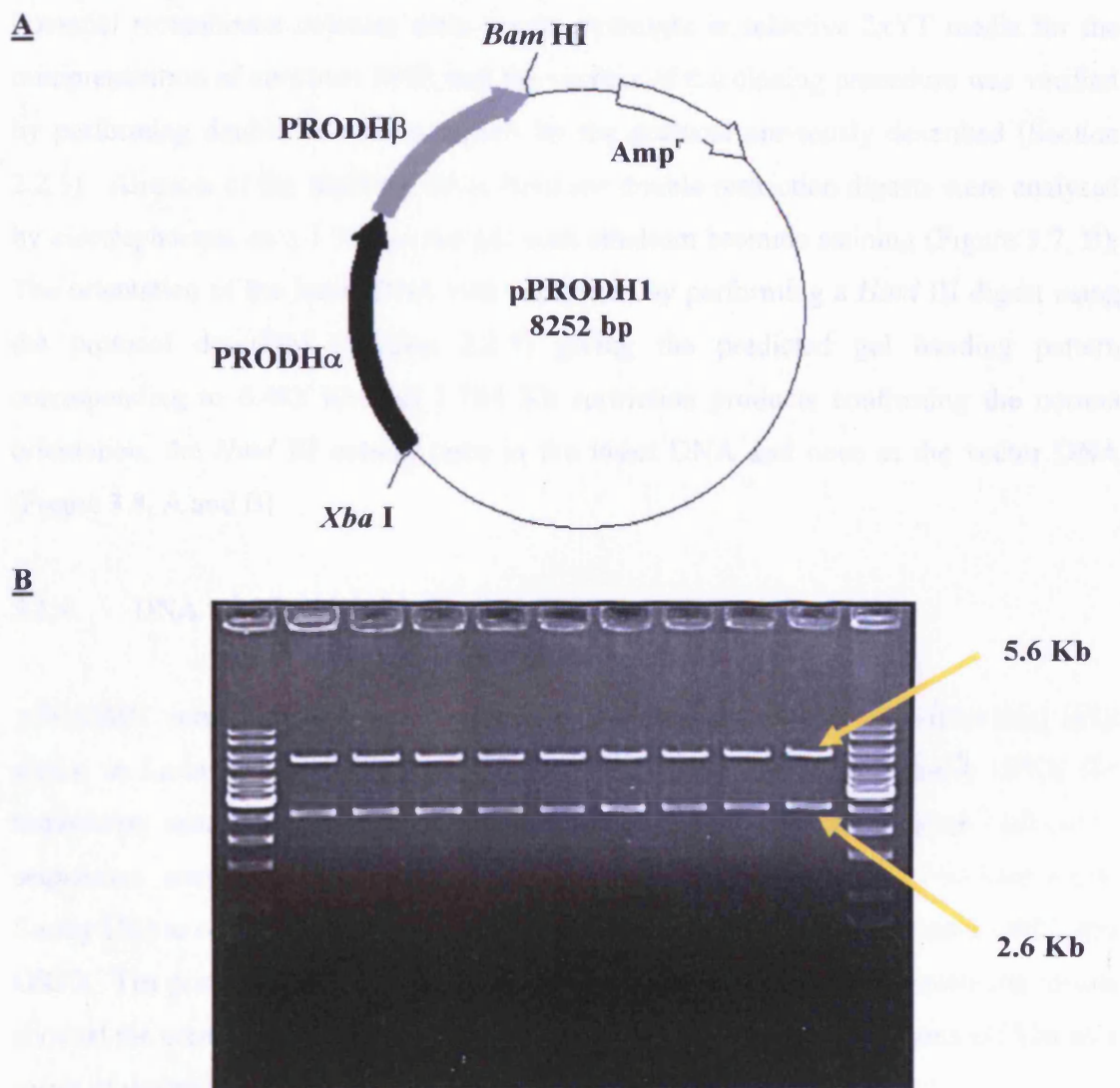
Figure 3. 7. Map of the pPRODH1 construct harbouring the cloned target DNA sequence and restriction digest analysis of plasmid to confirm positive clones. *Panel A*, diagram of the pPRODH1 construct map. The relative position of the first ORF (encoding the PRODH α subunit [PRODHα]) is shown coloured black and the second ORF (encoding the PRODH β subunit [PRODHβ]) immediately downstream of ORF1 is coloured grey. The *Xba* I and *Bam* HI restriction sites engineered for directional cloning of the target DNA are illustrated and the gene encoding β-lactamase to confer ampicillin resistance on the host cell is coloured white (designated Amp^r). *Panel B*, 1 % agarose gel of electrophoresed pPRODH1 digest products of a double restriction reaction with the type II restriction endonucleases *Xba* I and *Bam* HI. Lanes 2-10, the upper band is the larger linearised pET11d vector DNA (5.6 Kb) and the lower band is the smaller cloned insert DNA (2.6 Kb). The restriction lanes are flanked either side by a 1 Kb DNA molecular weight ladder (lanes 1 and 11), the bright band in the centre of the marker ladder has a molecular weight of 3 Kb.

Potential recombinant colonies were grown overnight in selective 2xYT media for the minipreparation of construct DNA and the success of the cloning procedure was verified by performing double restriction digests by the protocol previously described (Section 2.2.5). Aliquots of the resulting DNA from the double restriction digests were analysed by electrophoresis on a 1 % agarose gel with ethidium bromide staining (Figure 3.7, B). The orientation of the insert DNA was confirmed by performing a *Hind* III digest using the protocol described (Section 2.2.5) giving the predicted gel banding pattern corresponding to 6.482 Kb and 1.764 Kb restriction products confirming the correct orientation, the *Hind* III cutting once in the insert DNA and once in the vector DNA (Figure 3.8, A and B).

3.2.4. DNA SEQUENCING

pPRODH1 construct DNA was purified by minipreparation from XL1-Blue host cells grown in Luria-Bertani (LB) broth for optimal propagation of high quality DNA for sequencing using the protocol described (Section 2.2.5). MJ BaseStation automated sequencers were employed utilizing BigDye sequencing chemistry (GRI Genomics, Surrey UK) to completely sequence the insert region of pPRODH1 comprising ORF1 and ORF2. Ten primers were used for the sequencing cycles (Table 2.3). Sequencing results showed the complete native sequence had been preserved with no mutations evident as a result of the two PCR experiments (Figure 3.9).

3.2.5. MOLECULAR BIOLOGY OF THE SYSTEM USED FOR RECOMBINANT EXPRESSION

The *E. coli* strain BL21(DE3) contains a chromosomal copy of the gene that encodes T7 RNA polymerase. These BL21(DE3) hosts contain lysogenic DE3 bacteriophage that are lambda derivatives containing the immunity region of phage 21, the promoter region *lacUV5*, the *lacI* gene and the gene encoding T7 RNA polymerase (Studier and Moffatt, 1986). T7 RNA polymerase transcription is mediated solely by the *lacUV5* promoter, which in turn can be chemically induced by isopropyl-β-D-thiogalactopyranoside (IPTG).

A

ORFs:
a: 492 aa
b: 382 aa

Hind III

Hind III

pPRODH1
8252 bp

B

1   2   3   4   5

Undigested

6.48 Kb

1.76 Kb
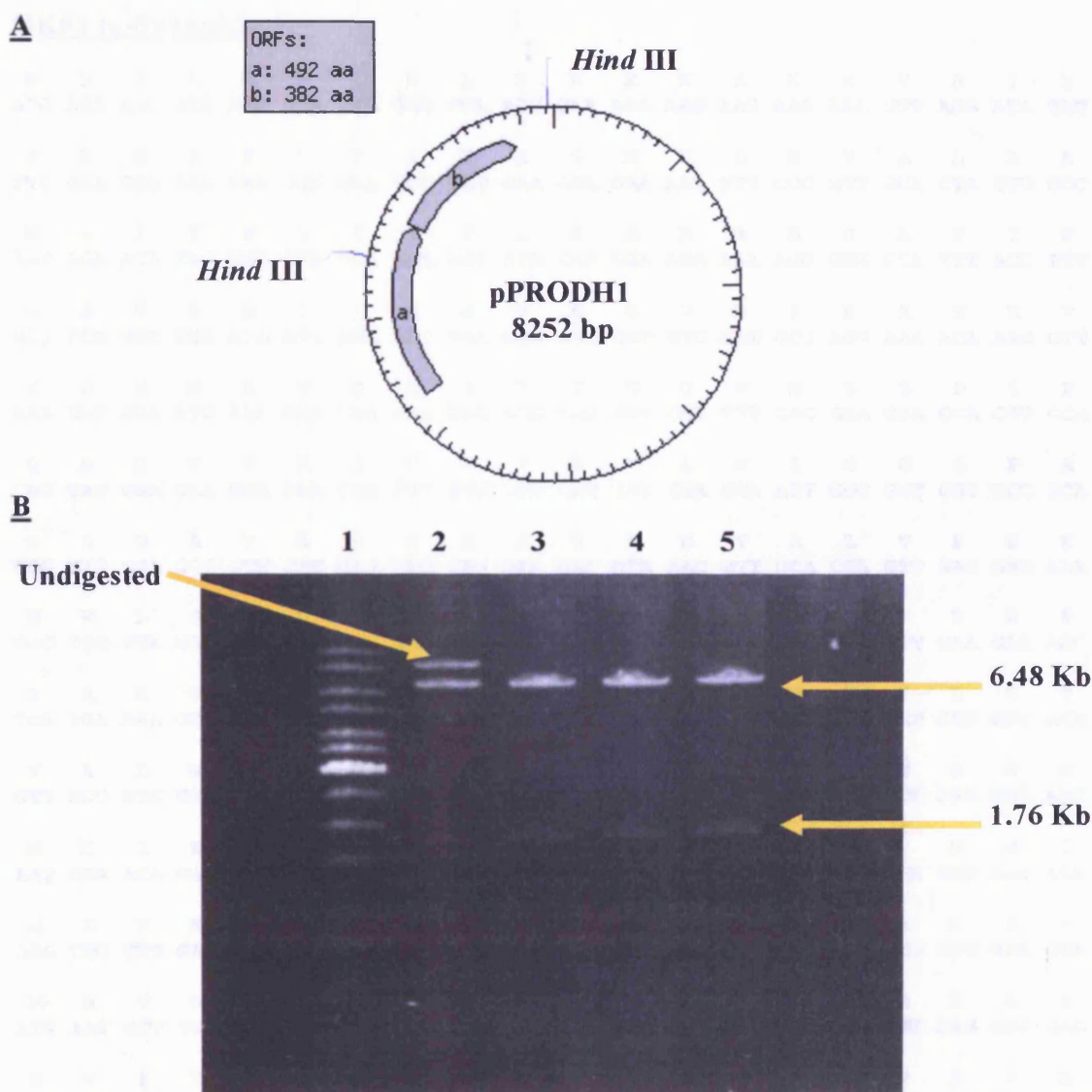
Figure 3. 8. *Hind* **III restriction digest analysis of pPRODH1 construct to confirm the correct orientation of the cloned target DNA insert.** *Panel A,* figure of the pPRODH1 construct map showing the location of the two *Hind* III restriction sites relative to the position of the cloned DNA region that is illustrated by the two grey shaded arrows (a and b refer to ORF1 and ORF2 respectively). The amino acid sequence length of the ORF expression products are given in the key. The construct map was generated using NEB cutter V.2.0 (http://tools.neb.com/NEBcutter2/index.php). *Panel B,* 1% agarose gel of electrophoresed pPRODH1 digest products of a restriction reaction with the type II restriction endonuclease *Hind* III that cuts once in the cloned insert DNA sequence and once in the vector DNA sequence. Lane 1, 1 Kb DNA molecular weight ladder; lanes 2-5, *Hind* III digested pPRODH1. The 6.48 Kb and 1.76 Kb restriction products confirmed that the target DNA was ligated into the pET11d vector in the correct orientation.

ORF1 (α-Subunit)

```
M   R   N   L   R   P   L   D   L   T   E   K   K   K   K   K   V   R   I   Y
ATG AGA AAC TTG AGG CCA CTA GAC TTA ACG GAA AAG AAG AAG AAA AAA GTT AGG ATA TAT

F   E   G   K   E   L   E   A   Y   E   G   E   K   L   P   V   A   L   L   A
TTC GAA GGG AAG GAA CTG GAA GCC TAT GAA GGA GAA AAA TTG CCC GTT GCA CTA TTG GCC

N   G   I   Y   W   L   T   T   S   L   E   G   R   K   R   G   A   F   T   F
AAT GGA ATA TAC TGG CTA ACA ACA AGC CTA GAA GGA AGA AAA AGG GGG GCA TTT ACC TTT

G   P   V   P   M   I   I   N   G   V   K   G   V   D   A   R   K   T   K   V
GGT CCA GTC CCA ATG ATC ATA AAT GGA GTA AAG GGT GTC GAT GCT AGG AAA ACA AAG GTT

K   D   G   M   K   V   Q   R   Q   T   Y   G   D   F   H   E   E   P   L   P
AAA GAT GGA ATG AAA GTA CAA AGA CAA ACC TAC GGT GAT TTT CAC GAA GAA CCA CTT CCA

Q   D   G   E   V   K   Q   V   V   V   D   V   L   V   I   G   G   G   P   A
CAG GAT GGA GAA GTA AAA CAA GTT GTG GTT GAT GTT TTA GTA ATT GGC GGT GGC CCC GCA

G   L   G   A   V   L   E   M   Q   E   H   L   N   V   A   L   V   E   E   K
GGG CTG GGA GCT GTT CTT GAG ATG CAG GAA CAC CTA AAC GTT GCA CTA GTT GAG GAG AAA

G   W   L   G   G   D   M   F   L   K   T   S   T   A   E   G   F   E   E   S
GGC TGG TTA GGT GGG GAT ATG TTT TTA AAG ACT TCA ACA GCG GAG GGC TTT GAA GAA AGC

S   R   K   V   V   D   K   L   A   K   E   V   K   A   N   V   Y   L   G   T
TCA AGA AAA GTC GTT GAT AAG CTC GCT AAA GAA GTT AAA GCT AAT GTA TAT CTT GGC ACA

V   A   L   G   V   F   D   K   G   E   Y   F   L   V   P   A   T   K   G   N
GTT GCC CTG GGA GTT TTT GAT AAA GGG GAA TAC TTT CTA GTT CCA GCA ACT AAA GGA AAT

N   L   I   E   F   L   A   K   R   V   V   L   A   T   G   A   V   D   N   I
AAT CTA ATA GAA TTT CTG GCT AAA AGG GTA GTT TTA GCT ACT GGT GCG GTG GAT AAC ATA

M   L   F   E   N   N   D   M   P   G   V   F   R   R   D   F   A   L   E   V
ATG CTC TTT GAA AAC AAC GAC ATG CCT GGG GTC TTT AGG CGT GAT TTT GCG CTT GAG GTA

M   N   V   W   E   V   A   P   G   W   N   V   A   V   T   G   S   K   A   E
ATG AAC GTT TGG GAA GTA GCT CCA GGT TGG AAT GTA GCT GTT ACT GGA AGT AAG GCG GAG

E   V   I   Y   E   L   E   R   W   G   I   D   Y   V   E   V   P   S   V   K
GAA GTA ATA TAT GAA CTC GAG AGA TGG GGA ATT GAT TAC GTA GAG GTG CCC TCT GTA AAA

R   V   E   G   K   E   K   V   E   K   V   I   D   F   N   G   N   E   Y   K
AGG GTT GAA GGG AAA GAG AAG GTT GAG AAG GTT ATT GAC TTC AAT GGA AAT GAG TAC AAG

V   D   A   I   I   F   A   D   G   K   R   P   D   I   N   P   I   T   Q   A
GTT GAT GCA ATA ATA TTT GCT GAT GGT AAA AGG CCT GAC ATA AAT CCC ATT ACC CAG GCA

G   G   K   L   H   F   R   R   G   Y   Y   R   P   V   V   N   E   Y   N   Q
GGA GGA AAA TTA CAC TTT AGG AGG GGA TAT TAT AGG CCC GTT GTA AAT GAA TAT AAC CAG

I   R   E   G   V   Y   V   A   G   S   A   V   T   I   K   P   H   Y   T   N
ATT AGA GAG GGG GTA TAT GTA GCA GGC AGT GCA GTG ACG ATA AAG CCC CAC TAT ACA AAT

Y   L   E   G   R   L   V   G   A   Y   I   L   R   E   F   G   I   D   S   E
TAC CTG GAA GGA AGG CTA GTT GGA GCA TAT ATT CTT AGG GAA TTT GGA ATA GAT TCA GAA

P   C   I   Y   K   E   K   L   K   E   F   E   P   E   A   L   P   V   P   K
CCA TGC ATA TAC AAA GAA AAG CTT AAG GAA TTT GAA CCT GAA GCT CTT CCT GTG CCA AAA
```

```
I   P   I   N   K   L   N   L   D   D   V   Q   I   C   G   C   D   V   S   L
ATC CCA ATA AAC AAG CTG AAC TTG GAT GAC GTC CAG ATA TGT GGA TGT GAT GTC TCC TTA

R   K   V   Y   D   V   V   E   K   G   I   T   D   L   Q   I   I   K   R   L
AGA AAG GTA TAT GAT GTA GTC GAA AAG GGC ATA ACA GAT CTT CAA ATA ATT AAA AGG TTA

T   H   L   A   M   G   F   C   Q   G   R   F   C   L   F   N   G   A   A   V
ACC CAT CTA GCT ATG GGC TTT TGC CAG GGA CGT TTC TGC CTC TTC AAT GGG GCA GCA GTT

V   S   Q   V   T   G   I   K   L   G   E   I   D   L   P   V   A   R   P   P
GTT TCC CAG GTT ACG GGA ATT AAG CTA GGT GAA ATA GAC CTA CCT GTG GCA AGG CCC CCA

I   K   T   V   K   L   G   I   L   S   R   R   *
ATA AAA ACC GTA AAG TTA GGA ATT CTA TCT AGG AGG TGA (1479 bp) GAGGG
                                            ‾‾‾‾‾‾‾   ‾‾‾‾‾‾‾‾‾‾‾‾‾‾
```

ORF2 (β-Subunit)   ORF2 RBS   *SPACER SEQUENCE*

```
M   I   P   E   K   S   E   I   V   V   I   G   G   G   I   V   G   V   T   I
ATG ATT CCA GAA AAA AGT GAA ATT GTC GTG ATT GGT GGG GGT ATT GTT GGA GTT ACG ATA

A   H   E   L   A   K   R   G   E   E   V   T   L   V   E   K   R   F   I   G
GCT CAT GAG CTC GCT AAG AGA GGA GAA GAA GTT ACC CTC GTT GAG AAG AGG TTC ATT GGT

S   G   S   T   F   R   C   G   T   G   I   R   Q   Q   F   N   D   E   A   N
TCT GGC TCA ACT TTT AGA TGT GGA ACG GGA ATT AGA CAG CAA TTT AAC GAT GAA GCA AAC

V   Q   V   M   K   R   S   V   E   L   W   K   K   Y   S   E   E   Y   G   F
GTT CAA GTT ATG AAG CGC TCT GTA GAG CTT TGG AAG AAG TAC AGT GAA GAA TAT GGT TTT

K   F   E   Q   T   G   Y   L   F   L   L   Y   D   D   E   E   V   E   I   F
AAG TTC GAG CAA ACA GGT TAC CTC TTC TTA TTG TAT GAT GAT GAG GAA GTT GAG ATA TTT

K   Q   N   I   K   I   Q   N   K   F   G   V   P   T   R   L   I   T   P   E
AAG CAA AAC ATA AAG ATC CAG AAC AAA TTT GGA GTT CCT ACT AGG TTG ATA ACC CCA GAA

E   A   K   E   I   V   P   L   L   D   I   S   E   V   I   A   A   S   W   N
GAG GCG AAG GAG ATA GTT CCA CTC TTG GAT ATA AGC GAA GTA ATC GCA GCT TCG TGG AAT

P   T   D   G   K   A   D   P   F   H   S   T   T   A   F   A   L   K   A   K
CCA ACG GAT GGA AAA GCA GAT CCG TTT CAC TCT ACA ACG GCC TTT GCA CTT AAG GCA AAG

E   Y   G   A   K   I   L   E   Y   T   E   V   K   G   F   I   I   E   N   N
GAG TAT GGT GCA AAA ATA CTT GAA TAC ACG GAG GTA AAG GGA TTT ATC ATC GAA AAT AAT

E   I   K   G   V   K   T   N   R   G   V   I   K   T   G   I   V   V   N   A
GAG ATT AAG GGA GTA AAA ACA AAT AGA GGG GTA ATA AAG ACG GGG ATT GTT GTA AAC GCA

T   N   A   W   A   K   L   I   N   A   M   A   G   I   K   T   S   I   P   I
ACT AAT GCA TGG GCA AAG TTG ATA AAT GCT ATG GCT GGT ATT AAA ACT TCC ATT CCA ATT

E   P   Y   K   H   Q   A   V   I   T   Q   P   I   K   R   G   T   I   K   P
GAG CCC TAC AAG CAT CAA GCA GTG ATA ACC CAA CCG ATT AAA AGA GGA ACT ATA AAG CCG

M   V   I   S   F   K   Y   G   H   A   Y   L   T   Q   T   A   H   G   G   I
ATG GTC ATA TCT TTC AAG TAT GGT CAC GCT TAT TTA ACA CAA ACT GCG CAT GGA GGG ATT

I   G   G   V   G   Y   E   V   G   P   T   Y   D   L   T   P   T   Y   E   F
ATA GGA GGA GTT GGT TAT GAA GTG GGG CCA ACA TAT GAC TTG ACT CCA ACT TAT GAG TTT

L   R   E   V   S   Y   Y   F   S   K   I   I   P   A   L   K   N   L   L   I
CTA AGA GAA GTT AGC TAC TAT TTC TCA AAG ATA ATA CCA GCT CTA AAG AAT CTA CTA ATC
```

```
 L   R   T   W   A   G   Y   Y   A   K   T   P   D   S   N   P   A   I   G   K
CTA AGA ACC TGG GCA GGT TAT TAC GCA AAA ACT CCC GAC AGT AAC CCA GCT ATC GGG AAA

 V   E   G   V   S   D   Y   Y   I   A   A   G   F   S   G   H   G   F   M   M
GTT GAA GGT GTA AGT GAT TAT TAC ATC GCT GCA GGA TTT TCA GGG CAT GGA TTT ATG ATG

 A   P   A   V   A   E   M   V   A   D   L   I   T   K   G   K   T   E   L   P
GCT CCA GCG GTA GCT GAG ATG GTT GCT GAT TTA ATC ACA AAA GGT AAG ACA GAA CTT CCA

 V   E   W   Y   D   P   H   R   F   E   R   G   E   L   R   T   V   A   L   Q
GTA GAG TGG TAC GAT CCT CAC AGA TTT GAA AGG GGA GAA TTA AGA ACT GTT GCT CTT CAA

 M   G   *
ATG GGT TGA(1149 bp)
```

Figure 3. 9. Sequence of the cloned target DNA region holding ORF1 and ORF2 that comprise the operon that encodes for the α and β subunits of PRODH in *P. furiosus*. The initiation codon of both ORF's are shown in blue. The cognate amino acid residue is given above each corresponding DNA codon. The termination codon of each ORF is highlighted by a red asterisk. The ribosome-binding site (RBS) for ORF2 translation is labelled and shown double-underlined and italicised. The spacer sequence between the RBS and initiation codon of ORF2 is labelled and underlined.

Therefore, the BL21(DE3) lysogen strain is a good host for recombinant protein expression since addition of mM amounts of IPTG to a growing culture induces T7 RNA polymerase expression, the T7 RNA polymerase in turn mediating expression of the target gene sequence in pPRODH1. The translation vector pET11d was used to construct pPRODH1 as to increase plasmid stability, post transformation. There is still some basal level of T7 RNA polymerase expression in λDE3 lysogens from the _lacUV5_ promoter even in the complete absence of IPTG. This is a major problem if the target gene product is toxic to the host cell, therefore preventing plasmid establishment. pET11d, as previously stated carries the T7_lac_ promoter (Studier _et al._, 1990), the _lac_ operator sequence downstream of the T7 promoter and the _lac_ repressor (_lacI_) which is positioned as to result in the divergence of both the T7 _lac_ and _lacI_ promoters. When pET11d is transformed into BL21(DE3), the _lac_ repressor interacts with both the _lacUV5_ promoter in the BL21(DE3) chromosome as to repress T7 RNA polymerase gene transcription by the host polymerase and with the T7_lac_ promoter carried by pET11d as to inhibit target gene transcription by any surplus T7 RNA polymerase that is expressed. Therefore, using pET11d as the translation vector to carry the target gene increases the possibility of plasmid establishment within the host cell.

3.2.6.   STRAIN SCREENING FOR RECOMBINANT EXPRESSION OF PRODH FROM pPRODH1

Expression strain screening was carried out as previously described (Section 2.4.2). No expression of the α and β subunits of PRODH was observed with BL21(DE3) competent cells, therefore, BL21(DE3)pLysS competent cells were screened for expression suitability in the subsequent expression trial utilising the pLysS plasmid to provide additional stability to the target gene. The pLysS compatible plasmid expresses small quantities of T7 lysozyme that works as to inhibit T7 RNA polymerase (Mofatt and Studier, 1987), pLysS therefore makes plasmid constructs carrying target genes encoding gene products toxic to the _E.coli_ host cell more stable. A third strain of BL21(DE3) derivative cells called Rosetta(DE3)pLysS were also screened for heterologous expression suitability. This strain carries a compatible plasmid called pLysSRARE that

contains a chloramphenicol-resistance gene and carries genes that encode tRNAs for the codons AUA AGG AGA CUA CCC GGA that are rarely used in *E. coli* but which manifest in the archaeal cloned DNA sequence of the pPRODH1 construct. The high frequency of rare codons in target gene sequences has been shown experimentally to be a cause of low level recombinant protein expression (Zhang *et al.*, 1991; Sorensen *et al.*, 1989). This translational inhibitory effect appears to be most acute when multiple rare codons are apparent at the amino terminus (Chen and Inouye 1990) and more specifically, when these rare codons are the Arginine codons AGA and AGG appearing consecutively (Brinkmann *et al.*, 1989; Hua *et al.*, 1994; Schenk *et al.*, 1995; Zhan, 1996; Calderone *et al.*, 1996). Of these codons classified as rare in highly expressed *E.coli* genes, only a subset have cognate charged tRNA molecules that are present in low enough cellular concentrations as to have an inhibitory effect on translation elongation (Ikemura, 1985). Rare codons apparent in the primary sequence of the α and β subunits of PRODH are given in Tables 3.2 and 3.3, respectively.

SDS-PAGE results showed recombinant protein expression of both the PRODH α and β subunits in the Rosetta(DE3)pLysS cells and possible isolated expression of the β subunit in the BL21(DE3)pLysS cells (Figure 3.10). Recombinant expression of the α subunit of PRODH in Rosetta(DE3)pLysS cells occurs because the second codon in ORF1 of the PRODH operon in pPRODH1 is the rare Arg codon (AGA) that is translated by the cognate charged tRNA molecule expressed from the pLysSRARE compatible plasmid of the Rosetta strain. The β subunit was unable to be purified after isolated expression in BL21(DE3)pLysS cells possibly due to instability of the subunit when not in complex with the α subunit. Also, lower levels of β subunit expression in the BL21(DE3)pLysS cells in comparison to the Rosetta(DE3)pLysS cells could be a direct result of the translational coupling mechanism employed for the cloned operon. Translation of the distal gene (β subunit) is partially inhibited by the inability of the BL21(DE3)pLysS host to translate the proximal gene (α subunit encoding) due to the presence of rare codons in the proximal gene for which this cell line does not harbour sufficient amounts of the cognate charged tRNA molecules. The Rosetta(DE3)pLysS competent cells were therefore used for the expression of PRODH for the remainder of the project.

Amino Acid	Rare Codon	Frequency of Occurrence
Arginine	CGA	0
	CGG	0
	AGG	17
	AGA	7
Glycine	GGA	22
	GGG	9
Isoleucine	AUA	18
Leucine	CUA	13
Proline	CCC	7
Threonine	ACG	3

Table 3. 2. Table showing the frequency of rare codons and the amino acid encoded for in the DNA sequence of ORF1. The genes encoding the cognate charged tRNA molecules for the rare codons found in the DNA sequence of ORF1 are all carried on the compatible plasmid pLysSRARE of the Rosetta(DE3)pLysS expression host strain. The rare arginine codons 'AGA' (codon two) and 'AGG' (codon five) are situated early in the ORF1 DNA sequence and may have contributed to the inhibition of recombinant expression of the α subunit of PRODH in non-pLysSRARE harbouring expression host strains such as BL21(DE3)pLysS.

Amino Acid	Rare Codon	Frequency of Occurrence
Arginine	CGA	0
	CGG	0
	AGG	3
	AGA	9
Glycine	GGA	15
	GGG	7
Isoleucine	AUA	15
Leucine	CUA	5
Proline	CCC	2
Threonine	ACG	6

Table 3. 3. Table showing the frequency of rare codons and the amino acid encoded for in the DNA sequence of ORF2. The genes encoding the cognate charged tRNA molecules for the rare codons found in the DNA sequence of ORF2 are all carried on the compatible plasmid pLysSRARE of the Rosetta(DE3)pLysS expression host strain. Non of the rare codons are situated early enough in the DNA sequence of ORF2 to adversely affect recombinant expression of the β subunit of PRODH with the rare glycine codon 'GGG' being the earliest of the specified rare codons at sequence position thirteen.
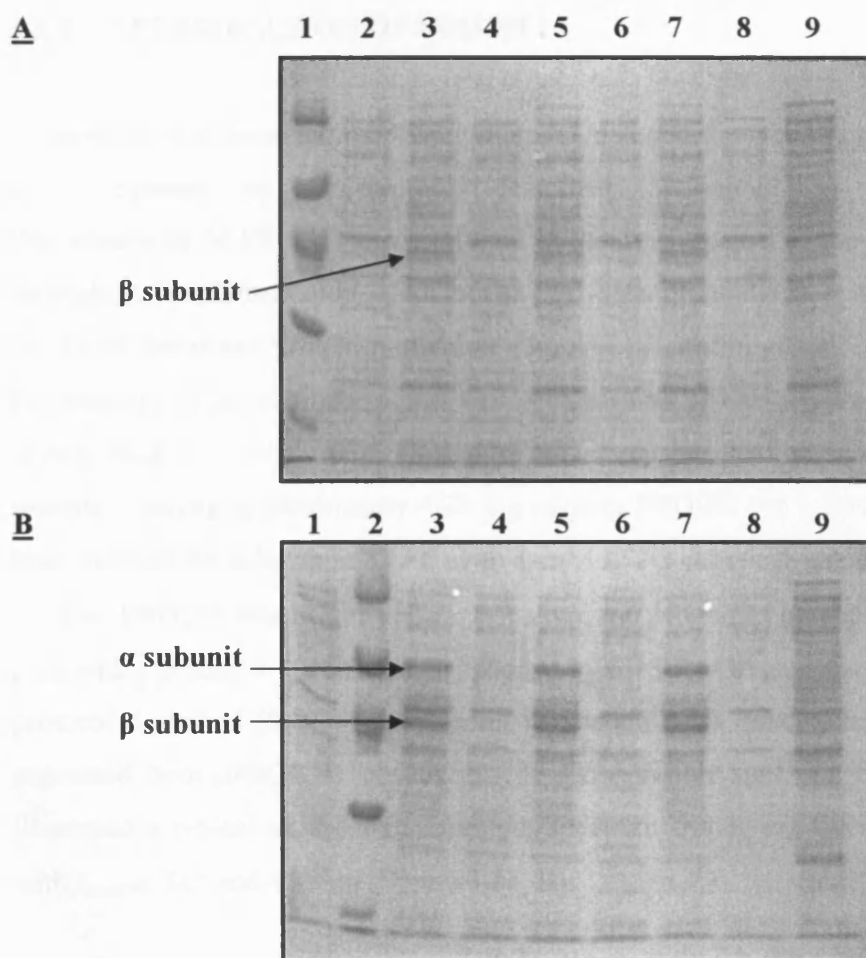
Figure 3. 10. SDS-PAGE analysis of the expression of recombinant PRODH during the screening of various DE3 lysogen expression host cells transformed with pPRODH1. *Panel A*, expression trial with *E. coli* strain BL21(DE3)pLysS as host cell: Lane 1, low molecular weight marker (97, 66, 45, 30, 20.1 and 14.4 KDa from top to bottom of the gel); lanes 2, 4, 6 and 8, cell lysate samples of uninduced cells; lanes 3, 5, 7, and 9, lysate samples of the same cell cultures after chemical induction with IPTG to 1 mM final concentration. Isolated expression of the β subunit of PRODH is evident from analysis of the gel. The protein band corresponding to the approximate molecular weight of the β subunit is labelled in lane 3 (induced). Moreover, no protein band of the same molecular weight is observed in any of the uninduced lysate samples. *Panel B*, expression trial with *E. coli* strain Rosetta(DE3)pLysS as host cell: Lane 2, low molecular weight marker as for panel A; lanes 1, 4, 6 and 8, cell lysate samples of uninduced cells; lanes 3, 5, 7 and 9, lysate samples of the same cell cultures after chemical induction with IPTG to 1 mM final concentration. Stoichiometric expression of both the α and β subunits of PRODH is evident from analysis of the gel. The protein bands corresponding to the induced expression of the recombinant α and β subunits are labelled in lane 3 (induced). No observable expression of protein bands of the same molecular weight is evident in any of the uninduced lysate samples.

3.2.7. PURIFICATION OF PRODH

A purification scheme for PRODH was developed and the recombinant enzyme purified to homogeneity by the protocol described (Section 2.4.3). The exceptional thermostability of PRODH was exploited in the development of the purification scheme through the implementation of an initial heat-denaturation step at 80 °C/1 hr post cell lysis with denatured protein particulate removal by centrifugation. This step denatured the majority of contaminating host cell proteins and proved a very effective and time-saving stage of purification. The entire three-step purification scheme took 48 hrs to execute, yielding approximately 4.25 mg of pure PRODH per 1 litre of culture that had been induced for 8 hours at 37 °C with 1 mM IPTG chemical inducer (Figure 3.11, A). Purified PRODH was bright yellow in colour and judged to be approximately 90-95 % pure with a subunit 1:1 stoichiometry judged by SDS-PAGE analysis performed using the protocol described (Section 2.4.1; refer to section 3.2.8 concerning purity of PRODH expressed from pPRODH1 construct). The UV-Visible spectrum for purified PRODH illustrated a typical oxidised flavoprotein spectrum displaying flavin absorbance peaks with λ_{max} at 365 and 450 nm (Figure 3.11, B).

3.2.8. N-TERMINAL SEQUENCING OF PRODH

N-terminal sequencing of the α and β subunits of PRODH and that of a contaminating intermediate band visualised by SDS-PAGE (see Figure 3.11, A) was performed by the Protein and Nucleic Acid Sequencing Laboratory (PNACL), University of Leicester, UK using the protocol described (Section 2.5.1). The results of this analysis confirmed that the purified subunits were that of PRODH expressed from the pPRODH1 construct and also identified the intermediate contaminating band to be a sub-population of truncated α subunit. Approximately 13.2 % of the α subunit was shown to be truncated based on the pmol yield from automated N-terminal sequence analysis (Table 3.4). The sequence MKVQRQ was obtained for the truncated α subunit N-terminal sequence, whereas the sequence MRNLRP was obtained for approximately 86.8 % of the sample (full length α subunit). These results indicated that the truncation in the α subunit is located 83 amino

A

B
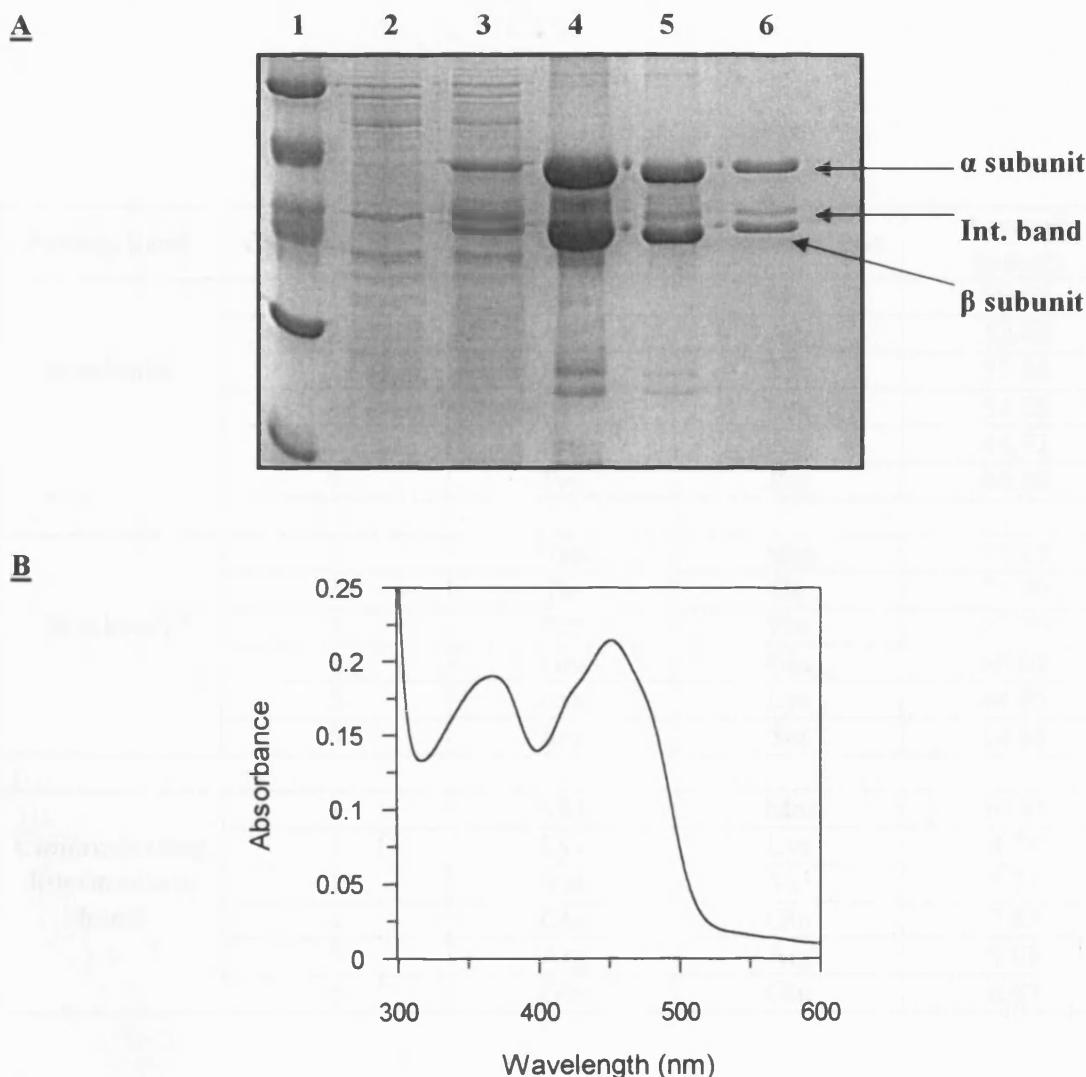
Figure 3. 11. SDS-PAGE analysis of the purification of recombinant wild-type PRODH from *E. coli* strain Rosetta(DE3)pLysS transformed with pPRODH1 and UV-visible spectrum of pure PRODH. *Panel A*, SDS-PAGE purification gel: Lane 1, molecular weight marker (97, 66, 45, 30 and 20.1 KDa from top to bottom of the gel); lane 2, uninduced cell lysate; lane 3, Induced cell lysate (1 mM IPTG); lane 4, sample after heat-denaturation at 80 °C and clarification by centrifugation; lane 5, pooled fractions following anion-exchange chromatography (Q-sepharose); lane 6, pooled fractions following size-exclusion chromatography (Superdex 75) showing the pure α and β subunits of PRODH. A contaminating band was evident with a larger molecular weight than the PRODH β subunit as indicated on the gel (Int. band) that accounted for approximately 5-10 % of protein in the purified solution. *Panel B*, UV-visible absorption spectrum of recombinant wild-type PRODH of *P. furiosus* expressed from construct pPRODH1. The absorption spectrum recorded between 300-600 nm is typical of a flavoprotein spectrum. Flavin peaks are at 365 and 450 nm. Conditions: 100mM potassium phosphate buffer pH 7.5; 25 °C, enzyme concentration 13 μM.

Protein band	Cycle number	Predicted residue	Actual residue	Amount (pmol)
α-subunit	1	Met	Met	59.04
	2	Arg	Arg	52.08
	3	Asn	Asn	57.66
	4	Leu	Leu	54.28
	5	Arg	Arg	44.91
	6	Pro	Pro	46.80
β-subunit	1	Met	Met	75.15
	2	Ile	Ile	71.70
	3	Pro	Pro	67.79
	4	Glu	Glu	60.03
	5	Lys	Lys	44.85
	6	Ser	Ser	14.63
Contaminating intermediate band	1	Met	Met	10.81
	2	Lys	Lys	4.71
	3	Val	Val	8.71
	4	Gln	Gln	7.83
	5	Arg	Arg	9.03
	6	Gln	Gln	6.93

Table 3. 4. Table showing the N-terminal sequencing results for the recombinant α and β subunits of PRODH expressed from construct pPRODH1 and the intermediate molecular weight contaminating band observed by SDS-PAGE analysis. The first six amino-terminal residues of each protein band were sequenced and results confirmed the predicted sequence for both the α and β subunits with translation starting from the correct predicted initiating methionine residue. Sequencing of the contaminating protein band showed this to be truncated α subunit. 13.2 % of the α subunit was found to be truncated as judged from the pmol yield of the sequencing results.

acids downstream from the initiating methionine residue in the full-length α subunit. The N-terminal sequence of the β subunit, MIPEKS was not contaminated with underlying sequence, indicating that the β subunit is intact and the protein sequence initiates as predicted by the gene sequence. The purified sample therefore consisted of 93.1 % pure full length αβ heterodimeric PRODH. Initially, the truncated α subunit was thought to be the result of endopeptidase activity, therefore protease inhibitors (Complete protease inhibitor cocktail tablets) were added to cells during the initial cell lysis stage of PRODH purification and the entire purification procedure was performed at 4 °C to minimise proteolysis of the recombinant α subunit. These efforts had a negligible effect on the amount of truncated α subunit produced. The DNA sequence for the region encoding the N-terminal of the truncated contaminating α subunit was therefore re-examined. A putative internal ribosome-binding site with the sequence 'AAGG' was identified within the DNA sequence encoding the α subunit just eleven nucleotides upstream from the initiating methionine residue of the truncated product. This putative internal ribosome-binding site was eradicated by site-directed mutagenesis, the results of which are now discussed in the proceeding section.

3.2.9. SITE-DIRECTED MUTAGENESIS FORMING EXPRESSION CONSTRUCT pPRODH2 TO ERADICATE A GENE-INTERNAL RIBOSOME-BINDING SITE IDENTIFIED IN ORF1

A silent mutation was introduced within the region of the putative internal ribosome-binding site in ORF1 in an effort to diminish the sequence affinity and binding energy between this region and the 3' end of the 16S rRNA sequence of the translating ribosome complex. It was essential that this procedure did not alter the native translated primary sequence of the PRODH α subunit. The AAG codon of Lys79 in ORF1 that formed the main core of the identified 'AAGG' putative internal ribosome-binding site sequence was mutated to the alternative lysine codon sequence AAA in a single site-directed mutagenesis step according to the protocol described (Section 2.2.7). Mutants were identified by DNA sequencing performed by the PNACL by the protocol described

(Section 2.2.7; Figure 3.12). The new construct harboring the silent mutation was designated pPRODH2.

Purification of PRODH expressed from the pPRODH2 construct was achieved using the same purification scheme developed for PRODH expressed from the initial pPRODH1. The enzyme was purified to homogeneity in three steps and in the oxidised monoflavinylated (FAD-bound) form. The crystal structure of PRODH (Section 5.2.5) revealed that the enzyme has three cofactors, one molecule of FAD non-covalently bound to the β subunit, one ATP molecule bound to the α subunit and one molecule of FMN bound non-covalently at the $\alpha\beta$ subunit interface. Binding of the FMN cofactor in PRODH was found to be unstable under the purification conditions employed for solution studies and this aspect of the enzymes solution properties was exploited to isolate PRODH in monoflavinylated form with FAD bound at the active site on the β subunit. PRODH was buffer exchanged against high concentration phosphate buffer pH 7.5 to compete off FMN at the subunit interface as the phosphate moiety of both FMN cofactor and phosphate buffer are mutually exclusive at this binding site. All solution data detailed in this thesis therefore corresponds to the FAD-bound form of recombinant wild-type PRODH unless stated otherwise.

Subsequent SDS-PAGE analysis revealed that the mutagenesis procedure had successfully impeded the expression of the truncated α subunit contaminant (Figure 3.13, A). The UV-visible absorption spectrum of pure PRODH expressed from construct pPRODH2 displayed flavin absorbance peaks with λ_{max} at 367 and 450 nm (Figure 3.13, B). The yield of purified PRODH expressed from pPRODH2 was also greater in comparison to that achieved through pPRODH1 expression with a notable increase in pure protein climbing from an average of 4.25 mg/l culture prior to mutagenesis, to an average yield of 10.23 mg/l culture post-mutation. This increase in protein expression can be explained in terms of ribosome competition. Prior to mutagenesis, in addition to ribosomes translating from the 'correct' ribosome-binding sites for both ORF1 and ORF2, the internal ribosome-binding site in ORF1 would also have hosted ribosome

A
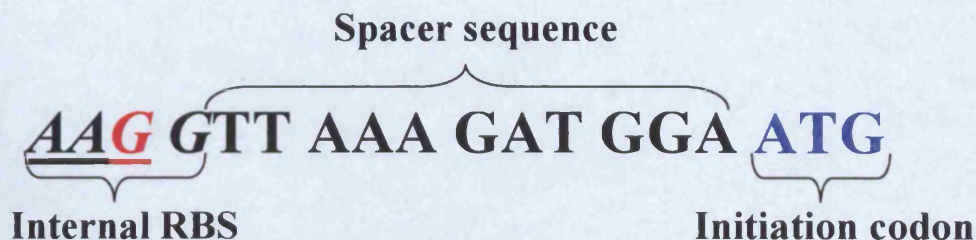
B
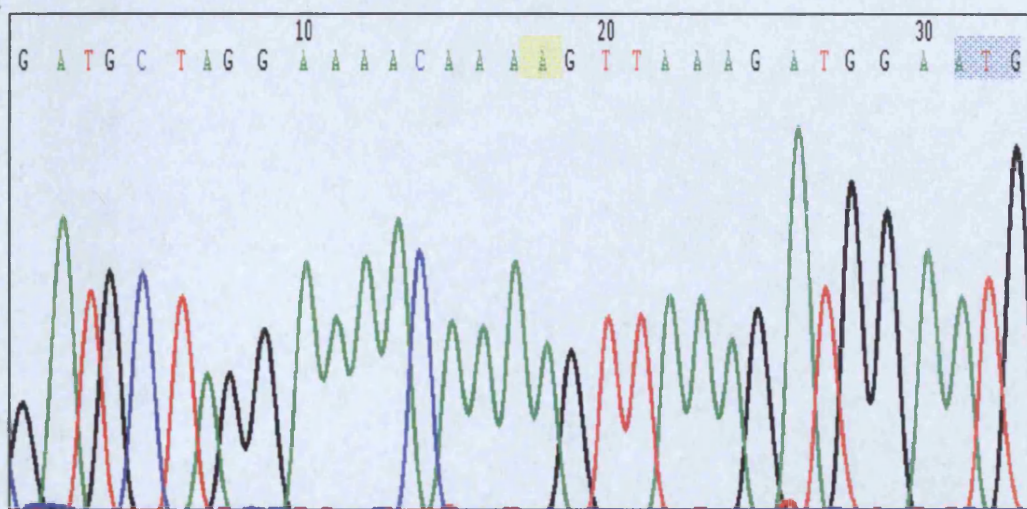
Figure 3. 12. DNA sequence of the region within ORF1 where translation of the truncated α subunit is initiated. *Panel A*, N-terminal sequencing results for the truncated α subunit allowed the initiating methionine codon within ORF1 to be located (blue). Subsequent analysis of the DNA sequence immediately upstream of this codon revealed a putative four nucleotide gene-internal RBS 'AAGG' (italic) eleven nucleotides from the initiation codon. Site-directed mutagenesis of the codon for Lys79 (underlined) from 'AAG' to 'AAA' (nucleotide targeted for mutagenesis is highlighted red) whilst not altering the native sequence at the amino acid level destroyed the gene-internal RBS and effectively eradicated expression of the truncated α subunit form. *Panel B*, chromatogram showing the DNA sequencing results confirming successful mutagenesis of the targeted nucleotide (highlighted yellow). The internal initiation codon is highlighted blue. Chromatograms of DNA sequence data were produced using Chromas v.2.3 (Technelysium).

A

B
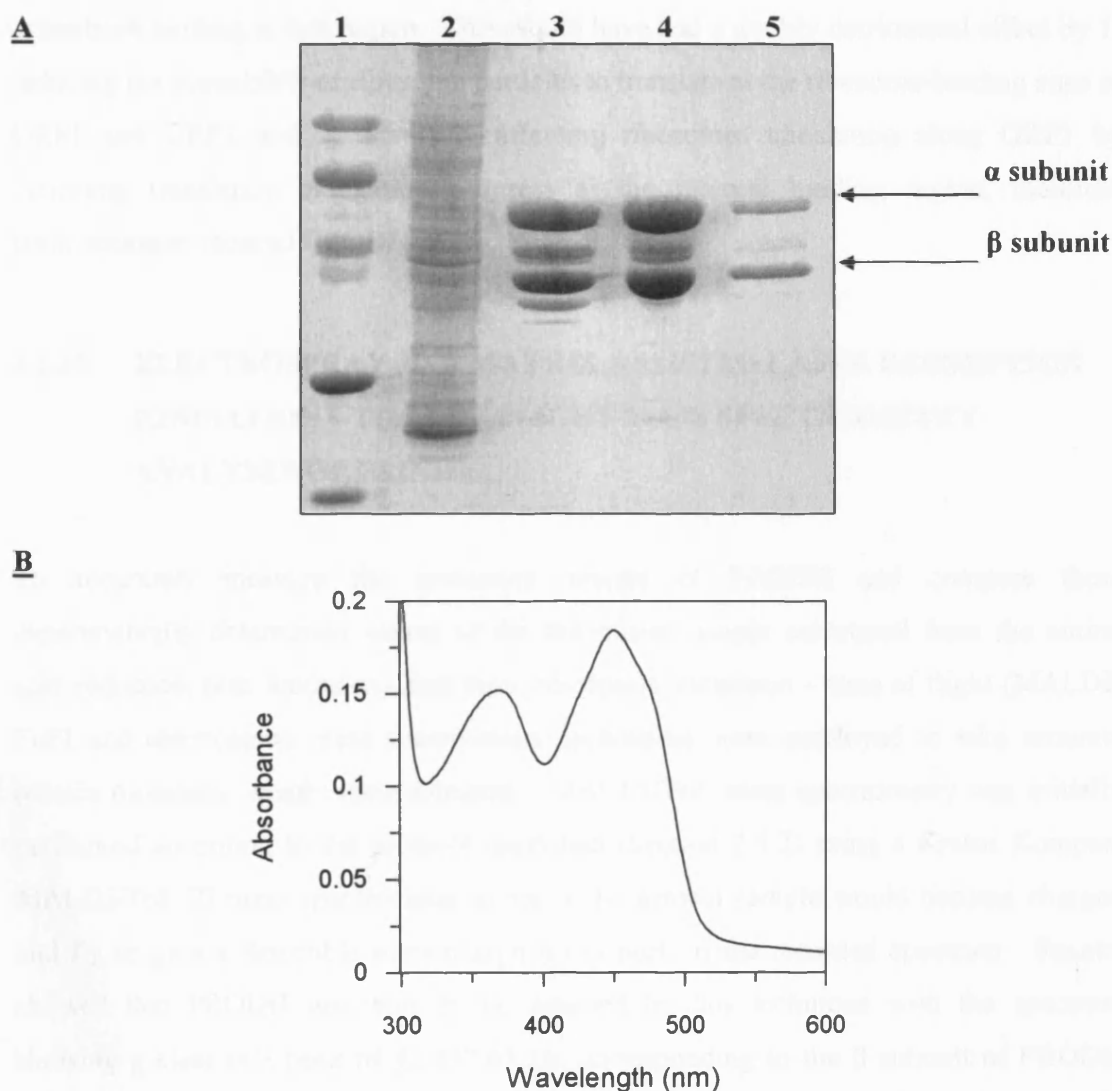
Figure 3. 13. SDS-PAGE analysis of the purification of recombinant wild-type PRODH from *E. coli* strain Rosetta(DE3)pLysS transformed with pPRODH2 and UV-visible spectrum of pure PRODH. *Panel A*, SDS-PAGE purification gel: Lane 1, molecular weight marker (97, 66, 45, 30 and 20.1 KDa from top to bottom of the gel); lane 2, uninduced cell lysate; lane 3, sample after heat-denaturation at 80 °C and clarification by centrifugation; lane 4, pooled fractions following anion-exchange chromatography (Q-sepharose); lane 5, pooled fractions following size-exclusion chromatography (Superdex 75) showing the pure α and β subunits of PRODH. *Panel B*, UV-visible absorption spectrum of recombinant wild-type PRODH of *P. furiosus* expressed from construct pPRODH2. The absorption spectrum recorded between 300-600 nm is typical of a flavoprotein spectrum. Flavin peaks are at 367 and 450 nm. Conditions: 100mM potassium phosphate buffer pH 7.5; 25 °C, enzyme concentration 9 μM.

assemblies binding at this region. This would have had a doubly detrimental effect by 1) reducing the availability of ribosome particles to translate at the ribosome-binding sites of ORF1 and ORF2 and 2) adversely affecting ribosomes translating along ORF1 by inhibiting translation elongation progress at the internal binding region, therefore contributing to reduced PRODH yield.

3.2.10. ELECTROSPRAY AND MATRIX-ASSISTED LASER DESORPTION IONISATION – TIME OF FLIGHT MASS SPECTROMETRY ANALYSES OF PRODH

To accurately measure the molecular weight of PRODH and compare these experimentally determined values to the theoretical weight calculated from the amino acid sequence, both matrix-assisted laser desorption ionisation – time of flight (MALDI-ToF) and electrospray mass spectrometry techniques were employed to take accurate protein molecular weight measurements. MALDI-ToF mass spectrometry was initially performed according to the protocol described (Section 2.5.2) using a Kratos Kompact MALDI-ToF III mass spectrometer to see if the protein sample would become charged and fly to give a detectible mass/charge (m/z) peak in the recorded spectrum. Results showed that PRODH was able to be detected by this technique with the spectrum showing a clear m/z peak of 42,437.65 Da corresponding to the β subunit of PRODH (Figure 3.14) which compares favourably to the predicted mass of 42,481.2 Da from the amino acid sequence of the β subunit. However, the α subunit was unable to be detected by this method possibly due to insufficient laser energy for desorption and ionisation of the larger subunit. Electrospray mass spectrometry was therefore performed to gain a more accurate molecular weight measurement for the β subunit and to see if this technique was capable of detecting the larger α subunit of PRODH. Electrospray mass spectrometric measurements were taken using the protocol described (Section 2.5.2) on a Waters Micromass LCT Time of Flight Mass Spectrometer. Again, no detectible m/z peaks corresponding to the α subunit were evident in the resulting spectrum, although a clear m/z peak of 42,474.0 Da corresponding to the β subunit was evident (Figure 3.15). This value is significantly closer to the predicted molecular mass of the β subunit when
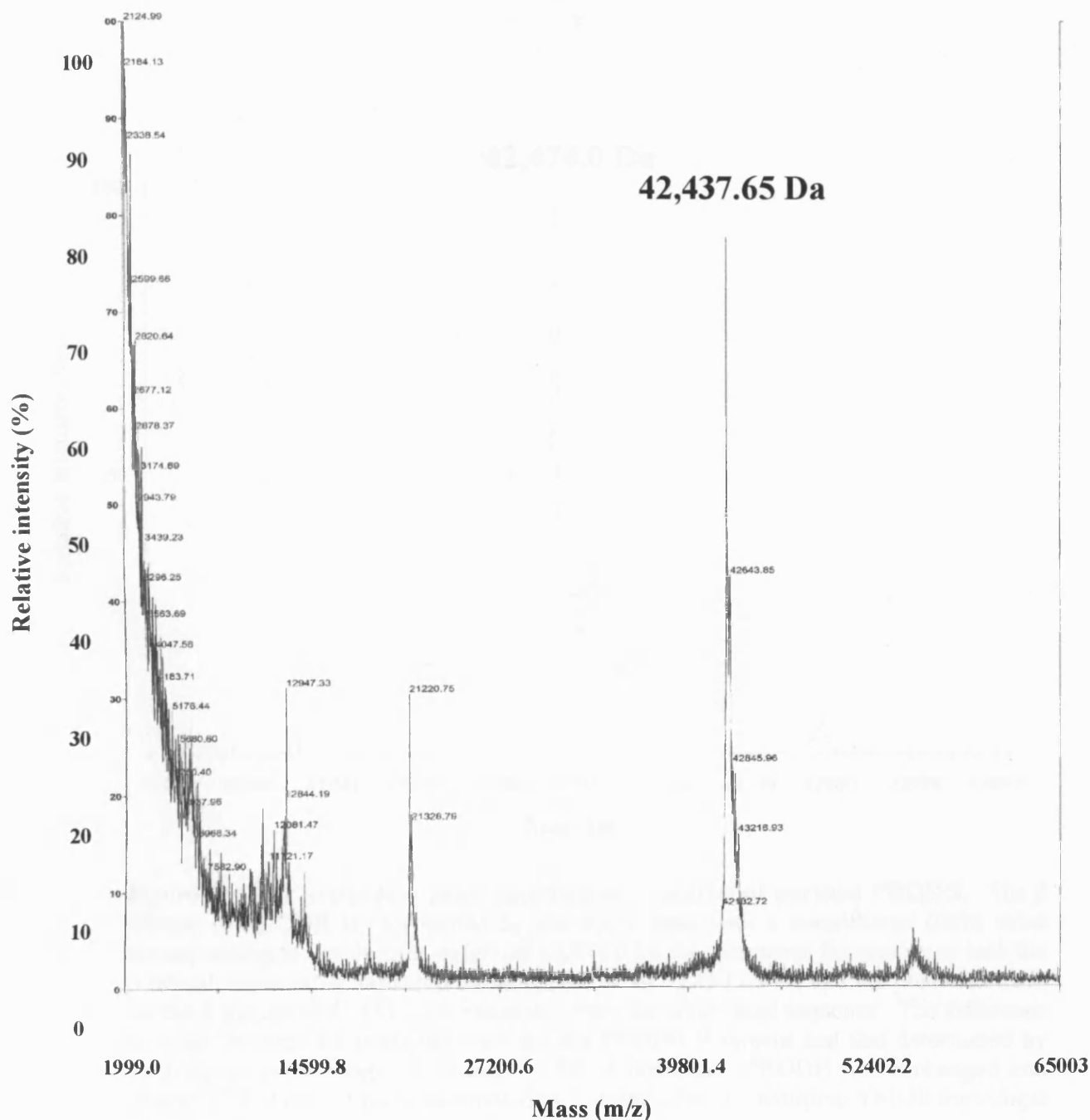
Figure 3. 14. MALDI-ToF mass spectrometry analysis of purified PRODH. The β
subunit of PRODH is clearly visible with a mass/charge (m/z) peak corresponding to a
molecular weight of 42,437.65 Da that compares favourably to the predicted mass for the
β subunit of 42,481.2 Da calculated from the amino acid sequence. Conditions: PRODH
was exchanged into filtered ddH₂O pH 7.0 and concentrated to 1 mg/ml using a
Centriprep YM-30 centrifugal filter membrane.
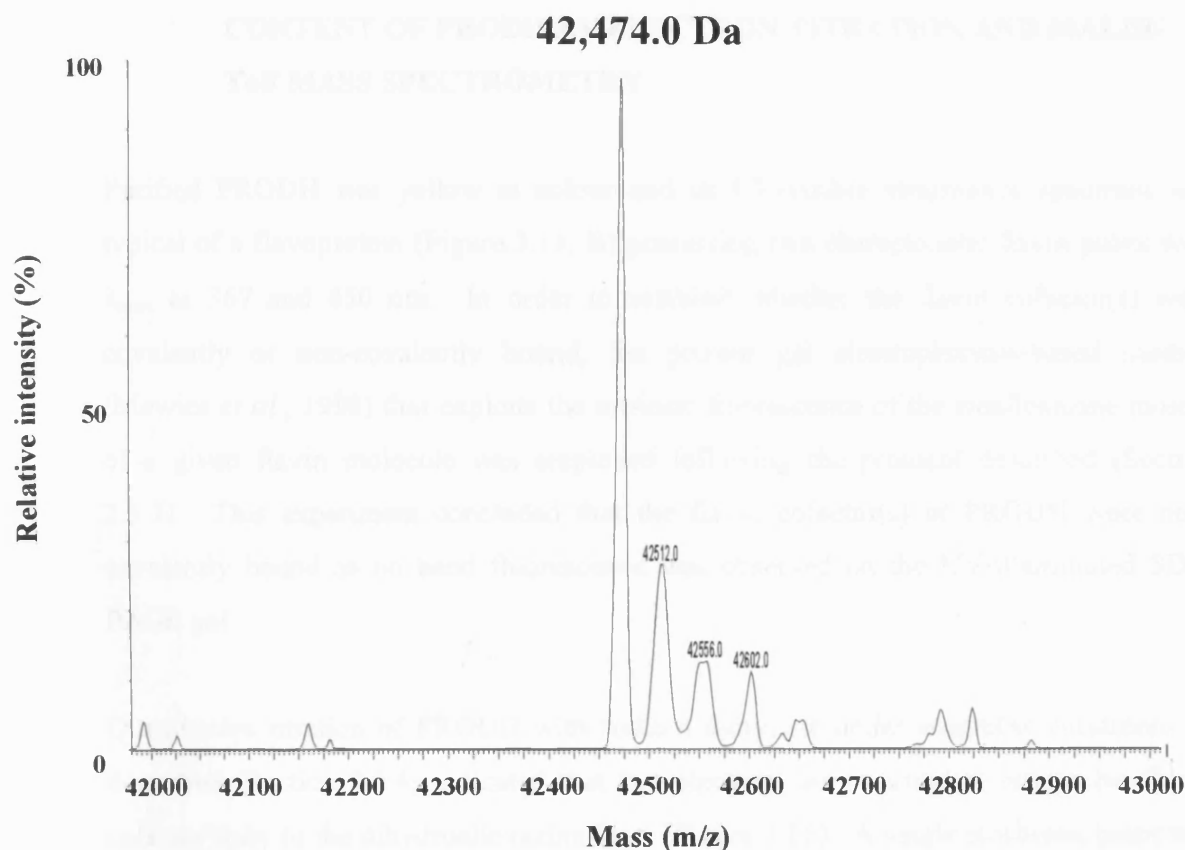
42,474.0 Da

Figure 3. 15. Electrospray mass spectrometry analysis of purified PRODH. The β subunit of PRODH is represented by the major peak with a mass/charge (m/z) value corresponding to a molecular weight of 42,474.0 Da that compares favourably to both the β subunit mass value measured by MALDI-ToF of 42,437.65 Da and the predicted mass for the β subunit of 42,481.2 Da calculated from the amino acid sequence. The difference in value between the predicted mass for the PRODH β subunit and that determined by electrospray experimentation is only 7.2 Da. Conditions: PRODH was exchanged into filtered ddH$_2$O pH 7.0 and concentrated to 1 mg/ml using a Centriprep YM-30 centrifugal filter membrane.

compared to the mass value determined by MALDI-ToF mass spectrometry with only 7.2 Da separating the predicted value from that determined by electrospray for the β subunit.

3.2.11. IDENTIFICATION AND QUANTITATION OF THE COFACTOR CONTENT OF PRODH BY ELECTRON TITRATION AND MALDI-ToF MASS SPECTROMETRY

Purified PRODH was yellow in colour and its UV-visible absorbance spectrum was typical of a flavoprotein (Figure 3.13, B) possessing two characteristic flavin peaks with λ_{max} at 367 and 450 nm. In order to establish whether the flavin cofactor(s) were covalently or non-covalently bound, the protein gel electrophoresis-based method (Mewies et al., 1998) that exploits the intrinsic fluorescence of the isoalloxazine moiety of a given flavin molecule was employed following the protocol described (Section 2.5.3). This experiment concluded that the flavin cofactor(s) of PRODH were non-covalently bound as no band fluorescence was observed on the UV-illuminated SDS-PAGE gel.

Quantitative titration of PRODH with sodium dithionite under anaerobic conditions as described (Section 2.5.4) indicated that two electrons are required to reduce the flavin cofactor fully to the dihydroalloxazine form (Figure 3.16). A single isosbestic point was observed at 340 nm and evidence for a semiquinone species was not obtained during titration with sodium dithionite. For MALDI-ToF mass spectrometric identification of the non-covalently bound cofactor, samples of concentrated PRODH were denatured by incubation in boiling water to promote cofactor release and precipitated protein removed by centrifugation. The cofactor content of PRODH in the resulting supernatant was analysed against authentic FAD, FMN, ATP, ADP and AMP standard solutions according to the protocol described (Section 2.5.5) using a Bruker Biflex mass spectrometer. The spectrum produced for the PRODH cofactor sample illustrated clear detection of peaks corresponding to the positively charged quasimolecular ion of FAD ($[M+H]^+$) with a mass/charge peak at 787 and the FAD-potassium adduct with a mass/charge peak at 825. Partial hydrolysis of FAD cofactor during heat treatment was
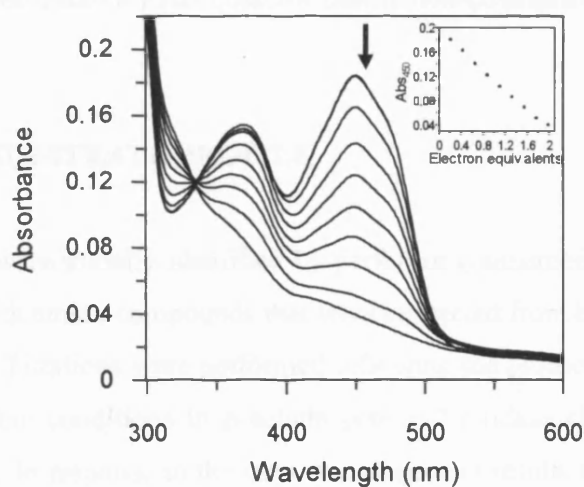
Figure 3. 16. **Spectral changes accompanying the reductive titration of monoflavinylated (FAD-bound) PRODH of *P. furiosus* DSM 3638 with sodium dithionite.** Arrow indicates direction of absorption change. A single isosbestic point was observed at 340 nm. *Inset*, a plot of absorbance at 450 nm versus electron equivalents, which demonstrates that reduction is complete following addition of two electrons. Conditions: 50 mM potassium phosphate buffer pH 7.5 at 25 °C; enzyme concentration 9 μM.

highlighted by mass/charge peaks at 348 and 458 assigned to AMP and FMN ([M+H$^+$]) hydrolysis products respectively. The spectrum also contained a mass/charge peak at 496 correlating to the FMN-potassium adduct species (Figure 3.17). Hydrolysis of labile ATP cofactor may also have contributed to the AMP detection signal. The potassium ions present in the PRODH cofactor sample are from the purification buffers. The spectrum obtained for the flavin cofactor released from purified PRODH is consistent with assignment as FAD and the quantitative titration with sodium dithionite as reductant indicates a single redox-active FAD cofactor that is non-covalently associated with the purified enzyme.

3.2.12. PRODH SUBSTRATE PROFILE

Reactive substrates were initially identified by performing anaerobic optical titrations of oxidised PRODH with amine compounds that were suspected from bioinformatics data to reduce the enzyme. Titrations were performed following the protocol described (Section 2.5.6) under anaerobic conditions to preclude potential oxidase chemistry the enzyme may have catalysed. In response to the sequence alignment results that clearly suggested PRODH to be an amine-specific oxidoreductase highlighting residue conservation with active site residues His225, Tyr259 and Gly270 in DMGO, screening of various primary, secondary and tertiary amine compounds was undertaken. Enzyme-substrate reactivity was established by observing the bleaching of the PRODH flavoprotein spectrum on addition of amine compound. Of the amine compounds screened for reducing activity, the enzyme was found to oxidise only secondary amine compounds, namely sarcosine, L-proline and L-pipecolic acid. L-proline was found to be the most effective reducing substrate ($t_{\frac{1}{2}} = \sim 105$ s^{-1} for spectral bleaching of the absorbance at 450 nm), followed by L-pipecolic acid ($t_{\frac{1}{2}} = \sim 110.5$ s^{-1}) a structural analogue of L-proline, and lastly sarcosine ($t_{\frac{1}{2}} = \sim 654$ s^{-1}) which unlike L-proline and L-pipecolic acid lacks a ring moiety (Figure 3.18). Glycine betaine, glycine, dimethylglycine and D-proline did not reduce the enzyme flavin. The common structural link between these identified substrates for PRODH is that they are all secondary alpha-amino acids (Figure 3.18, E). Addition of sodium sulphite to purified PRODH did not perturb the flavin absorption spectrum
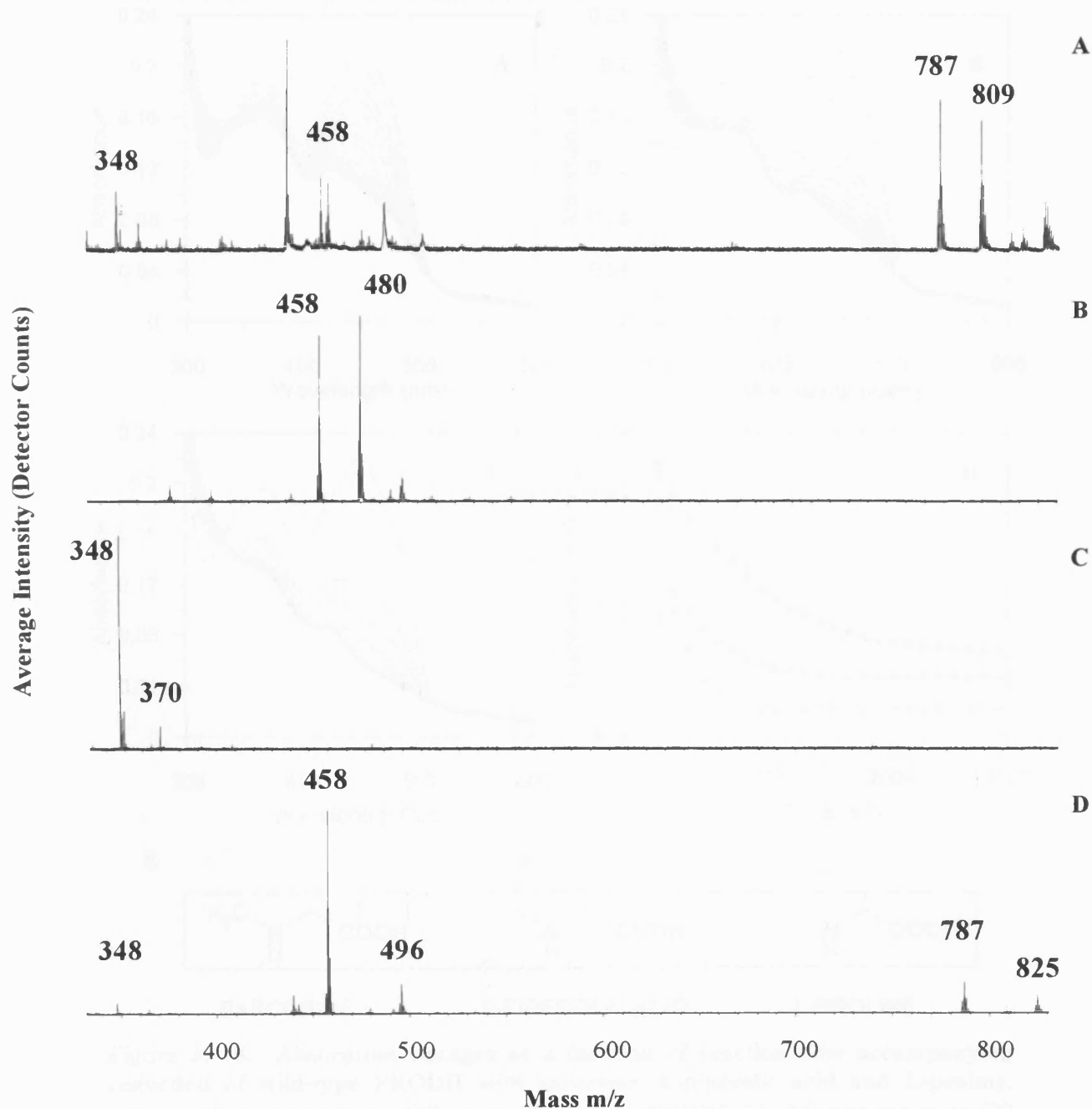
Figure 3. 17. MALDI-ToF mass spectrometry of the isolated flavin cofactor of PRODH. *Spectrum A*, authentic FAD showing the ([M+H]$^+$) ion of FAD (m/z 787) and FAD-Na$^+$ adduct (m/z 809). *Spectrum B*, authentic FMN showing the [M+H]$^+$ ion (m/z 458) and FMN-Na$^+$ adduct (m/z 480). *Spectrum C*, authentic AMP showing the [M+H]$^+$ ion (m/z 348) and AMP-Na$^+$ adduct (m/z 370). *Spectrum D*, released PRODH cofactor showing the [M+H]$^+$ ion of FAD (m/z 787) and FAD-K$^+$ adduct (m/z 825). The [M+H]$^+$ ion of AMP (m/z 348) and FMN (m/z 458) and the FMN-K$^+$ adduct (m/z 496) result from hydrolysis of FAD and ATP. Conditions: Samples were prepared in ddH$_2$O pH 7.0.
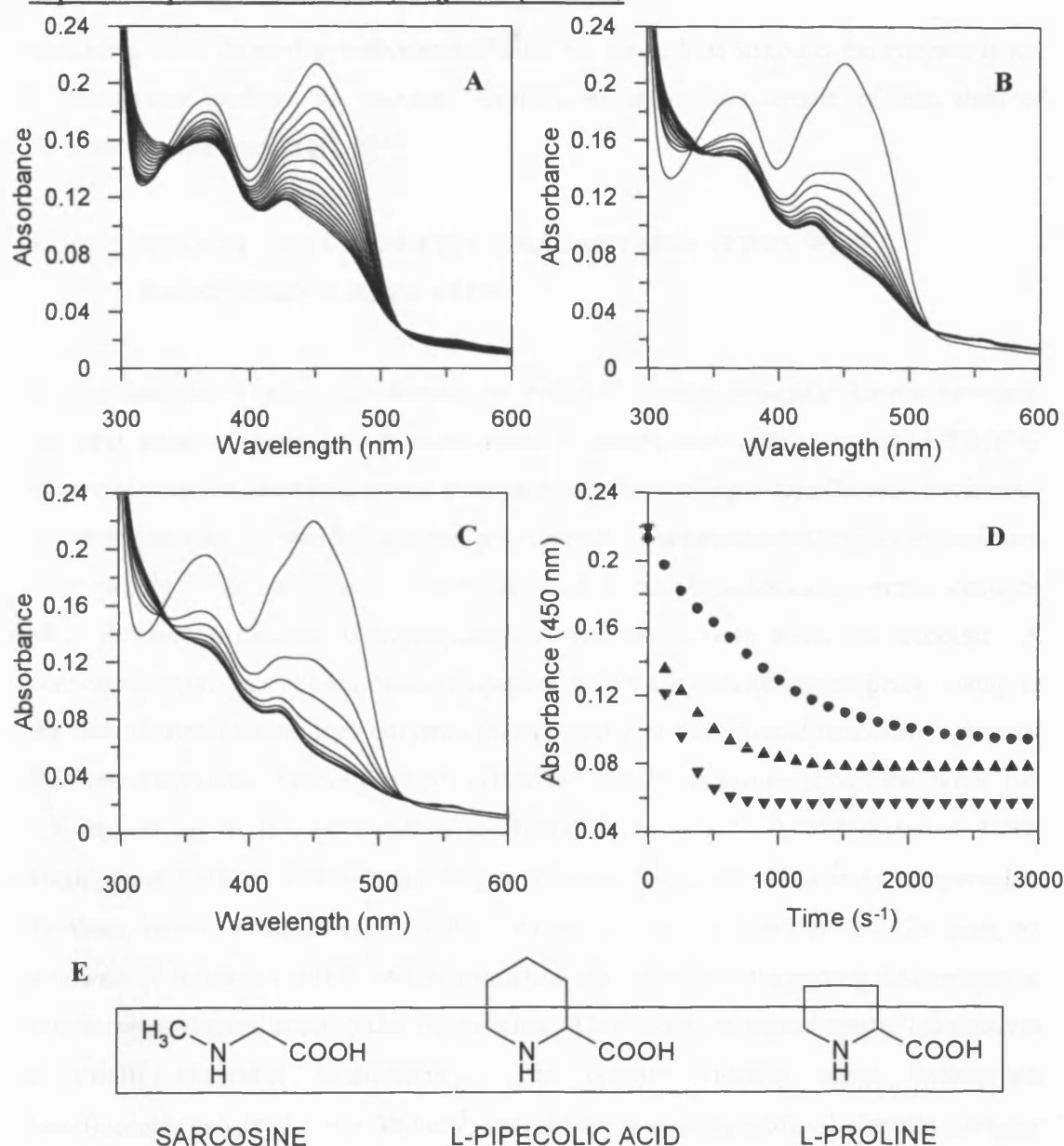
Figure 3. 18. Absorption changes as a function of reaction time accompanying reduction of wild-type PRODH with sarcosine, L-pipecolic acid and L-proline. *Panel A*, absorption changes following reduction of PRODH (13 µM) with sarcosine (20 mM). *Panel B*, as for panel A, but with L-pipecolic acid (20 mM). *Panel C*, as for panel A, but with L-proline (20 mM). *Panel D*, plot of absorbance change at 450 nm as a function of time for each of the spectral changes shown in panels A to C. Symbols: sarcosine (●), L-pipecolic acid (▲) and L-proline (▼). Conditions: 100 mM potassium phosphate buffer pH 7.5; 80 °C. *Panel E*, Structural formulae for the three secondary amine molecules sarcosine, L-pipecolic acid and L-proline. Boxed areas illustrate the common moiety suggested to be important to binding in the PRODH active site. Note: The structure of sarcosine permits free rotation about the illustrated bonds.

143

indicating that a flavin-N5-sulfite adduct does not form. This suggests the enzyme is not a flavoprotein oxidase, as reactivity with sulfite is a characteristic of this class of flavoenzyme (Massey *et al.*, 1969).

3.2.13. STEADY-STATE KINETIC CHARACTERISATION WITH IDENTIFIED SUBSTRATES

Having determined reducing substrates for PRODH through anaerobic kinetic titrations, the next stage of investigation necessitated a steady-state kinetic study of PRODH reactivity with the identified amine substrates. In developing a suitable and continuous turnover assay for the purified enzyme at an elevated temperature (80 °C) as to represent more closely the catalytic activity of PRODH under the physiological growth conditions of *P. furiosus*, a number of experimental design issues were taken into account. A continuous assay was chosen because coupled assays are usually inappropriate owing to the lack of suitable accessory enzymes that are stable at the elevated temperature desired for experimentation. Assays were performed in 100 mM potassium phosphate buffer, pH 7.5, chosen for its low temperature coefficient [$d(\text{p}K_a)/dT$ = -0.0028 (Stevens, 1992; Beynon and Easterby 1996)] permitting a very stable solution pH at assay temperature. Previous kinetic titration of PRODH with sodium sulfite (Section 3.2.12) gave no evidence of flavin-N5-sulfite adduct formation (oxidase trait) suggesting that oxygen is not the physiological acceptor for the enzyme. This finding is logical since *P. furiosus* is a strictly anaerobic heterotroph. The potent oxidising agent ferricenium hexafluorophosphate (E'_0 = + 380 mV) was therefore used as artificial electron acceptor (Lehman *et al.*, 1990). The molecular thermostability of this electron acceptor was analysed spectrophotometrically prior to commencing kinetic investigations to establish whether the high assay temperature would compromise the compounds structural/oxidising integrity (Figure 3.19). Results indicated that ferricenium would be adequately stable over the short time periods of data collection for each substrate concentration during steady-state experimentation (Appendix, Figure A1.1). Steady-state assays were performed at 80 °C with both L-proline and L-pipecolic acid as substrate. A comparison of steady-state turnover under aerobic and anaerobic conditions indicated that
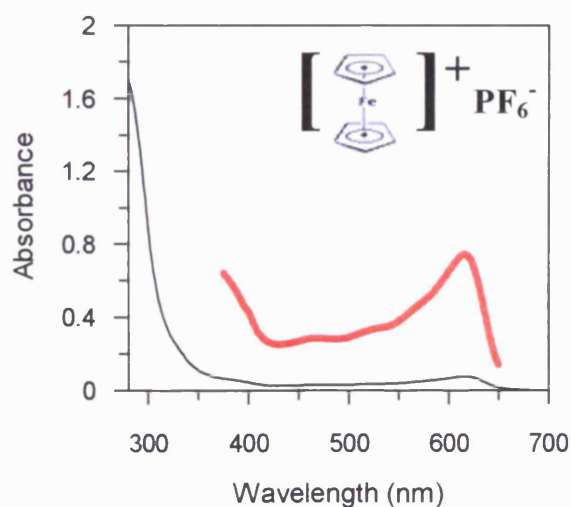
Figure 3. 19. **UV-visible absorption spectrum of the artificial electron acceptor ferricenium hexafluorophosphate ($Fc^+PF_6^-$).** The spectrum was measured between 280-700 nm. A magnification (x10) of the spectrum between 375-650 nm is shown in red. *Inset*, structural formula of the organometallic oxidant ferricenium hexafluorophosphate. Conditions: Spectrum was recorded in 10 mM HCl, 25 °C, 182 μM ferricenium hexafluorophosphate.

the presence of oxygen did not affect turnover reaction rates, consistent with the enzyme not being of the oxidase class. Consequently, steady-state kinetic parameters were determined under aerobic conditions according to the protocol described (Section 2.6.1). To confirm that the observed initial velocity readings taken during steady-state experiments were a consequence of enzyme-catalysed substrate oxidation, initial velocity measurements were analysed as a function of enzyme concentration. This data revealed that the initial velocity of reaction had a linear dependence on the concentration of PRODH in the assay mixture, allowing the conclusion that the assay was effectively measuring enzyme activity (Figure 3.20, A and B). Analysis of hyperbolic plots of initial velocity as a function of substrate concentration yielded apparent K_m values of 30.8 ± 1.1 mM and 212.3 ± 17.0 mM for L-proline and L-pipecolic acid as substrate, respectively (Figure 3.21, A and B). The corresponding apparent k_{cat} values were 18.1 ± 0.2 s^{-1} and 0.4 ± 0.02 s^{-1} for L-proline and L-pipecolic acid, respectively, with calculated specificity constants (k_{cat}/K_m) of 0.6 ± 0.03 s^{-1} mM^{-1} for L-proline and 0.002 ± 0.0002 s^{-1} mM^{-1} for L-pipecolic acid (Table 3.5). It is deduced that L-proline is the preferred substrate and that the enzyme therefore represents one of a new class of hyperthermophilic L-proline dehydrogenase (PRODH) that is distinct from the structurally elucidated L-proline dehydrogenase 'PutA' of *Escherichia coli* (Lee *et al.*, 2003).

3.3.   DISCUSSION

3.3.1.   RECOMBINANT EXPRESSION AND SUBSEQUENT MUTAGENIC ERADICATION OF N-TERMINALLY TRUNCATED α-SUBUNIT

Regarding the initial expression and purification of PRODH expressed from the pPRODH1 construct, the production of an N-terminally truncated α subunit by recombinant expression in *E. coli* was a surprising observation. After peptidase activity and subunit instability were both ruled out as the cause of this truncation, the fact that N-terminal sequencing showed methionine to be the first residue of the truncation therefore demanded a re-examination of the DNA sequence immediately upstream of the codon for this Met1 residue. The presence of an 'AAGG' motif 11 nucleotides upstream of the

A

B
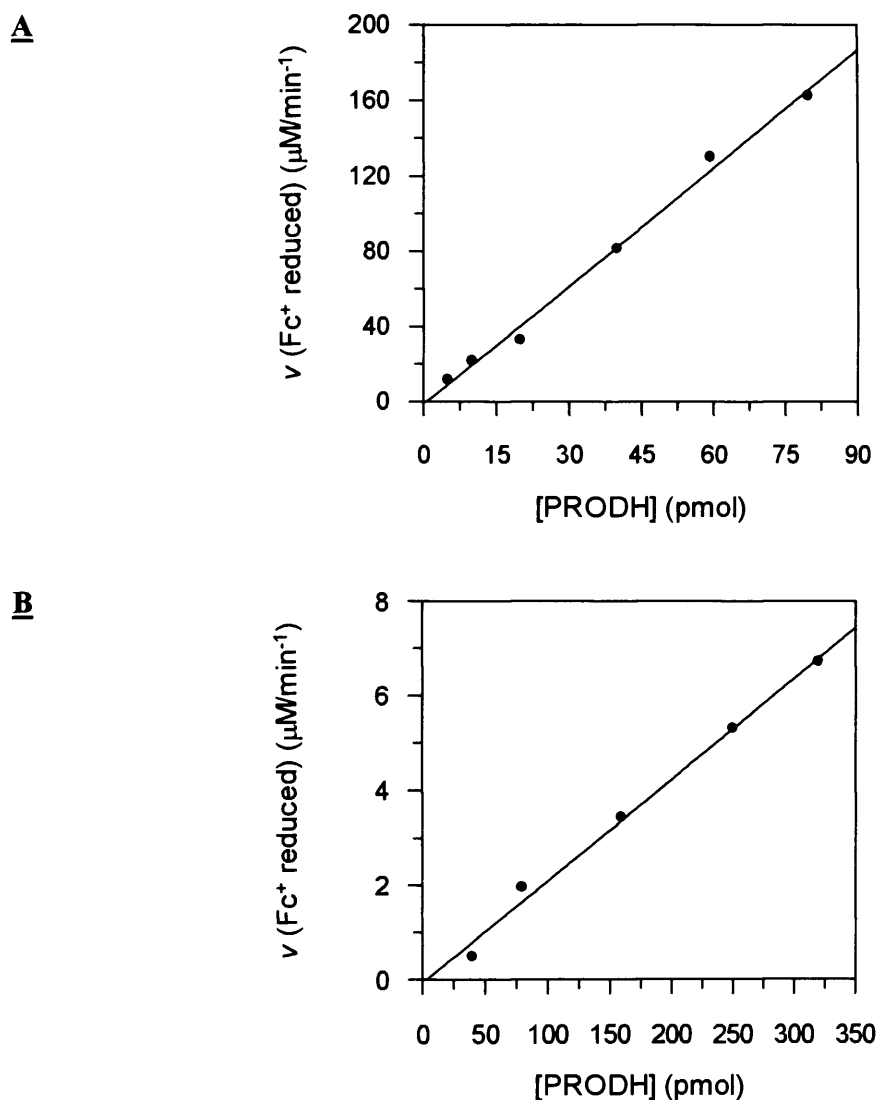
Figure 3. 20. Linear plots of reaction velocity as a function of PRODH concentration. *Panel A*, plot of initial velocity of the reduction of the artificial electron acceptor ferricenium hexafluorophosphate ($Fc^+PF_6^-$) as a function of PRODH concentration in a standard steady-state reaction containing 125 mM L-proline as substrate. *Panel B*, as for panel A, but with the standard reaction mixture containing 125 mM L-pipecolic acid as substrate. Conditions: 100 mM potassium phosphate buffer pH 7.5, 200 μM ferricenium hexafluorophosphate, 125 mM substrate (L-proline or L-pipecolic acid) and variable concentrations of PRODH (5-320 pmol); 80 °C.
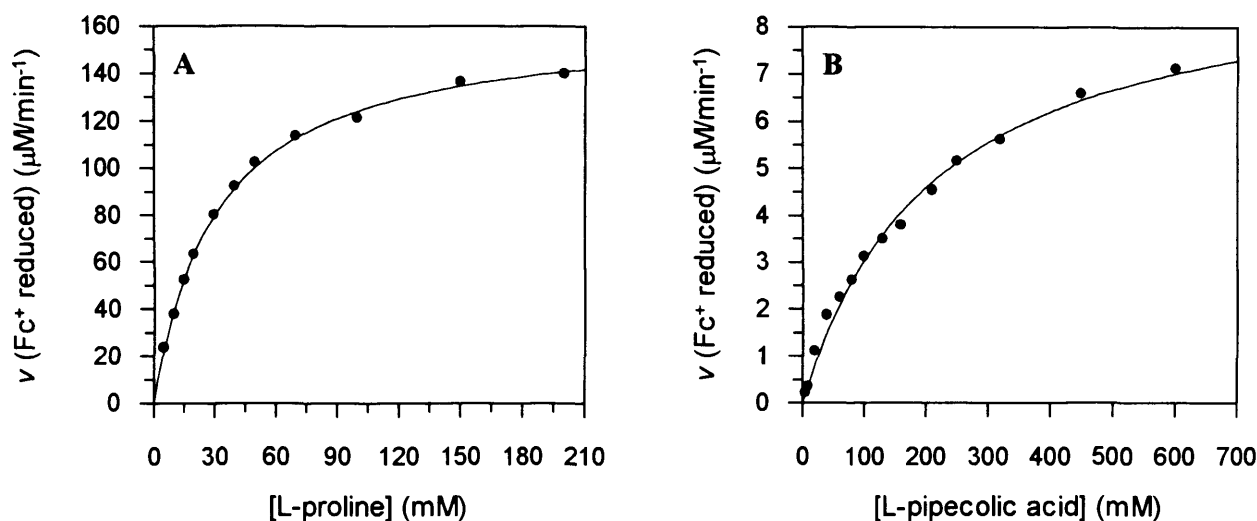
Figure 3. 21. Plots of initial velocity as a function of substrate concentration for reactions catalysed by PRODH. *Panel A*, steady-state hyperbolic plot for the reaction of PRODH-catalysed L-proline oxidation. *Panel B*, as for panel A, but with L-pipecolic acid (L-proline homologue with six-membered ring) as substrate. Initial velocities are given as ferricenium ion reduced to ferrocene (μM/min^{-1}). Data were fitted to the standard Michaelis-Menten rate equation (Equation 2.1). Conditions: 100 mM potassium phosphate buffer pH 7.5, 200 μM ferricenium hexafluorophosphate, PRODH 74.5 nM (Panel A) and 200 nM (Panel B) and variable substrate concentrations between 5-200 mM L-proline (Panel A) and 5-600 mM L-pipecolic acid (Panel B); 80 °C.

Substrate	Acceptor	V_{max} (μM/min^{-1})	k_{cat} (s^{-1})	K_m (mM)	k_{cat}/K_m (s^{-1}/mM^{-1})
L-proline	Ferricenium	81.06 ± 1.0	18.1 ± 0.2	30.8 ± 1.1	0.6 ± 0.03
L-pipecolic acid	Ferricenium	4.8 ± 0.4	0.4 ± 0.02	212.3 ± 17.0	0.002 ± 0.0002

Table 3. 5. Table of steady-state parameters for the reaction of PRODH with L-proline and L-pipecolic acid as substrate. The table displays the apparent steady-state kinetic constants corresponding to the Michaelis-Menten plots in figure 3.21. Note; V_{max} is expressed as substrate oxidised (μM/min^{-1}) as opposed to ferricenium ion reduced. Conditions: As stated in figure 3.21.

Met1 codon highlighted the possibility that host ribosome complex may have been forming transient base paired attachments with this sequence via the 16S rRNA polynucleotide therefore allowing the 30S ribosomal subunit to bind to the mRNA transcript resulting in translation initiation from this region. The AGG nucleotide triplet appeared to be a critical determinant for ribosomal recognition of this sequence as a gene-internal ribosome-binding site, a hypothesis based on the Shine-Dalgarno consensus sequence 5'-AGGAGGU-3' of _E. coli_ (Shine and Dalgarno, 1974) that clearly shows the 'AGG' triplet being core and critical for recognition. The short nucleotide sequence of the proposed internal ribosome-binding site along with its low binding energy and spacing from the initiation codon are likely contributing factors to the overall yield of truncated α subunit being approximately 13.2 % in comparison to the expression levels of the full length α subunit. The mutagenesis of the Lys79 codon from 'AAG' to 'AAA' (whilst not altering the native sequence at the amino acid level) effectively eradicated expression of the truncated α subunit, thus confirming the hypothesis for the presence of a gene-internal ribosome-binding site. The obvious question that initially springs to mind asks, why is translation also initiated at this internal site within ORF1 during recombinant expression in _E. coli_ and is this internal site utilised by the translation machinery of _P. furiosus_ during physiological expression? With reference to the observed low level translation of truncated polypeptide, it seems unlikely that translation initiation occurs from this site in _P. furiosus_ and if residual expression does occur, the product is likely to be rapidly targeted for degradation. The truncated product may well have formed a stable tertiary complex with the αβ heterodimer as judged from its co-purification with the full length subunits, but it appeared to have no beneficial kinetic or thermostabilising influence on PRODH. An explanation for the observed low level gene-internal translation during recombinant over-expression in _E. coli_ may be found by comparing the phylogenetic ordering of source and host species (Figure 3.22). A noticeable concurrence is generally found when comparing the ordering of organisms based on the information content of their ribosome-binding site sequences to their relative phylogenetic ordering (Frishman _et al._, 1999). _E. coli_ belonging to the γ-subdivision of Gram-negative bacteria has a ribosome-binding site signal strength of 2.55 compared to 2.73 for the archaebacterium _P. furiosus_. These values were determined from automatically derived
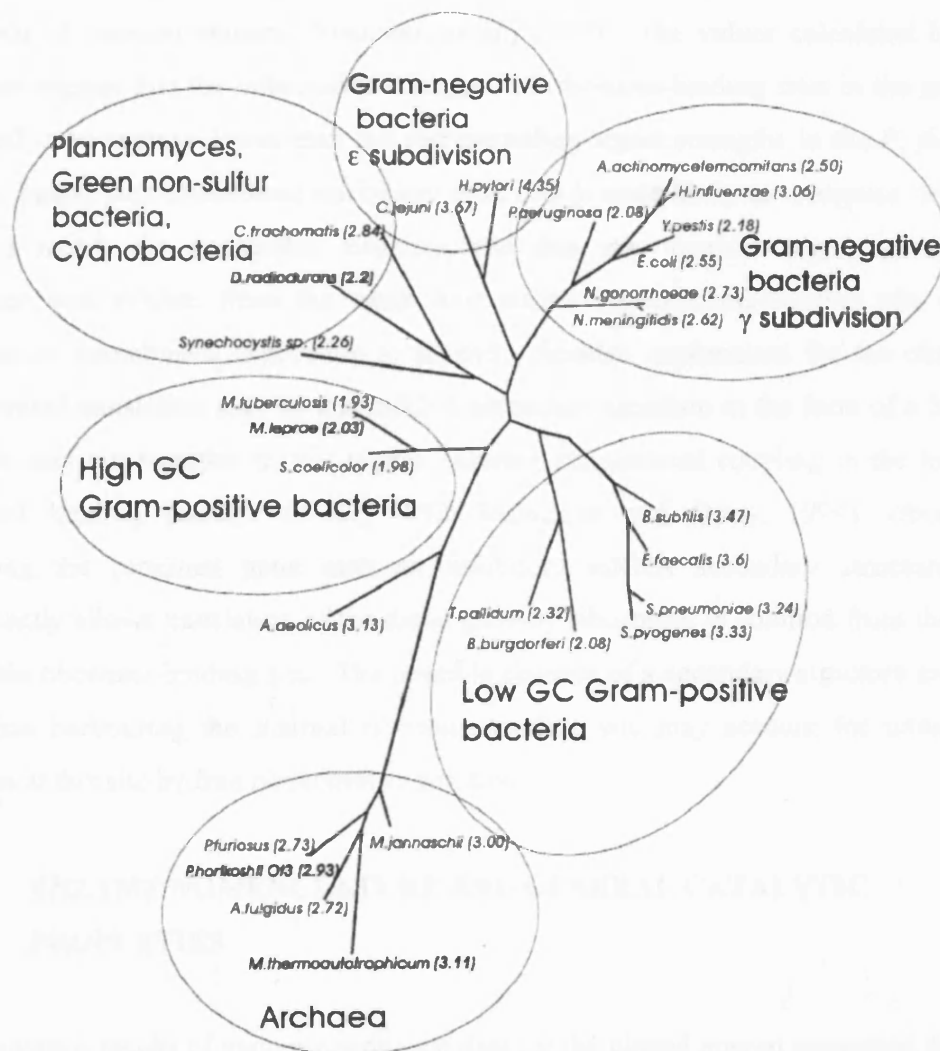
Figure 3. 22. **Phylogenetic tree comprising 28 prokaryotes grouped by maximum likelihood analysis of small subunit rRNA sequences (PHYLIP, Felsenstein, 1993).** The numbers in the parentheses correspond to RBS information content. The figure is taken from Frishman *et al.*, 1999.

ribosome-binding site alignments predicted using ORPHEUS gene recognition software (Frishman _et al._, 1998) that were analysed by a two-stage iterative procedure which upon convergence gives a binding profile corresponding to the nucleotide weight matrix and the vector of position weights (Frishman _et al._, 1999). The values calculated by this algorithm suggest that the informational content of ribosome-binding sites in the genome of _E. coli_ is on average lower than the corresponding signal strengths in the _P. furiosus_ genome, hence, the translational machinery of _E. coli_ is more likely to recognise 'weaker' sequence motifs for translation initiation and this may explain why gene-internal translation was evident from the weak four nucleotide ribosome-binding site within ORF1 upon recombinant expression in _E. coli_. Another explanation for the observed gene-internal translation may be that mRNA secondary structure in the form of a hairpin structure may not manifest in this region. During translational coupling in the form of facilitated binding (Lesage _et al._, 1992; Dallmann and Dunn, 1994), ribosomes translating the proximal gene melt an inhibitory mRNA secondary structure that subsequently allows translation of the distal gene by ribosomes in solution from the now accessible ribosome-binding site. The possible absence of a secondary structure motif in the region harbouring the internal ribosome-binding site may account for translation initiation at this site by free ribosomes in solution.

3.3.2.   ENZYME NOMENCLATURE AND GENERAL CATALYTIC PROPERTIES

Bioinformatics results of genomic sequence data for the cloned operon suggested that the physiological substrate for PRODH was sarcosine based on the sequence identity that PRODH holds with experimentally characterised sarcosine oxidases of various species. Anaerobic kinetic titrations of PRODH during the initial screening and identification of reactive substrates revealed that the enzyme had catalytic activity towards the three secondary amine compounds L-proline, L-pipecolic acid and sarcosine.   The bioinformatics data available in the preliminary stages of this investigation was therefore invaluable as an indicator of the chemical nature of the putative physiological substrate and greatly aided the selection of amine compounds for the screening process.   This

experimentally observed substrate promiscuity of PRODH is in stark contrast to the catalytic activity of the recently identified dye-linked L-proline dehydrogenase (PDH1) of _P. horikoshii_ OT-3 that was found to act exclusively on L-proline; L-pipecolic acid and sarcosine were shown to be inert as substrates (Kawakami _et al._, 2005).

The observed multiple substrate reactivity of PRODH has also been documented for a number of covalent flavoproteins belonging to the MSOX family. One of the most recently characterised of this family is NikD from _S. tendae_ Tü901, a novel flavoprotein important in the biosynthesis of nikomycin antibiotics catalysing the oxidation of Δ^1 or Δ^2-piperideine-2-carboxylate to yield picolinate (Venci _et al._, 2002). The initial molecular characterisation of NikD found that the enzyme, like PRODH can also oxidise L-pipecolic acid and the nitrogen heterocycle L-proline. 3,4-dehydro-L-proline was also confirmed as an alternative substrate of NikD highlighting that the enzyme catalyses oxidation of a carbon-nitrogen bond in this substrate resulting in an unstable tautomer that after rearrangement yields pyrrole-2-carboxylate, a stable aromatic tautomer (Venci _et al._, 2002). The substrate specificity profile of monomeric sarcosine oxidase (MSOX), the enzyme by which the aforementioned covalent flavoprotein family is named after also manifests catalytic activity towards multiple amine compounds. Aside from MSOX catalysing the oxidative demethylation of sarcosine to produce glycine and formaldehyde, the enzyme from _Bacillus sp._ B-0618 was also found to oxidise _N_-methyl-L-alanine with an apparent catalytic efficiency (k_{cat} / K_m) of 220 vs. 610 mM^{-1} min^{-1} when compared to sarcosine indicating that the active site of MSOX is tolerant of a methyl group in place of one of the sarcosine α-hydrogen atoms. An approximate 60-fold decrease in apparent catalytic efficiency was observed during catalysis with _N_-ethyl-glycine solely resulting from an increase in apparent K_m from 4.5 ± 0.1 mM for sarcosine to 260 ± 10 mM. Like PRODH, MSOX was also able to oxidise L-proline but with the lowest catalytic efficiency of all the identified substrates (0.19 mM^{-1} min^{-1}) and MSOX was also unable to oxidise tertiary amines such as dimethylglycine (Wagner and Jorns, 2000) analogous to the catalytic traits of PRODH illustrating dimethylglycine to be inert as substrate. Additional enzymes identified with catalytic activity towards sarcosine, L-pipecolic acid and L-proline are peroxisomal sarcosine oxidase isolated from rabbit kidney (Reuber _et_

_al._, 1997) and L-pipecolic acid oxidase isolated from monkey liver (Mihalik _et al._, 1991). A comparison of the relative catalytic constants of these oxidases toward the three secondary amine compounds is given in Table 3.6. A similar catalytic reaction mechanism is likely for these enzymes with the theoretical catalytic oxidation products of L-proline and L-pipecolic acid being Δ^1-pyrroline-5-carboxylate and Δ^1-piperideine-6-carboxylate respectively, and the products of sarcosine oxidation being glycine and formaldehyde. Comparison of the chemical structures of these three substrates also illustrates a common imino moiety suggesting that this group is key to recognition and substrate binding at the active site (Figure 3.18, E). Regarding the overall sequence identity and moreover, the conservation between active site residues in DMGO from _Arthrobacter globiformis_ and PRODH from _P. furious_, the contrast in substrate preference between these two flavoproteins is intriguing. Unlike PRODH, catalytic activity has been observed for DMGO towards both secondary and tertiary amine compounds. The physiological substrate of DMGO is dimethylglycine a tertiary amine molecule, but as demonstrated by anaerobic spectral kinetic reduction experiments DMGO also oxidises the secondary amine sarcosine, albeit at an exceptionally slow rate with full reduction of enzyme occurring over approximately 1 hour after the addition of 20 mM sarcosine (Basran _et al._, 2002).

Steady-state characterisation of PRODH with both L-proline and L-pipecolic acid as substrate gave apparent K_m values of 30.8 ± 1.1 mM and 212.3 ± 17.0 mM, respectively with corresponding apparent k_{cat} values of 18.1 ± 0.2 s^{-1} and 0.4 ± 0.02s^{-1} at 80 °C/pH 7.5. The apparent K_m determined for PDH1 of _P. horikoshii_ with L-proline as substrate is 4 mM using 2,6-dichloroindophenol as electron acceptor at 50 °C/pH 8.0 (Kawakami _et al._, 2005). The millimolar K_m value determined using L-proline as substrate for PRODH at first glance seems high but is actually lower in comparison to the Michaelis constants determined for the trifunctional L-proline oxidising enzyme PutA from the enteric bacteria _E. coli_ and _S. typhimurium_ with apparent K_m values of 105 and 50 mM respectively (Menzel and Roth, 1981; Graham _et al._, 1984). In bacteria, cytosolic levels of amino acids including L-proline are in the low mM concentration range (Krämer,

	Recombinant sarcosine oxidase	Rabbit kidney sarcosine oxidase	Monkey liver L-pipecolic acid oxidase
Sarcosine	46 %	100 %	10 %
L-pipecolic acid	53 %	30 %	100 %
L-proline	100 %	23 %	23 %

Table 3. 6. Table showing relative catalytic constants of three oxidases. Recombinant sarcosine oxidase is a fusion with maltose binding protein and data was with a substrate concentration of 9.8 mM. Data for sarcosine oxidase from rabbit kidney was taken at a substrate concentration of 9.8 mM. Data for L-pipecolic acid from monkey liver was taken at a substrate concentration of 5 mM. The data are not catalytic efficiencies as K_m values were not determined in each case. The table is adapted from Reuber *et al.*, 1997.

1994). In the absence of L-proline, *E. coli* PutA is located in the cytoplasm and acts as an autogeneous transcriptional repressor of the *putP* and *putA* genes of the proline utilisation (*put*) regulon by binding to the *put* control intergenic DNA region (Brown and Wood, 1992; Ostrovsky *et al.*, 1991). When proline is available in the cytoplasm, PutA relocates to the membrane with concomitant activation of *put* gene transcription, thus allowing proline oxidation (Brown and Wood, 1993). Stopped-flow fluorescence measurements of FAD reduction by L-proline substrate in *E. coli* PutA showed flavin reduction to preceed the critical conformational change that mediates the transition of PutA from acting as a transcriptional repressor to a membrane-bound protein (limiting rate constant for the reduction of PutA FAD by L-proline = 133 ± 6 s^{-1}). Residue W211 in the flexible region of the PutA L-proline dehydrogenase domain was also shown to be the critical molecular marker for the conformational change caused by L-proline oxidation (Zhu and Becker, 2005). The apparent affinity that *E. coli* PutA displays towards L-proline substrate in the presence of membrane vesicles representing the membrane-bound form of the enzyme is >20-fold higher manifesting an apparent K_m = 4.3 mM (Graham *et al.*, 1984). No substantial increase in substrate affinity in the presence of membrane vesicles was observed for the PutA$_{669}$ truncated polypeptide (K_m = ~80 mM) that carries only the L-proline dehydrogenase domain of the enzyme, although an apparent catalytic turnover of 16 s^{-1} recorded for PutA$_{669}$ was >2-fold faster than the apparent k_{cat} of 7.5 s^{-1} determined for full length PutA (Vinod *et al.*, 2002). Bifunctional PutA from the soil microbe *Bradyrhizobium japonicum* (BjPutA) lacks the DNA-binding domain present in *E. coli* PutA and does not therefore act as a transcriptional repressor. However, consistent with kinetic data collected for its *E. coli* homologue, the apparent K_m of BjPutA utilising L-proline as substrate falls from 150 ± 11 mM to 45 ± 5 mM in the presence of polar lipids with a corresponding increase in apparent k_{cat} values from 5.6 ± 0.7 to 18 ± 2 s^{-1} (Krishnan and Becker, 2005).

Kinetic studies of various other amine catabolising enzymes have described millimolar K_m values with examples including monomeric sarcosine oxidase from *Bacillus sp. B-0618* with an apparent K_m^{sarc} = 9.4 mM (Wagner and Jorns, 2000) and dimethylglycine oxidase from *Arthrobacter globiformis* with an apparent K_m^{DMG} = 2.4 mM (Basran *et al.*,

2002). The ostensible low binding affinity these amine oxidases carry toward their given substrates likely results from the relative availability of substrate ionic species at solution pH during oxidative catalysis. It has been suggested that these flavoprotein oxidase enzymes utilise the deprotonated form of substrate under physiological conditions. However, at physiological pH values, the predominant substrate species is the zwitterionic form (e.g., L-proline α-amino group $pK_a = 10.6$). Structural studies with DMGO suggest that residues His225 and Tyr259, which are conserved in PRODH, might also facilitate deprotonation of substrate close of physiological pH values. In this regard, it is important to note that at physiological pH, the millimolar value of the Michaelis constant determined for PRODH with L-proline as substrate is representative of the sum of zwitterionic and anionic species (and strictly speaking, the cationic species, although contribution by this species at physiological pH will be negligible), and the 'true' K_m value is actually in the micromolar range corresponding to the concentration of the deprotonated form of substrate. Using the Henderson-Hasselbalch equation (Appendix, Section A1.3), at pH 7.5, the K_m for L-proline expressed in terms of the unprotonated form only, is 24.5 μM. Kinetic studies with TMADH show that the pK_a for substrate ionisation is sufficiently perturbed during formation of the Michaelis complex from pH 9.8 to ~pH 6.5. This shift of 3.5 pH units favours formation of the free base form of trimethylamine and implies that the unprotonated substrate form is reactive (Basran *et al.*, 2001a), also consistent with proposed mechanisms of flavoprotein catalysed amine oxidation (Scrutton, 2004).

Concerning the finding that PRODH possesses oxidase activity toward multiple substrates, the catalytic efficiency of PRODH for these secondary amine substrates was calculated to determine which substrate is predominantly metabolised under competing substrate conditions (Cornish-Bowden, 1979). Calculated specificity constants (k_{cat}/K_m) of 0.59 ± 0.03 s^{-1} mM^{-1} for L-proline and 0.002 ± 0.0002 s^{-1} mM^{-1} for L-pipecolic acid as substrate clearly indicated that L-proline is the preferred substrate of PRODH when alternative substrates are present, as is the case under physiological conditions in the cell cytoplasm. It was therefore concluded that PRODH represents one of a new class of hyperthermophilic L-proline dehydrogenases (EC 1.5.99.8) that appears to be common in

the order *Thermococcales* with similar PRODH gene clusters being evident in the genome of *P. abyssi* (*PAB1842-PAB1843*) and *P. horikoshii* (*PH1363, PH1364*), the later of which has recently been characterised and confirmed to be a dye-linked L-proline dehydrogenase (Kawakami *et al.*, 2005; Tsuge *et al.*, 2005).

3.4   SUMMARY

This chapter has reported the cloning and recombinant expression of two open reading frames from the genome of *P. furiosus* DSM 3638 that show some sequence homology with bacterial amine specific flavoprotein oxidases/dehydrogenases. The encoded enzyme has been purified by a scheme that engineers the isolation of the monoflavinylated enzyme form with FAD non-covalently bound, as identified by MALDI-ToF mass spectrometry and quantified by reductive titration with sodium dithionite (FAD bound at the active site on the β subunit as revealed by elucidation of the X-ray crystal structure, Chapter 5). The enzymes reactivity towards the secondary amine compounds L-proline, L-pipecolic acid and sarcosine has been demonstrated with optimal catalytic activity measured towards L-proline. Robust, high-temperature steady-state assay conditions have been developed and steady-state parameters for both L-proline and L-pipecolic acid as substrate have been determined at 80 °C. Results confirm PRODH as a new member of the recently identified class of L-proline dehydrogenase of hyperthermophilic origin that is distinct from the structurally characterised L-proline dehydrogenase (PutA) of *E. coli* (EC 1.5.99.8). PRODH, in terms of cofactor content and redox chemistry is simpler than the heterotetrameric dye-linked L-proline dehydrogenase from the hyperthermophilic archaeon, *Thermococcus profundus*, an analogue of which is also encoded in the genome of *P. furiosus*. This initial work therefore demonstrates the structural diversity amongst the hyperthermophilic L-proline dehydrogenase enzymes and PRODH from *P. furiosus* represents a novel model system to advance the current understanding of the mechanistic basis of flavoprotein-catalysed amine oxidation reactions.

CHAPTER FOUR

A COMPREHENSIVE DESCRIPTION OF STEADY-STATE KINETIC PROPERTIES AND THERMODYNAMIC ANALYSIS OF PRODH REDOX CHEMISTRY

CHAPTER FOUR

A COMPREHENSIVE DESCRIPTION OF STEADY-STATE
KINETIC PROPERTIES AND THERMODYNAMIC ANALYSIS OF
PRODH REDOX CHEMISTRY

4.1. INTRODUCTION

High temperature is a salient feature of the geothermally heated marine sediment that
constitutes the habitat of the hyperthermophile *P. furiosus*. The enzymes from this and
other extremophiles serve as useful model systems for researchers from various scientific
fields of expertise interested in discovering and understanding fundamental aspects of
nature such as the molecular basis of protein thermostability, deciphering the mechanisms
of enzyme catalysis at the atomic and sub-atomic level, and enzyme adaptation through
evolution. Extremophilic enzymes stable up to and exceeding solution temperatures of
100 °C have a variety of research advantages. These enzymes can be used to study
catalytic reactions under conditions usually too harsh and destructive for their mesophilic
counterparts, such as analysis with chaotropic agents and organic solvents, since many
heat stable enzymes are also resistant to proteolysis and denaturants at room temperature.
Reactions catalysed by hyperthermophiles can also be analysed closely by reducing assay
temperatures to slow reactions down without the need to employ cryosolvents. Perhaps
the most useful asset of using hyperthermophilic enzymes as research subjects is the
ability to probe the effects of temperature on enzyme parameters over a wide temperature
range (Daniel and Danson, 2001), therefore allowing a more accurate thermodynamic
profile of the enzyme system. In developing and validating a robust and reliable assay
utilising the artificial electron acceptor ferricenium hexafluorophosphate (as described in
Chapter 3) to analyse the kinetics of PRODH of *P. furiosus* in the steady-state,
experiments were initiated to characterise the dependence of PRODH steady-state kinetic
parameters on solution temperature and pH in order to obtain a detailed description of the

thermodynamics and ionisation events respectively, of the catalytic reaction with the identified physiological substrate L-proline.

Oxidation-reduction (redox) potentiometry is an essential research tool for studying the energetics of electron transfer events in biological systems. The information gained through this technique provides key insights into the workings of electron transfer in fundamental biological processes such as respiration, photosynthesis, enzyme-catalysed metabolic processes and drug detoxification mechanisms (Dutton, 1978). Elucidating the high temperature redox chemistry of hyperthermophilic oxidoreductases and electron-carrier proteins is a niche research area now gaining increased attention from the scientific community, and thermodynamic analyses of hyperthermophilic redox enzymes in terms of biological equilibrium electron transfer potentials may provide clues as to the structural mechanisms employed in optimising catalytic activity at physiological (evolved) temperatures (Smith, _et al._, 1995). Numerous conflicting and contrasting reports of apparently 'unusual' redox chemistry in _P. furiosus_ have been published, with biphasic and non-linear temperature dependences of the midpoint potential (E_m) of ferredoxin and rubredoxin electron carrier proteins respectively, of _P. furiosus_ being described (Park _et al._, 1991; Adams, 1992). These early experimental observations of the change in equilibrium reduction potential with temperature have been interpreted by theoretical modeling in terms of an internal protein dielectric constant that changes non-linearly with temperature using a numerical solution to the Poisson-Boltzmann equation (Christen, _et al._, 1996). In addition, molecular dynamic simulations have been utilised to explain and understand the unusual temperature dependence of the redox potential of _P. furiosus_ rubredoxin by evaluating the temperature effects on the physical properties of the protein such as the structure, bond energies and solvation parameters (Swartz and Ichiye, 1996). A later report concerning the redox chemistry of heterologously expressed wild-type ferredoxin from _P. furiosus_ described observations of a 'normal' linear temperature dependence of the E_m measured by the direct electrochemistry method of cyclic voltammetry at a glassy carbon electrode (Brereton _et al._, 1998). The hyperthermophilic ferredoxin showed no temperature-dependent transition of the E_m between 0-80 °C in the latter study. These data are in stark contrast to the measurements

taken by EPR-monitored redox titrations that suggested a biphasic temperature dependence of the E_m of the same enzyme with an observed break-point at 80 °C (Figure 4.1; Park *et al.*, 1991). Rationale for the observed break-points in midpoint potential/temperature dependence profiles of various proteins studied has manifested in the proposal that the 'phase-transition' is an intrinsic property of the given protein that likely occurs as a result of a change in hydration (Koller and Hawkridge, 1988; Tanaguichi *et al.*, 1993). Further evidence to corroborate the observations of Brereton *et al.*, (1998) of a 'normal' linear dependence of the E_m of ferredoxin on temperature came from direct cyclic voltammetry experiments with both *P. furiosus* ferredoxin and rubredoxin proteins (Hagedoorn *et al.*, 1998). This study recorded the temperature dependence of the E_m of both the electron carrier proteins under investigation over the temperature range of 20-90 °C and showed the redox chemistry of these two hyperthermophilic proteins to be regular, with linear temperature dependences apparent for the redox midpoint potential of both enzymes (Figure 4.2; Hagedoorn *et al.*, 1998).

The conflicting data in the literature regarding the 'hot' redox biochemistry of hyperthermophilic systems, and moreover, the different methods utilized in collecting potentiometric measurements heralded the question; what methodology obtains redox data that most closely represents the true redox behaviour of the enzyme under investigation at a given solution temperature? A comparative electrochemical analysis of rubredoxin and ferredoxin of *P. furiosus* using both EPR-monitored redox titrations and direct cyclic voltammetry methodology has been performed by Hagedoorn and colleagues (Hagedoorn *et al.*, 1998) to assess the validity of potentiometric measurements obtained by these two contrasting methods. This study found that EPR derived E_m measurements gave values approximate to those determined voltammetrically and subsequently linearly extrapolated to a solution temperature corresponding to 0 °C or below. As a direct consequence of the small molecular weight of the electron transferring proteins in question, the observed redox data was interpreted in terms of the flexibility of the protein tertiary structure. The level of structural flexibility possessed by the *P. furiosus* ferredoxin and rubredoxin was stipulated to permit a rapid conformational adjustment (< 0.5 s^{-1}) upon flash-freezing the proteins in liquid N_2 (dead time, $t \approx 5$ s^{-1}) or
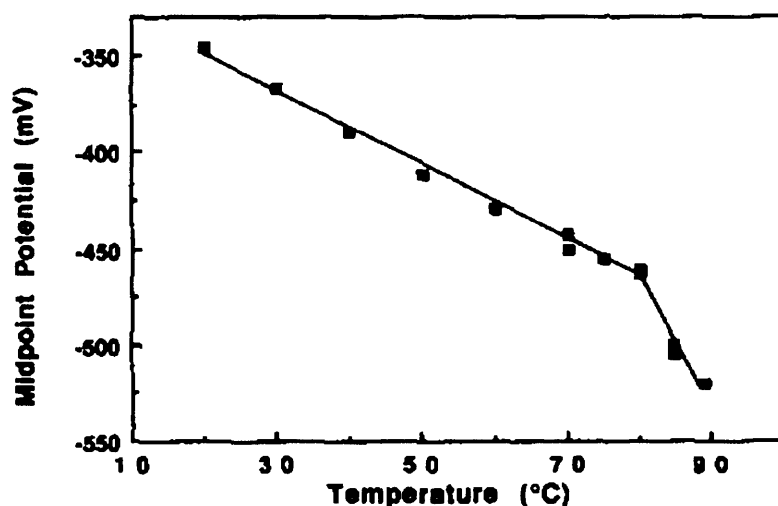
Figure 4.1. Graph showing the temperature dependence of the E_m of the small iron-sulfur protein ferredoxin of _P. furiosus_. The midpoint potential of ferredoxin was determined by bulk redox titration monitored by EPR spectroscopy with data illustrating a biphasic temperature dependence of the E_m characterised by an observed break-point at 80 °C. The figure is taken from Park _et al._, (1991).
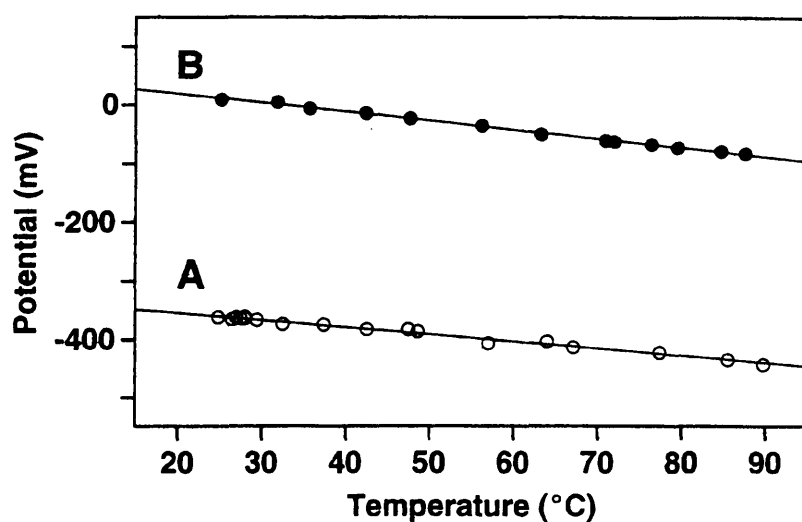
**Figure 4.2. Graph showing the temperature dependence of the midpoint reduction
potential of the small iron-sulfur proteins rubredoxin and ferredoxin of *P. furiosus*.**
The midpoint potential of ferredoxin (A, open circles) and rubredoxin (B, closed circles,
B) were determined by the direct electrochemistry method of cyclic voltammetry.
Evidence of a 'non-linear' or 'biphasic' temperature dependence for rubredoxin and
ferredoxin, respectively, was not observed in this study. These results are in conflict with
previous observations from studies that employed EPR spectroscopy. The figure is taken
from Hagedoorn *et al.*, (1998).

cold isopentane ($t \approx 0.5$ s^{-1}) so that the redox state of the frozen enzyme in EPR experiments corresponded to the equilibrated state near the freezing point of the aqueous solvent. The logical consequence of this proposal therefore concludes that EPR-monitored redox titrations of small proteins only give E_m measurements relevant to the redox state of the protein at or near the freezing point of the aqueous solution (Hagedoorn *et al.*, 1998).

In order to further extend the study of redox chemistry in hyperthermophilic systems, temperature dependence studies of the E_m of recombinant wild-type PRODH of *P. furiosus* were initiated using spectrophotometric methods under anaerobic conditions to optically assess PRODH-flavin redox states during the course of potentiometric reductive titration with sodium dithionite according to the method of Dutton (1978). In addition to the critical thermodynamic characterisation of PRODH redox chemistry, these studies also evaluate the experimental validity of redox potentiometric/spectrophotometric titration methodology for acquiring redox data on hyperthermophilic systems in comparison to EPR/cyclic voltammetric methods, and corroborates this method as an invaluable technique for the modern enzymologist.

This chapter documents the pH-dependence and thermodynamic description of the steady-state kinetics of PRODH of *P. furiosus* with substrate L-proline. Measurement of the E_m value of the redox centre of recombinant wild-type PRODH in monoflavinylated form (active site non-covalent FAD) and investigation of the temperature dependence of the enzyme midpoint potential is described together with a thermodynamic analysis of the electron transfer energetics of the system. Identification of the reaction product of PRODH catalysed L-proline oxidation is described utilising MALDI-ToF and electrospray mass spectrometry approaches.

4.2. RESULTS

4.2.1. PRODH REACTION PRODUCT IDENTIFICATION

4.2.1.1. CHEMICAL ASSAY FOR THE PRODUCTION OF Δ^1-PYRROLINE-5-CARBOXYLATE

The reaction product of the PRODH-catalysed oxidation of L-proline was identified by a colorimetric assay using a modified method to that described for the PutA protein of enteric bacteria (Wood, 1987; Section 2.7). This assay determined the reaction product of the oxidation of substrate L-proline by PRODH of *P. furiosus* to be Δ^1-pyrroline-5-carboxylate (P5C; Figure 4.3) as judged by the formation of the P5C-*o*-aminobenzaldehyde adduct chromophore followed spectrophotometrically at 443 nm. The rate constant for the bimolecular reaction of P5C with *o*-aminobenzaldehyde was found to be first-order with respect to *o*-aminobenzaldehyde concentration (Figure 4.4, A). Previous studies have shown the spontaneous reaction of P5C with *o*-aminobenzaldehyde to be first-order with respect to P5C concentration (Wood, 1987). From the gradient of the plot of $\log(V_f-V_t)$ as a function of time, where V_f is the final rate attained and V_t is the rate at time t, the $t_{1/2}$ for the steady-state rate of colour development was determined by the relationship: $t_{1/2} = -\ln2/(2.303 \times \text{slope})$. The $t_{1/2}$ is equal to $\ln2/k$, where k is the pseudo-first-order rate constant for the reaction. The bimolecular reaction therefore yielded an overall second order rate constant of 42.4 $s^{-1} M^{-1}$ (Figure 4.4, B) and analysis of the stoichiometry of conversion indicated that the ratio of L-proline oxidised to *o*-aminobenzaldehyde-P5C formed was 0.59. The observed partial conversion of free P5C to form the covalent adduct chromophore is readily interpretable with reference to the chemical properties of the two reagents participating in the bimolecular reaction. Primarily, the labile nature of the catalytic reaction product P5C is well documented (Mezl and Knox, 1976; Hu *et al.*, 1996; Zhang *et al.*, 2004) and spontaneous hydrolysis of the P5C ring moiety in generating stable γ-glutamic semialdehyde is a crucial non-enzymatic step in the reaction catalysed by the multifunctional PutA enzyme of *E. coli* (Lee *et al.*, 2003) that converts L-proline to glutamate via two distinct catalytic reaction
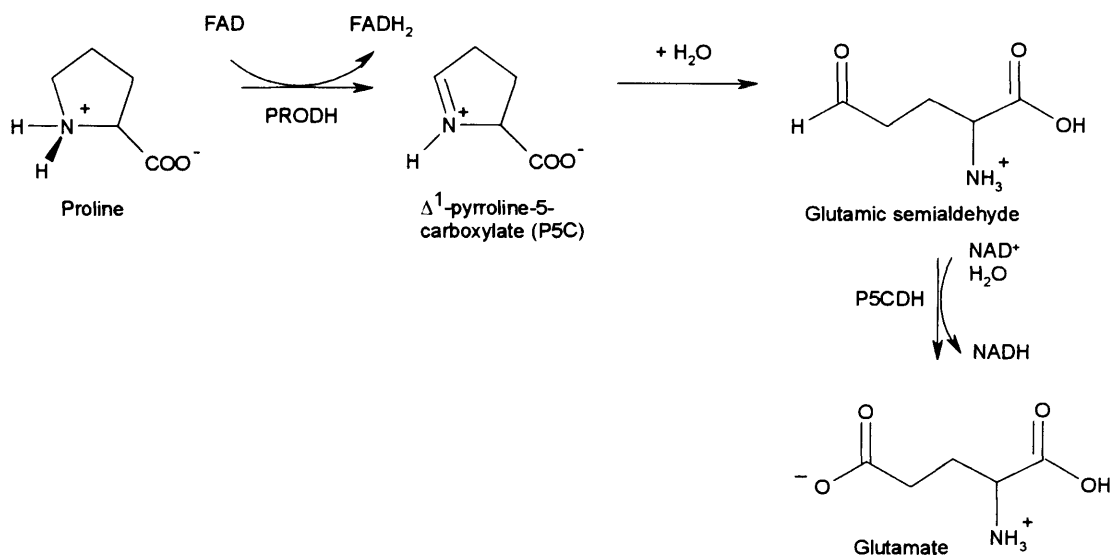
Figure 4.3. Reactions catalyzed by the multifunctional PutA protein of enteric bacteria. The first step of the reaction illustrating initial oxidation of L-proline to Δ^1-pyrroline-5-carboxylate (P5C) is analogous to the catalytic reaction of L-proline substrate oxidation by the PRODH of *P. furiosus*. Oxidation of L-proline with concomitant two-electron reduction of the non-covalent FAD cofactor of PRODH enzyme yields P5C product. Hydrolysis of P5C is nonenzymatic. In eukaryotes, distinct enzymes (PRODH and P5CDH) encoded by separate genes catalyse these reactions.
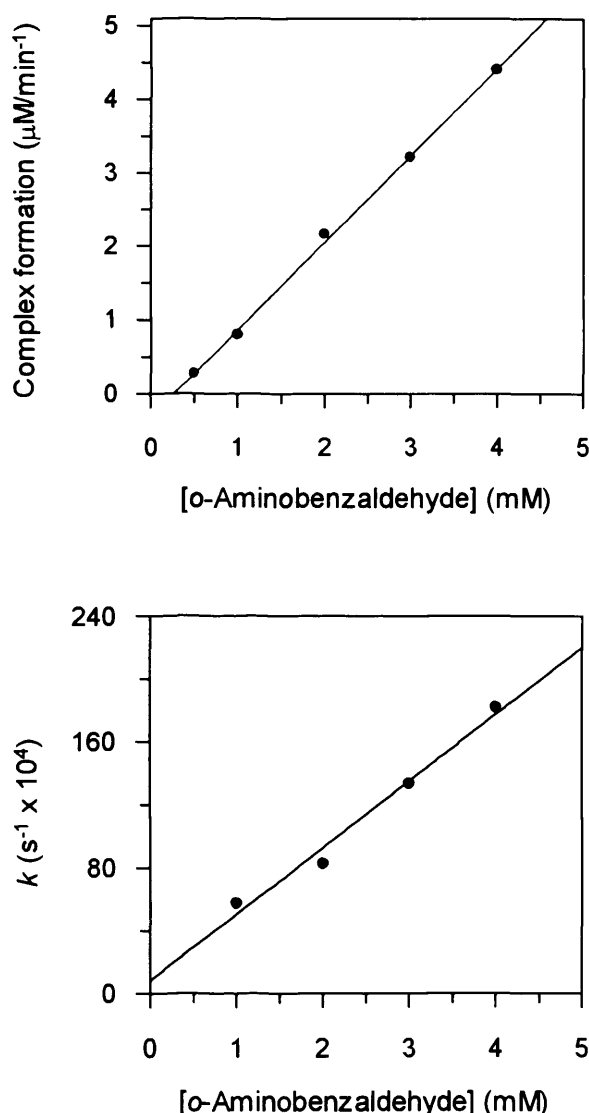
Figure 4.4. Graph showing the rate of P5C-*o*-aminobenzaldehyde adduct formation
as a function of *o*-aminobenzaldehyde concentration. *Panel A*, the rate of P5C-*o*-
aminobenzaldehyde adduct formation was a direct linear function of *o*-
aminobenzaldehyde concentration in the bimolecular reaction. *Panel B*, the pseudo-first-
order rate constant for the reaction of P5C with *o*-aminobenzaldehyde was a direct
function of *o*-aminobenzaldehyde concentration, yielding a value for the second-order
rate constant of 42.4 $s^{-1} M^{-1}$ calculated from the slope of the plot. Condition: 100 mM
potassium phosphate buffer pH 7.5, L-proline 200 mM, ferricenium 200 μM, PRODH 75
nM and *o*-aminobenzaldehyde to final concentrations of 0.5-4.0 mM.

steps (Figure 4.3). Oxidation of L-proline catalysed by hyperthermophilic PRODH necessitated an assay temperature of 60 °C to permit substrate oxidation within a reasonable experiment time-scale, therefore, it is plausible that partial non-enzymatic hydrolysis of P5C generated during the enzyme assay may have occurred. Furthermore, the elevated temperature employed for the PRODH assay likely accelerated the hydrolysis of P5C product during the short time-course of the reaction. Secondly, _o_-aminobenzaldehyde self-polymerises readily in solution (Owston and Shaw, 1988; Jircitano _et al._, 1994) and efforts to reduce the rate of polymerisation involved the use of 20 % ethanol as solvent with storage at -20 °C. Despite these measures, limited polymerisation of _o_-aminobenzaldehyde was observed during the experiments and together, the hydrolysis of P5C and rapid polymerisation of free _o_-aminobenzaldehyde likely accounted for the remaining 0.41 fraction not spectrophotometrically detected as _o_-aminobenzaldehyde-P5C chromophore.

4.2.1.2. ELECTROSPRAY MASS SPECTROMETRY ANALYSIS OF P5C-AROMATIC ALDEHYDE CONDENSATION PRODUCT

The presence of P5C which is the major intermediate that accumulates endogenously as a consequence of the inherited disorder hyperprolinemia type II resulting from a lack of the enzyme Δ^1-pyrroline-5-carboxylate dehydrogenase (EC 1.5.1.12; Phang _et al._, 1995) has been investigated as a potential cause of vitamin B_6 deficiency identified in patients with this type of hyperprolinemia as their primary diagnosis (Farrant _et al._, 2001). This study found that P5C acts as a unique endogenous vitamin antagonist. By a combination of high resolution ^1H nuclear magnetic resonance spectroscopy and mass spectrometry, this study demonstrated that pyridoxal phosphate (vitamin B_6 coenzyme) is de-activated by P5C through a Claisen condensation reaction. This reaction was proposed to involve the activated C-4 carbon of the pyrroline ring of P5C and the pyridoxal phosphate carbonyl group. Following the addition of the activated C-4 carbon of P5C to the aldehyde function of pyridoxal phosphate redolent of a Knoevenagel reaction whereby the imine moiety of activated P5C operates similarly to the carbonyl in the conventional ketone-aldehyde reaction, an olefin is formed through the elimination of water. Observations of

P5C reactivity towards aliphatic and aromatic aldehydes and ketones at physiological pH imply that the proposed condensation reaction mechanism may be a generic reaction concerning activated carbonyl compounds (Farrant *et al.*, 2001). Pyridoxal phosphate, like the reagent *o*-aminobenzaldehyde upon which the chemical test for the presence of P5C is based, are both aromatic aldehydes (Figure 4.5). This condensation reaction may therefore be applicable regarding the reaction of P5C with *o*-aminobenzaldehyde, forming the adduct chromophore monitored by the colorimetric assay during PRODH turnover as previously described (Section 2.7). To investigate this proposal further, the P5C-*o*-aminobenzaldehyde adduct was analysed by electrospray mass spectrometry to determine if the adduct mass corresponded to the calculated mass of the product of a Claisen condensation (Figure 4.6). The spectrum highlighted a single peak with a mass/charge ratio of 217 representing the positively charged quasimolecular ion ($[M+H]^+$) of the condensation product of P5C with *o*-aminobenzaldehyde (Figure 4.6, [4]). A point to note is that the stereochemistry of this olefin was not determined, but can be resolved by double-pulse field gradient nOe experiments (Neuhaus and Williamson, 2000). The nature of the colorimetric assay does not permit enough pure product to be available for this type of stereochemical investigation which requires a downstream HPLC purification procedure, and this level of analysis was beyond the scope of the present study.

4.2.1.3. DIRECT MALDI-ToF MASS SPECTROMETRY ANALYSIS OF THE L-PROLINE OXIDATION PRODUCT P5C

Direct analysis of the P5C reaction product of the PRODH-catalysed oxidation of substrate L-proline was also performed using MALDI-ToF mass spectrometry as previously described (Section 2.7). Following enzyme turnover, a peak at a mass/charge ratio of 114.1 was observed corresponding to the positively charged quasimolecular ion ($[M+H]^+$) of P5C. A second peak was also evident with a mass/charge ratio of 116.1 representative of the $[M+H]^+$ ion of surplus L-proline substrate in the assay mixture (Figure 4.7).

Keto   Pyridoxal phosphate   Enol

o-aminobenzaldehyde
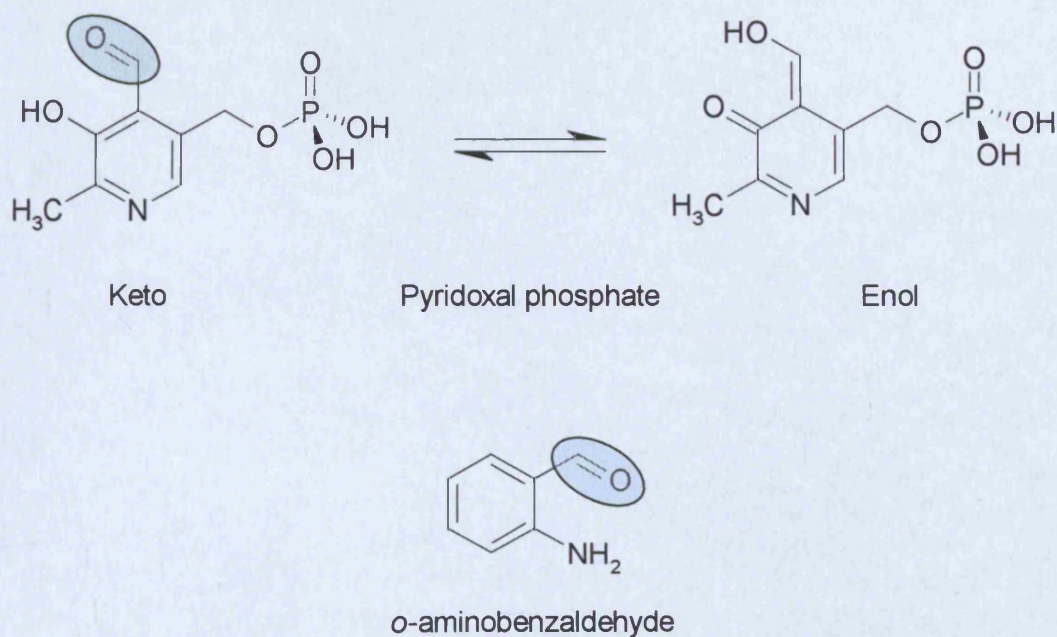
Figure 4.5. Structural formulae of pyridoxal phosphate (vitamin B$_6$ coenzyme) and the reagent *o*-aminobenzaldehyde used in the chemical test for P5C. The active coenzyme form of vitamin B$_6$ is the keto tautomer. The common carbonyl function of both the pyridoxal phosphate keto tautomer and *o*-aminobenzaldehyde that are involved in the proposed Claisen condensation reaction with the activated C-4 carbon of P5C are highlighted in blue. P5C is a unique endogenous vitamin B$_6$ antagonist and de-activation of vitamin B$_6$ may be a contributing factor to seizures presenting in patients with the inherited disorder hyperprolinemia type II.

217
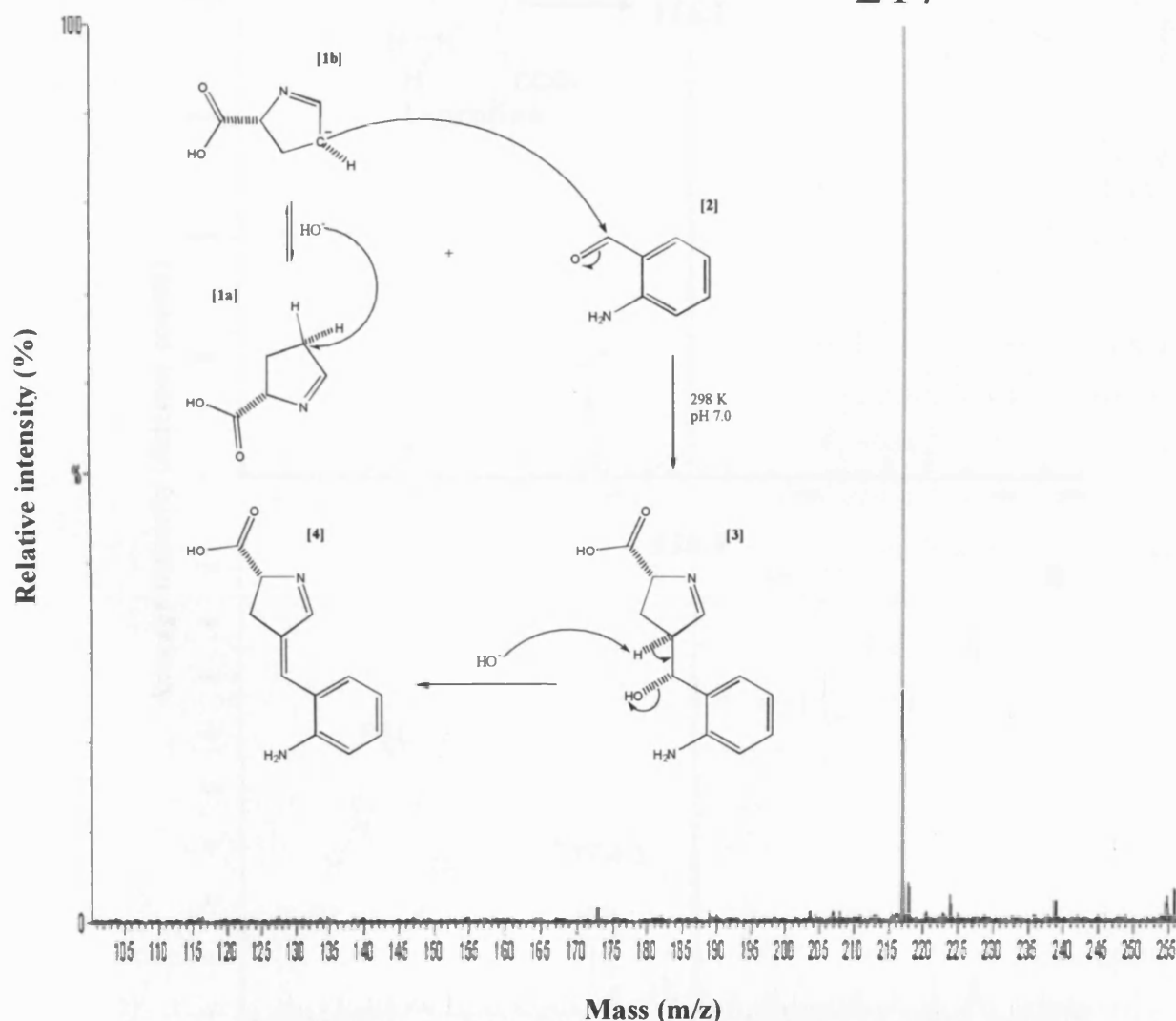
Figure 4.6. Electrospray mass spectrometry of the *o*-aminobenzaldehyde adduct of the catalytic reaction product P5C generated during the oxidation of L-proline by PRODH of *P. furiosus* DSM 3638. The ionisation mode used produced the positively charged quasimolecular ion ([M+H]$^+$) species. The spectrum shows a m/z peak of 217 that represents the stable P5C-*o*-aminobenzaldehyde adduct. Inset: the proposed mechanism for the reaction of P5C (1a) and *o*-aminobenzaldehyde (2). Following addition of activated P5C (1b) C4 carbon to the aldehyde function of *o*-aminobenzaldehyde redolent of a Knoevenagel reaction whereby the imine moiety of activated P5C is comparable to the carbonyl in a conventional ketone-aldehyde reaction, the adduct precursor (3) forms following condensation and elimination of water forms a stable adduct (4). The reaction is analogous to that of P5C with pyridoxal phosphate (Farrant *et al.*, 2001). An alternative reaction mechanism based on a nucleophilic enamine is equally viable (Appendix, Figure A1.2).
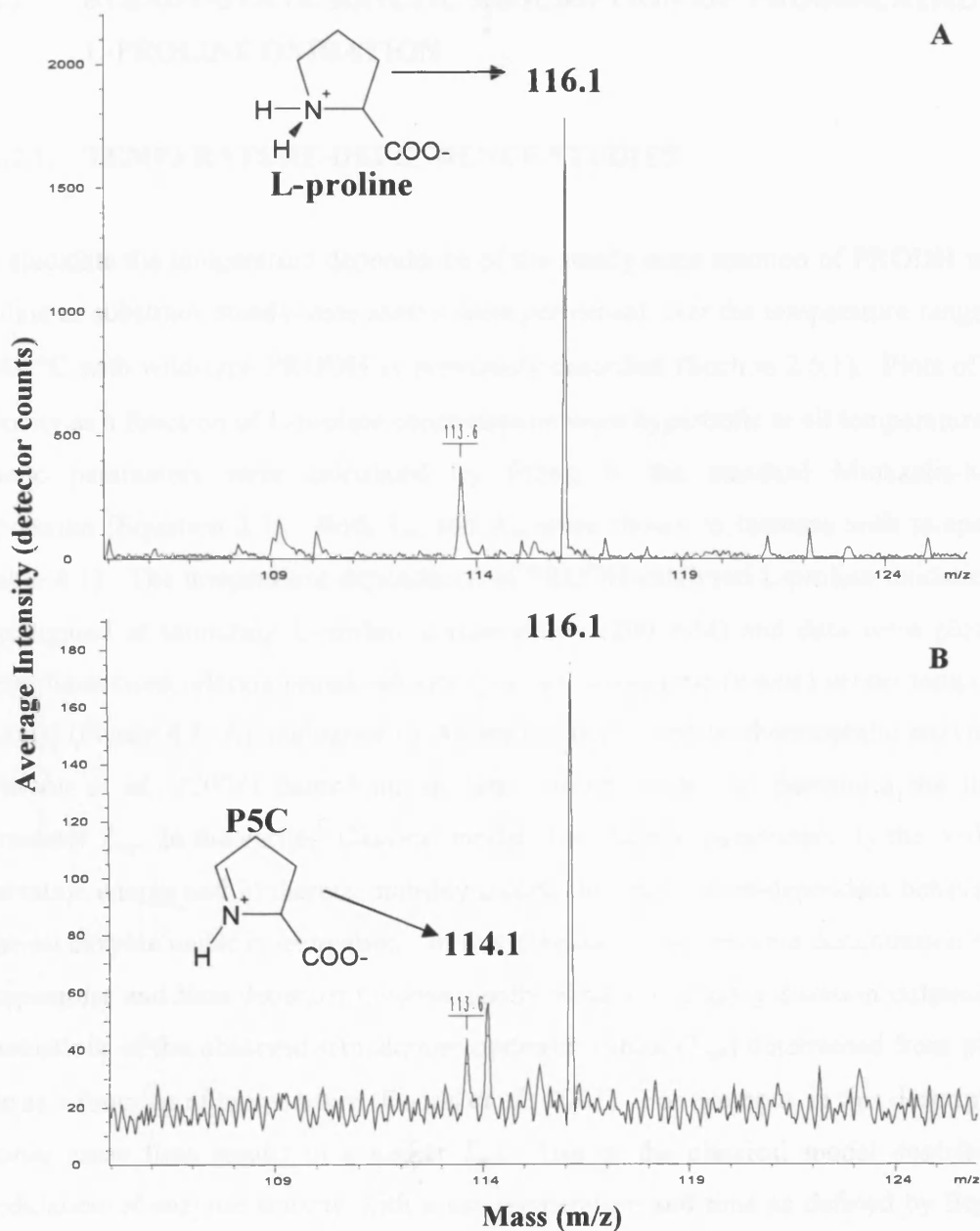
Figure 4.7. MALDI-ToF mass spectrometry of P5C produced from the oxidation of substrate L-proline catalysed by PRODH of *P. furiosus* DSM 3638. *Spectrum A*, authentic L-proline showing a m/z peak at 116.1 representing the positively charged quasimolecular ion ($[M+H]^+$) species. *Spectrum B*, sample of assay mixture containing excess L-proline (200 mM), 75 nM PRODH and limiting ferricenium ion (200 µM). The reduction of ferricenium ion was to completion as monitored by the absorbance change at 300 nm for complete reduction of ferricenium ion to ferrocene. The $[M+H]^+$ ion of both surplus L-proline and the reaction product P5C are represented by the m/z peaks at 116.1 and 114.1 respectively. The matrix used was gentisic acid.

4.2.2.   STEADY-STATE KINETIC DESCRIPTION OF PRODH-CATALYSED L-PROLINE OXIDATION

4.2.2.1.   TEMPERATURE-DEPENDENCE STUDIES

To elucidate the temperature dependence of the steady-state reaction of PRODH with L-proline as substrate, steady-state assays were performed over the temperature range of 40 to 80 °C with wild-type PRODH as previously described (Section 2.6.1). Plots of initial velocity as a function of L-proline concentration were hyperbolic at all temperatures, and kinetic parameters were calculated by fitting to the standard Michaelis-Menten expression (Equation 2.1). Both k_{cat} and K_m were shown to increase with temperature (Table 4.1). The temperature dependence of PRODH-catalysed L-proline oxidation was investigated at saturating L-proline concentration (200 mM) and data were plotted in three-dimensions relating initial velocity (y-axis) _versus_ time (x-axis) _versus_ temperature (z-axis) (Figure 4.8, A) analogous to the studies performed on thermophilic enzymes by Peterson _et al._, (2004) describing an 'equilibrium model' to determine the thermal parameter T_{eq}. In the earlier 'classical model' two thermal parameters, 1) the Arrhenius activation energy and 2) thermal stability dictate the temperature-dependent behaviour of a given enzyme under investigation. In this classical model enzyme denaturation is both temperature and time dependent, consequently variation of assay duration culminates in fluctuations of the observed temperature optimum values (T_{opt}) determined from plots of rate as a function of temperature (Daniel _et al._, 2001). For example, in this description, a shorter assay time results in a higher T_{opt}. Use of the classical model describes the modulation of enzyme activity with assay temperature and time as defined by Equation 4.1.

$$V_{max} = k_{cat} \cdot [E]_0 \, e^{-k_{inact} \cdot t}$$

Equation 4. 1

Where V_{max} is maximal enzyme velocity, k_{cat} is the catalytic constant, $[E]_0$ is the total enzyme concentration, k_{inact} is the thermal inactivation rate constant and t is assay duration. The rate constants k_{cat} and k_{inact} are both temperature dependent giving rise to

Temperature (°C)	K_m (mM)	k_{cat} (s^{-1})	k_{cat}/K_m (s^{-1}/mM^{-1})
40	5.6 ± 0.4	0.4 ± 0.005	0.08 ± 0.006
45	5.6 ± 0.2	0.8 ± 0.005	0.1 ± 0.005
50	5.3 ± 0.4	1.3 ± 0.02	0.2 ± 0.02
55	8.0 ± 0.4	2.5 ± 0.02	0.3 ± 0.02
60	9.9 ± 0.4	4.0 ± 0.04	0.4 ± 0.02
65	11.6 ± 1.0	5.9 ± 0.1	0.5 ± 0.05
70	19.9 ± 2.3	10.4 ± 0.4	0.5 ± 0.08
75	25.9 ± 1.3	14.8 ± 0.2	0.6 ± 0.04
80	30.8 ± 1.1	18.01 ± 0.2	0.6 ± 0.03

Table 4.1. Steady-state kinetic parameters for the reaction of PRODH with L-proline determined at different solution temperatures. Both the apparent Michaelis constant (K_m) and the apparent turnover number (k_{cat}) generally increase with assay temperature. The relationship of the apparent kinetic parameters results in a steady increase in the calculated specificity constant (k_{cat}/K_m) with increasing temperature. Conditions: 100 mM potassium phosphate buffer, pH 7.5 at each assay temperature.
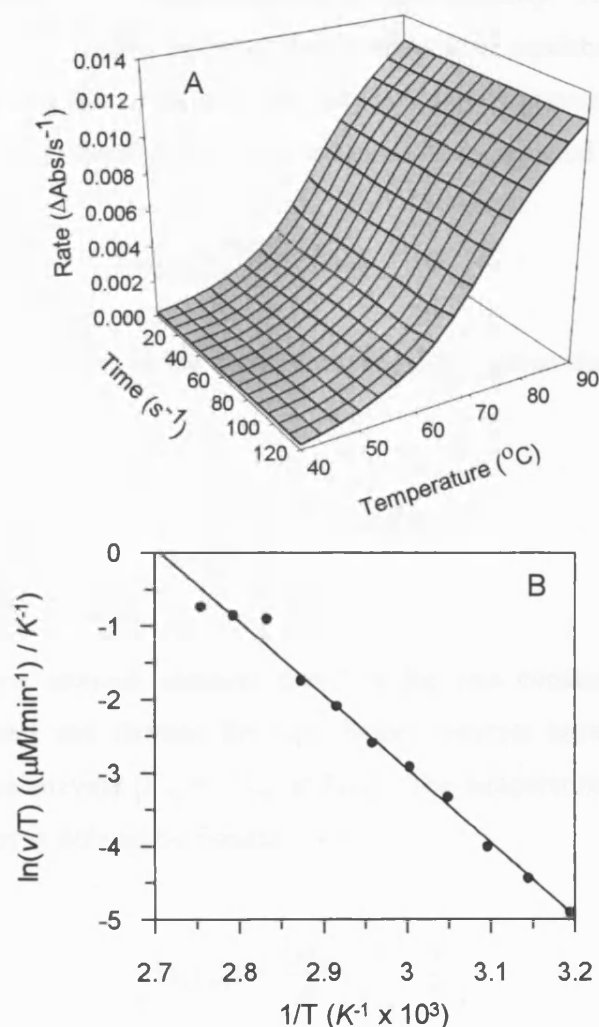
Figure 4.8. Temperature dependence and Eyring analysis of initial velocity data for wild-type PRODH reacting with L-proline. *Panel A*, three-dimensional plot showing initial velocity (y-axis) *versus* time (x-axis) *versus* temperature (z-axis). Reactions were performed with saturating L-proline (200 mM) over the temperature range of 40-90 °C. The dimension of time demonstrates any potential loss of activity due to enzyme thermal inactivation/denaturation at elevated temperatures (not observed for PRODH-catalysed oxidation of L-proline up to 90 °C). The plot was generated using SigmaPlot v9.0 for Windows. Curve-fitting used the Loess transformation to smooth data by local regression that applies a tricube weight function to elicit trends from noisy data (Cleveland, 1993). This trend was then used to extrapolate data back to time-point zero to compensate for the time lag between reaction initiation and the start of data collection. Conditions: 100 mM potassium phosphate buffer pH 7.5. *Panel B*, Eyring plot of initial velocity data for PRODH with L-proline as substrate. Thermodynamic parameters derived from fitting of the data to the Eyring equation are $\Delta H^{\ddagger} = 83.4 \pm 2.9$ kJ·mol^{-1}, $\Delta S^{\ddagger} = 27.2 \pm 1.0$ J·mol^{-1}·K^{-1} and $\Delta G^{\ddagger}_{373} = 73.3$ kJ·mol^{-1} at 100 °C.

T_{opt} values that are not a 'true' intrinsic thermal enzyme property. The latest 'equilibrium model' (Peterson *et al.*, 2004) proposes that a reversible equilibrium exists between active (E_{act}) and inactive (E_{inact}) forms of an enzyme and that irreversible denaturation of the inactive form leads to the thermal denatured state (X) as depicted in Scheme 4.1.

$$E_{act} \rightleftharpoons E_{inact} \longrightarrow X \qquad \textbf{Scheme 4. 1}$$
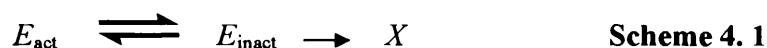
The concentration of enzyme in the active form (E_{act}) at a given time point is described by Equation 4.2.

$$(E_{act}) = \frac{(E_0) - (X)}{1 + K_{eq}} \qquad \textbf{Equation 4. 2}$$

Where K_{eq} is a new enzyme constant that like the rate constants k_{cat} and k_{inact} is temperature-dependent and defines the equilibrium constant between the active and inactive forms of the enzyme [$K_{eq} = (E_{inact})/(E_{act})$]. The temperature dependence of this new enzyme property is defined by Equation 4.3.

$$\ln(K_{eq}) = \frac{\Delta H_{eq}}{R}\left(\frac{1}{T_{eq}} - \frac{1}{T}\right) \qquad \textbf{Equation 4. 3}$$

Where ΔH_{eq} is the enthalpic change relating to the conversion of E_{act} to E_{inact} forms of the enzyme and T_{eq} is the temperature where the concentrations of both the E_{act} and E_{inact} enzyme forms are equal ($K_{eq} = 1$). This new intrinsic thermal enzyme parameter (T_{eq}) represents a sub-millisecond timescale-reversible temperature-dependent equilibrium between active enzyme and inactive (or less active) forms (Peterson *et al.*, 2004). The effect of a shift in T_{eq} is up to two orders of magnitude greater than the contribution of thermal denaturation on a decrease in enzyme activity above the optimal temperature. The application of this proposed equilibrium model however, may be restricted to monomeric enzymes as the model does not take into account the complicating effects of thermally induced subunit dissociation of oligomeric enzymes (Peterson *et al.*, 2004).

Curve-fitting of the three dimensional plot of PRODH activity was performed using the SigmaPlot software package, Version 9.0, by employing a Loess transformation to smooth the data set based on local regression that applies a tricube weight function to elicit trends from noisy data (Cleveland, 1993). The trend elicited from the smoothing process was then used to extrapolate data back to time-point zero to compensate for the time lag between the addition of enzyme to initiate the reaction and the start of data collection. The dimension of 'time' was necessary in the three-dimensional data-set as to observe any potential loss in activity due to enzyme thermal inactivation/denaturation at elevated temperature equal to and exceeding the source (evolved) temperature, though no loss in the rate of catalytic L-proline oxidation by PRODH was apparent from this data. Thermodynamic parameters were obtained by fitting to the Eyring equation (Equation 2.3) describing a unimolecular reaction. Plotting temperature dependence data using Equation 2.3 for the calculation of thermodynamic parameters is preferred over the use of the classical Arrhenius plot, namely a plot of $\ln(k)$ as a function of $1/T$. Although data appears linear in the corresponding Arrhenius plot over the accessible temperature range of experimentation, the Arrhenius equation and hence the data fit is actually curved and asymptotically approaches infinity at elevated temperatures (Scrutton, et al., 1999).

Initial velocity was strongly dependent on temperature and analysis of the data using the Eyring plot (Figure 4.8, B) gave thermodynamic parameters $\Delta H^{\ddagger}$ = 83.4 ± 2.9 kJ·mol^{-1}, $\Delta S^{\ddagger}$ = 27.2 ± 1.0 J·mol^{-1}·K^{-1} and $\Delta G^{\ddagger}$ = 73.3 kJ·mol^{-1} (at 373 K). Incubation of PRODH at elevated temperatures prior to activity assay showed the enzyme is extremely stable with no loss of activity evident up to 100 °C; above this temperature, thermal denaturation of PRODH is apparent with complete loss of activity realised after 10 minutes of incubation in glycerol buffer at temperatures ≥ 115 °C (Figure 4.9, A). Thus, PRODH from P. furiosus is the most thermostable L-proline dehydrogenase described to date, exceeding the thermal stability limit described for PDH1 of P. horikoshii with optimal activity at ~90 °C (Kawakami et al., 2005; Figure 4.9, B).
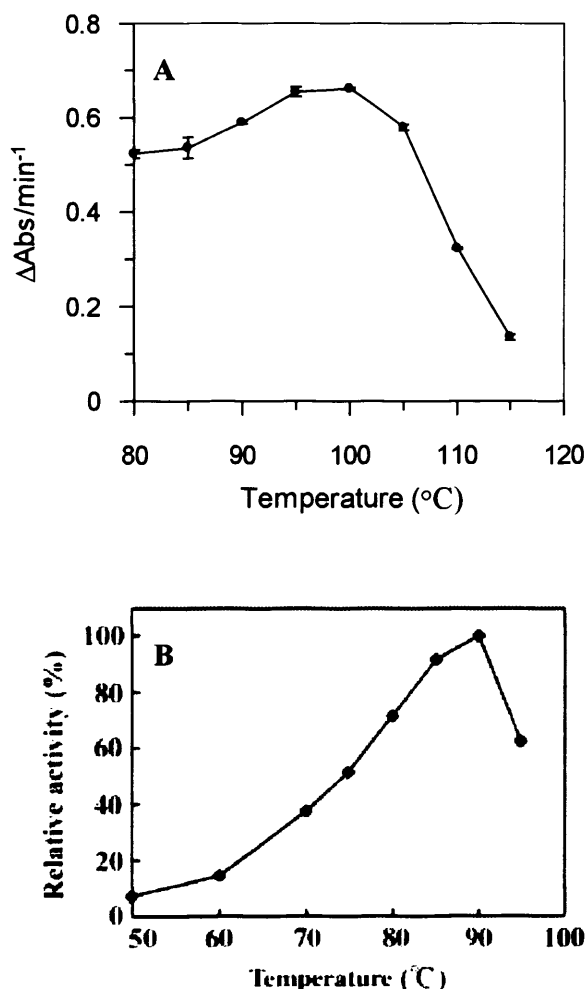
Figure 4.9. Graphs illustrating the thermostability of PRODH of *P. furiosus* DSM 3638 and the dye-linked L-proline dehydrogenase (PDH1) of *P. horikoshii* OT-3. *Panel A*, the effect of temperature on the activity of PRODH from *P. furiosus* highlights that thermoinactivation of the enzyme occurs at solution temperatures $\geq 100\ ^\circ C$. *Panel B*, the corresponding thermostability profile for PDH1 of *P. horikoshii* reveals an optimum temperature for activity of ~90 $^\circ$C. PRODH of *P. furiosus* is therefore the most thermostable L-proline dehydrogenase described to date. Conditions: (A), 100 mM potassium phosphate buffer pH 7.5, 200 mM L-proline, 200 μM ferricenium, 75 nM PRODH. Assay mixtures were incubated in glycerol baths at the elevated temperatures described in sealed reaction vessels. (B), data regarding PDH1 of *P. horikoshii* was collected using ferricyanide as the artificial electron acceptor. Figure 4.9, B, is taken from Kawakami *et al.*, (2005).

177

4.2.2.2. pH-DEPENDENCE STUDIES

No previous studies regarding L-proline oxidising enzymes from thermophilic/hyperthermophilic sources has documented any detailed pH dependence studies of an extremophilic L-proline dehydrogenase system. Therefore, to provide a comprehensive pH profile of the reaction catalysed by PRODH of _P. furiosus_, steady-state turnover assays were performed aerobically with L-proline substrate at 60 °C over the pH range 5.5 - 10.0 to identify kinetically influential ionisations in the catalytic mechanism of L-proline oxidation as previously described (Section 2.6.1). Ionic strength across the pH range was kept constant using a three-component buffer system. All plots of initial velocity as a function of L-proline concentration were hyperbolic and kinetic parameters were calculated by fitting to the Michaelis-Menten expression (Equation 2.1; Table 4.2). For wild-type PRODH the pH dependence of k_{cat}/K_m was found to be bell-shaped and fitting of the data (Equation 2.6) yielded macroscopic pK_a values of 7.0 ± 0.2 (acid limb) and 7.6 ± 0.2 (alkali limb) (Figure 4.10, A). Assuming no change in rate-limiting step across the pH range, these macroscopic pK_a values most likely represent the ionisation of residues in the free enzyme, following the process described in Scheme 4.2.

$$E + S \xrightarrow{\;k_{cat}/K_m\;} E + P$$
Scheme 4. 2

By analogy with other amine oxidases/dehydrogenases that share similarity at the sequence level with PRODH (Chapter 3, Figure 3.6), it was initially speculated that the pK_a of 7.0 ± 0.2 might be attributed to the ionisation of the conserved His-225 (pK_a of the ionising side chain of free histidine = 6.0), a potential active site base residue. The pH dependence of k_{cat} exhibited a simple sigmoid behaviour, and analysis by fitting of the data (Equation 2.5) produced a macroscopic pK_a value of 7.7 ± 0.1 (Figure 4.10, B) representing the pK_a of the enzyme-substrate complex according to the process depicted in Scheme 4.3.

$$ES \xrightarrow{\;k_{cat}\;} E + P$$
Scheme 4. 3

178

pH	k_{cat} (s^{-1})	K_m (mM)	k_{cat}/K_m (s^{-1} mM^{-1})
5.5	1.1 ± 0.06	10.0 ± 2.	0.1 ± 0.03
6.0	1.7 ± 0.03	5.8 ± 0.5	0.3 ± 0.03
6.5	2.4 ± 0.02	1.1 ± 0.1	2.2 ± 0.2
7.0	4.1 ± 0.04	1.3 ± 0.1	3.2 ± 0.3
7.5	6.8 ± 0.1	1.8 ± 0.3	3.8 ± 0.7
8.0	11.7 ± 0.3	5.8 ± 0.7	2.0 ± 0.3
8.5	16.4 ± 0.5	19.5 ± 1.7	0.8 ± 0.1
9.0	16.4 ± 0.3	42.4 ± 1.6	0.4 ± 0.02
9.5	16.5 ± 0.4	87.2 ± 4.2	0.2 ± 0.01
10.0	18.0 ± 1.1	138.0 ± 15.1	0.1 ± 0.02

Table 4.2. Steady-state kinetic parameters determined for the reaction of PRODH with L-proline at different pH values and at constant ionic strength. The values determined for the apparent k_{cat} increase with increasing solution pH. The apparent K_m increases dramatically from neutral to alkaline solution pH. Conditions: Buffer comprised of MES, TAPSO and diethanolamine at final concentrations of 0.052, 0.052 and 0.1 M, respectively, pH corrected at an assay temperature of 60 °C.
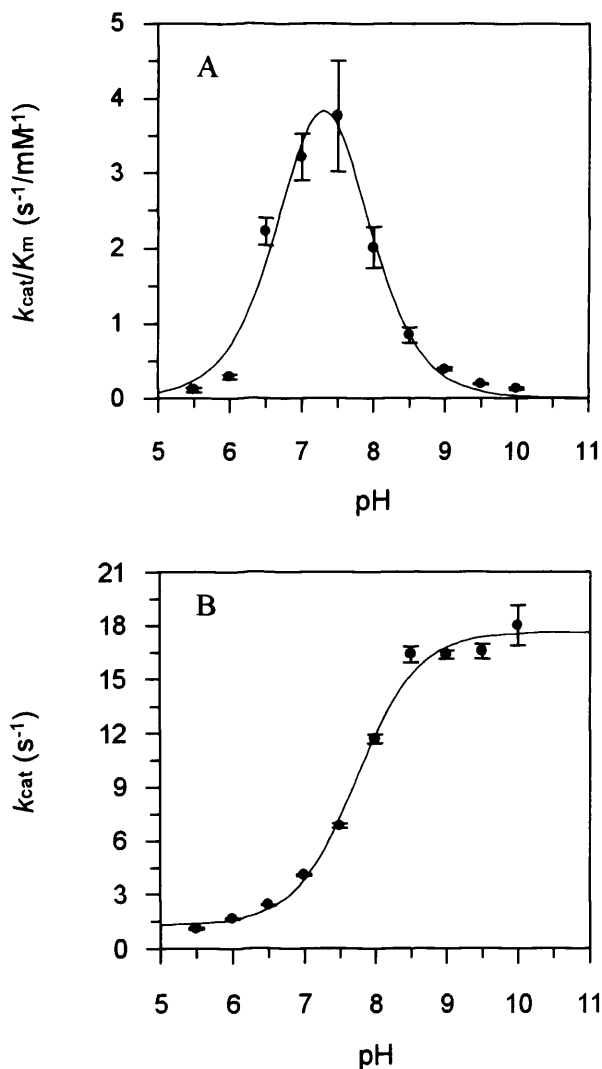
Figure 4.10. Dependence of steady-state kinetic parameters on solution pH for the PRODH-catalysed oxidation of L-proline. *Panel A*, pH dependence of k_{cat}/K_m following ionisations in the free enzyme and substrate. Fitting of data to Equation 2.6 (Section 2.6.1) gave two pK_a values of 7.0 ± 0.2 and 7.6 ± 0.2. *Panel B*, pH dependence of k_{cat} following the pK_a of the enzyme-substrate complex. Fitting of data to Equation 2.5 (Section 2.6.1) showed a simple sigmoid relationship giving a pK_a of 7.7 ± 0.1. This value is tentatively assigned to deprotonation of the substrate L-proline. Conditions: A three-component buffer system comprising 0.052, 0.052 and 0.1 M of MES, TAPSO and diethanolamine, respectively; 60 °C.

The pK_a value for the protonation of free proline is 10.6, but this might be lowered on binding to enzyme in the Michaelis complex by 2.9 pH units. Precedent for stabilisation of the free base form of amine substrates at physiological pH values is available in studies with trimethylamine dehydrogenase (TMADH) (Basran *et al.*, 2001a), and is consistent with mechanistic proposals that require the unprotonated form of the amine substrate to react with the enzyme-bound flavin (Scrutton, 2004).

4.2.3. REDOX POTENTIOMETRY AND ENERGETICS OF ELECTRON TRANSFER

The midpoint potential (E_m) of PRODH-bound FAD cofactor was determined by potentiometric redox titration with sodium dithionite at ambient temperature and pH 7.0 as previously described (Section 2.8). During the course of reductive titration, the oxidised flavin was reduced directly to the dihydroflavin form without visible population of a flavin semiquinone species indicating that the potential of the oxidised/semiquinone couple is much lower than the semiquinone/hydroquinone couple (Figure 4.11, A). Data were fitted to the concerted two-electron Nernst function (Equation 2.7) by least squares regression analysis and gave a two-electron midpoint potential value of -192 ± 3 mV and a corresponding '$2.303RT/nF$' (RTF) value of 28.9 ± 0.4 mV, consistent with the expected theoretical value (29.5 mV) for a two-electron reduction of the enzyme-bound FAD (Figure 4.11, B).

The temperature dependence of the two-electron midpoint potential of enzyme-bound FAD was investigated to assess whether a 'linear' or 'non-linear'/'bi-phasic' dependence on solution temperature was apparent for this hyperthermophilic dehydrogenase system. Midpoint reduction potentials were measured within the range 7.5 – 31 °C, the accessible temperature limits were imposed by the performance of the measurement electrode (Figures 4.12 and 4.13). In concurrence with redox data acquired by cyclic voltammetry characterising the rubredoxin and ferredoxin proteins of *P. furiosus* (Hagedoorn *et al.*, 1998), a 'normal' linear temperature dependence over the accessible temperature range was observed (Figure 4.14, A and B). The temperature dependence of the midpoint
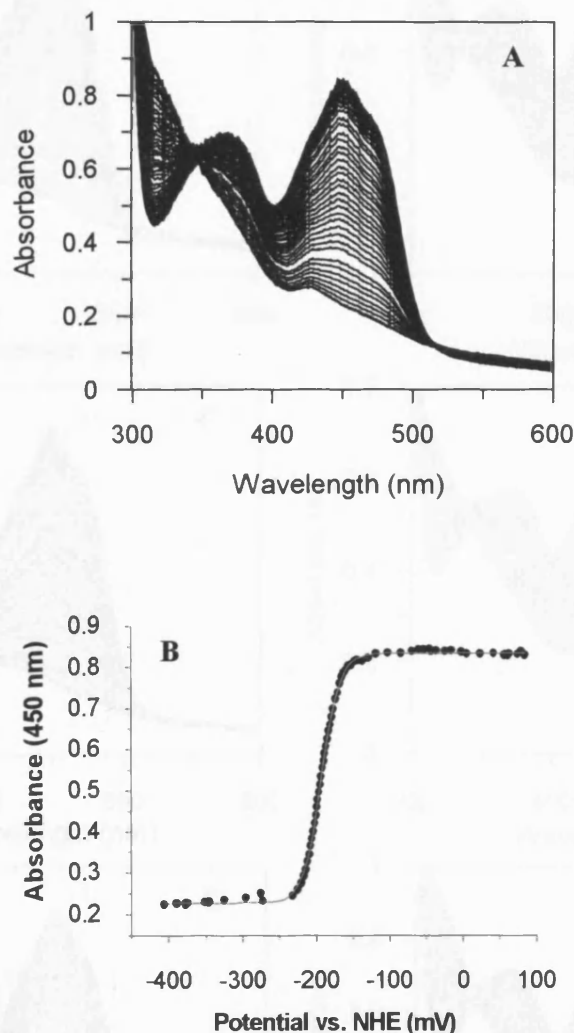
Figure 4.11. Redox potentiometric titration of wild-type monoflavinylated PRODH with sodium dithionite. *Panel A*, spectral changes accompanying reductive titration of PRODH with sodium dithionite at ambient temperature. *Panel B*, plot of absorbance at 450 nm *versus* the observed potential (corrected against the normal hydrogen electrode). The data are fitted to the Nernst equation (Equation 2.7) for a two-electron reduction process giving a midpoint reduction potential (E_m) of -192 ± 3 mV and an RTF value of 28.9 ± 0.4 mV. Conditions: 100 mM potassium phosphate buffer, pH 7.0. Mediator dyes used: methyl viologen (0.3 μM), benzyl viologen (1 μM), HNQ (7 μM) and PMS (2 μM).
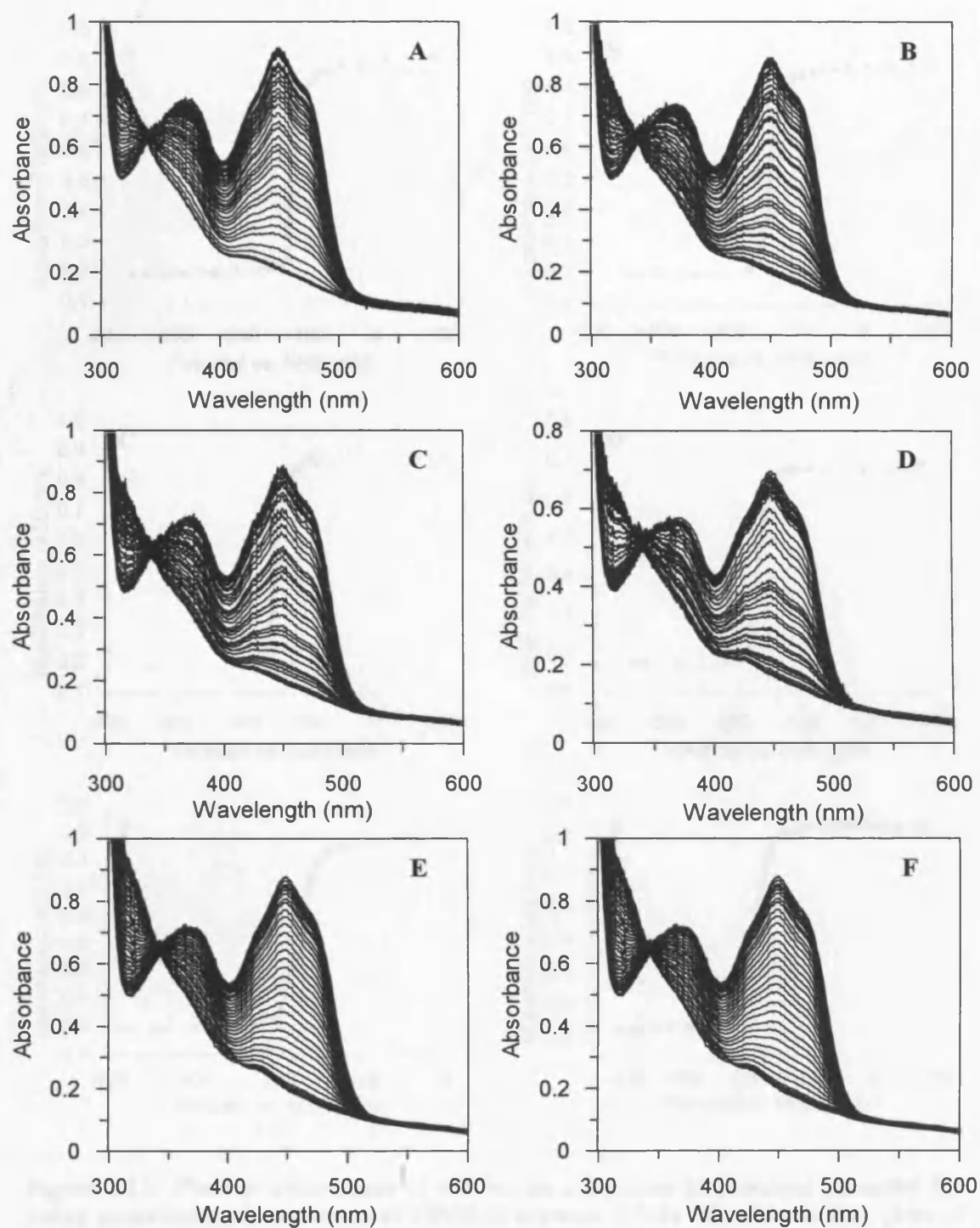
Figure 4.12. Redox potentiometric titration of PRODH with sodium dithionite at different solution temperatures. *Panels A-F*, Spectral changes accompanying reductive titration of PRODH with sodium dithionite at solution temperatures of 7.5, 13.1, 17.3, 21.1, 25.5 and 31.0 °C, respectively. Conditions: As described in figure 4.11.
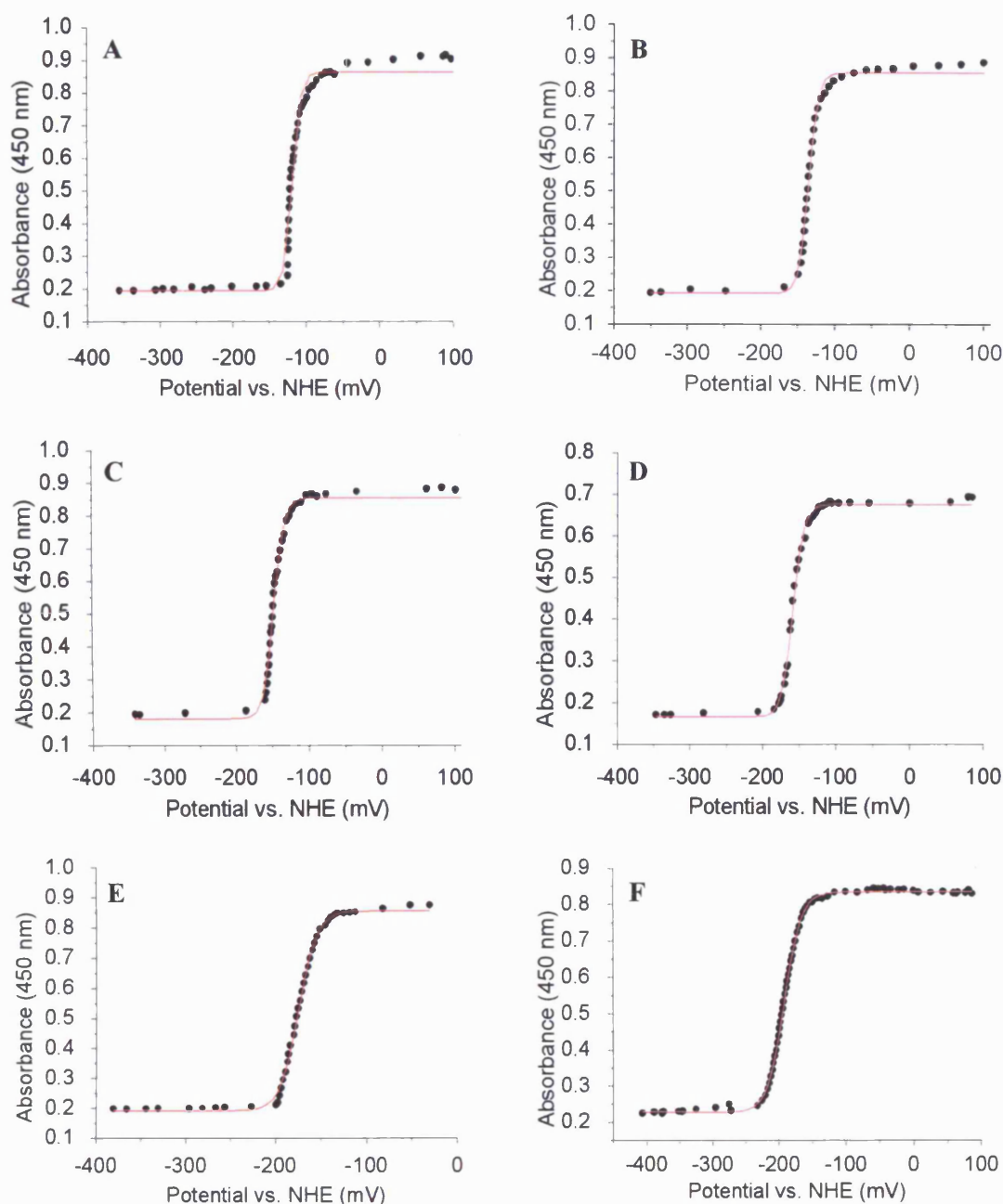
Figure 4.13. **Plots of absorbance at 450 nm as a function of observed potential for redox potentiometric titrations of PRODH between 7.5-31 °C.** *Panels A-F*, plots of PRODH flavin absorbance at 450 nm as a function of the observed potential collected during potentiometric titration of wild-type monoflavinylated PRODH at solution temperatures of 7.5, 13.1, 17.3, 21.1, 25.5 and 31.0 °C, respectively. The reductive titration spectra corresponding to each plot are shown in figure 4.12. Data are fitted to the Nernst equation (Equation 2.7) for a two-electron reduction process.
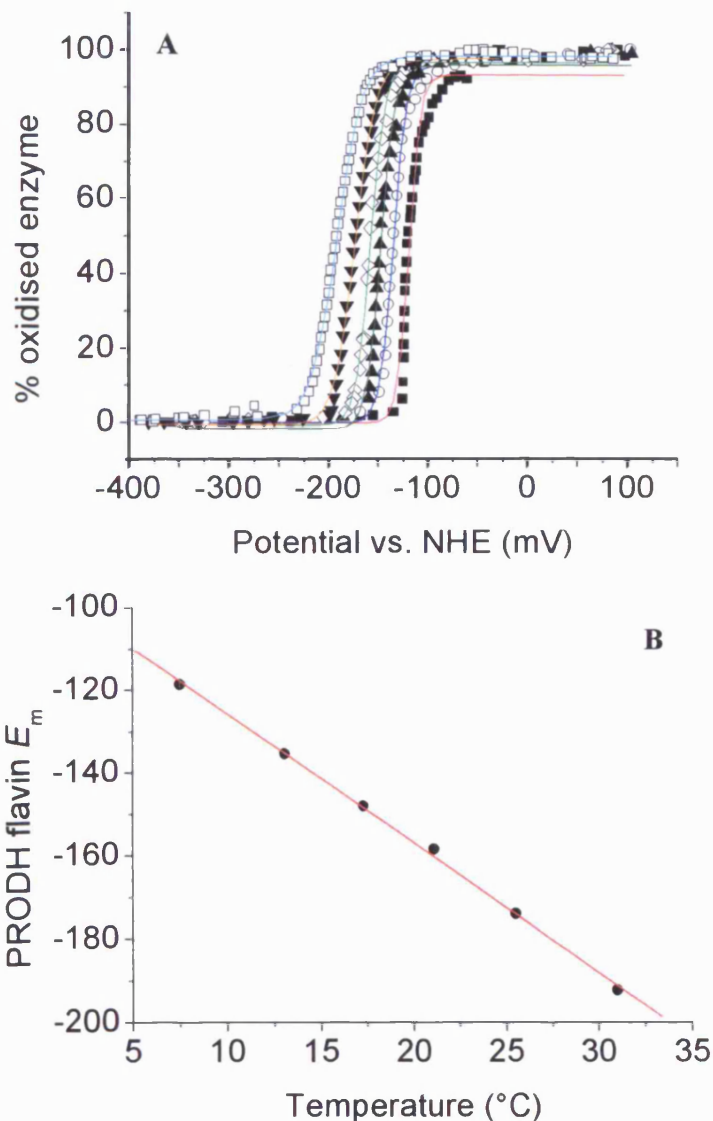
Figure 4.14. Redox potentiomtric titration of wild-type monoflavinylated PRODH and temperature dependence of E_m. *Panel A*, overlay of plots showing % oxidised enzyme as a function of potential for titration of PRODH at 7.5 °C (filled squares, red curve), 13.1 °C (open circles, blue curve), 17.3 °C (closed triangles, olive curve), 21.1 °C (open diamonds, light green curve), 25.5 °C (closed inverted triangles, orange curve) and 31.0 °C (open squares, cyan curve). Data are fitted to the Nernst equation (Equation 2.7) for a two-electron reduction process. *Panel B*, plot of E_m versus temperature illustrating a normal 'linear' dependence with a gradient of -3.1 ± 0.05 mV/ °C. The plot extrapolates to an operational midpoint potential at physiological temperature (100 °C for *P. furiosus*) of -407 ± 5 mV.

potential was calculated to be -3.1 ± 0.05 mV/°C from the gradient of the plot. Extrapolation to physiological temperature (_i.e._ 100 °C for _P. furiosus_) indicated an operational midpoint potential for PRODH of -407 ± 5 mV (assuming no hysteretic behaviour at elevated temperatures beyond the accessible temperature range of the experiment). Thermodynamic parameters for the reduction of PRODH by sodium dithionite were calculated from the temperature dependence of the two-electron midpoint potential and the standard free energy change ($\Delta G^{\circ\prime}$) of the reaction was calculated directly (Equation 2.8) giving a value for the spontaneous reaction: $\Delta G^{\circ\prime}{}_{298} = -41.1$ kJ·mol^{-1} at 25 °C. Calculation of the Gibbs free energy change therefore allowed the determination of the equilibrium constant ($K^{\prime}{}_{eq}$) for the redox reaction (Equation 2.9), giving $K^{\prime}{}_{eq} = 1.59 \times 10^{7}$ and thus, revealed the direction of the reaction. The standard entropy change of the reaction ($\Delta S^{\circ\prime}$) was determined using Equation 2.10 giving $\Delta S^{\circ\prime} = -290.4$ J·mol^{-1}·K^{-1} and from this, the standard enthalpy change of the reaction ($\Delta H^{\circ\prime}$) was derived from Equation 2.11 giving $\Delta H^{\circ\prime} = -127.6$ kJ·mol^{-1}.

The reduction potential for the L-proline/P5C couple has been measured previously at 20 °C and shown to be -123 mV with a corresponding Nernst slope of 30 mV consistent with a two-electron transfer process (Figure 4.15; Becker and Thomas, 2001). At this temperature, the E_m value of FAD cofactor of PRODH is -157 mV (as determined from the linear fit of the temperature dependence; Figure 4.14, B), therefore, the potential difference ($\Delta E^{\circ\prime}$) between the L-proline/P5C couple and the FAD cofactor bound to PRODH is -34 mV which correlates to a thermodynamically unfavourable Gibbs free energy change of +6.56 kJ·mol^{-1} for the reaction, highlighting that the electron transfer energetics of the catalytic reaction of PRODH with physiological substrate at 20 °C is endergonic, consistent with kinetic observations of negligible enzyme activity with substrate at solution temperatures ≤ 25 °C.
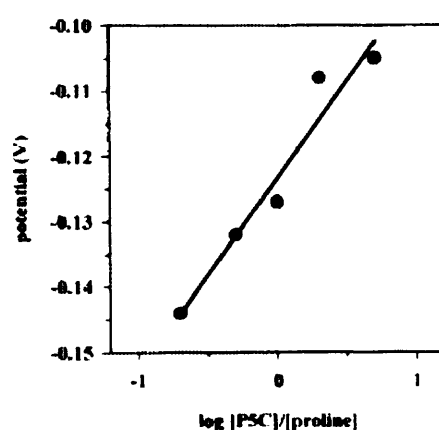
Figure 4.15. Nernst plot of potentiometric measurements taken with various ratios of L-proline:P5C. A reduction potential for the L-proline/P5C couple of -123 mV was determined from the plot with a slope of 30 mV consistent with a two-electron process. Conditions: 70 mM Tris buffer pH 7.5, L-proline:P5C ratio of 5:1, 2:1, 1:1, 1:2 and 1:5 at 600 μM final concentration and 1 μM PutA at 20 °C. Figure taken from Becker and Thomas, (2001).

4.3. DISCUSSION

4.3.1. KINETIC PROPERTIES OF PRODH

Thermodynamic studies have revealed that the steady-state reaction of PRODH from _P. furiosus_ with the physiological substrate L-proline is extremely temperature dependent illustrated by a large enthalpy of activation ($\Delta H^{\ddagger}$) deduced from Eyring analysis of the raw data. The $\Delta H^{\ddagger} = 83.4 \pm 2.9$ kJ·mol^{-1} is greater than the enthalpies of activation documented for the flavoprotein tetrameric sarcosine oxidase (Harris _et al._, 2000) and the quinoproteins methylamine dehydrogenase (MADH) from _Methylophilus methylotrophus_ (Basran _et al._, 1999) and aromatic amine dehydrogenase (AADH) from _Alcaligenes faecalis_ (Hothi _et al._, 2005). Determination of the rate-limiting step in the reaction pathway of L-proline oxidation by PRODH by implementing high-temperature rapid-reaction kinetic experiments with selectively deuterated substrate is required in order to shed more light on the observed thermodynamic parameters.

PRODH of _P. furiosus_ has been demonstrated to oxidise the C-N bond of the physiological substrate L-proline, and the active site of the enzyme can sterically accommodate the six-membered ring moiety of the secondary amine L-pipecolic acid (slower substrate). The enzyme has also been demonstrated to catalyse the oxidation of the equivalent methyl group of sarcosine (slowest substrate). Despite a concerted international effort to resolve the mechanistic basis of flavoprotein-catalysed amine oxidation, fundamental aspects of the flavoenzymes mechanistic strategy remain unconcluded.

To further address these questions regarding the mechanistic basis of flavoenzyme-catalysed amine oxidation, and to elucidate a description of the mechanism employed by PRODH for the oxidation of L-proline substrate, pH-dependence studies were performed to identify kinetically influential ionisations in the catalytic reaction as previously described (Section 2.6.1). Inspection of the pH profile of the PRODH reaction with L-

proline indicates a strong pH dependence on kinetic parameters k_{cat} and k_{cat}/K_m. A single macroscopic pK_a of value 7.7 ± 0.1 is observed in the plot of k_{cat} versus pH that identifies ionisation in the enzyme-substrate complex (Scheme 4.3) and maximum activity is realised on the alkaline side of this ionisation. This is consistent with kinetic studies of other amine oxidising flavoproteins such as TMADH (Basran _et al._, 2001a), where the ionisation has been attributed to the deprotonation of the cationic form of the substrate. This implies the unprotonated form of the substrate is reactive, consistent with proposed mechanisms of amine substrate oxidation by flavoprotein enzymes (Scrutton, 2004). Biologically relevant amines typically exhibit pK_a values that exceed physiological pH (pK_a of L-proline = 10.6). On binding substrate, the pK_a for the substrate ionisation is sufficiently perturbed to favour formation of the deprotonated form at physiological pH. In the case of TMADH, stopped-flow studies indicate there is a shift in pK_a of about 3.5 pH units (from pH 9.8 to ~pH 6.5) for the substrate ionisation on forming the enzyme-substrate complex (Basran _et al._, 2001a). Studies into the pH dependence of the reaction of monomeric sarcosine oxidase (MSOX) from _Bacillus_ sp. B-0618 with the slow substrate L-proline suggest that the pK_a of the MSOX-bound L-proline may decrease by >2.5 pH units in comparison to the pK_a of free L-proline (Zhao and Jorns, 2005). The data for _P. furiosus_ PRODH suggests that a similar shift in pK_a of about 2.9 pH units (from 10.6 to 7.7) occurs on binding L-proline to the enzyme, although unequivocal demonstration of this must await detailed stopped-flow studies with protiated and deuterated substrate. In contrast to observations with PRODH of _P. furiosus_, a flavin-ligand charge transfer interaction is observed in the MSOX–L-proline complex represented by a long wavelength absorption band in the UV-visible spectrum (Figure 4.16, A). The charge transfer complex comprises the oxidised flavin cofactor and electron-rich L-proline anion (Figure 4.16, B) that was determined to be pH dependent harbouring a pK_a essentially identical to the kinetically determined pK_a describing the ionisation in the enzyme-substrate complex (pK_a of 7.9 and 8.0 respectively; Zhao and Jorns, 2005; Zhao and Jorns, 2002).

Mutagenesis studies of TMADH have indicated a role for residues His-172 and Tyr-60 in perturbing the pK_a of the substrate (Basran _et al._, 2001b), and structural studies of DMGO
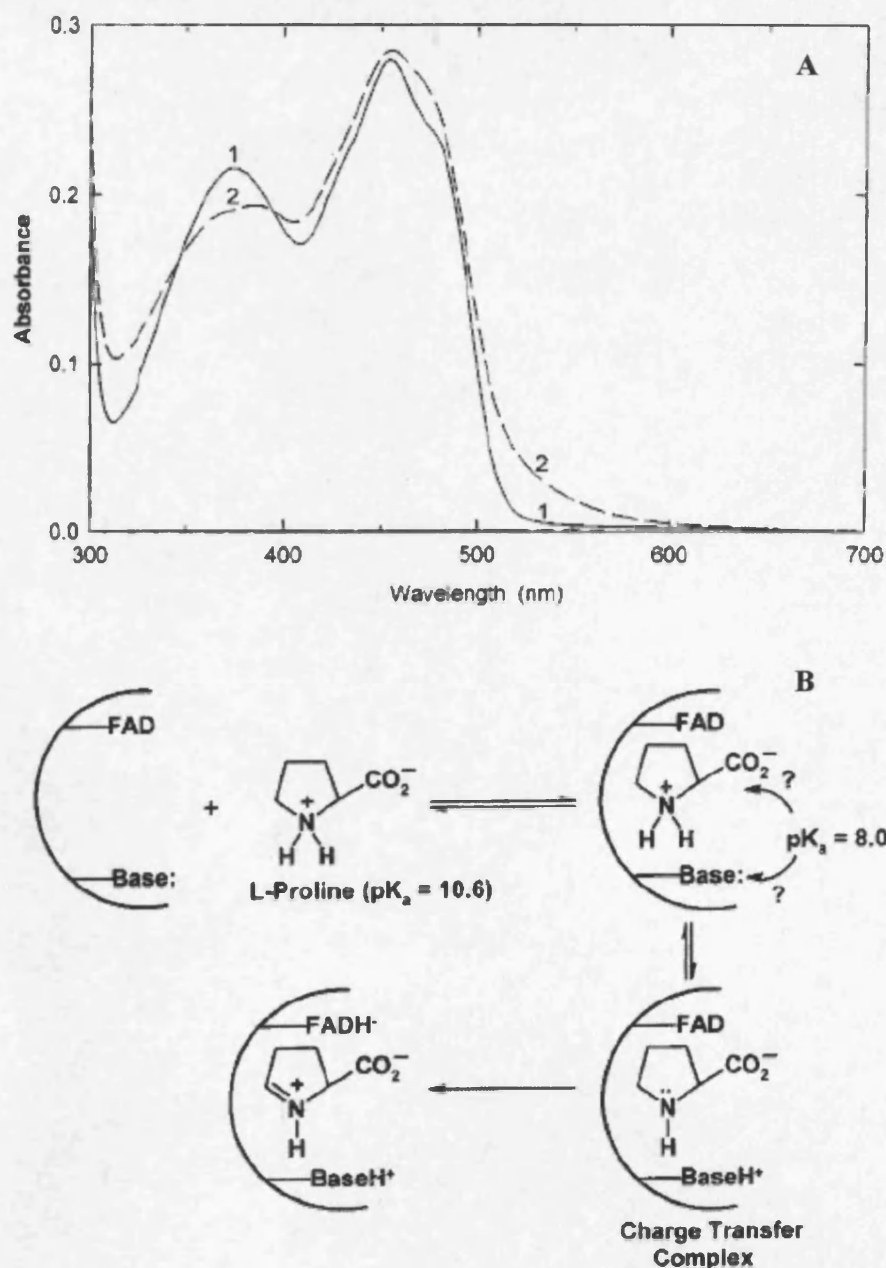
Figure 4.16. **UV-visible spectrophotometric evidence of a flavin-ligand charge transfer interaction in the complex formed with L-proline and MSOX enzyme.** *Panel A*, curve 1 (solid line) is uncomplexed enzyme. Curve 2 (dashed line) represents the spectrum recorded immediately after the addition of saturating L-proline showing the presence of a long wavelength band (λ_{max} = 512 nm, deduced from difference spectra) characteristic of a charge transfer interaction. Conditions: 50 mM potassium phosphate buffer pH 8.0, 600 mM L-proline, 4 °C. *Panel B*, proposed mechanism of electron transfer from L-proline substrate to the MSOX flavin cofactor via charge-transfer complexation. Figures taken from Zhao and Jorns, (2002).

suggest that residues His-225 and Tyr-259, which are conserved in PRODH, might also facilitate deprotonation of substrate close of physiological pH values (Leys *et al.*, 2003). Fitting of the bell-shaped dependence observed for k_{cat}/K_m on solution pH gave macroscopic pK_a values of 7.0 ± 0.2 (acid limb) and 7.6 ± 0.2 (alkali limb) (Figure 4.10, A). Based on the structural observations of DMGO and the conservation of key active site residues of DMGO in the primary sequence of PRODH, the pK_a of 7.0 ± 0.2 might be attributed to the ionisation of the conserved His-225 residue (pK_a of the ionising side chain of free histidine = 6.0), a putative active site base residue. Further investigations into the mechanism of PRODH catalysed L-proline oxidation and the assignment of ionisations was performed by mutagenesis strategies, results of these experiments are reported in Chapter 5.

It should be noted that the macroscopic pK_a values derived from the curve-fitting of the pH-dependence plots may not be an accurate reflection of the 'true' pK_a values of the catalytic reaction due to the relatively few data points defining each curve and, with reference to the k_{cat}/K_m plot, the narrowness of the bell-shaped curve. These aspects of the analysis lend the pH-profile to be seen as a more qualitative indicator of the presence of kinetically influential ionisations in the enzyme reaction and emphasis must not be placed on the exact pK_a values obtained from curve-fitting (Basran *et al.*, 2001b).

At this stage, changes in rate-limiting step or contributions from other ionisable groups could not be unequivocally ruled out as the origin of the observed dependence of the kinetic parameters of PRODH on solution pH. With reference to Briggs-Haldane kinetics (Scheme 4.4).

$$E + S \underset{k_{-1}}{\overset{k_1}{\rightleftharpoons}} ES \xrightarrow{k_2} E + P \qquad \textbf{Scheme 4.4}$$
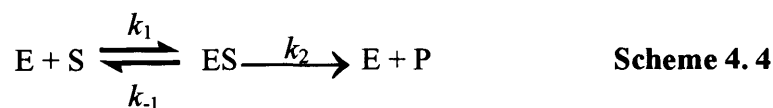
In an acute manifestation of this class of kinetics, the rate constant for the chemical step (k_2) is greater than the corresponding rate constant describing the dissociation of the enzyme-substrate complex. In this scenario, the value of k_{cat}/K_m is equal to k_1. If the activity of the enzyme requires a group to be in a basic form, at high solution pH, $k_2 > k_{-1}$.

On the other hand, when the pH of the solution is lowered and the catalytic base becomes protonated, k_2 will decrease and eventually be slower than k_{-1}. In the corresponding pH profile of k_{cat}/K_m for this enzymatic reaction, the apparent pK_a values determined from the curve-fitting will be lower than the pK_a of the catalytic base. In such a case, the apparent pK_a extracted from curve-fitting is termed a 'kinetic pK_a' that results from a change in rate-limiting step in the enzyme-catalysed reaction (Renard and Fersht, 1973).

4.3.2. THERMODYNAMIC ANALYSIS OF THE PRODH FLAVIN MIDPOINT POTENTIAL

Previous studies into the high temperature redox characterisation of proteins from hyperthermophiles has largely focused on the redox chemistry of the small iron-sulfur proteins rubredoxin and ferredoxin (Park *et al*, 1991; Smith *et al.*, 1995; Brereton *et al.*, 1998; Hagedoorn *et al.*, 1998). In an effort to establish if the molecular nature of the redox chemistry of hyperthermophilic enzyme systems holds fundamental distinctions with respect to structure-function correlations to that of the regular redox biochemistry described for mesophilic and psychrophilic proteins, potentiometric experimentation using a variety of electrochemical techniques has been reported for these small electron-carrier proteins. The conflicting claims reporting unusual redox properties for these extremophilic proteins clearly illustrates that further work in this area of hyperthermophile research is necessary to gain an informed understanding of the 'hot' redox biochemistry of *P. furiosus* and other extremophile systems.

Evident from cross-referencing data from previous studies of *P. furiosus* ferredoxin are the apparent disparities in the documented E_m values ascertained by different electrochemical methods. Redox midpoint potential measurements of the 4Fe form of ferredoxin of *P. furiosus* using cyclic voltammetry gave a value of -370 mV (Smith *et al.*, 1995) that was in very close agreement with the corresponding reduction potential of -365 mV previously derived by bulk electrochemical/EPR redox titrations (Park *et al.*, 1991). Similarly, the reduction potential determined for the 3Fe form of ferredoxin in two separate studies using the same direct electrochemistry technique gave comparable

values of -203 mV (Brereton _et al._, 1998) and -190 mV (Smith _et al._, 1995). However, the reduction potentials determined by direct electrochemical techniques (cyclic voltammetry, differential pulse) are ~30-40 mV more negative than the corresponding values determined by bulk electrochemical titration monitored by rapid-freeze EPR spectroscopy (Brereton _et al._, 1998; Aono _et al._, 1989). A possible explanation for the observed differences in the E_m values determined by direct methods and EPR-monitored bulk redox titrations was proposed by Hagedoorn and colleagues (Hagedoorn _et al._, 1998) who stipulated that the flash-freezing process required for EPR spectroscopy analysis of these small iron-sulfur proteins renders the protein in a redox state that approximates the equilibrated state near the freezing point of the aqueous solution. The redox data gathered by EPR-monitored bulk redox titration is therefore representative of the protein reduction potential close of 0 °C. Also, peculiar to the EPR-monitored bulk redox titration method are the observations of break-points in the temperature dependence of the determined E_m that apparently represent a transition temperature (Park _et al._, 1991; Smith _et al._, 1995) representative of a phase-transition arising from an alteration in hydration state (Koller and Hawkridge, 1988) with observations relating this transition point with the onset of catalytic activity (Smith _et al._, 1995). Later studies to resolve the electrochemistry of the same protein using cyclic voltammetry found no evidence of a transition phase at elevated temperatures and concluded that observations using the EPR-monitored bulk redox titration method describing a break-point in the temperature dependence plots of the E_m were incorrect and the transition point deduced by this method may actually be an artefact of freezing the protein necessary for spectroscopic analysis by EPR (Brereton _et al._, 1998).

Conclusions drawn from theoretical studies using a macroscopic continuum model explaining a protein dielectric constant that changes non-linearly with solution temperature (Christen _et al._, 1996) have endorsed experimental observations of a temperature dependent transition manifested by a break-point at 80 °C in the temperature profile of the E_m of _P. furiosus_ ferredoxin (Adams, 1992). Molecular dynamic (MD) simulations to evaluate temperature dependent differences in the protein structural parameters of _P. furiosus_ rubredoxin (Swartz and Ichiye, 1996) have claimed that the

temperature dependence of the calculated average electrostatic potential at the Fe site ($\Delta\phi$) correlates very well with the experimentally determined temperature dependence of the E_m reported by studies using bulk redox titrations monitored by EPR (Adams, 1992). This (MD) study found that the only major structural difference in terms of the protein or solvent elicited by an elevation in solution temperature was the lack of water penetration and this may therefore account for the observed transition in temperature dependence. Critically, the experimental work on which these theoretical studies are based is suspected to be erroneous based on more recent data collected by direct cyclic voltammetry that illustrated a normal 'linear' dependence of both the ferredoxin and rubredoxin E_m values as a function of solution temperature (Hagedoorn *et al.*, 1998) that is corroborated by data presented in this thesis reporting a normal 'linear' dependence on solution temperature of the reduction potential of PRODH from *P. furiosus*. The validity of the theoretical data published concerning the small electron transfer proteins has therefore been falsified by these later observations.

In *E. coli, Salmonella typhimurium* and soil microbes such as *Pseudomonas putida*, the expression of *put* genes is dependent on the intracellular location of the protein PutA, and the proline-dependent translocation of PutA from the cytoplasm to a peripheral position on the membrane has been the subject of detailed studies (Wood, 1987; Brown and Wood, 1993; Muro-Pastor *et al.*, 1997; Surber and Maloy, 1999). The redox properties of the PutA protein from *E. coli* are well established and detailed electrochemical analyses have alluded that the redox state of the FAD cofactor of PutA is a central determinant of PutA conformation. In the absence of L-proline substrate, PutA acts as an autogeneous transcriptional repressor of the proline utilisation (*put*) regulon (Brown and Wood, 1992) by binding to the *put* control intergenic DNA region (Ostrovsky *et al.*, 1991; Brown and Wood, 1992). When L-proline becomes available, PutA switches from the cytoplasm to the membrane, therefore activating transcription of the *put* regulon allowing proline oxidation. In a series of elegant experiments coupling the redox state of PutA protein to conformational changes in the enzymes structure based on fragment analysis of limited proteolysis treatment and mapping of protease susceptibility sites (Zhu and Becker, 2003), the study discovered that FAD cofactor reduction caused concomitant

changes in the conformation of the enzyme that were transmitted to domains outside the active site where L-proline oxidation emanates. Tryptophan fluorescence spectroscopy with truncated (residues 86-601) wild-type and mutant forms of PutA86-601 revealed that residue W211 in a flexible domain near the L-proline dehydrogenase active site of PutA is the primary molecular marker of the conformational change associated with the catalytic oxidation of L-proline (Zhu and Becker, 2005). This study showed that addition of L-proline to wild-type PutA86-601 protein caused a 36 % reduction in the observed tryptophan fluorescence with an apparent rate constant of 0.59 ± 0.06 s^{-1} determined for the fluorescence change by stopped-flow fluorescence methods, that in comparison to the limiting rate constant for the reduction of the FAD cofactor of PutA by L-proline substrate of 133 ± 6 s^{-1} demonstrated that the reduction of FAD precedes the conformational transition detected by tryptophan fluorescence spectroscopy.

Substrate binding has been found not to have a regulatory effect on the flavin cofactor redox properties of PutA of *E. coli* since addition of an L-proline/P5C (1:1) mixture to PutA does not dramatically influence the reduction potential of the bound FAD cofactor (Zhu *et al.*, unpublished data). However, the reduction potential of the L-proline/P5C couple has been determined at 20 °C/pH 7.5 to be -123 mV with a corresponding RTF value of 30 mV consistent with a two-electron transfer (Becker and Thomas, 2001) that in comparison to the midpoint reduction potential of PutA of -76 mV determined under the same experimental conditions demonstrates that the reduction of PutA by substrate L-proline is thermodynamically driven by a potential difference ($\Delta E^{\circ'}$) between the L-proline/P5C couple and the PutA-bound FAD cofactor of ~45-50 mV (Becker and Thomas, 2001). In contrast, the potential difference ($\Delta E^{\circ'}$) between the L-proline/P5C couple and the FAD cofactor of PRODH at 20 °C is -34 mV correlating to a thermodynamically unfavourable Gibbs free energy change of +6.56 kJ·mol^{-1} for the reaction. Electron transfer during the catalytic reaction of PRODH with substrate L-proline is therefore endergonic at this reaction temperature, consistent with the observed kinetic behaviour of PRODH that shows negligible enzyme activity towards substrate L-proline at assay temperatures ≤ 25 °C.

It would appear at first glance from the temperature dependence of the E_m of the PRODH flavin cofactor (−3.1 ± 0.05 mV/°C) that the catalytic reaction with physiological substrate would become more endergonic as solution temperature increases considering the increasingly negative value of the PRODH flavin E_m at elevated temperatures. However, binding of substrate to the active site of PRODH in contrast to observations with PutA protein of *E. coli* may shift the redox midpoint potential of the FAD cofactor of substrate-bound PRODH to sufficiently perturb the E_m value of the non-covalently bound flavin, therefore governing the redox poise of the FAD cofactor to permit a thermodynamically favourable electron transfer event to elicit the catalytic oxidation of L-proline with concomitant reduction of enzyme flavin cofactor. This aspect of the redox chemistry of PRODH in the presence of saturating L-proline will be an immediate subject of future potentiometric experiments, and the temperature dependence of the L-proline/P5C redox couple must also be evaluated in any future analyses.

4.4.   SUMMARY

This chapter has reported the steady-state characterisation of PRODH of *P. furiosus* in the engineered monoflavinylated form to isolate the L-proline dehydrogenase activity of the enzyme with FAD non-covalently bound at the active site situated on the β subunit. Structural studies of the flavoprotein dimethylglycine oxidase (DMGO) suggest that residues His-225 and Tyr-259, conserved in PRODH (residues His-225 and Tyr-251, respectively), may facilitate deprotonation of substrate close of physiological pH values and subsequent pH dependence studies documented in this chapter have described a single macroscopic pK_a with a value of 7.7 ± 0.1 that is observed in the plot of k_{cat} versus pH and has been initially attributed to the substrate ionisation in the Michaelis complex with data suggesting that a shift in pK_a of about 2.9 pH units (from 10.6 for free L-proline to 7.7) occurs on binding L-proline to the enzyme, although unequivocal demonstration of this must await detailed stopped-flow studies with protiated and deuterated substrate. On binding substrate, the pK_a for the substrate ionisation is sufficiently perturbed to favour formation of the deprotonated form at physiological pH. This is consistent with kinetic reports concerning other oxidising flavoproteins such as trimethylamine

dehydrogenase (TMADH) with stopped-flow studies indicating that there is a shift in pK_a of about 3.5 pH units (from pH 9.8 to ~pH 6.5) for the substrate ionisation on forming the enzyme-substrate complex (Basran *et al.*, 2001a). Other data consistent with this mechanistic proposal is apparent from studies with the flavoprotein monomeric sarcosine oxidase (MSOX) from *Bacillus* sp. B-0618, suggesting that the pK_a of the MSOX-bound L-proline substrate may decrease by >2.5 pH units in comparison to the pK_a of free L-proline (Zhao and Jorns, 2005). Macroscopic pK_a values of 7.0 ± 0.2 (acid limb) and 7.6 ± 0.2 (alkali limb) were determined from the curve-fitting of the pH dependence of k_{cat} /K_m and these values most likely account for ionisation of residues in the free enzyme. By analogy with the structurally elucidated flavoprotein DMGO for which PRODH shares conserved residues implicated in the active site catalytic mechanism of substrate oxidative demethylation, it is speculated that the pK_a of 7.0 ± 0.2 might be attributed to the ionisation of the conserved His-225, a potential active site base residue, assuming no change in rate-limiting step across the experimental pH range. Further investigations into the origins of these observed pK_a's are reported in Chapter 5 using mutagenesis strategies to target potential active site residues in evaluating the active site components of PRODH.

Redox potentiometry data describing a normal 'linear' dependence of the E_m of the PRODH flavin cofactor are in agreement with measurements of the temperature dependence of the reduction potentials of the small iron-sulfur proteins ferredoxin and rubredoxin of *P. furiosus* recorded by direct cyclic voltammetry with both proteins manifesting a normal 'linear' dependence. The corroborative data described in this chapter regarding normal 'linear' temperature dependences of redox protein midpoint potentials further discounts earlier claims of the experimental observations of break-points in E_m temperature dependence plots evoked by so-called phase-transition events of protein molecule hydration, these early observations now thought to be endemic to the method of bulk redox titration monitored by EPR spectroscopy that necessitates flash-freezing of protein samples for analysis.

Results described in this chapter also conclude that P5C is the product of the PRODH-catalysed oxidation of L-proline substrate and analysis of the P5C-o-aminobenzaldehyde stable adduct by electrospray mass spectrometry lends further evidence to the mechanistic proposal of Farrant and colleagues who suggest that the reported condensation reaction between P5C and aliphatic/aromatic aldehyde and ketone compounds at physiological pH might be a generic reaction of 'activated' carbonyl compounds (Farrant *et al.*, 2001). These interactions occur *in vivo* in the inherited disorder hyperprolinemia type II, for example, P5C with acetoacetic acid.

The experimental results described in this chapter provide a good framework upon which to design and execute future experimental work regarding a high-temperature rapid-reaction kinetic description of the PRODH-catalysed oxidation of physiological substrate L-proline and the slow substrates L-pipecolic acid and sarcosine.

CHAPTER FIVE

MECHANISTIC ASPECTS OF PRODH-CATALYSED AMINE OXIDATION: STRUCTURAL BIOLOGY AND ASSIGNMENT OF SUBSTRATE IONISATION STABILISED IN THE MICHAELIS COMPLEX

CHAPTER FIVE

MECHANISTIC ASPECTS OF PRODH-CATALYSED AMINE OXIDATION: STRUCTURAL BIOLOGY AND ASSIGNMENT OF SUBSTRATE IONISATION STABILISED IN THE MICHAELIS COMPLEX.

5.1. INTRODUCTION

The principle nonaqueous components of living cells are the macromolecules comprising the proteins, carbohydrates and nucleic acids. Enzymes, constituting the largest and most diverse class of the protein macromolecules are responsible for catalysing the majority of biochemical reactions within the cell. In order to gain a detailed understanding of the molecular processes that dictate such specific, enzyme-catalysed reactions, an accurate three-dimensional description of these macromolecules permitting the resolution of individual atoms lends vital clues and a structural element towards alluding the mechanistic basis of a given physiological reaction process. The knowledge of macromolecular three-dimensional structure is not only critical in driving fundamental biochemistry research, but is also of indispensable value to the biotechnology industry. Structural description of the active site of a given enzyme identified for example, as having a key role in a defective metabolic or regulatory pathway resulting in a disease pathology allows rational design of new drug compounds to inhibit or otherwise affect the action of that enzyme (McPherson, 1994). Visualisation of the three-dimensional structure of an enzyme macromolecule also provides the physical and chemical basis of the rational, targeted mutation of amino acid residues in the design and enhancement of enzyme activity (McPherson, 2004), and structural data in conjunction with kinetic data for rationally designed mutant enzyme forms are together essential in the determination of mechanistic strategies employed during enzyme-catalysed reaction processes.

199

The two main techniques utilised for the determination of three-dimensional structures of biomacromolecules to atomic resolution are, nuclear magnetic resonance (NMR) spectroscopy and X-ray crystallography. These techniques are complementary with respect to the relative advantages and constraints of these distinct methodologies. For example, NMR spectroscopy permits structural information to be obtained for a macromolecule in the solution state, thus providing valuable information regarding the dynamics of the macromolecule. In contrast, X-ray crystallography necessitates crystallisation of the macromolecule under investigation prior to X-ray diffraction analysis towards structural elucidation in the crystalline state. Conversely, NMR spectroscopy is presently limited to the structural resolution of macromolecules with molecular weights < 30,000 Da whereas X-ray crystallography is applicable for the structural determination of macromolecules up to at least 10^6 Da (Drenth, 1999). The limitations of NMR spectroscopy in this respect are often critical in favouring X-ray crystallography for the three-dimensional structure determination of proteins.

The 1930s saw the first pioneering applications of X-ray diffraction analysis of crystallised proteins, with J. D. Bernal and Dorothy Crowfoot recording sharp diffraction patterns from crystals of pepsin (Bernal and Crowfoot, 1934), and by 1958, the first X-ray crystallographic data concerning a globular protein molecule were reported for sperm-whale myoglobin at low resolution (Kendrew, 1958). This first glimpse into the complexity of protein three-dimensional structure was remarked upon by John Kendrew following his structural determination of myoglobin at the Medical Research Council Laboratory of Molecular Biology, in Cambridge, by expressing "Perhaps the most remarkable features of the molecule are its complexity and its lack of symmetry. The arrangement seems to be almost totally lacking in the kind of regularities which one instinctively anticipates, and it is more complicated than has been predicted by any theory of protein structure." With hindsight, it is now accepted that the complex and irregular structures of enzyme molecules is a fundamental trait both commanded and illustrated by the diverse and specific functions they perform in the cell.

Progress in the 1970s in the development of recombinant DNA technology (Backman *et al.*, 1976) permitting researchers to express and purify copious amounts of protein for structural analysis, and the fervent interest of the biotechnology industry concerning protein structure and function for rational drug design has fuelled huge progress in the fields of X-ray crystallography and structural biology. Completion of the human genome project along with the concerted sequencing efforts of an array of other genome sequencing projects now underway, leads to the conclusion that the next logical progression in our understanding of the workings of the cell is the determination of the three-dimensional structures of all the proteins that the genome encodes. This strategy, under the broad rubric of 'structural genomics' will provide a comprehensive structural description of the cellular machinery at the atomic level (Bravo and Aloy, 2006). However, concerning individual protein-protein interactions that occur in the cell, it will take two decades before the representative three-dimensional structure for each type of interaction are known, of which there is estimated to by approximately 10,000 different interaction types (Aloy and Russell, 2004). The Southeast Collaboratory for Structural Genomics (SECSG) is one example of a high-throughput gene-to-structure factory comprising of four working groups (protein production, X-ray crystallography, NMR spectroscopy, and bioinformatics) that aims to develop high-throughput structural genomics research aimed at both prokaryotic and eukaryotic systems (Adams *et al.*, 2003).

The data presented so far in this thesis describes the cloning, recombinant expression and solution properties of recombinant wild-type PRODH of *P. furiosus* in terms of steady-state kinetic and redox potentiometric parameters. In this chapter, the key three-dimensional structure features of PRODH resolved by X-ray crystallography are detailed and discussed with particular emphasis on the molecular definition of the cofactor binding sites and the molecular architecture of the amine substrate (L-proline) active site. Kinetic and potentiometric data for three active site mutant enzyme forms (H225A, H225Q and Y251F) are presented and discussed in relation to the structural description of wild-type PRODH and conclusions drawn from these data toward a coherent depiction of the chemical mechanism utilised for substrate amine oxidation catalysed by PRODH.

5.2. RESULTS

5.2.1. PROTEIN CRYSTALLISATION TRIALS

The technique of single-crystal X-ray crystallography for the structural determination of a protein requires, as the title implies, the growth of suitable protein crystals of sufficient quality and size. The crystal specimen provides the X-ray diffraction pattern, the raw data from which the crystal structure of the macromolecule in the crystalline state is calculated and refined. The crystal therefore represents the 'keystone element' in the whole structure determination process (McPherson, 1989) and the size, perfection and physical qualities of the crystal are all parameters that contribute to the level of structural resolution observable in the final refined structure.

Knowledge of the scientific basis underlying the phenomena involved in protein crystallisation is limited at present and as a result there is no comprehensive theory when first attempting to crystallise a protein from solution. Crystallisation of macromolecules is a trial-and-error procedure (Drenth, 1999) and must ideally be performed systematically, searching for possible crystallisation conditions followed by optimisation of these conditions to enhance crystal quality. This is a complex and difficult process where each parameter, e.g. salt, buffer, ion concentration along with temperature and pH must be incrementally altered around the initial 'hit' condition where promising crystallisation results where initially observed (Bergfors, 1999). Factors effecting the crystallisation of proteins are highlighted in Table 5.1. The protein used for crystallisation screening must be a homogeneous sample, if the protein is not highly pure, contaminants could affect its efficacy for crystallisation. The pure protein is concentrated close of its solubility maximum and placed into a 'drop' containing a precipitant solution known as the 'mother liquor'. The solution is then brought to 'supersaturation' achieved by a variety of techniques (hanging drop and sitting drop vapour diffusion techniques, batch method, liquid-liquid diffusion and dialysis). Supersaturation drives both nucleation and crystal growth, governing both the extent and kinetics of each event. The nucleation event represents a first-order process of phase-transition where the protein molecules pass from a disordered to ordered state (McPherson, 2004). The 'critical

| PHYSICAL	CHEMICAL	BIOCHEMICAL
Temperature/Temperature variation	pH	Purity of the macromolecule/impurities
Surfaces	Precipitant type	Ligands/inhibitors/effectors
Methodology/Approach to equilibrium	Precipitant concentration	Aggregation state of the macromolecule
Gravity	Ionic Strength	Post-translational modifications
Pressure	Specific ions	Source of macromolecule
Time	Degree of supersaturation	Proteolysis/hydrolysis
Vibrations/Sounds/Mechanical perturbations	Reductive/Oxidative environment	Chemical modifications
Electrostatic/Magnetic fields	Concentration of the macromolecules	Genetic modifications
Dielectric properties of the medium	Metal ions	Inherent symmetry of the macromolecule
Viscosity of the medium	Crosslinkers/polyions	Stability of the macromolecule
Rate of equilibration	Detergents/surfactants/amphophiles	Isoelectric point
Homogeneous of heterogeneous nucleants	Non-macromolecular impurities	History of the sample

Table 5. 1. Table showing the various factors that effect crystallisation. Factors grouped as physical, chemical and biochemical in nature are described. The table information is taken from McPherson, 2004.

nuclei' representing a small, completely ordered protein assembly will then promote crystal growth, as long as there is a degree of supersaturation.

Crystallographic analysis of proteins from hyperthermophilic origin has continued to gain increased attention in the field of structural biology since the first three-dimensional structure of a hyperthermophilic protein, rubredoxin from *P. furiosus* was resolved to 1.8 Å in 1992 (Day *et al.*, 1992). This interest in hyperthermophilic protein structure has been incited by efforts to understand the structural basis of thermostability, to characterise novel enzyme cofactors and to assess the structural similarities between hyperthermophilic and mesophilic/psychrophilic homologues through structural genomics initiatives (Rees, 2001). These hyperthermophilic proteins provide attractive targets for structural analysis since by conventional wisdom, the thermostability of these proteins lends them to be more robust in comparison to their mesophilic counterparts, and these proteins are therefore more resilient to withstanding the harsh solution conditions toward supersaturation and also the timescales of crystallisation screens.

Crystallisation trials with wild-type recombinant PRODH of *P. furiosus* where initiated using the sitting-drop method of vapour diffusion (Figure 5.1). In this method, equilibrium is reached by the diffusion of vapour from the precipitating solution to the drop containing PRODH, or *vice versa*, therefore bringing the protein solution to supersaturation to promote a nucleation event. Crystallisation screens were performed as previously described (Monaghan *et al.*, 2005; Section 2.9). Initial crystal screens were performed with PRODH expressed from construct pPRODH1 and purified to homogeneity as described previously (Section 2.4.3). The preliminary screen (Molecular Dimensions Clear Strategy Screen MD 1-14, Screen I) consisted of 24 conditions at each given buffer pH from pH 6.0 to pH 8.5 with 0.5 pH unit increments (Appendix, Table A1.1). The concentration of PRODH was 16.4 mg/ml. After 3-4 days incubation at 19 °C, these preliminary screens yielded crystals that were yellow in colour, with a needle topology (Figure 5.2) in the condition comprising, 0.8 M sodium formate, 8 % PEG 20K and 8 % PEG 550 MME at pH 7.5 buffered by 100 mM Tris-HCl. Selected crystals from this condition were taken to the European Synchrotron Radiation Facility (ESRF),
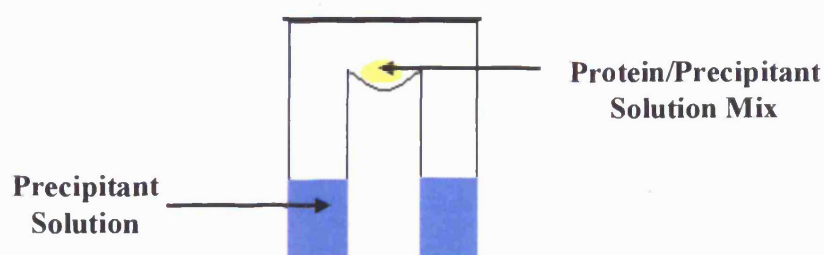
Figure 5. 1. Schematic of the sitting-drop method of vapour diffusion for the crystallisation of protein. The chamber is sealed and equilibrium is reached by vapour diffusion between the precipitant solution in the well (Blue) and the drop containing the protein (Yellow). A gradual approach to equilibrium leads to supersaturation of the protein and a nucleation event to spur the crystallisation of protein from solution.

Figure 5.2. Light microscope image of preliminary crystals obtained from the initial crystallisation screen with purified wild-type recombinant PRODH expressed from construct pPRODH1. The crystals were yellow in colour and had a needle stick topology. Diffraction analysis highlighted low diffraction resolution (~6 Å) and a high crystal mosaicity. Conditions: 0.8 M sodium formate, 8 % PEG 20K and 8 % PEG 550 MME at pH 7.5 buffered by 100 mM Tris-HCl. Protein stock concentration was 16.4 mg/ml.

Grenoble, France, for X-ray diffraction analysis. All crystals diffracted to extremely low resolution (~6 Å) and showed high mosaicity. Systematic optimisation of the initial crystallogenesis trial was therefore performed through secondary screening around the condition that produced the initial 'hit' of crystal growth. In this subsequent screen, the concentration of sodium formate (0.2-0.8 M), the concentration and nature (molecular weight) of the polyethylene glycol (PEG) utilised and the buffer pH of the mother liquor (pH 6.0-8.5) were all varied, as shown in Table A1.2 (Appendix). PRODH concentration was also subsequently reduced to 12.2 mg/ml to reduce the level of observed precipitation. This optimised screen produced yellow crystals with a similar needle topology in the condition comprising, 0.6 M sodium formate, 22 % PEG 3000 at pH 8.5 buffered by 100 mM Tris-HCl (Figure 5.3). This optimisation did produce slightly larger crystals with a smoother topology, but subsequent diffraction analysis showed negligible improvement in both diffraction resolution and mosaicity. Further screens varying type of salt in the mother liquor (Appendix, Table A1.3) and the concentration of ammonium sulphate in the mother liquor (Appendix, Table A1.4) yielded no crystal specimens.

The high level of mosaicity observed in the diffraction data for the initial crystal specimens pointed to a problem regarding crystal packing. The purification gel of PRODH expressed from construct pPRODH1 (Figure 3.11, A) highlighted an intermediate protein band identified as truncated α subunit by N-terminal sequence analysis (Table 3.4). This contaminating band constituting ~7.0 % of the protein sample (Section 3.2.8) was therefore thought to be causing the high mosaicity in the crystal specimens. Therefore, a new crystallogenesis screening project was initiated using purified PRODH expressed from construct pPRODH2 (Section 3.2.9; Figure 3.13, A) avoiding expression of truncated α subunit. Initial screens were performed with Molecular Dimensions Clear Strategy Screen MD 1-14 Screen I (Appendix, Table A1.1) and MD 1-15 Screen II (Appendix, Table A1.5) at pH 7.5 and pH 8.5 buffered by 100 mM Tris-HCl, using a PRODH stock concentration of 6.1 mg/ml as previously described (Monaghan _et al._, 2005; Section 2.9). After 3-4 days incubation at 19 °C, yellow crystals with cubic topology were observed in two separate conditions containing 0.2 M potassium thiocyanate, 8 % PEG 20K and 8 % PEG 550 MME, pH 7.5, 100 mM Tris-
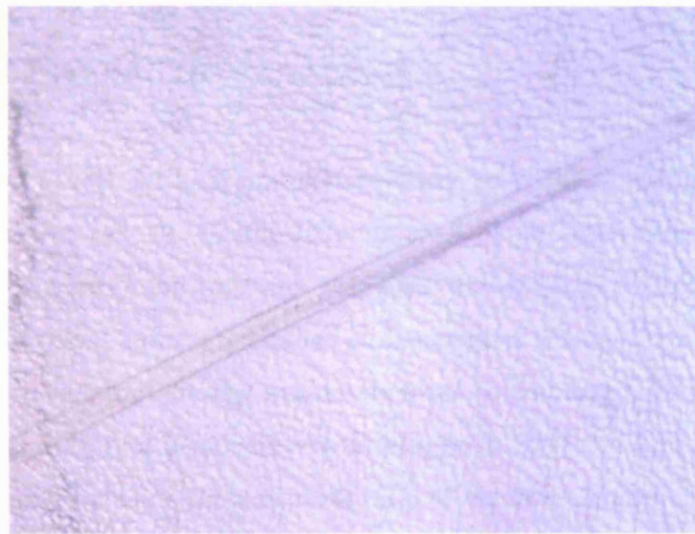
Figure 5. 3. Light microscope image showing a crystal of wild-type recombinant PRODH after optimisation of the crytallisation conditions. The crystals were yellow in colour with a needle stick topology. The crystals were slightly larger and smoother than the crystals grown in the initial screen, but diffraction analysis highlighted negligible improvement in diffraction resolution and mosaicity. Conditions: 0.6 M sodium formate, 22 % PEG 3000 at pH 8.5 buffered by 100 mM Tris-HCl. Protein stock concentration was 12.2 mg/ml.

HCl (Crystal form 1; Figure 5.4, A), and 0.2 M sodium formate, 8 % PEG 20K and 8 % PEG 550 MME, pH 8.5, 100 mM Tris-HCl (Crystal form 2; Figure 5.4, B). The average dimensions of these new crystals were 40 x 250 x 250 μm (form 1) and 50 x 50 x 200 μm (form 2). Prior to data collection at 100 K, selected crystals were soaked in mother liquor with 10 % PEG 200 as cryoprotectant and flash-cooled in liquid nitrogen for storage and transport as described previously (Section 2.9).

5.2.2. X-RAY DIFFRACTION ANALYSIS

For a given object to diffract light and consequently be visible under magnification, the wavelength (λ) of the light the object diffracts must be no larger than the object being visualised. By analogy, in order to visualise the individual atoms of a protein macromolecule, in which atoms are bonded at distances of around 1.5 Å, electromagnetic radiation with wavelength of similar magnitude must be employed. X-rays with λ of $10^{-7} - 10^{-11}$ m (1000-0.1 Å) first discovered by Roentgen in 1895 fall into this category and are therefore suitable for the structural resolution of macromolecules at the atomic level (Table 5.2). Proteins are made up predominantly of the 'light' elements carbon, nitrogen and oxygen that carry only a few electrons which are responsible for diffraction of the primary X-ray beam. These light atoms scatter X-rays much more weakly than in comparison to heavier elements. Also, the large size of protein macromolecules in comparison to small organic compounds for example, invariably means that fewer molecules are present in the protein crystal. These two factors necessitate the use of an intense X-ray beam to permit data collection. The most powerful source of electromagnetic radiation available to the crystallographer is that of synchrotron radiation. Synchrotrons are giant ring structures within which electrons circulate at near speed of light velocity steered by precise magnets. The forced curved motion of the charged body (electron) promotes the emission of energy in a magnetic field (synchrotron radiation) in the form of X-rays which are focussed by mirrors and monochromators tangential to the storage ring that provide intense monochromatic X-ray beams of selectable wavelength (Rhodes, 1993).

A

B
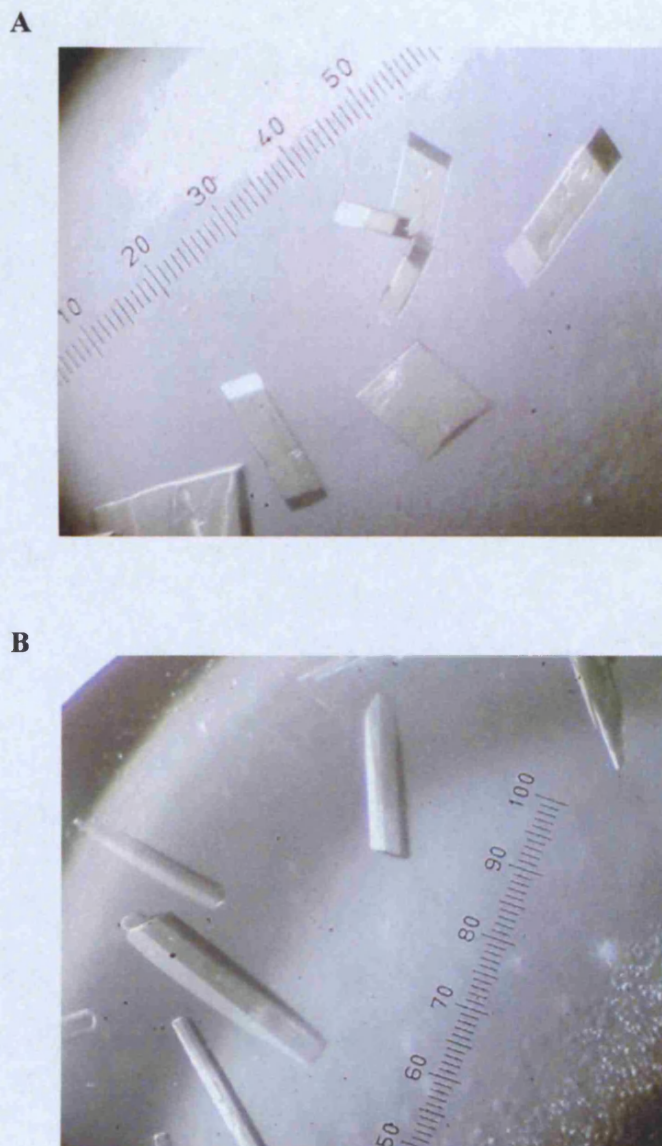
Figure 5. 4. Light microscope images showing crystals of purified recombinant PRODH expressed from construct pPRODH2. *Panel A*, Crystal form 1 of PRODH. Conditions: 0.2 M potassium thiocyanate, 8 % PEG 20K and 8 % PEG 550 MME, pH 7.5, 100 mM Tris-HCl. *Panel B*, Crystal form 2 of PRODH. Conditions: 0.2 M sodium formate, 8 % PEG 20K and 8 % PEG 550 MME, pH 8.5, 100 mM Tris-HCl. After 3-4 days incubation at 19 °C, yellow crystals with cubic topology were observed in both of these conditions. The average dimensions of these new crystals were 40 x 250 x 250 μm (form 1) and 50 x 50 x 200 μm (form 2).

THE ELECTROMAGNETIC SPECTRUM			
Wave Type	**Wavelength (m)**	**Frequency (Hz)**	**Energy (J)**
Radio Waves	> 0.1	$< 3 \times 10^9$	$< 2 \times 10^{-24}$
Microwaves	$10^{-3} - 0.1$	$3 \times 10^9 - 3 \times 10^{11}$	$2 \times 10^{-24} - 2 \times 10^{-22}$
Terahertz Waves	$10^{-3} - 10^{-4}$	$3 \times 10^{11} - 3 \times 10^{12}$	$2 \times 10^{-22} - 2 \times 10^{-21}$
Infrared	$7 \times 10^{-7} - 10^{-3}$	$3 \times 10^{11} - 4 \times 10^{14}$	$2 \times 10^{-22} - 3 \times 10^{-19}$
Visible Light	$4 \times 10^{-7} - 7 \times 10^{-7}$	$4 \times 10^{14} - 7.5 \times 10^{14}$	$3 \times 10^{-19} - 5 \times 10^{-19}$
Ultraviolet	$10^{-8} - 4 \times 10^{-7}$	$7.5 \times 10^{14} - 3 \times 10^{16}$	$5 \times 10^{-19} - 2 \times 10^{-17}$
X-rays	$10^{-11} - 10^{-8}$	$3 \times 10^{16} - 3 \times 10^{19}$	$2 \times 10^{-17} - 2 \times 10^{-14}$
Gamma Rays	$< 10^{-11}$	$> 3 \times 10^{19}$	$> 2 \times 10^{-14}$

Table 5. 2. Table showing approximate wavelengths, frequencies and energies for selected regions of the electromagnetic spectrum denoted by wave type. The wavelength of X-rays (10^{-11}-10^{-8} m) distinguish this radiation as ideally suited to the resolution of molecular structures at the atomic level.
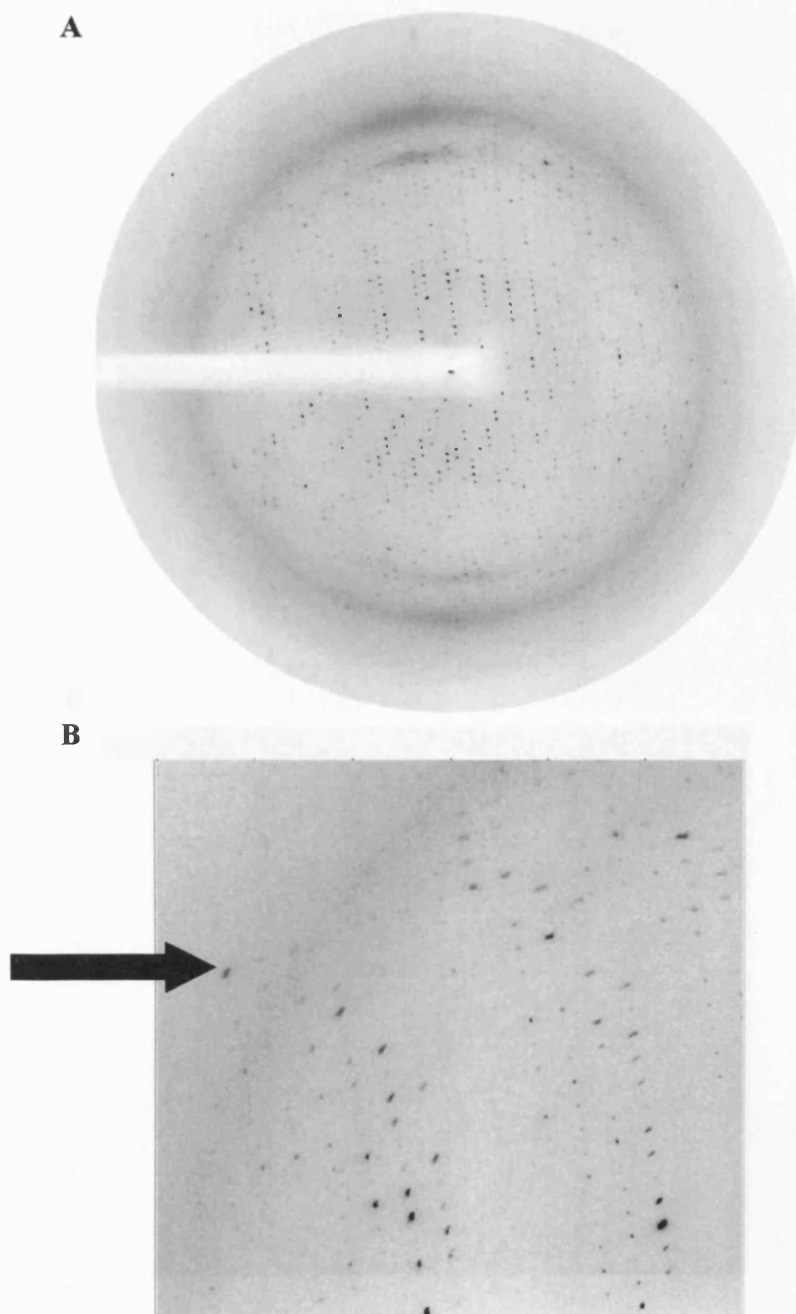
Diffraction data for PRODH crystal forms 1 and 2 were collected from cryocooled crystals (100 K) using a Quantum ADSC (Area Detector Systems Corporation) CCD detector on beamline ID 14-3 at the European Synchrotron Radiation Facility (ESRF), Grenoble, France. Crystals were mounted on a goniometer and diffraction data was collected using 1° oscillations with the crystal-to-detector distance set to 230 mm and the resulting diffraction data analysed as previously described (Monaghan _et al.,_ 2005; Section 2.9). Crystals of form 1 diffracted to a resolution of 3.6 Å (Figure 5.5, A and B) and belonged to the triclinic space group $P1$, with unit cell parameters $a = 93.7$, $b = 116.3$, $c = 126.9$ Å, $\alpha = 97.3$, $\beta = 99.9$, $\gamma = 104.6°$. Crystals of form 2 diffracted to a resolution of 3.3 Å (Figure 5.6, A and B) and again belonged to space group $P1$, with unit cell parameters $a = 91.3$, $b = 136.3$, $c = 203.8$ Å, $\alpha = 94.5$, $\beta = 99.4$, $\gamma = 102.7°$. Diffraction data collection and processing statistics for crystal form 1 and 2 of wild-type recombinant PRODH of _P. furiosus_ are given in Table 5.3.

5.2.3.   PRODUCTION OF SELENOMETHIONINE-SUBSTITUTED PRODH FOR THE PURPOSE OF MULTIWAVELENGTH ANOMALOUS DIFFRACTION (MAD)

Selenomethionine-substituted PRODH was produced following the protocol described previously (Section 2.4.5) for the purpose of multiwavelength anomalous diffraction (MAD) experiments. This method has become the most widely implemented for solving the phasing problem in protein X-ray crystallography (Hendrickson _et al.,_ 1990). The use of reducing agents such as dithiothreitol (DTT) and β-mercaptoethanol are often used in attempts to avoid selenomethionine oxidation (Smith and Thompson, 1998) as mixtures of oxidised and reduced selenomethionine in selenomethionyl derivatives is known to be deleterious to the phasing power of a MAD experiment (Thomazeau _et al.,_ 2001).

Full substitution of methionine residues with selenomethionine was assessed by electrospray mass spectrometry of the PRODH selenomethionyl derivative against native PRODH as previously described (Section 2.5.2). Only the β subunit of PRODH was detectible by electrospray mass spectrometry, an observation previously noted and

Figure 5. 5. X-ray diffraction pattern collected for PRODH crystal form 1 using a Quantum ADSC CCD detector on Beamline ID 14-3 at the ESRF. *Panel A*, Full diffraction pattern taken for PRODH crystal form 1 collected at a crystal-to-detector distance of 230 mm. *Panel B*, magnified picture of the diffraction edge of the diffraction pattern shown in panel A. The arrow highlights the diffraction limit corresponding to a resolution of ~3.6 Å.

A

B
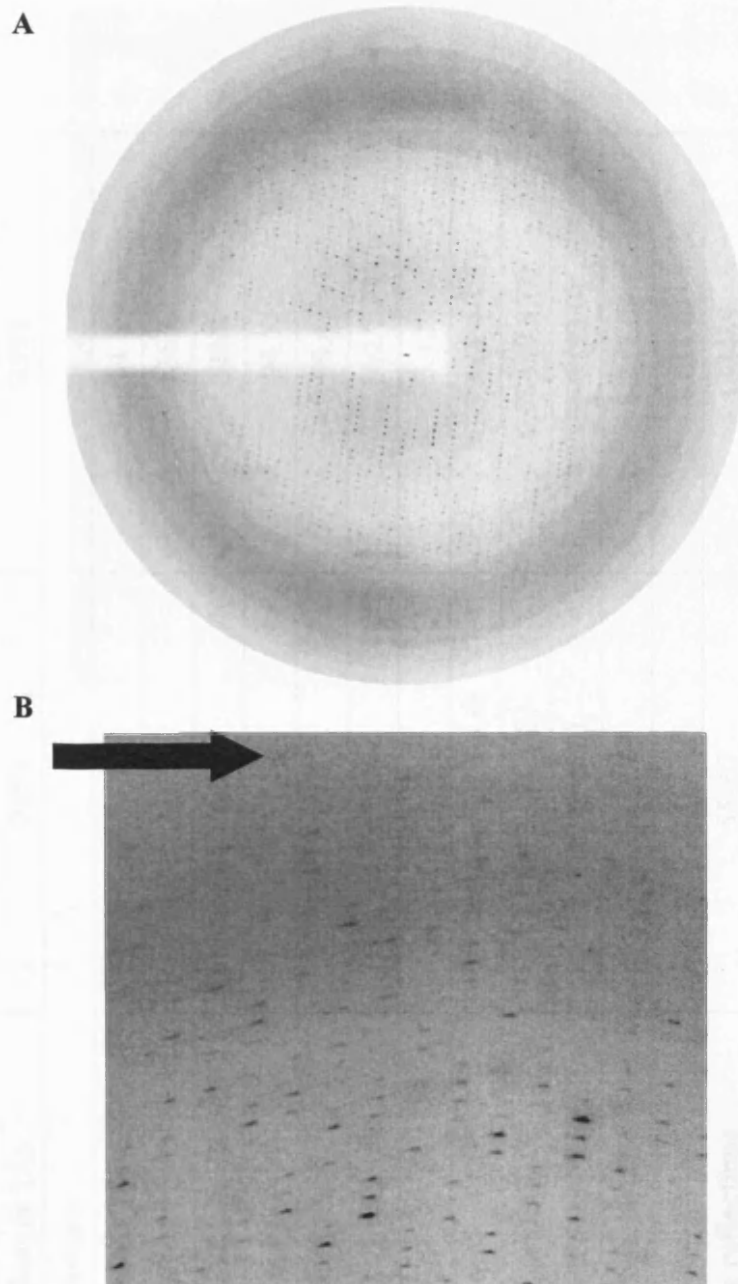
Figure 5. 6. X-ray diffraction pattern collected for PRODH crystal form 2 using a Quantum ADSC CCD detector on Beamline ID 14-3 at the ESRF. *Panel A*, Full diffraction pattern taken for PRODH crystal form 2 collected at a crystal-to-detector distance of 230 mm. *Panel B*, magnified picture of the diffraction edge of the diffraction pattern shown in panel A. The arrow highlights the diffraction limit corresponding to a resolution of ~3.3 Å.

Crystal form	1	2
Synchrotron radiation	Beamline ID 14-3, ESRF	Beamline ID 14-3, ESRF
Space group	*P1*	*P1*
Wavelength (Å)	0.931	0.931
Unit cell parameters:		
a (Å)	93.7	91.3
b (Å)	116.3	136.3
c (Å)	126.9	203.8
α (Å)	97.3	94.5
β (Å)	99.9	99.4
γ (Å)	104.6	102.7
Matthews coefficient (Å^3 Da^{-1})	3.34	3.12
Resolution (Å)	30-3.6 (3.8-3.6)	30-3.3 (3.4-3.3)
R_{merge} (%)	0.120 (0.432)	0.084 (0.357)
Completeness (%)	96.4 (95.0)	96.0 (93.0)
Average $I/\sigma(I)$	6.2 (1.8)	8.2 (2.0)
Average redundancy	2.5 (2.3)	1.9 (1.8)
Unique reflections	55367	132489

Table 5. 3. Data-collection and processing statistics for crystal form 1 and form 2 of wild-type recombinant PRODH of *P. furiosus* DSM 3638. The table highlights the synchrotron radiation source and wavelength used for diffraction analysis, the space group of each crystal form and unit cell parameters. Values in parentheses are for the highest resolution shell.

discussed (Section 3.2.10). The spectrum of native PRODH clearly showed a predominant mass/charge peak corresponding to the β subunit of PRODH measuring a molecular weight of 42,474.0 Da for the wild-type recombinant PRODH form (Figure 5.7, A). The corresponding spectrum for the selenomethionine-substituted PRODH derivative again showed a clear predominant peak with a mass/charge of 42,848.0 Da (Figure 5.7, B). The β subunit of PRODH has eight methionine residues in its amino acid sequence. If all eight residue positions are converted from methionine to selenomethionine, the mass difference between a sulfur and selenium atom, multiplied by eight is calculated as 375.1. The experimentally determined number for the molecular mass difference between the native and the selenomethionyl derivative of the PRODH β subunit measured by electrospray mass spectrometry was 374. These data therefore confirm that the β subunit of PRODH is fully selenated, and it is therefore likely, although not conclusively demonstrated, that the α subunit will also be selenated. To what degree the α subunit is selenated remains undetermined.

An initial crystallisation screen with selenomethionine-substitutes PRODH using the Molecular Dimensions Clear Strategy Screen MD 1-14 Screen I (Appendix, Table A1.1) yielded small yellow crystals with needle stick topology in conditions containing 0.2 M potassium thiocyanate, 8 % PEG 20K and 8 % PEG 550 MME, pH 7.5, 100 mM Tris-HCl (Figure 5.8).

5.2.4. GENERAL SELF-ROTATION FUNCTION

A self-rotation function describes the angular relationship between identical units within an asymmetric unit. It is a method useful in determining the relative orientation of molecular axes and thus provides information of the point symmetry of an oligomeric complex, therefore permitting the number of subunits or monomers that the complex is composed of to be determined (Rossmann, 1990). This self rotation function can be derived from the X-ray diffraction data taken of the protein crystal under analysis by

A

42,474.0 Da

B   **42,848.0 Da**

42200   42300   42400   42500   42600   42700   42800   42900   43000

Mass (m/z)
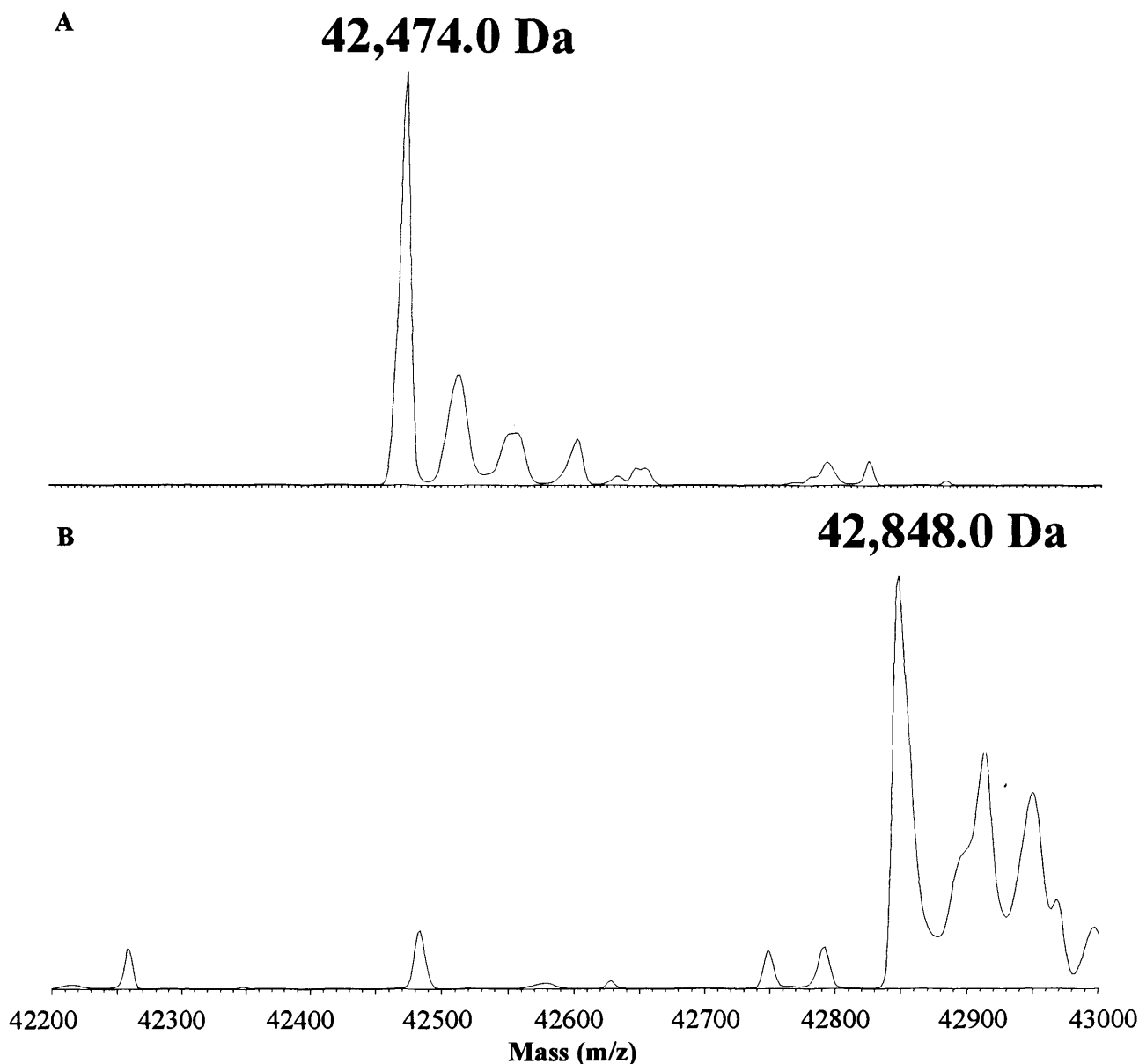
Figure 5. 7. **Electrospray mass spectrometry analysis of native and selenomethionine-substituted forms of PRODH of *P. furiosus* DSM 3638.** *Panel A*, electrospray mass spectrum of native PRODH showing a mass peak at 42,474.0 Da corresponding to the molecular weight of the native β subunit of PRODH. *Panel B*, electrospray mass spectrum of selenomethionyl-derivative PRODH showing a mass peak at 42,848.0 Da corresponding to the molecular weight of the selenated β subunit of PRODH. The data highlights a mass difference between native and selenomethionyl-derivative PRODH β subunit forms of 374, confirming that all eight methionine residues in the β subunit of PRODH were successfully substituted to selenomethionine during expression in strain B834(DE3) in the presence of DL-selenomethionine. Conditions: Both PRODH forms were exchanged into filtered ddH₂O pH 7.0 and concentrated to 1 mg/ml using a Centriprep YM-30 centrifugal filter membrane.

217

Figure 5. 8. Light microscope image showing a crystal of the selenomethionine-subtituted form of PRODH expressed in the selenomethionine auxotroph strain B834(DE3) from construct pPRODH2.   These preliminary crystals were yellow in colour indicating that the presence of selenomethionine residues in the protein had no effect on flavin cofactor binding.   Crystals had a branched, needle stick topology. Conditions: 0.2 M potassium thiocyanate, 8 % PEG 20K and 8 % PEG 550 MME, pH 7.5, 100 mM Tris-HCl.

superimposition of two Patterson maps. The self-Paterson vector distribution is the same for all identical molecules (or subunits) in the asymmetric unit with the exception of a rotation that is equal to their non-crystallographic rotational symmetry in real space.

The space of all the possible rotations in three-dimensional space are commonly parameterised in terms of Eulerian angles (Goldstein, 1959) or spherical polar rotation angles (Rossmann and Blow, 1962). In searching for non-crystallographic symmetry, the spherical polar rotation method is the most convenient (Drenth, 1999), a Cartesian lattice of which is illustrated in Figure 5.9. The polar angles ψ and ϕ specify the longitude and colatitude of the axis and therefore determine the position of the rotation axis, and the azimuthal angle κ specifies the rotation about this axis. The x, y and z axes depict real space.

Using the program MOLREP (Vagin and Teplyakov, 1997) that performs rotational searches using the fast rotational function (Crowther, 1972), a general self rotation function was computed for a number of defined κ angles (60, 90, 120 and 180°) to test for the presence of non-crystallographic twofold, threefold, fourfold and sixfold axes. A self-rotation function computed from the crystal form 1 data set indicates the presence of three perpendicular twofold axes in the unit cell, which strongly suggests that the protein is a heterooctamer, with heterodimers arranged in *222* non-crystallographic symmetry (Figure 5.10, A and B). Data for the peaks observed in the self-rotation analysis with regard to the polar angles are shown in Table 5.4. Four heterodimers (one heterooctamer) per unit cell, totalling 388.8 KDa, corresponded to a Matthews coefficient of 3.34 $\text{Å}^3 \text{Da}^{-1}$ and a solvent content of ~62.8 % (Matthews, 1968). No evidence for the presence of non-crystallographic symmetry could be found from self rotation functions of the data set of crystal form 2. However, two heterooctamers per unit cell, totalling 777.6 KDa, corresponds to a Matthews coefficient of 3.12 $\text{Å}^3 \text{Da}^{-1}$ and a solvent content of ~60.2 % (Monaghan *et al.*, 2005).
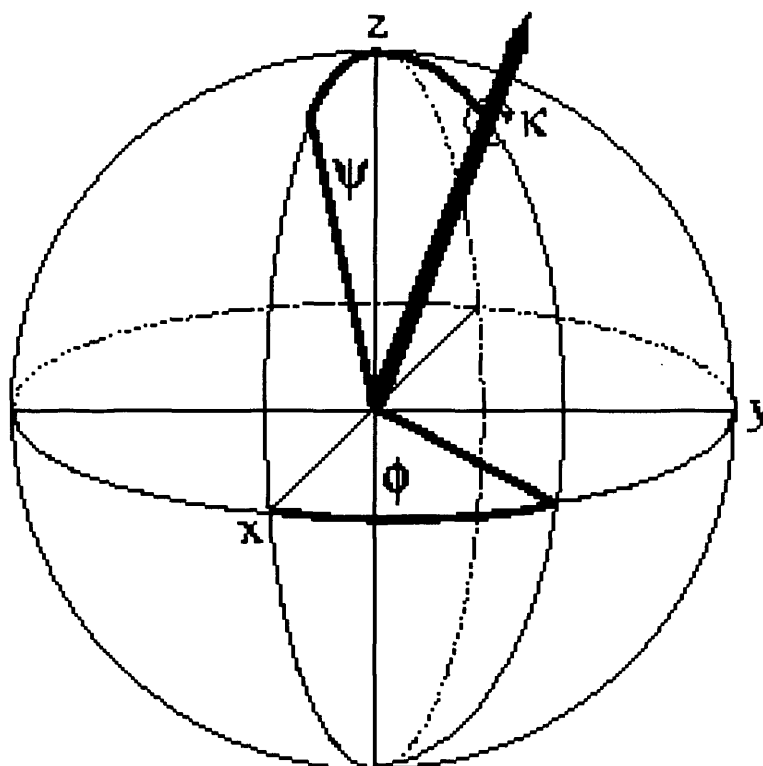
Figure 5. 9. Cartesian lattice illustrating spherical polar rotation, highlighting the polar angles κ, ψ and φ. The polar angles ψ and φ specify the longitude and colatitude of the axis and therefore determine the position of the rotation axis, and the azimuthal angle κ specifies the rotation about this axis. The x, y and z axes depict real space.

A

RFmax = 3.757

B

PRODH
heterodimer
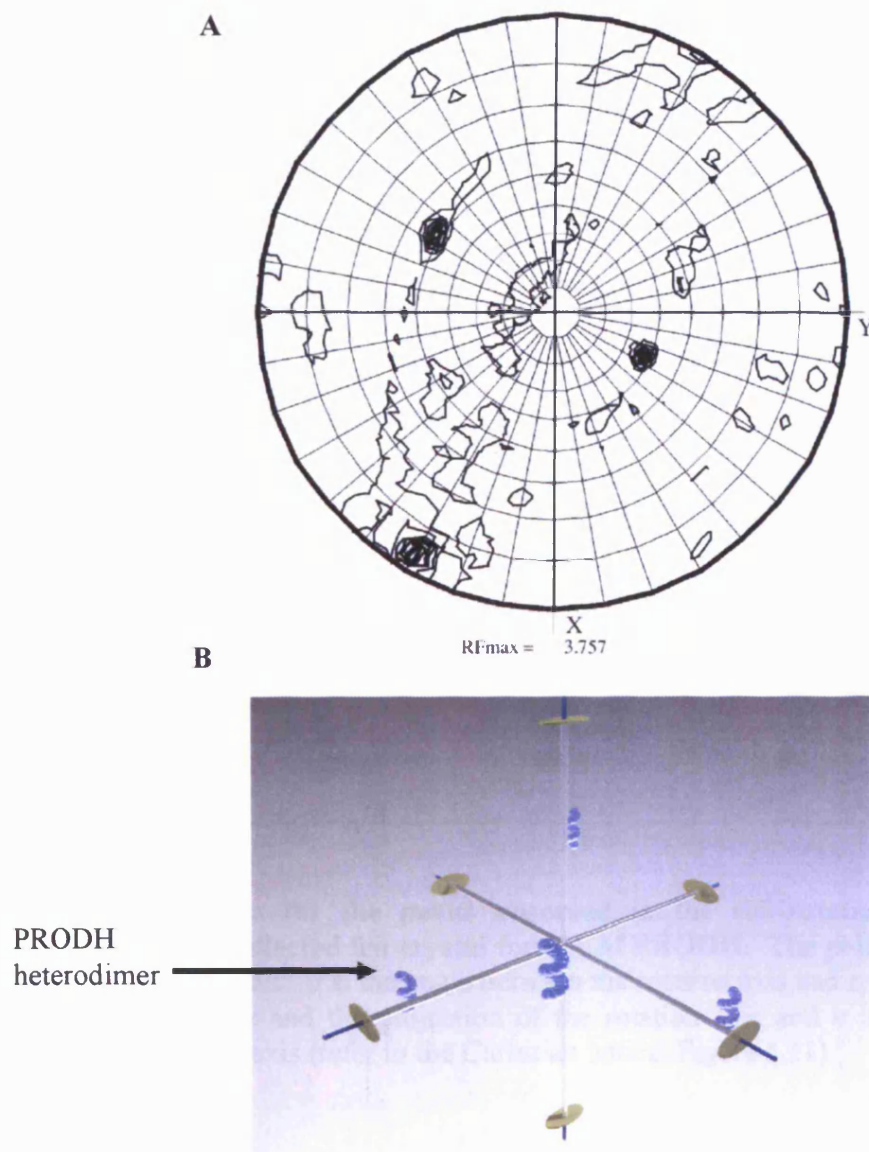
Figure 5. 10. Self-rotation function calculated with the crystal form 1 data between 30-3.6 Å and a 50.0 Å radius of integration. _Panel A_, The very strong peaks in the κ = 180° plot indicate the presence of three perpendicular twofold axes in the unit cell, which strongly suggests that the protein is a heterooctamer, with heterodimers arranged in _222_ non-crystallographic symmetry. _Panel B_, Schematic representation of the oligomeric arrangement and relative orientation of the PRODH complex with four heterodimers (one heterooctamer) per unit cell, totalling 388.8 KDa, corresponds to a Matthews coefficient of 3.34 $Å^3 Da^{-1}$ and a solvent content of ~62.8 % (Matthews, 1968).

Peak	ψ (°)	φ (°)	κ (°)	Rf/σ
1	86.6	-30.9	180	10.6
2	127.9	57.1	180	10.5
3	38.3	64.3	180	9.7

Table 5. 4. Data for the peaks observed in the self-rotation analysis of the diffraction data collected fro crystal form 1 of PRODH. The polar angles ψ, φ and κ are defined as follows: ψ is the angle between the rotation axis and z, φ is the angle in the xy plane between x and the projection of the rotation axis and κ is the rotation angle around the rotation axis (refer to the Cartesian lattice; Figure 5.11).

5.2.5. STRUCTURAL DETERMINATION: MOLECULAR REPLACEMENT

Proteins that share amino acid sequence homology display similar folds or motifs of the polypeptide chain evident in the secondary and tertiary structures of the homologous globular protein macromolecules. This structural redundancy is the basis of the method of 'molecular replacement' that utilises a homologous protein structure as a phasing model to establish a set of initial phases and a 'first model' of the protein structure to be determined. Calculation of initial phases by this method requires placing a structure model of the known protein into the unit cell of the new protein. The molecular replacement method was pioneered by Michael Rossmann and David Blow during their work in theoretical crystallography, namely, approaches for the combination of different kinds of phase information (Rossmann and Blow, 1962). A three-stage process represented the initial concept of the molecular replacement method. The first stage involved determining the relative rotation (orientation) of homologous structures within the same crystal form. The information from this stage was then utilised in stage two known as 'translation' to determine the local non-crystallographic operator positions relative to crystallographic symmetry elements. Knowledge of the non-crystallographic operators derived in stages one and two allowed phase determination in stage three of the scheme (Rossmann, 1990).

Structure determination of wild-type recombinant PRODH was performed by the method of molecular replacement using the heterooctameric protein PDH1 of *P. horikoshii* (PDB accession code 1Y56; Tsuge *et al.*, 2005) as the phasing model and the diffraction data collected for PRODH crystal form 1. Molecular replacement was an applicable technique due to the high degree of amino acid sequence identity between these two *Pyroccocal* enzymes with the α subunits sharing 75 % sequence identity (Figure 5.11) and the β subunits sharing 90 % sequence identity at the amino acid level (Figure 5.12) as computed by the bioinformatics sequence alignment program 'ClustalW' (http://www.ebi.ac.uk/clustalw/). Molecular replacement was performed using the AMoRe software package (Navaza, 1994). Improvement of the first model of the PRODH structure was an iterative process that included manual tracing of the

```
PRODHa    MRNLRPLDLTEKKKKKVRIYFEGKELEAYEGEKLPVALLANGIYWLTTSLEGRKRGAFTF 60
PDH1a     -MLMRPLDLTEKRGKKVTIYFEGKELEAYEGEKLPVALLANEIYWLTTSNEGRKRGAFTF 59
          ********  ***  ************************  *******  *********

PRODHa    GPVPMIINGVKGVDARKTKVKDGMKVQRQTYGDFHEEPLPQDGEVKQVVVDVLVIGGGPA 120
PDH1a     GPVPMTVNGVKGLEARRIKVKDGMKIERQGYYDFHEEPVVEPGEIERVVVDVAIIGGGPA 119
          *****  ***** **  ******* **  ** ****** **   **  *****  ******

PRODHa    GLGAVLEMQEHLNVALVEEKGWLGGDMFLKTSTAEGFEESSRKVVDKLAKEVKAN--VYL 178
PDH1a     GIGAALELQQYLTVALIEERGWLGGDMWLKGIKQEGFNKDSRKVVEELVGKLNENTKIYL 179
          * *** **  *  **** ** ****** **    *** ***** *   *     *   **

PRODHa    GTVALGVFDKGEYFLVPATKGNNLIEFLAKRVVLATGAVDNIMLFENNDMPGVFRRDFAL 238
PDH1a     ETSALGVFDKGEYFLVPVVRGDKLIEILAKRVVLATGAIDSTMLFENNDMPGVFRRDFAL 239
          *  ************** *   *  *** ********** *  ******************

PRODHa    EVMNVWEVAPGWNVAVTGSKAEEVIYELERWGIDYVEVPSVKRVEGKEKVEKVIDFNGNE 298
PDH1a     EVMNVWEVAPGRKVAVTGSKADEVIQELERWGIDYVHIPNVKRVEGNEKVERVIDMNNHE 299
          ***********   ********* ****  *********** *  *****  ****  *  *

PRODHa    YKVDAIIFADGKRPDINPITQAGGKLHFRRGYYRPVVNEYNQIREGVYVAGSAVTIKPHY 358
PDH1a     YKVDALIFADGRRPDINPITQAGGKLRFRRGYYSPVLDEYHRIKDGIYVAGSAVSIKPHY 359
          *****  ***** ******************  **  *** *   *   ********* *****

PRODHa    TNYLEGRLVGAYILREFGIDSEPCIYKEKLKEFEPEALPVPKIPINKLNLDDVQICGCDV 418
PDH1a     ANYLEGKLVGAYILKEFGYDAQPCIYEEKLREYEPESLSIPRIPLDKFNLEDVQICGCDV 419
          ***** ******* *** **   ***** ** ** *** *    *  *  ** *********

PRODHa    SLRKVYDVVEKGITDLQIIKRLTHLAMGFCQGRFCLFNGAAVVSQVTGIKLGEIDLPVAR 478
PDH1a     SLKKVDEVIRKGITDLQIIKRLTHLAMGFCQGRYCLFNGAVVVSQRTGKKLSEIDLPVAR 479
          ** **   *  ************************ ****** ****** **  **  ********

PRODHa    PPIKTVKLGILSRR 492
PDH1a     SPIKNVKMGILARR 493
          ***  **  ***  **
```

Figure 5. 11. Sequence alignment data for the α subunit of PRODH of *P. furiosus* DSM 3638, and the α subunit of PDH1 of *P. horikoshii* OT3. The primary structure of the α subunit of PRODH of *P. furiosus* (PRODHa) was analysed for sequence identity with the amino acid sequence of the α subunit of PDH1 of *P. horikoshii* (PDH1a). 75 % sequence identity was observed between the two input sequences using the multiple sequence alignment tool 'ClustalW' (http://www.ebi.ac.uk/clustalw/). The residues that comprise the dinucleotide-binding motif are highlighted in yellow where residues are conserved and grey where not. The GG-doublet five nucleotides downstream of the dinucleotide-binding motif is highlighted in red and the ATG-motif is highlighted in green. Residue conservation throughout the two sequences analysed is indicated by an asterisk.

```
PRODHb    MIPEKSEIVVIGGGIVGVTIAHELAKRGEEVTLVEKRFIGSGSTFRCGTGIRQQFNDEAN 60
PDH1b     MLPEKSEIVVIGGGIVGVTIAHELAKRGEEVTVIEKRFIGSGSTFRCGTGIRQQFNDEAN 60
          * ********************************* ************************

PRODHb    VQVMKRSVELWKKYSEEYGFKFEQTGYLFLLYDDEEVEIFKQNIKIQNKFGVPTRLITPE 120
PDH1b     VRVMKRSVELWKKYSEEYGFSFKQTGYLFLLYDDEEVKTFKRNIEIQNKFGVPTKLITPE 120
          * ****************** * ************* ** ** ********* *****

PRODHb    EAKEIVPLLDISEVIAASWNPTDGKADPFHSTTAFALKAKEYGAKILEYTEVKGFIIENN 180
PDH1b     EAKEIVPLLDISEVIAASWNPTDGKADPFEATTAFAVKAKEYGAKLLEYTEVKGFLIENN 180
          ***************************** ***** ******** ********* ****

PRODHb    EIKGVKTNRGVIKTGIVVNATNAWAKLINAMAGIKTSIPIEPYKHQAVITQPIKRGTIKP 240
PDH1b     EIKGVKTNKGIIKTGIVVNATNAWANLINAMAGIKTKIPIEPYKHQAVITQPIKRGTINP 240
          ******** * ************** ********** ********************* *

PRODHb    MVISFKYGHARLTQTAHGGIIGGVGYEVGPTYDLTPTYEFLREVSYYFSKIIPALKNLLI 300
PDH1b     MVISFKYGHARLTQTFHGGIIGGIGYEIGPTYDLTPTYEFLREVSYYFTKIIPALKNLLI 300
          ************** ******** *** *********************** *********

PRODHb    LKTWAGYTAKTPDSNPAIGKVEGVSDYYIAAGFSGHGFMMAPAVAEMVADLITKGKTELP 360
PDH1b     LKTWAGYTAKTPDSNPAIGRIEELNDYYIAAGFSGHGFMMAPAVGEMVAELITKGKTKLP 360
          *******************  *       ************* ****** ****** **

PRODHb    VEWYDPHRFERGELRTVALQMG 382
PDH1b     VEWYDPYRFERGELRTAALQMG 382
          ****** ********* *****
```

Figure 5. 12. Sequence alignment data for the β subunit of PRODH of *P. furiosus* DSM 3638, and the β subunit of PDH1 of *P. horikoshii* OT3. The primary structure of the β subunit of PRODH of *P. furiosus* (PRODHb) was analysed for sequence identity with the amino acid sequence of the β subunit of PDH1 of *P. horikoshii* (PDH1b). 90 % sequence identity was observed between the two input sequences using the multiple sequence alignment tool 'ClustalW' (http://www.ebi.ac.uk/clustalw/). The residues that comprise the dinucleotide-binding motif are highlighted in yellow where residues are conserved and grey where not. Residues Arg52β, Tyr251β, Tyr308β and His336β on the *re* face of the FAD cofactor isoalloxazine ring that are conserved in MSOX are highlighted in green. Arg302β on the *si* face of the isoalloxazine moiety of the FAD cofactor in both PRODH and PDH1 and conserved in MSOX is highlighted in red. Residue conservation throughout the two sequences analysed is indicated by an asterisk.

polypeptide chain to the electron density map. Atomic and B-factor refinement was performed using the Refmac5 program (Murshudov *et al.*, 1997) of the Collaborative Computational Project Number 4 (CCP4) suite for maximum-likelihood-based macromolecular refinement, alternated with manual rebuilding using the model-building/map-fitting program Coot (Emsley and Cowtan, 2004) of the CCP4 program suite. Using Refmac5 after an initial stage of interactive map fitting enabled refinement of the current coordinates. Coot was subsequently re-employed to read the new set of refined coordinates and MTZ file for an ensuing stage of model building. All stages of the molecular replacement, model building and refinement procedures were performed with Dr David Leys, University of Manchester, UK. Refinement statistics for the molecular replacement structure of PRODH are given in Table 5.5.

As suggested by the general self-rotation function for the diffraction data of form 1 crystals of PRODH (Section 5.2.4), the native oligomeric structure of PRODH of *P. furiosus* does indeed assemble as a $(\alpha\beta)_4$ heterooctameric complex displaying *222* non-crystallographic symmetry (Figure 5.13). This tetrameric complexation of $\alpha\beta$ heterodimers gives a native oligomeric mass for PRODH totalling a substantial 388.8 KDa. This high degree of oligomerisation presented by PRODH is a structural strategy likely employed to impart increased protein thermostability (Backmann and Schäfer, 2001), with the native quaternary complex (heterooctamer) possessing increased packing density, hydrogen bonds, salt bridges, and ion pair networks in comparison to the $\alpha\beta$ heterodimer alone. The three-dimensional structure of PRODH highlights the presence of three cofactors, ATP bound to the α subunit, FAD non-covalently bound to the β subunit and FMN non-covalently bound at the $\alpha\beta$ subunit interface.

The α subunit comprises of four domains, an N-terminal domain, a central domain, an ATP-binding domain and a Cys-clustered domain. A dinucleotide binding motif is present in the α subunit amino acid sequence (Section 3.2.1) that forms the common Rossmann fold (Rossmann *et al.*, 1974; dinucleotide-binding domain) consisting of a five-stranded parallel β-sheet motif flanked by a three-stranded anti-parallel β-sheet on one side and two-helices to the other side, this fold accommodating the ATP cofactor of

Refinement Target	Maximum Likelihood
Resolution Range High (Å)	3.24
Resolution Range Low (Å)	29.66
Completeness for range (%)	100
Number of Reflections	131297
R Value (Working + Test Set)	0.24960
R Value (Working Set)	0.24750
Free R Value	0.28920
Free R Value Test Set Size	5 %
Free R Value Test Set Count	6944
Mean B-Value	79.631
Correlation Coefficient $F_o - F_c$	0.910
Correlation Coefficient $F_o - F_c$ Free	0.879
Number of Non-Hydrogen Atoms Used in Refinement	55368

Table 5. 5. Refinement statistics for the molecular replacement structure of PRODH of *P. furiosus* DSM 3638. Protein PDH1 of *P. horikoshii* OT3 was used as the phasing model using diffraction data collected for PRODH crystal form 1. Molecular replacement was performed using the 'AMoRe' software package (Navaza, 1994). Atomic and B-factor refinement was performed using the 'Refmac5' program (Murshudov *et al.*, 1997) of the Collaborative Computational Project Number 4 (CCP4) suite for maximum-likelihood-based macromolecular refinement, alternated with manual rebuilding using the model-building/map-fitting program 'Coot' (Emsley and Cowtan, 2004) of the CCP4 program suite.
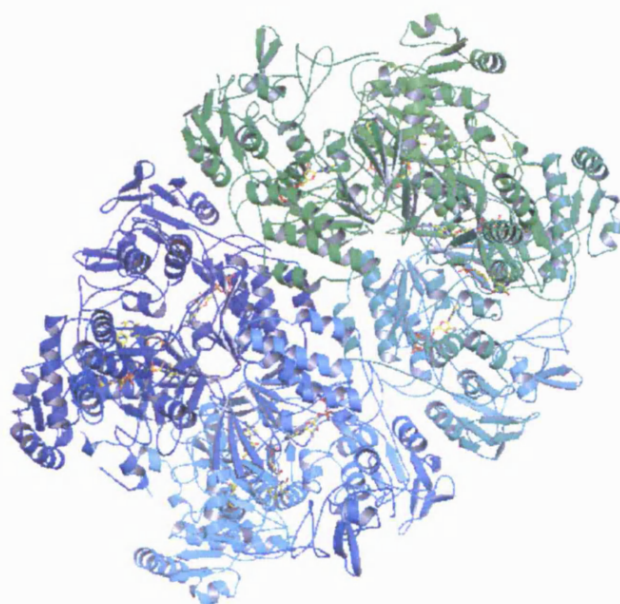
Figure 5. 13. Native oligomeric structure of PRODH of *P. furiosus* DSM 3638. PRODH is displayed in ribbons format with monomers defined by individual colouring. Figure constructed using PyMOL v.0.99 (DeLano, 2002; http://www.pymol.org).

PRODH. In this ATP-binding domain, three consecutive glycine residues (Gly113-115α) run parallel to the phosphodiester backbone of the ATP cofactor with the Glu135α side chain carboxyl group making contact with the O2' and O3' atoms of the ATP cofactor ribose moiety. Residues His356α and Asn359α are positioned approximal to, and administrate binding of the ATP cofactor γ-phosphate (Figure 5.14).

The β subunit of PRODH is composed of two domains, an FAD-binding domain illustrated by a Rossmann fold similar to the dinucleotide-binding motif apparent in the α subunit and accommodating non-covalent FAD cofactor. The other domain is an interface domain comprised of a two-part anti-parallel β-sheet structure. Describing the environment of bound FAD cofactor, Cys47β forms a parallel contact with the *si* face of the isoalloxazine ring moiety, whilst the residues occupying the area on the *re* face of the FAD flavin ring shape the substrate-binding site with participating residues including Tyr308β, Gly335β, His336β, Met339β, Tyr87β, Arg52β and Ile243β in collaboration with residues His225β and Tyr251β (Figure 5.15) that are conserved in the active site of DMGO and implicated in the enzymes catalytic mechanism during the oxidative demethylation of dimethylglycine substrate (Leys *et al.*, 2003; Figure 3.6).

The β subunit interface domain together with the four α helices Cys-clustered domain of the α subunit mediate binding of non-covalent FMN cofactor at the αβ subunit interface. The α subunit and β subunit each possess a key hydrophobic residue, Met444α and Trp304β, respectively, that stack either side of the isoalloxazine ring moiety of the FMN cofactor with Trp304β participating in π-π interactions with the flavin ring system. The phosphate group at the base of the ribitol function of FMN is secured at the subunit interface by the basic β subunit residues Arg46β and Arg302β (Figure 5.16). The Pfam database (Protein Family database; Bateman *et al.*, 2004), predicted the presence of a [2Fe-2S] cluster in the α subunit from its primary structure. In the structure of the phasing model (PDH1), an electron density feature at 5σ, was attributed to the presence of Fe^{3+} (Tsuge *et al.*, 2005) and similar electron density corresponding to a putative Fe is apparent in the molecular replacement structure of PRODH. The Fe ligand is in close proximity to the four cysteine residues Cys413α, Cys415α, Cys447α and Cys452α that
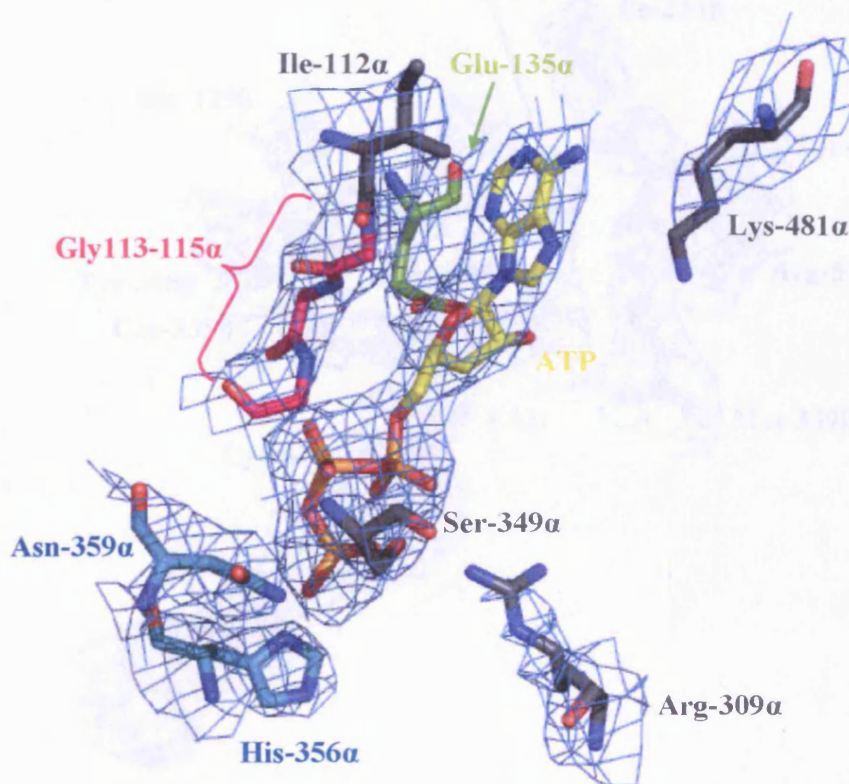
Figure 5. 14. Three-dimensional structure of the ATP cofactor bound to the α subunit of PRODH and residues participating in ATP binding. Glycine residues 113-115α (pink) run parallel to the ATP backbone. The Glu-135α side chain carboxyl group (Green) makes contact with the O2' and O3' atoms of the ATP cofactor ribose moiety (Yellow). His-356α and Asn-359α (Cyan) comprise the ATP γ-phosphate binding site. Electron density for the ATP cofactor and surrounding residues is shown as sky blue mesh (contoured at 2.0 σ). Figure constructed in stick representation using PyMOL v.0.99 (DeLano, 2002; http://www.pymol.org).
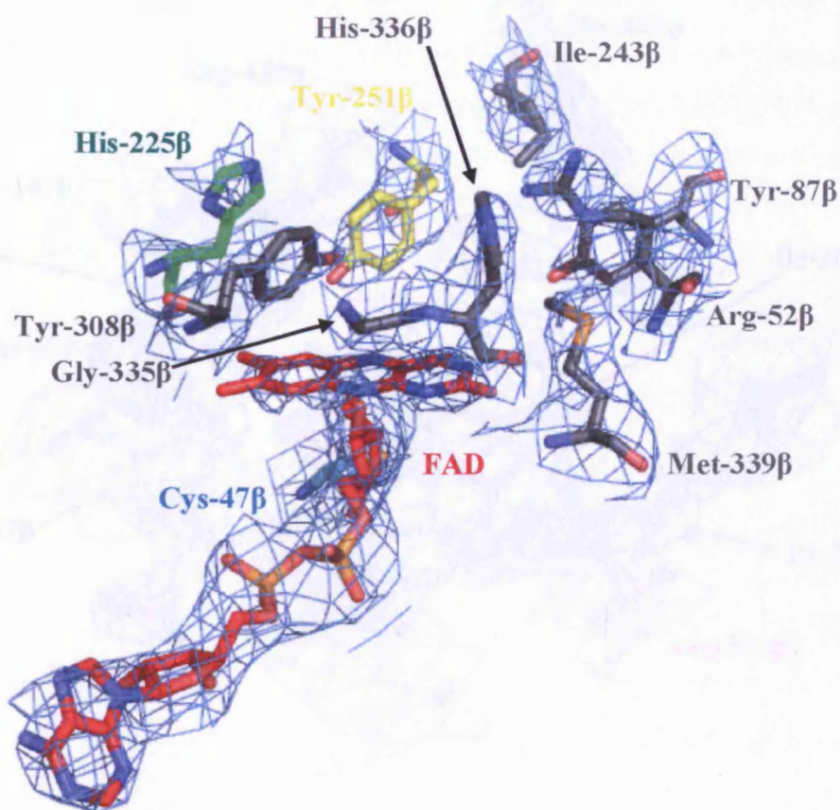
Figure 5. 15. **Three-dimensional structure of the FAD cofactor non-covalently bound to the β subunit of PRODH and the amino acid residues on the *re* face of the flavin isoalloxazine ring that form the L-proline substrate binding site.** Residue Cys-47β (Cyan) makes parallel contact with the FAD cofactor isoalloxazine moiety (Red) approaching the *si* face of the flavin ring. Residues on the *re* face of the FAD isoalloxazine ring function that form the active site architecture for amine substrate oxidation in the β subunit of PRODH are coloured grey. The active site residues His-225β and Tyr-251β targeted for mutation are coloured green and yellow, respectively. Electron density for the FAD cofactor and active site residues is shown as sky blue mesh and contoured at 2.0 σ. Figure constructed in stick representation using PyMOL v.0.99 (DeLano, 2002; http://www.pymol.org).

231
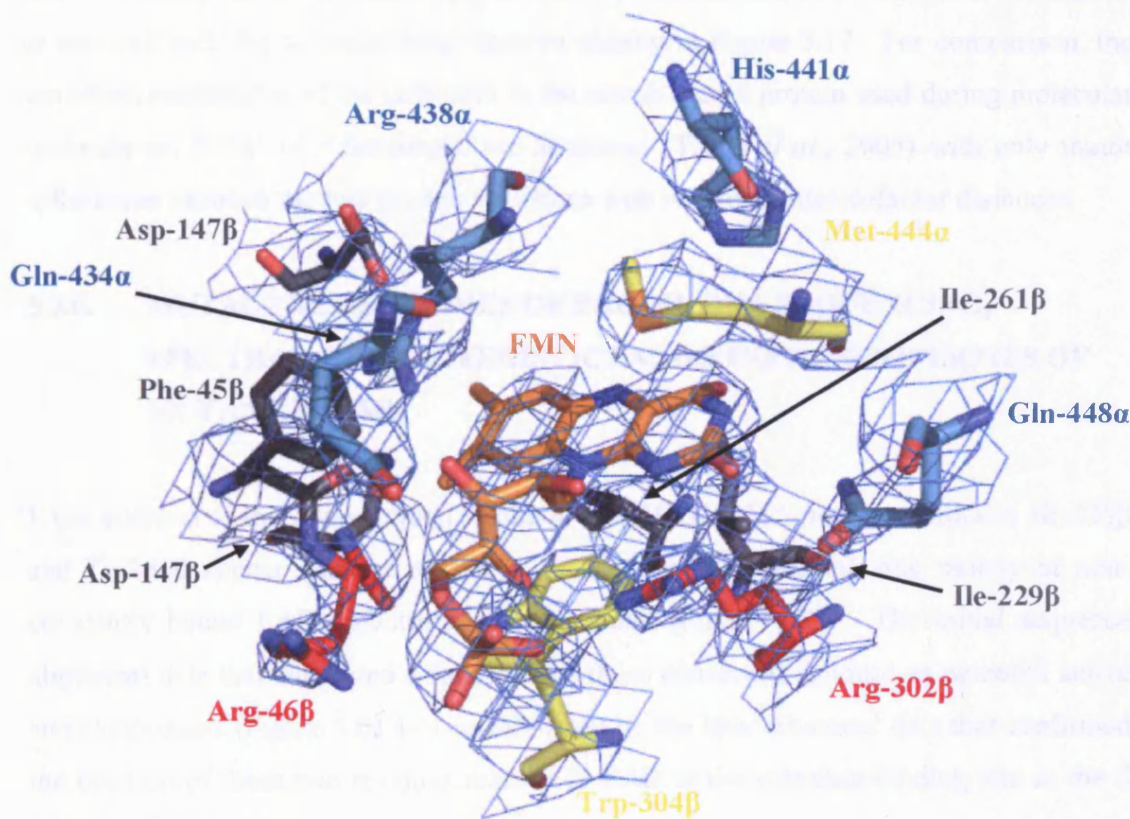
Figure 5. 16.   Three-dimensional structure of the FMN cofactor non-covalently bound at the αβ subunit interface in PRODH between the Cys-clustered domain of the α subunit and the interface domain of the β subunit. The FMN cofactor of PRODH (Orange) is stacked between the hydrophobic residues Met-444α and Trp-304β (Yellow residues). Arg-46β and Arg-302β (Red residues) are the basic residues that secure the phosphate group of FMN cofactor in position at the binding site. Additional participating residues of the α and β subunits are shown in teal and grey, respectively. Electron density for the FMN cofactor and the residues that constitute the cofactor binding site is shown as sky blue mesh and contoured at 2.0 σ. Figure constructed in stick representation using PyMOL v.0.99 (DeLano, 2002; http://www.pymol.org).

constitute in part the Cys-clustered domain of the α subunit. Noticeably, Cys413α and Cys452α establish a disulfide bridge. The relative structural orientation and proximity of each cofactor (ATP, FMN and FAD) and the Cys-cluster within the structure of PRODH is depicted with the corresponding electron density in Figure 5.17. For comparison, the structural relationship of the cofactors in the search model protein used during molecular replacement, PDH1 of _P.horikoshii_ are described (Tsuge _et al._, 2005) with only minor differences between the two protein structures with regard to inter-cofactor distances.

5.2.6. MUTAGENESIS STUDIES OF PRODH; DNA SEQUENCING, SPECTRAL CHARACTERISTICS AND KINETIC PROPERTIES OF MUTANT FORMS

From analysis of the X-ray crystal structure of PRODH of _P. furiosus_, residues His225β and Tyr251β appear situated on the _re_ face of the isoalloxazine ring moiety of non-covalently bound FAD cofactor in the β subunit (Figure 5.15). The initial sequence alignment data that suggested a function for these conserved residues as potential active site components (Figure 3.6) was corroborated by the later structural data that confirmed the position of these two residues relative to FAD at the substrate-binding site in the β subunit of PRODH.

pH-dependence studies with wild-type recombinant PRODH in the monoflavinylated FAD-bound form yielded macroscopic pK_a values of 7.0 ± 0.2 and 7.6 ± 0.2 from the data fit of the secondary plot describing the pH dependence of k_{cat}/K_m (Figure 4.10, A). Since the pH dependence of the specificity constant follows ionisations in the free enzyme and free substrate (Scheme 4.2), the pK_a value of 7.0 ± 0.2 on the acid limb of the pH dependence plot was in the first instance tentatively attributed to ionisation of the conserved His225β, a potential active site base residue (pK_a of the ionising side chain of free histidine = 6.0). Additionally, the corresponding pH-dependence of k_{cat} that follows the pK_a of the enzyme-substrate complex (Scheme 4.3) was sigmoidal and fitting of the data described a single macroscopic pK_a value of 7.7 ± 0.1 (Figure 4.10, B) that, by analogy with other flavoenzyme dehydrogenases such as TMADH (Basran _et al._, 2001a)
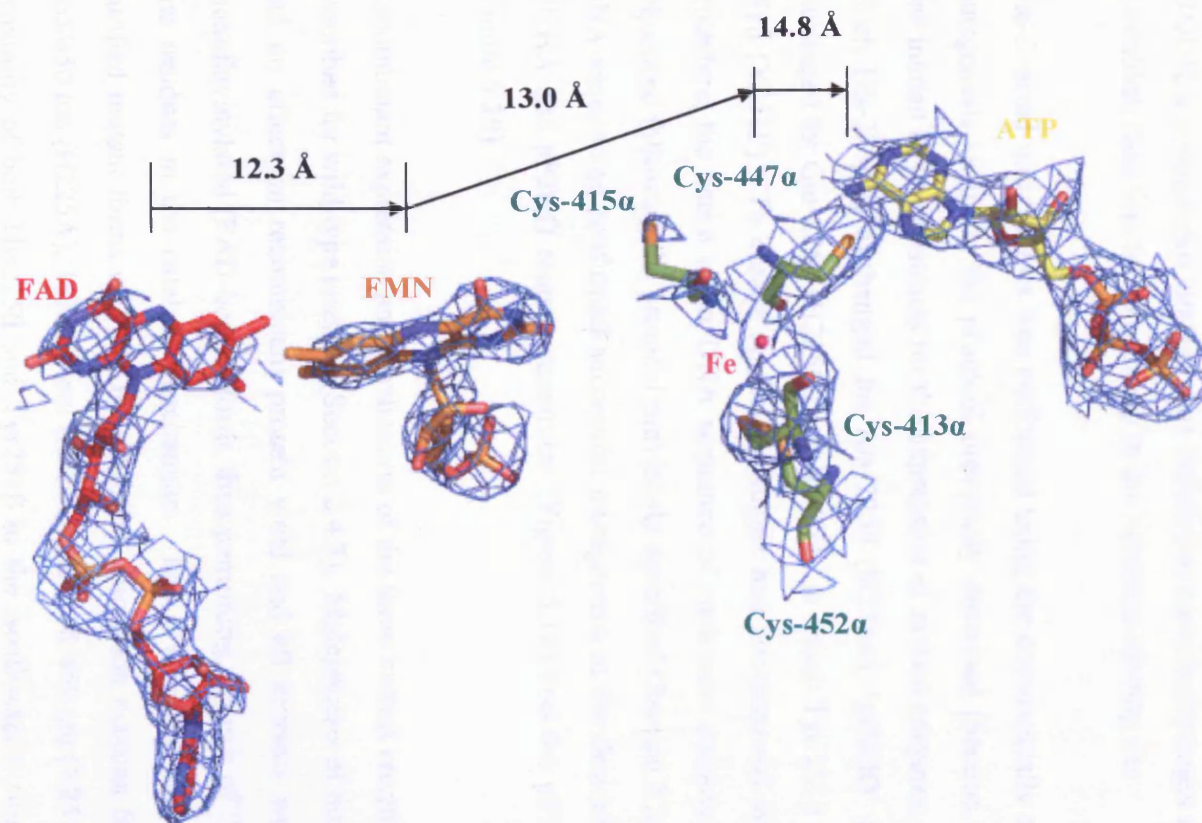
Figure 5. 17. Three-dimensional structure of the three cofactors and Cys-rich region of PRODH of *P. furiosus* DSM 3638. The proximity and relative orientation of the non-covalently bound FAD (Red), FMN (Orange) and ATP (Yellow) cofactors of PRODH are highlighted including the cysteine residues (Green) of the Cys-clustered domain of the α subunit involved in coordination of Fe ligand (Pink sphere). Distances between the FAD, FMN, Cys-cluster and ATP are indicated by the arrows. Electron density for the FAD, FMN and ATP cofactors, the Fe ligand and cysteine residues of the Cys-clustered domain is shown as sky blue mesh and contoured at 2.0 σ. Figure constructed in stick representation using PyMOL v.0.99 (DeLano, 2002; http://www.pymol.org).

and MSOX (Zhao and Jorns, 2005) may represent the ionisation of substrate L-proline in the Michaelis complex. The pK_a value corresponding to the protonation of free L-proline is 10.6 and stabilisation of the deprotonated form of L-proline in the Michaelis complex appears evident by a shift of -2.9 pH units to a pK_a of 7.7. To assess the potential role of these two conserved residues in the catalytic mechanism of L-proline oxidation by PRODH, a mutagenesis strategy was initiated to specifically target these residues in order to establish their functional capacity in the substrate-binding site.

Site-directed mutagenesis was performed using the commercially available QuikChange mutagenesis kit using the protocol previously described (Section 2.2.7) to produce the new mutant DNA constructs for the expression of mutant enzymes; construct 'pP2HA' in which His-225β is exchanged for Ala-225β (H225A), 'pP2HQ' in which His-225β is exchanged for Gln-225β (H225Q) and 'pP2YF' in which Tyr-251β is exchanged for Phe-251β (Y251F). To ensure spurious changes had not occurred during the mutagenesis procedure, the entire insert DNA sequence of each new construct was completely re-sequenced following the protocol previously described (Section 2.2.6). The results of the DNA sequencing confirmed successful mutagenesis at the desired target regions in the pP2HA and pP2HQ mutant constructs (Figure 5.18) and the pP2YF mutant construct (Figure 5.19).

Recombinant expression and purification of the three mutant enzymes of PRODH was as described for wild-type enzyme (Section 2.4.3). Mutagenesis of these active site residues had no effect on recombinant protein yield and all mutants were purified in stable monoflavinylated (FAD-bound) form, thus permitting analysis of the role of these active site residues in the catalytic mechanism. The UV-visible absorption spectra of the purified mutant forms of PRODH exhibited absorption maxima for the flavin peaks of 365/450 nm (H225A), 363/450 nm (H225Q) and 368/450 nm (Y251F). Despite the close proximity of both His225β and Tyr251β to the isoalloxazine ring moiety of the FAD cofactor, no major perturbations in the UV-visible absorption properties of the enzyme-bound flavin were evident as a consequence of mutagenesis when compared to the wild-type PRODH UV-visible flavin absorption peaks at 367/450 nm (Figure 5.20).

G A G C C C T A C A A G C A T C A A G C A G T G A T A

pPRODH2 (Wild-Type)

G A G C C C T A C A A G G C T C A A G C A G T G A T A

pP2HA (H225A)

G A G C C C T A C A A G C A G C A A G C A G T G A T A

pP2HQ (H225Q)
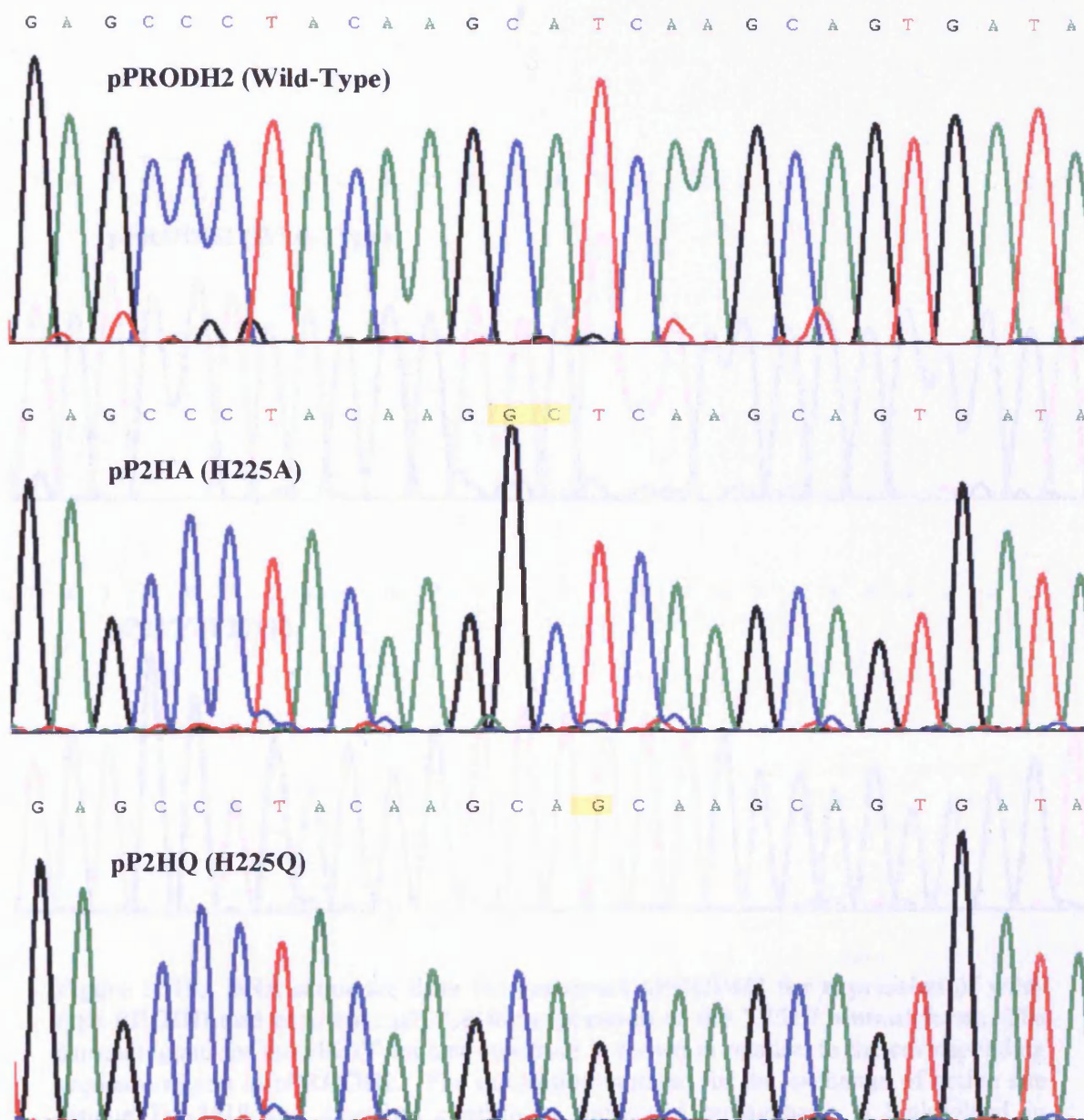
Figure 5. 18. DNA sequence data for construct pPRODH2 for expression of wild-type PRODH and the constructs pP2HA for expression of the H225A mutant form and pP2HQ for expression of the H225Q mutant form. Chromatograms for both the pP2Ha and pP2HQ mutant constructs are shown in relation to the corresponding sequence region in pPRODH2. Nucleotides mutated for the exchange of active site residue His-225β and therefore confirming successful mutagenesis are highlighted in yellow. Chromatograms of DNA sequence data were produced using Chromas v.2.3 (Technelysium).
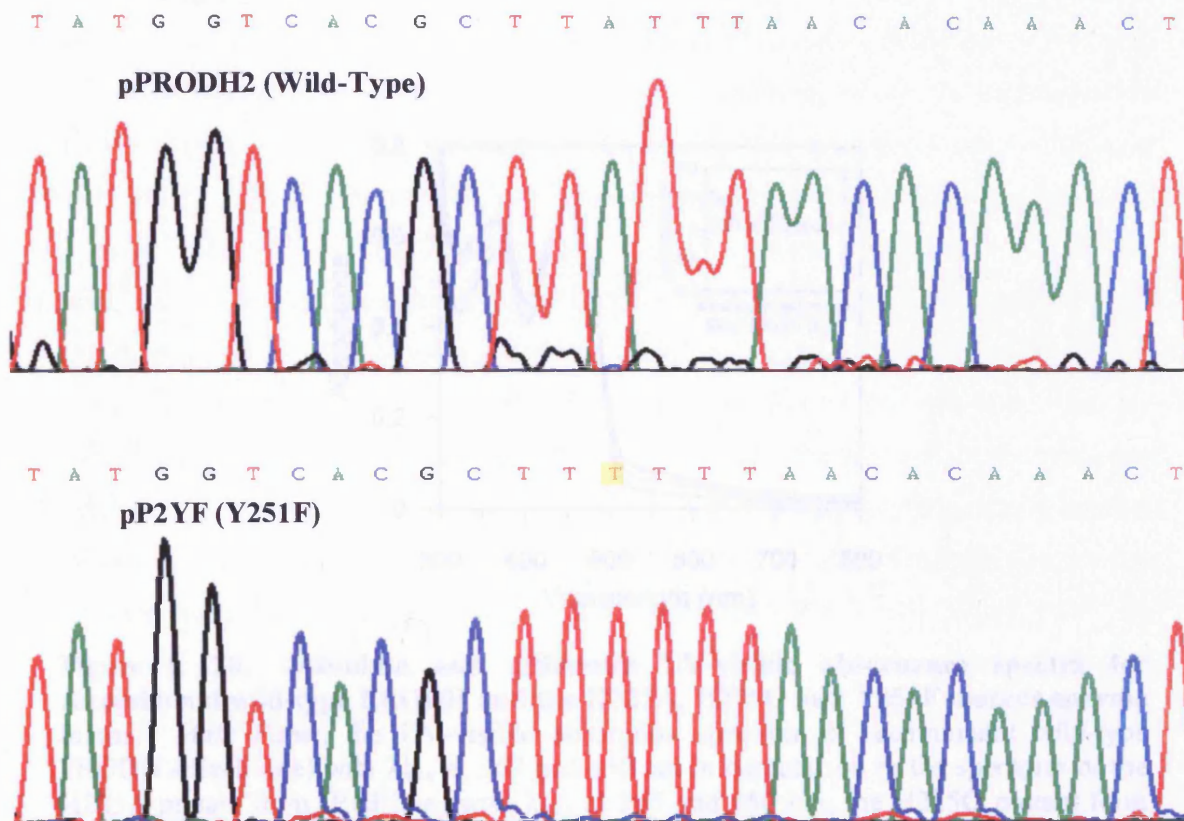
Figure 5. 19. DNA sequence data for construct pPRODH2 for expression of wild-type PRODH and construct pP2YF for expression of the Y251F mutant form. The chromatogram for the pP2YF mutant construct is shown in relation to the corresponding sequence region in pPRODH2. The nucleotide mutated for the exchange of active site residue Tyr-251β and therefore confirming successful mutagenesis is highlighted in yellow. Chromatograms of DNA sequence data were produced using Chromas v.2.3 (Technelysium).
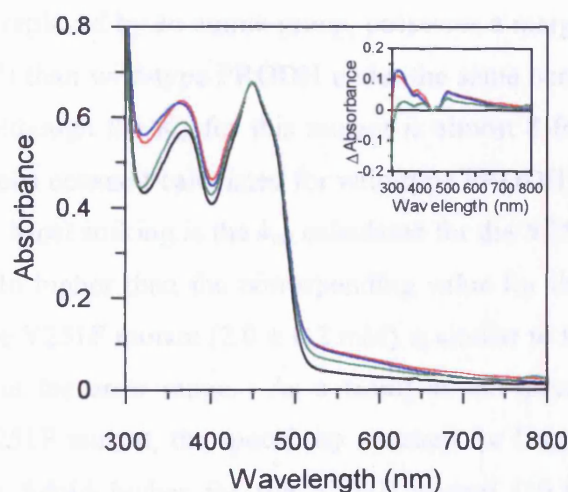
Figure 5. 20. **Absolute and difference UV-visible absorbance spectra for recombinant wild-type PRODH and the H225A, H225Q and Y251F mutant enzyme forms.** *Main Panel*, the UV-visible absorption spectrum of recombinant wild-type PRODH (Black line) with λ_{max} at 367 and 450 nm in comparison to the spectrum of the H225A mutant form (Red line) with λ_{max} at 365 and 450 nm, the H225Q mutant form (Blue line) with λ_{max} at 363 and 450 nm, and the Y251F mutant form (Green line) with λ_{max} at 368 and 450 nm. *Inset*, difference absorbance spectra for the three mutant forms H225A (Red line), H225Q (Blue line) and Y251F (Green line). The UV-visible absorbance spectrum of the Y251F mutant form is most similar to the corresponding spectrum of wild-type PRODH.

Initial steady-state experiments using a three-component buffer system at solution pH 7.5 showed major perturbations in the apparent kinetic constants calculated for each mutant enzyme in comparison to wild-type PRODH. The H225A mutant exhibited both the lowest k_{cat} (1.4 ± 0.01 s^{-1}) and highest K_m values (19.7 ± 0.8 mM) indicating that active site residue His-225β is implicated in the mechanism of L-proline oxidation by PRODH. The more conservative exchange in the H225Q mutant form where the imidazole side chain of His-225β is replaced by an amine group, possesses a marginally higher turnover number (9.0 ± 0.1 s^{-1}) than wild-type PRODH under the same conditions at solution pH 7.5 (6.8 ± 0.1 s^{-1}), although the K_m for this mutant is almost 8-fold higher (14.5 ± 0.8 mM) than the Michaelis constant calculated for wild-type PRODH (1.8 ± 0.3 mM) under the same conditions. Most striking is the k_{cat} calculated for the Y251F mutant (37.2 ± 1.2 s^{-1}), which is > 5-fold higher than the corresponding value for the wild-type. The K_m value obtained for the Y251F mutant (2.0 ± 0.2 mM) is similar to the value for wild-type enzyme and is within the error range. As a result of the elevated turnover number calculated for the Y251F mutant, the specificity constant for L-proline oxidation at this solution pH is over 5-fold higher for the Y251F mutant (19.1 ± 2.9 s^{-1} mM^{-1}) in comparison to wild-type PRODH (3.8 ± 0.7 s^{-1} mM^{-1}; Figure 5.21). Apparent kinetic parameters calculated for the three mutants in comparison to wild-type PRODH are summarised in Table 5.6.

Unlike for wild-type, H225A and H225Q enzyme, initial velocities recorded for the Y251F mutant were subject to inhibition at high L-proline concentration in the acid-to-neutral solution pH region (Figure 5.21, D). The apparent kinetic constants of the Y251F mutant enzyme for L-proline were derived by fitting data to a steady-state rate expression that incorporates substrate inhibition (Tipton, 1996; Equation 2.2). A possible explanation for the observed inhibition in the Y251F mutant is that, at high substrate concentrations, a molecule of L-proline may inhibit the catalytic site by binding close to the *re* face of the FAD cofactor isoalloxazine moiety, occupying volume that in wild-type PRODH is occluded by the phenolic hydroxyl group of the Tyr251β side chain. Marked inhibition has also been reported in studies of mutant forms of the flavoprotein
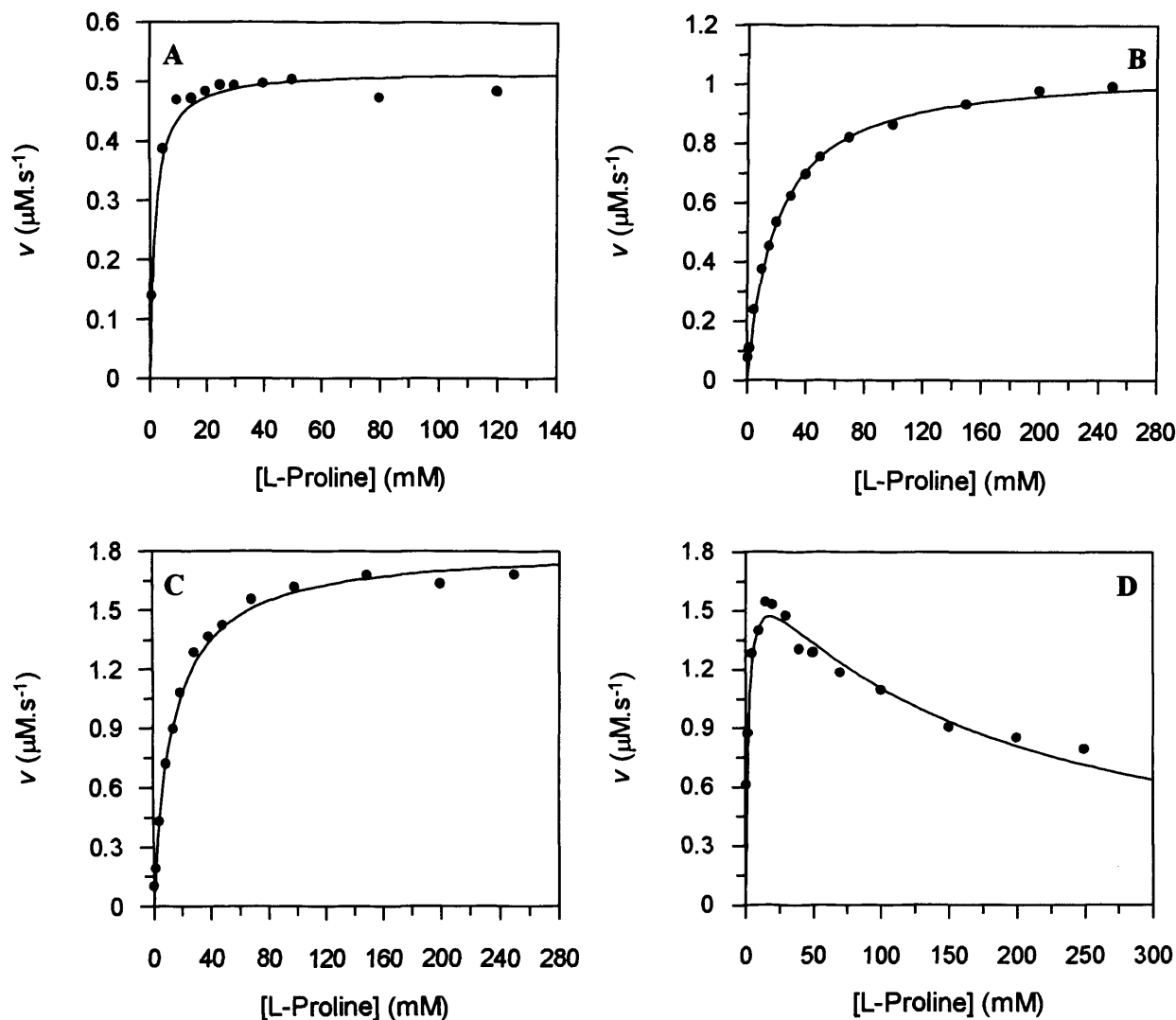
Figure 5. 21. Plots of initial velocity as a function of L-proline concentration for the steady-state kinetic activity of wild-type PRODH and the H225A, H225Q and Y251F mutant enzyme forms. *Panels A-C*, steady-state hyperbolic plots for the reactions of wild-type, H225A and H225Q enzyme forms, respectively, for the oxidation of substrate L-proline. Data were fitted to the standard Michaelis-Menten rate equation (Equation 2.1). *Panel D*, steady-state plot for the reaction of the Y251F mutant form for the oxidation of substrate L-proline. The Y251F mutant form of PRODH showed pronounced substrate inhibition at elevated substrate concentrations, therefore data for this mutant were fitted to a steady-state rate expression that incorporates substrate inhibition (Equation 2.2). Initial velocities are given as substrate oxidised ($\mu M/s^{-1}$). Conditions: Reactions were performed using a three-component buffer system comprising of MES, TAPSO and diethanolamine at final concentrations of 0.052, 0.052 and 0.1 M, respectively, solution pH 7.5, 60 °C.

PRODH	k_{cat} (s^{-1})	K_m (mM)	k_{cat}/K_m (s^{-1} mM^{-1})
Wild-Type	6.8 ± 0.1	1.8 ± 0.3	3.8 ± 0.7
H225A	1.4 ± 0.01	19.7 ± 0.8	0.07 ± 0.003
H225Q	9.0 ± 0.1	14.5 ± 0.8	0.6 ± 0.04
Y251F	37.2 ± 1.2	2.0 ± 0.2	19.1 ± 2.9

Table 5. 6. Table showing apparent steady-state kinetic parameters for wild-type PRODH and the H225A, H225Q and Y251F mutant enzyme forms. Reactions were performed using a three-component buffer system comprising of MES, TAPSO and diethanolamine at final concentrations of 0.052, 0.052 and 0.1 M, respectively. Conditions: Solution pH 7.5, 60 °C.

morphinone reductase under conditions of high substrate concentration (Messiha _et al._,
2005a; Messiha _et al._, 2005b).

5.2.7. pH-DEPENDENCE STUDIES OF PRODH MUTANT FORMS

To further probe the mechanistic aspects of PRODH-catalysed L-proline oxidation and to
establish a rationale at the molecular level to explain the observed kinetic behaviour
displayed by the three PRODH mutant enzymes, pH-dependence studies of the kinetics
of proline oxidation were performed. These studies revealed that the H225A enzyme was
unstable and precipitated from solution below pH 7.0 (Table 5.7). This affected the
accuracy of the data analysis in the acidic region. The H225Q mutant was relatively
stable displaying activity down to pH 6.0 (Table 5.7). The pH dependence of k_{cat} was
sigmoidal for both the H225A and H225Q enzymes and when fitted to Equation 2.5
produced a macroscopic pK_a value of 7.1 ± 0.1 for both of these enzymes. The Y251F
mutant enzyme was stable over the entire pH range of study (Table 5.7) with k_{cat} values
again showing a simple sigmoidal dependence on solution pH. Fitting data to Equation
2.5 gave a macroscopic pK_a value of 7.3 ± 0.1 that compares favourably to the values
determined for both wild-type (pK_a = 7.7 ± 0.1) and His-225β exchanged PRODH forms
(Figure 5.22, B1-3). In light of the similarity in the pK_a values obtained for wild-type and
mutant PRODH enzyme forms, the macroscopic pK_a of 7.7 ± 0.1 (wild-type PRODH)
was assigned to the ionisation of L-proline in the Michaelis complex. Like wild-type
PRODH, each mutant enzyme displayed a bell-shaped dependence in secondary plots of
k_{cat}/K_m as a function of solution pH and analysis of the data by fitting to Equation 2.6
(Figure 5.22, A1-3) produced macroscopic pK_a values of 6.8 ± 0.1 and 9.9 ± 0.1
(H225A), 6.8 ± 0.1 and 9.4 ± 0.2 (H225Q) and 6.0 ± 0.1 and 7.4 ± 0.1 (Y251F). Based
on these data, the pK_a value of 7.0 ± 0.1 initially assigned to the ionisation of the His-
225β imidazole side chain in wild-type enzyme has now been rejected as representing
this event. This pK_a value is not lost after mutation of His-225β to either alanine
(H225A) or glutamine (H225Q).

pH	k_{cat} (s^{-1})	K_m (mM)	k_{cat}/K_m (s^{-1} mM^{-1})
H225A			
7.0	0.9 ± 0.01	18.8 ± 0.9	0.05 ± 0.003
7.5	1.4 ± 0.01	19.7 ± 0.8	0.07 ± 0.003
8.0	1.6 ± 0.02	21.6 ± 1.1	0.07 ± 0.005
8.5	1.8 ± 0.02	22.9 ± 0.8	0.08 ± 0.003
9.0	1.9 ± 0.02	27.1 ± 1.0	0.07 ± 0.003
9.5	1.7 ± 0.01	25.9 ± 0.7	0.07 ± 0.002
10.0	1.9 ± 0.03	21.2 ± 1.3	0.1 ± 0.007
H225Q			
6.0	0.8 ± 0.02	26.1 ± 2.1	0.03 ± 0.003
6.5	2.6 ± 0.02	12.2 ± 0.5	0.2 ± 0.01
7.0	5.9 ± 0.03	13.5 ± 0.3	0.4 ± 0.01
7.5	9.0 ± 0.1	14.5 ± 0.8	0.6 ± 0.04
8.0	11.5 ± 0.1	19.4 ± 0.5	0.6 ± 0.02
8.5	13.4 ± 0.1	26.3 ± 0.6	0.5 ± 0.01
9.0	12.9 ± 0.1	28.3 ± 1.0	0.5 ± 0.02
9.5	12.2 ± 0.1	37.7 ± 1.3	0.3 ± 0.01
10.0	12.7 ± 0.2	37.3 ± 1.6	0.3 ± 0.02
Y251F			
5.5	3.9 ± 0.1	0.4 ± 0.04	9.3 ± 1.1
6.0	6.0 ± 0.2	0.3 ± 0.04	19.5 ± 3.3
6.5	10.1 ± 0.3	0.3 ± 0.1	31.3 ± 5.7
7.0	23.2 ± 0.7	0.9 ± 0.1	27.2 ± 4.3
7.5	37.2 ± 1.2	2.0 ± 0.2	19.1 ± 2.9
8.0	54.9 ± 2.0	5.4 ± 0.6	10.2 ± 1.6
8.5	63.2 ± 1.6	14.6 ± 0.9	4.3 ± 0.4
9.0	64.2 ± 2.3	35.8 ± 2.4	1.8 ± 0.2
9.5	60.9 ± 2.2	64.3 ± 3.4	0.9 ± 0.1
10.0	64.6 ± 3.6	84.4 ± 7.0	0.8 ± 0.1

Table 5. 7. Table showing the pH-dependence of apparent steady-state kinetic parameters calculated for the H225A, H225Q and Y251F mutant forms of PRODH. Reactions were performed using a three-component buffer system comprising of MES, TAPSO and diethanolamine at final concentrations of 0.052, 0.052 and 0.1 M, respectively, allowing a constant ionic strength across the pH range of study. Reactions were performed at 60 °C.
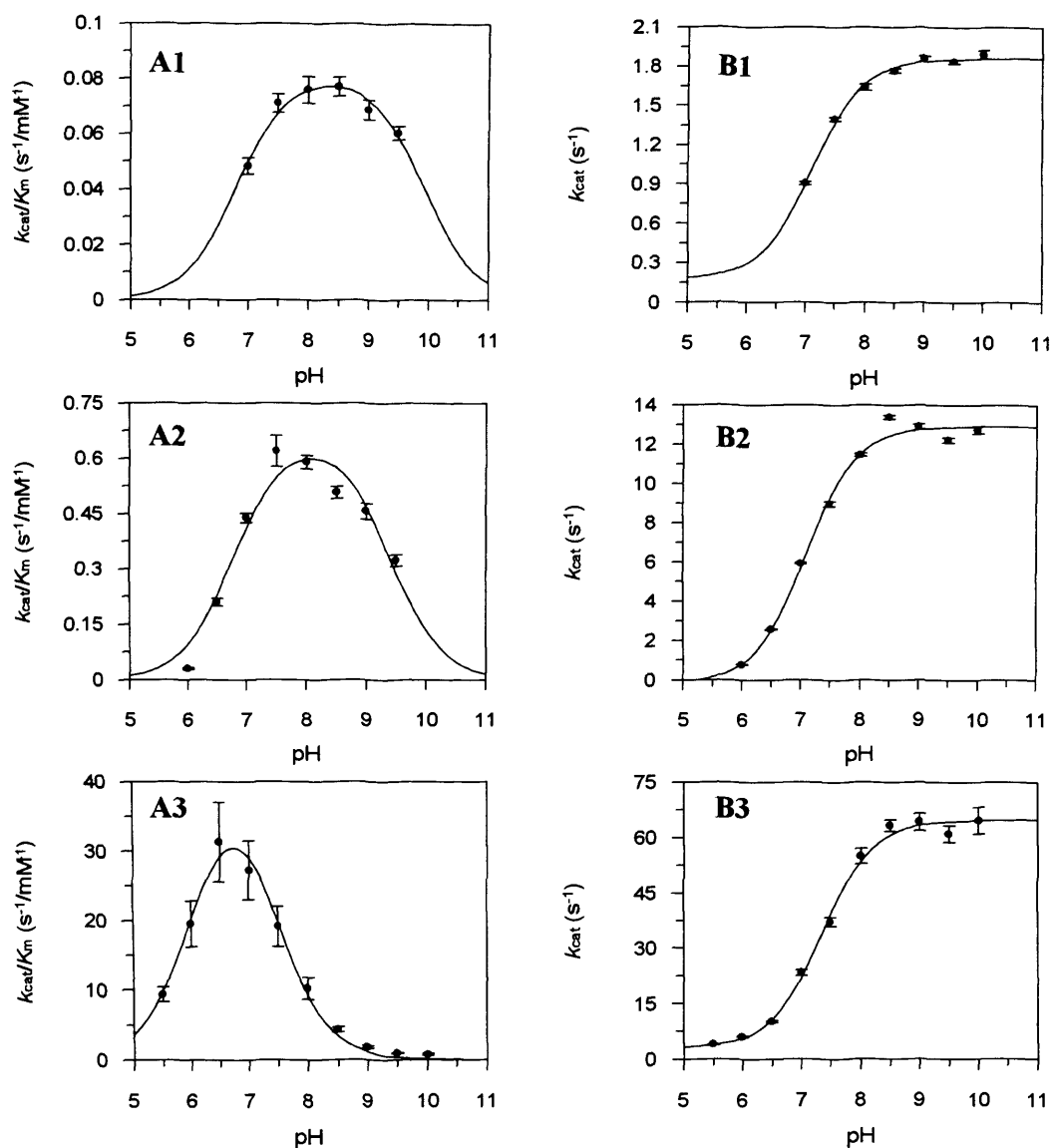
Figure 5. 22. Dependence of steady-state kinetic parameters on solution pH for the oxidation of L-proline substrate catalysed by the H225A, H225Q and Y251F PRODH enzyme forms. Panels A1, A2 and A3, pH dependence of k_{cat}/K_m following ionisations in the free enzyme and substrate during the reactions of H225A, H225Q and Y251F PRODH enzyme forms respectively. Fitting of data to Equation 2.6 showed a bell-shaped dependence of k_{cat}/K_m on solution pH for each mutant enzyme form giving two pK_a values from each plot; 6.8 ± 0.1 and 9.9 ± 0.1 (H225A), 6.8 ± 0.1 and 9.4 ± 0.2 (H225Q) and 6.0 ± 0.1 and 7.4 ± 0.1 (Y251F). Panels B1, B2 and B3, pH dependence of k_{cat} following the pK_a of the enzyme-substrate complex during the reactions of H225A, H225Q and Y251F PRODH enzyme forms respectively. Fitting of data to Equation 2.5 showed a simple sigmoid relationship of k_{cat} on solution pH for each mutant enzyme form giving a single pK_a value from each plot; 7.1 ± 0.1 (H225A), 7.1 ± 0.1 (H225Q) and 7.3 ± 0.1 (Y251F). Conditions: A three component buffer system comprising 0.052, 0.052 and 0.1 M of MES, TAPSO and diethanolamine respectively; 60 °C.

This analysis has revealed that all three mutant enzymes retain the ability to oxidise L-proline and that neither the His-225β nor Tyr-251β are active site base residues essential for catalysis. The results obtained suggest that PRODH stabilises the deprotonated form of L-proline substrate in the Michaelis complex analogous to substrate activation mechanisms observed in TMADH (Basran *et al.*, 2001a) and MSOX (Zhao and Jorns, 2005). Based on this finding and the absence of an active site residue that acts as base during the oxidation of L-proline, the data suggests that proline oxidation may occur by addition of L-proline base at the C4a position of the non-covalent FAD cofactor and abstraction of a substrate proton by the N5 atom of the flavin. Both are contemporary mechanisms of flavoprotein catalysed amine oxidation similar to those previously proposed for monoamine oxidase (Miller and Edmondson 1999; Rigby *et al.*, 2005) and TMADH (Basran *et al*, 2001b). However, these data are also consistent with a radical-based mechanismas proposed for MAO catalysis (Silverman *et al.*, 1980), and further studies including EPR spectroscopy are necessary to conclude which mechanism dictates PRODH catalysis. Crystallographic analysis with bound substrate and substrate analogues will shed more light on the nature of L-proline binding at the active site of PRODH and the participating residues involved in substrate binding. Macroscopic pK_a values obtained from the secondary plots for the solution pH-dependence of kinetic parameters k_{cat} (turnover number) and k_{cat}/K_m (specificity constant) are summarised in Table 5.8.

5.2.8. REDOX POTENTIOMETRIC TITRATIONS OF PRODH MUTANT FORMS

To establish if the mutation of His-225β and Tyr-251β active site residues had any effect on the redox poise of the FAD cofactor of PRODH, redox potentiometric titrations were performed to measure the midpoint potential of bound flavin in the three mutant forms as previously described (Section 2.8). Anaerobic redox potentiometric titration of the H225A, H225Q and Y251F mutant enzymes at 25 °C all showed reduction of oxidised flavin (FAD) directly to the dihydroflavin form without visible population of a flavin semiquinone species (Figure 5.23). Mutant data sets were fitted to the two-electron

245

Enzyme	Substrate pK_a	pK_a: bell-shaped curve (k_{cat}/K_m plot)	
		Acid limb	Alkali limb
Wild-type	7.7 ± 0.1	7.0 ± 0.2	7.6 ± 0.2
H225A	7.1 ± 0.1	6.8 ± 0.1	9.9 ± 0.1
H225Q	7.1 ± 0.1	6.8 ± 0.1	9.4 ± 0.2
Y251F	7.3 ± 0.1	6.0 ± 0.1	7.4 ± 0.1

Table 5. 8. Table giving a summary of the macroscopic pK_a values determined from the pH-dependence data for the oxidation of L-proline substrate catalysed by the wild-type and mutant PRODH enzyme forms. pK_a values determined from the sigmoidal pH-dependence of kcat are attributed to the ionisation of substrate L-proline stabilised in the Michaelis complex.
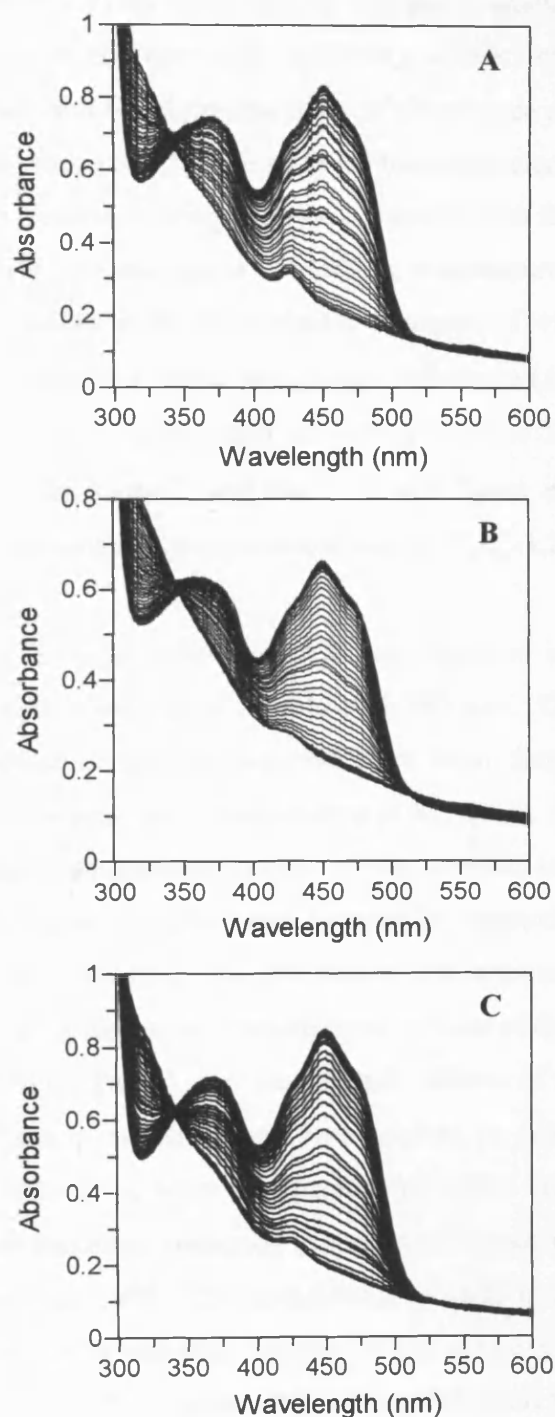
Figure 5. 23. Redox potentiometric titration of PRODH mutant enzyme forms with sodium dithionite. *Panels A-C*, Spectral changes accompanying the reductive titration of H225A, H225Q and Y251F mutant forms of PRODH with sodium dithionite. Conditions: 100 mM potassium phosphate buffer pH 7.0. Mediator dyes used: methyl viologen (0.3 μM), benzyl viologen (1 μM), HNQ (7 μM) and PMS (2 μM), 25 °C.

Nernst function (Equation 2.7) by least squares regression analysis and gave midpoint
two-electron potential values of -169 ± 3 mV (H225A), -155 ± 3 mV (H225Q) and -157 ±
3 mV (Y251F) extracted from the sigmoidal plots of absorbance at 450 nm as a function
of the observed potential (corrected for the standard hydrogen electrode) characterised by
a single inflection point observed during titration of each mutant form (Figure 5.24). The
midpoint potential of wild-type enzyme at a controlled temperature of 25 °C was -174 ± 3
mV, therefore, a perturbation in flavin midpoint potential of +5 mV observed in the
H225A mutant corresponded to a Gibbs free energy difference ($\Delta G^{\circ\prime}$) of -0.96 kJ·mol^{-1}.
Similarly, a flavin midpoint potential shift of +19 mV in the H225Q mutant enzyme
equated to a $\Delta G^{\circ\prime}$ of -3.66 kJ·mol^{-1} and the + 17 mV flavin midpoint potential shift
displayed in the Y251F mutant enzyme amounted to a $\Delta G^{\circ\prime}$ of -3.28 kJ·mol^{-1} (Table 5.9).

A positive shift in the flavin midpoint potential was observed in each of the PRODH
mutant forms relative to the redox poise of wild-type PRODH. Charged groups in close
proximity to flavin cofactors such as arginine have been demonstrated to influence
reduction potentials in flavoproteins (Maeda-Yorita et al., 1994). The midpoint reduction
potential for the oxidised/semiquinone couple of the electron transferring flavoprotein
(ETF) of Methylophilus methylotrophus was lowered by approximately 200 mV in the
R237A active site mutant revealing that this active site arginine residue has a major
regulatory role in stabilising the anionic semiquinone species of the FAD cofactor in ETF
(Talfournier et al., 2001). Indeed, the electrostatic effects of acidic residues on the
reduction potential of flavin cofactors has been studied in flavodoxin with evidence
showing a strong correlation between the quantity of acidic residues surrounding the
flavin cofactor and the measured reduction potential of the semiquinone/hydroquinone
couple (Zhou and Swenson, 1995). The mutagenesis of residues His-225β and Tyr-251β
in PRODH may cause conformational changes in the active site that induce charged
residues, for example Arg52β to undergo a subtle rearrangement in conformation relative
to the isoalloxazine moiety of bound FAD with the effect of stabilising the reduced
hydroquinone form. Structural data regarding the PRODH mutant forms will advance
this conjecture by highlighting potential differences in the conformation and proximity of

248
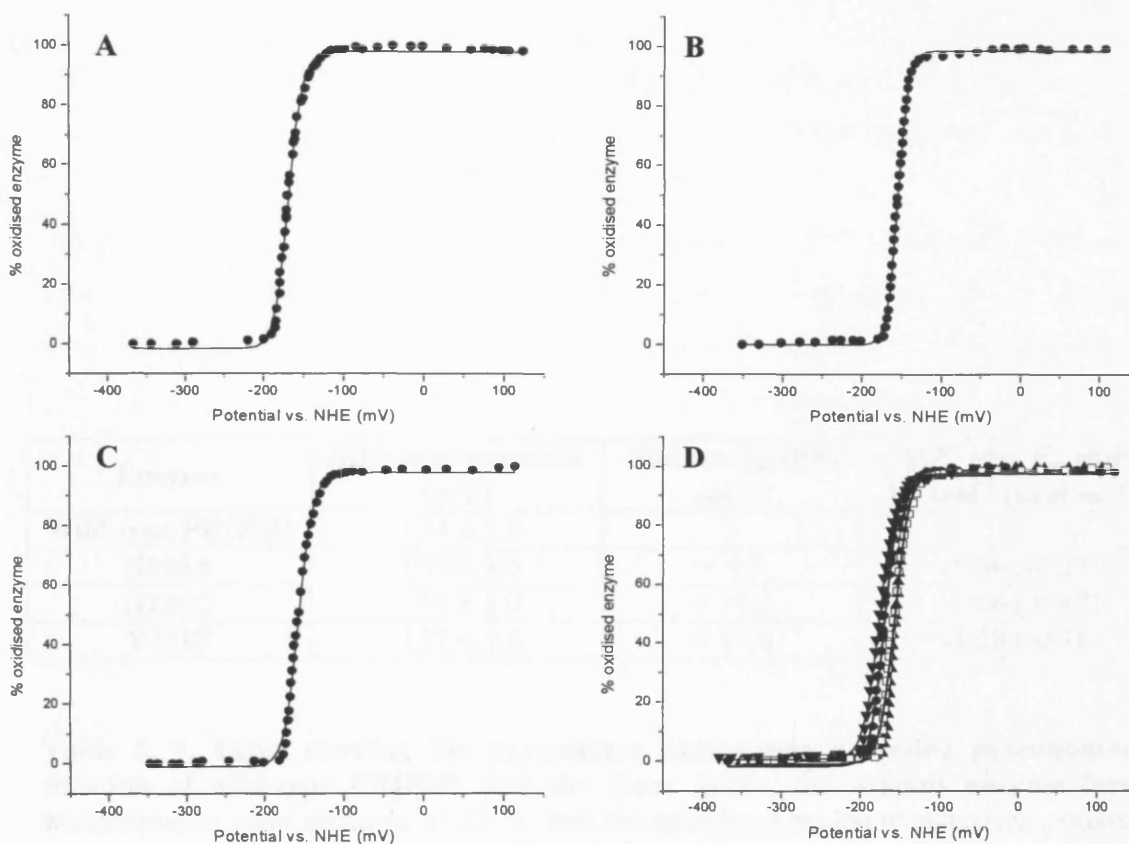
Figure 5. 24. Redox potentiometric titration of H225A, H225Q and Y251F mutant PRODH forms with sodium dithionite. *Panel A*, plot of % flavin oxidised monitored at 450 nm *versus* the observed potential for the H225A mutant enzyme form giving a midpoint reduction potential, E_m, of -169 ± 3 mV. *Panel B*, plot of % flavin oxidised at 450 nm *versus* the observed potential for the H225Q mutant enzyme form giving E_m, of -155 ± 3 mV. *Panel C*, plot of % flavin oxidised at 450 nm *versus* the observed potential for the Y251F mutant enzyme form giving E_m, of -157 ± 3 mV. *Panel D*, overlayed Nernst plots of % flavin oxidised monitored at 450 nm for the H225A mutant (*closed circles*), H225Q mutant (*closed triangles*) and Y251F mutant (*open squares*) forms in comparison to wild-type PRODH (*closed inverted triangles*). Observed potentials were corrected against the normal hydrogen electrode (NHE) and all data sets were fitted to the Nernst equation (Equation 2.7) for a two-electron reduction process. Conditions: 100 mM potassium phosphate buffer, pH 7.0. Mediator dyes used: methyl viologen (0.3 µM), benzyl viologen (1 µM), HNQ (7 µM) and PMS (2 µM); 25 °C.

Enzyme	Midpoint potential (mV)	Mutant E_m shift (mV)	$\Delta G^{\circ\prime}$ (for E_m shift) kJ mol^{-1} (kcal mol^{-1})
Wild-type PRODH	-174 ± 3.0	/	/
H225A	-169 ± 3.0	+ 5.0	-0.96 (-0.23)
H225Q	-155 ± 3.0	+ 19.0	-3.66 (-0.87)
Y251F	-157 ± 3.0	+ 17.0	-3.28 (-0.78)

Table 5. 9. Table showing the parameters determined by redox potentiometric titration of wild-type PRODH and the three active site mutant enzyme forms. Measurements were obtained at 25 °C and the calculated midpoint reduction potentials (E_m) were corrected for the normal hydrogen electrode.

acidic residues relative to the flavin ring in comparison to the structure of wild-type PRODH.

5.2.9. SPECTROPHOTOMETRIC SCREENING FOR A PUTATIVE PHYSIOLOGICAL ELECTRON ACCEPTOR OF PRODH

P. furiosus, the archaeal hyperthermophile from which PRODH was cloned, grows under anaerobic conditions. This habitat therefore rules out oxygen as the physiological electron acceptor for this protein, as confirmed by kinetic analysis (Section 3.2.12). In an effort to identify the physiological electron acceptor for reduced PRODH, a selection of nucleotide molecules and the small electron-carrier protein ferredoxin from _P. furiosus_ were screened for electron transfer activity by single and multiple enzyme turnover assays as previously described (Section 2.6.1). NAD^+, $NADP^+$, FAD and FMN were each assayed to assess if electrons were transferred to these small molecule electron acceptors from dithionite-reduced PRODH under anaerobic conditions and during steady-state turnover with L-proline substrate. Experiments were repeated using PRODH that had been purified in monoflavinylated form and subjected to prolonged incubation at room temperature with 10 mM FMN in MOPS buffer pH 7.5. No activity towards exogenous FMN, FAD, NAD^+ or $NADP^+$ was observed for PRODH during anaerobic assays. Furthermore, unlike the PutA multifunctional enzyme of enteric bacteria (Menzel and Roth, 1981), no activity towards NAD^+ was detected for the _P. furiosus_ PRODH in either multiple turnover or single turnover assays, which reinforces functional differences between the _P. furiosus_ and _E. coli/S. typhimurium_ enzymes.

Ferredoxin from _P. furiosus_ was generously supplied in the reduced form by Professor Wilfred Hagen of the Department of Biotechnology, Delft University of Technology, Delft, The Netherlands. _P. furiosus_ ferredoxin contains a 4Fe-4S cluster and two cysteine residues (Cys-21 and Cys-48) that form a disulfide bridge. Previous studies utilising a combination of NMR and EPR spectroscopy have shown that these thiol groups are redox active, allowing the ferredoxin to adopt four distinguishable redox states (Gorst _et al.,_ 1995) as illustrated in Figure 5.25. Prior to investigation, reduced ferredoxin was
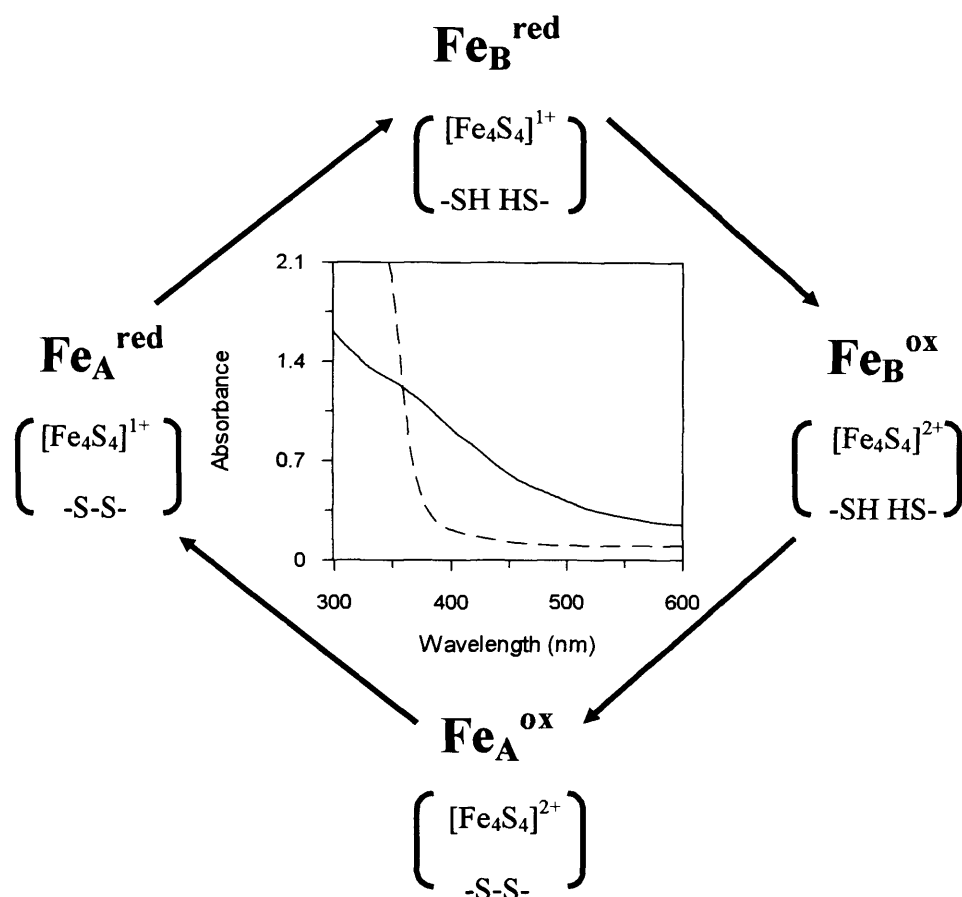
Figure 5. 25. The redox cycle of ferredoxin of _Pyrococcus furiosus_ DSM 3638 and UV-visible spectra of oxidised and reduced forms. Ferredoxin can exist in four different redox states. Purified under anaerobic and reducing conditions ferredoxin contains two free thiol groups (Cys-21 and Cys-48) designating the B form species (Fe_B). The reduced 4Fe cluster (Fe_B^{red}) is oxidised with oxygen exposure to Fe_B^{ox} with the thiols remaining reduced. Prolonged oxygen exposure ($t_{1/2}$ = 83 hours in air and 11 hours in oxygen) generates the disulfide bond characterising Form A (Fe_A^{ox}) with Fe_A^{red} being produced by treatment with the reductant sodium dithionite. The redox cycle illustration is adapted from Adams and Kletzin, 1996. _Central spectrum_, the UV-visible absorption sprectrum of the oxidised Fe_B^{ox} form (_black line_) and reduced Fe_B^{red} form (_dashed line_) of ferredoxin of _P. furiosus_ upon addition of 1 mM sodium dithionite. Conditions: 50 mM potassium phosphate buffer pH 7.0, _P. furiosus_ ferredoxin (58.8 µM), sodium dithionite (1 mM; _dashed line_), 80 °C.

oxidised in air for 2 hours with gentle agitation and monitored spectrophotometrically at 390 nm. Enzyme assays were performed in an anaerobic glovebox monitoring the reduction of 4Fe-4S ferredoxin (Fe_B^{ox} form; refer to Figure 5.25) at 390 nm by PRODH as described previously for aldehyde ferredoxin oxidoreductase activity (Mukund and Adams, 1991) using a molar extinction coefficient for oxidised ferredoxin at 390 nm (ε_{390}) of 17,000 M^{-1} cm^{-1} (Byrant and Adams, 1989), but using L-proline as substrate. Assays were performed at 80 °C in the presence of excess L-proline (200 mM) with ferredoxin at a final concentration of 90 μM. No activity towards ferredoxin was observed after prolonged incubation of the assay mixture (> 2 hours). As a positive control, and to confirm that *P. furiosus* ferredoxin was active and able to accept electrons in the assay mixture, an aliquot of sodium dithionite (μM concentration) was added to the assay mixture and the spectral change associated with the reduction of the small iron-sulfur ferredoxin was recorded between 300-600 nm (Figure 5.25).

5.2.10. ANAEROBIC GROWTH AND PURIFICATION OF WILD-TYPE PRODH

Activity assays utilising *P. furiosus* ferredoxin as electron acceptor produced no evidence for electron transfer from substrate-reduced PRODH to oxidised ferredoxin (Section 5.2.10). The anaerobic environment that *P. furiosus* inhabits led to the possibility that potential iron-sulfur clusters in the PRODH α subunit (inferred from sequence analysis) may be labile under aerobic conditions. Therefore, in an attempt to retain the iron-sulfur cluster in full occupancy, PRODH was expressed anaerobically and purified according to the protocol previously described (Section 2.4.4; Figure 5.26). Experiments were repeated with anaerobic PRODH with nucleotide electron acceptor candidates and *P. furiosus* ferredoxin as described for aerobic PRODH. No activity towards any of these was observed. Treatment of enzyme (anaerobically and aerobically purified forms) with ferrous ammonium sulfate (10 mM) had no effect in activity assays with these redox acceptors.
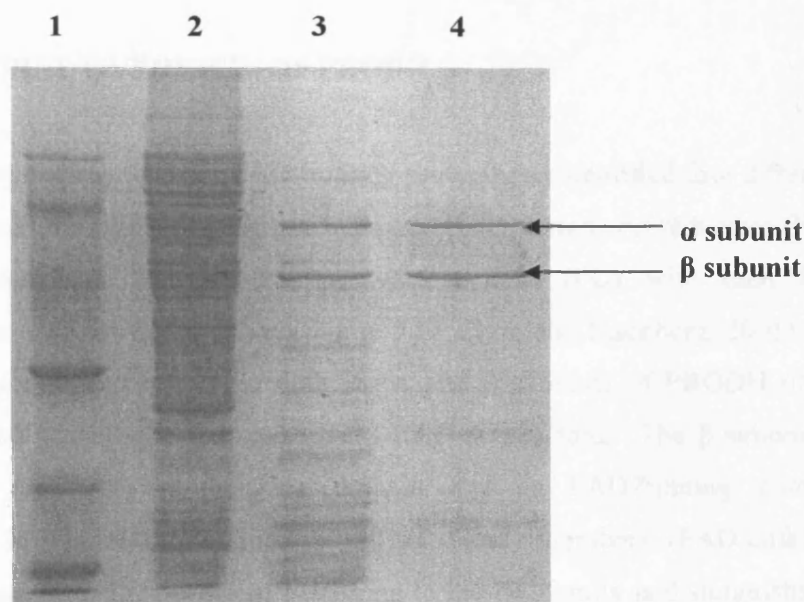
Figure 5. 26. SDS-PAGE analysis of the anaerobic purification of recombinant wild-type PRODH from *E. coli* strain Rosetta(DE3)pLysS transformed with pPRODH2. SDS-PAGE purification gel: Lane 1, molecular weight marker (97, 66, 45, 30, 20.1 and 14.4 KDa from top to bottom of the gel); lane 2, induced cell lysate (1 mM IPTG); lane 3, sample after heat-denaturation at 80 °C and clarification by centrifugation in a sealed air-tight tube; lane 4, pooled fractions following anion-exchange chromatography (DE52) performed in a Belle Technology anaerobic glovebox showing the pure α and β subunits of anaerobic PRODH.

The physiological electron acceptor for PRODH remains to be determined. A systematic screen of quinone compounds is the next logical phase in future experiments towards the determination of the physiological electron acceptor of PRODH of *P. furiosus*.

5.3. DISCUSSION

5.3.1. STRUCTURAL OVERVIEW OF PRODH

To date, structure-sequence analysis of FAD-binding proteins has identified four different FAD-family folds, exemplified by glutathione reductase (GR), ferredoxin reductase (FR), *p*-cresol methylhydroxylase (PCMH) and pyruvate oxidase (PO) with each fold represented by at least two protein families (Figure 5.27; Dym and Eisenberg, 2001). In terms of overall structure and topology, both the α and β subunits of PRODH of *P. furiosus* belong to the glutathione reductase (GR) FAD-family fold. The β subunit is composed of two domains, an interface domain and an FAD-binding domain characterised by the Rossmann fold adopted by all GR-family members. FAD cofactor binding and conformation in flavoproteins belonging to the GR-family is distinguishable by the elongated conformation adopted by the bound FAD with the isoalloxazine and adenine ring moieties positioned distally (Dym and Eisenberg, 2001). The β subunit of PRODH more specifically belongs to the GR_2 subfamily of the GR FAD-family fold exemplified by D-amino acid oxidase (Mattevi *et al.*, 1996). This subfamily is characterised by secondary structure insertions, particularly in the connections between β_2 to α_2 and α_2 to β_3 of the Rossmann fold (Dym and Eisenberg, 2001), consistent with members of the GR_2 subfamily only aligning with other GR family members in the N-terminal region (~ first 30 residues).

A point to note regarding the active site of PRODH is that only active site residue Arg302β on the *si* face of the FAD cofactor isoalloxazine ring is conserved between the β subunit of PRODH and the flavoprotein MSOX that carries 24 % sequence identity with PRODHβ at the amino acid level. Tyr251β, His336β, Tyr308β and Arg52β on the *re* face of the isoalloxazine ring moiety of the FAD cofactor are conserved in MSOX.

255
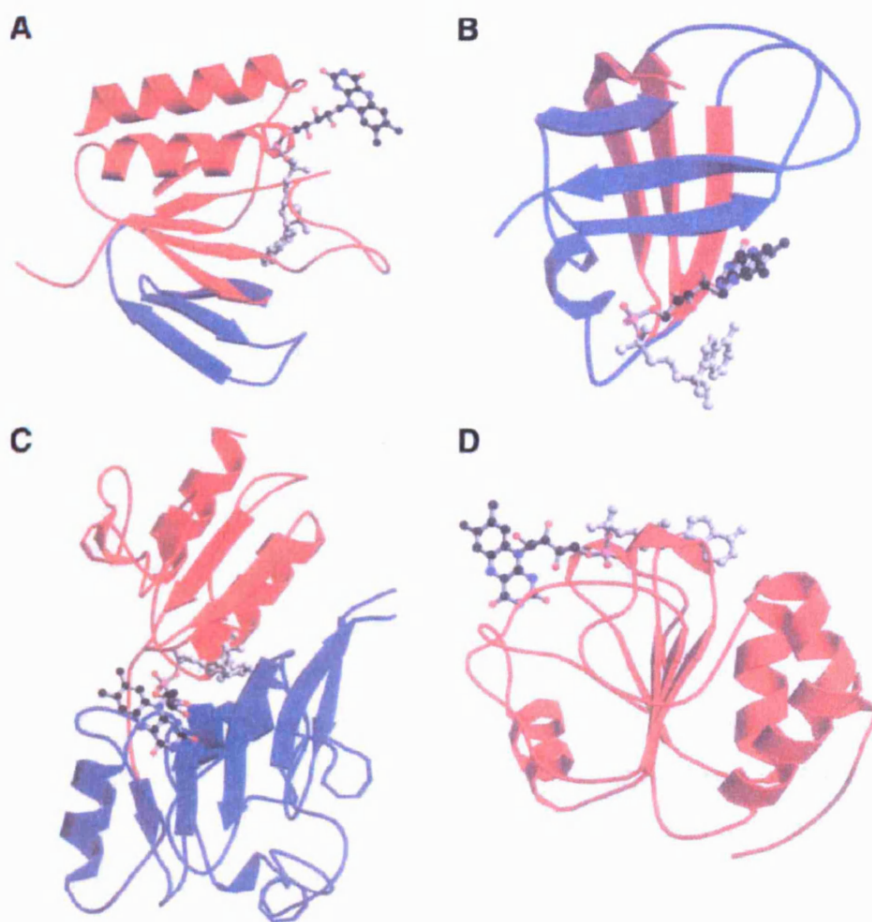
Figure 5. 27. The structures of the FAD-binding domains in complex with FAD cofactor for the four different FAD family folds. *Panel A*, ribbon representation of the Rossmann fold evident in the glutathione reductase (GR) family, with the central five-stranded parallel β-sheet surrounded by two α-helices is shown in red and the three-stranded anti-parallel β-sheet structure forming the crossover connection is shown in blue. The FAD cofactor is in an elongated conformation (ball and stick representation) and points towards the binding domain. *Panel B*, ribbon representation of the fold adopted by the ferredoxin reductase (FR) family members with the two anti-parallel three-stranded β-sheet secondary structures shown in red and blue and the FAD cofactor in a bent conformation with the isoalloxazine moiety (black, ball and stick representation) pointing towards the binding domain. *Panel C*, ribbon representation of the *p*-cresol methylhydroxylase (PCMH) family αβ fold with the three-stranded parallel β-sheet surrounded by α-helices is shown in red and the five anti-parallel beta strands surrounded by α helices is shown in blue. The FAD cofactor is positioned between the two subdomains in an elongated conformation (ball and stick representation). *Panel D*, the Rossmann fold shown in red adopted by the pyruvate oxidase (PO) family members. The FAD cofactor is located perpendicular to the β-sheet secondary structure in a elongated conformation. Figure taken from Dym and Eisenberg, 2001.

Additionally, whereas FAD is covalently attached via an 8α-S-cysteinyl linkage to Cys-315 in MSOX (Trickey _et al._, 1999), FAD cofactor is non-covalently bound to the β subunit of PRODH of _P. furiosus._

The α subunit of PRODH is composed of four domains, an ATP-binding domain, a central domain, an N-terminal domain and a Cys-clustered domain. One molecule of ATP cofactor is bound in the ATP-binding domain of the α subunit as observed in the X-ray crystal structure of PRODH (Figure 5.14). DALI analysis for protein structure comparison (Holm and Sander, 1995; http://www.ebi.ac.uk/dali/) revealed that the structure of this ATP-binding domain is related to the FAD-binding domain of the flavoprotein alkyl hydroperoxide reductase (Wood _et al._, 2001; PDB accession code: 1HYU), a member of the GR-family. This ATP cofactor has no obvious function from a mechanistic perspective, but may play a stabilising role under the harsh physiological conditions that _P. furiosus_ inhabits. The flavoenzyme TMADH is another example of a nucleotide-binding protein which harbours one equivalent of tightly bound ADP as cofactor with unknown function in addition to covalent FMN and a bacterial ferredoxin type 4Fe-4S centre (Lim _et al._, 1988). The central domain has limited parity with the NADPH-binding domain of glutathione reductase, although this nucleotide is not a demonstrated substrate for PRODH and no spectral/structural data gathered do date suggests NADPH binding in the α subunit.

The FMN cofactor of PRODH is non-covalently bound at the αβ subunit interface between the Cys-clustered domain of the α subunit and the interface domain of the β subunit forming π-π interactions with the hydrophobic side chains of residues Met444α and Trp304β, a coordination first observed in the PDH1 protein of _P. horikoshii_ OT-3 (Tsuge _et al._, 2005). Concerning intra-protein electron transfer in PRODH from _P. furiosus_, the FAD and FMN cofactor isoalloxazine ring co-planarity, close proximity and relative orientation of the dimethyl benzene sides intimates a probable directionality for the electron transfer events during amine substrate oxidation from the FAD to FMN (Figure 5.17). An atomic distance between the two flavin ring functions of ~8 Å correlates with efficient intramolecular electron transfer (Moser _et al._, 1992). The

presence of iron in the Cys-clustered domain of the α subunit thus provides the means to transfer electrons to a specific physiological electron acceptor protein from reduced FMN cofactor via this cluster. Indeed, electron density was observed in the Cys-clustered domain of the α subunit attributable to partial occupancy of iron coordination in $\alpha\beta$ heterodimers of the PRODH heterooctamer present in the unit cell (Figure 5.17).

5.3.2. MUTAGENESIS STUDIES WITH PRODH: IMPLICATIONS FOR MECHANISM AND EVIDENCE FOR STABILISATION OF THE DEPROTONATED FORM OF SUBSTRATE IN THE MICHAELIS COMPLEX

Comparative analysis of the pH-dependence data for wild-type PRODH and the respective data collected regarding the three mutant enzymes, indicates in the first instance that the two targeted residues (His-225β and Tyr-251β) are involved in the enzyme-catalysed oxidation of L-proline substrate, be it at the substrate recognition, binding or catalytic amine oxidation level. This is deduced from the major perturbations observed in the kinetic parameters resulting from mutagenesis (Table 5.6). Removal of ionisable groups in the active site of PRODH by mutagenesis of His-225β and Tyr-251β does not result in loss of the sigmoidal pH-dependence of k_{cat}, with minimal disparity observed in the macroscopic pK_a values extracted from the data fitting of wild-type (pK_a = 7.7), H225A (pK_a = 7.1), H225Q (pK_a = 7.1) and Y251F (pK_a = 7.3) pH-dependence plots (Table 5.8). These data support the initial conclusion that the pK_a value of 7.7 observed for wild-type PRODH represents ionisation of substrate L-proline, a shift of - 2.9 pH units from 10.6 for the pK_a of ionisation of free L-proline to 7.7 denoting stabilisation on binding of the deprotonated form of L-proline in the Michaelis complex. This mechanism is consistent with observation of the flavoprotein TMADH where, on binding substrate, the pK_a for the substrate ionisation is sufficiently perturbed to favour formation of the free base form at physiological pH. Stopped-flow studies with TMADH indicate there is a shift in pK_a of about 3.5 pH units (from pH 9.8 to ~pH 6.5) for the substrate ionisation on forming the enzyme-substrate complex (Basran *et al.*, 2001a). With regard to PRODH, unequivocal assignment of this pK_a must await detailed stopped-

flow analysis with both protiated and deuterated substrate. Additionally, a change in rate limiting step in the steady-state reaction will inevitably complicate the assignment of kinetically influential ionisations in the reaction of PRODH and future investigations with high temperature stopped-flow apparatus are therefore essential toward advancing possible chemical mechanisms of amine oxidation by PRODH.

If the above mentioned scenario describing the stabilisation of the free base form of substrate in the Michaelis complex is applicable for PRODH, the enzyme by logic will have evolved a higher affinity for the deprotonated form of L-proline compared to the zwitterionic and protonated cationic species. Indeed, evident from the pH-dependence of k_{cat}, the identical pK_a values observed for both the H225A and H225Q mutant forms of PRODH of 7.1, in comparison to the slightly elevated corresponding value for the Y251F mutant of 7.3, and larger still the analogous value determined with wild-type enzyme of 7.7 do correlate to a degree with the apparent K_m values determined for each enzyme form in the vicinity of these pK_a values at pH 7.5 (Table 5.6). These data illustrate that a marginal negative shift in the pK_a of the stabilised deprotonated form of substrate in the Michaelis complex of PRODH as a result of mutagenesis, suggesting further stabilisation of unprotonated L-proline in the enzyme-substrate complex. This presents major implications with regard to preferential binding of the deprotonated form of substrate, evident from the elevated apparent Michaelis constants for the mutant enzyme forms (since substrate concentration is measured as the sum of both the protonated cationic and deprotonated forms). These data strengthen the assignment of the pK_a value determined from the pH-dependence of k_{cat} for wild-type PRODH of 7.7 to ionisation of the deprotonated form of substrate L-proline in the Michaelis complex, highlighting this form of substrate as the likely active species.

On comparing the bell-shaped dependence of k_{cat}/K_m as a function of solution pH observed for wild-type PRODH and retained in all of the three mutant enzyme forms, immediately apparent is the elevated pK_a values depicted on the alkali limb of the plots for the H225A (pK_a = 9.9) and H225Q (pK_a = 9.4) mutant forms in relation to wild-type (pK_a = 7.6; Figure 5.22). This perturbation is possibly attributable to the effects of

removing a polar interaction between the replaced imidazole side chain of His-225β with a proximal residue, thus resulting in displacement of the ionising side chain pK_a of this residue to an elevated pH value. This conjecture is corroborated in part by the data collected for the Y251F mutant form where fitting of the bell-shaped dependence of k_{cat}/K_m on solution pH reveals a pK_a value of 7.4 corresponding to the descending alkali limb of the curve that is consistent and within the error range to the value obtained for wild-type PRODH with a pK_a of 7.6. Using this Y251F data as evidence to corroborate the postulation for the displacement of a proximal side chain pK_a to a higher pH value as a result of mutagenic replacement of the imidazole side chain of His-225β inevitably rules out such an interaction between Tyr-251β and His-225β in the active site.

Residues His-225β and Tyr-251β of PRODH are two of only three active site residues that are conserved within the family of sarcosine dehydrogenase (SDH)-like proteins, and based on the X-ray crystal structure of the flavoprotein DMGO, residues His-225 and Tyr-259 that align with the above mentioned residues in PRODH of _P. furiosus_ have been implicated in the deprotonation of zwitterionic substrate to the deprotonated species to facilitate reduction of the flavin cofactor by forming a His-225-Tyr-259 catalytic dyad for proton relay (Leys _et al._, 2003). Mutant studies with DMGO have revealed that like PRODH, H225Q and Y259F mutant forms of DMGO retain the ability to oxidise substrate indicating that neither residue is critical for enzyme activity (Basran _et al._, 2006). His-225 of DMGO has been demonstrated not to play a crucial role in the catalytic mechanism, though the presence of a water molecule in the H225Q crystal structure close of the Tyr-259 side chain may act to deprotonate Tyr-259 prior to substrate binding, therefore facilitating deprotonation of substrate by the active site base (Tyr-259) accounting for the residual activity observed in the H225Q mutant enzyme. This proposal is consistent with the steady-state kinetic behaviour observed with the H225A mutant form of PRODH. The Y259F mutant form of DMGO is severely compromised in terms of catalytic activity. Residual activity presented by the mutant enzyme may be accounted for if the enzyme binds deprotonated substrate over the protonated species, therefore negating the requirement for substrate deprotonation by Tyr-259 base prior to the catalytic event. In this case, the mutant should present a stable

turnover number consistent with wild-type and a dramatically elevated K_m, traits observed with His-225β mutant forms of PRODH.

Arguably, the most compelling observations of the mutant forms of PRODH of *P. furiosus* are the kinetic behaviour of the Y251F mutant form. In stark contrast to the residually active Y259F mutant form of DMGO, corresponding mutagenesis of the aligning Tyr-251β residue in PRODH to a phenylalanine with the effect of removing the phenolic hydroxyl group of the aromatic side chain results in a mutant enzyme with an apparent K_m value approximate to that measured for wild-type enzyme and, more surprisingly, an elevated k_{cat} at solution pH 7.5 that is >5-fold greater than the corresponding turnover number for wild-type PRODH. Furthermore, the Y251F mutant form displays pronounced substrate inhibition kinetics in the acid-to-neutral solution pH region (Figure 5.21, D), a characteristic similar to that previously documented in studies of mutant forms of the flavoprotein morphinone reductase under conditions of high substrate concentration (Messiha *et al.*, 2005a; Messiha *et al.*, 2005b). At high substrate concentrations, a molecule of L-proline may inhibit the catalytic site of PRODH by binding close to the *re* face of the FAD cofactor isoalloxazine moiety, occupying volume that in wild-type enzyme is occluded by the phenolic hydroxyl group of the Tyr251β side chain.

Overall, data points to PRODH preferentially binding and stabilising the free base form of L-proline substrate in the active site. Elevated Michaelis constants for the H225A and H225Q mutant forms suggests that His-225β may play a role in substrate binding, but this residue doesn't appear implicated in the mechanism of substrate amine oxidation and isn't critical for enzyme activity. pH-dependence data are consistent with a polar nucleophilic mechanism of L-proline oxidation by PRODH previously proposed for the mechanism of monoamine oxidase A (Miller and Edmondson, 1999) whereby nucleophilic attack by the substrate nitrogen on the flavin C4a atom leads to a transient covalent intermediate followed by proton abstraction by the flavin N5 atom, a very strong base with a pK_a value >30 (Figure 5.28). This mechanism is consistent with stabilisation of the free base form of substrate and the kinetic analyses concluding that neither active

Michaelis complex $pK_a = 7.7$

Free zwitterionic L-proline $pK'_a = 10.6$

Glutamic semialdehyde

P5C
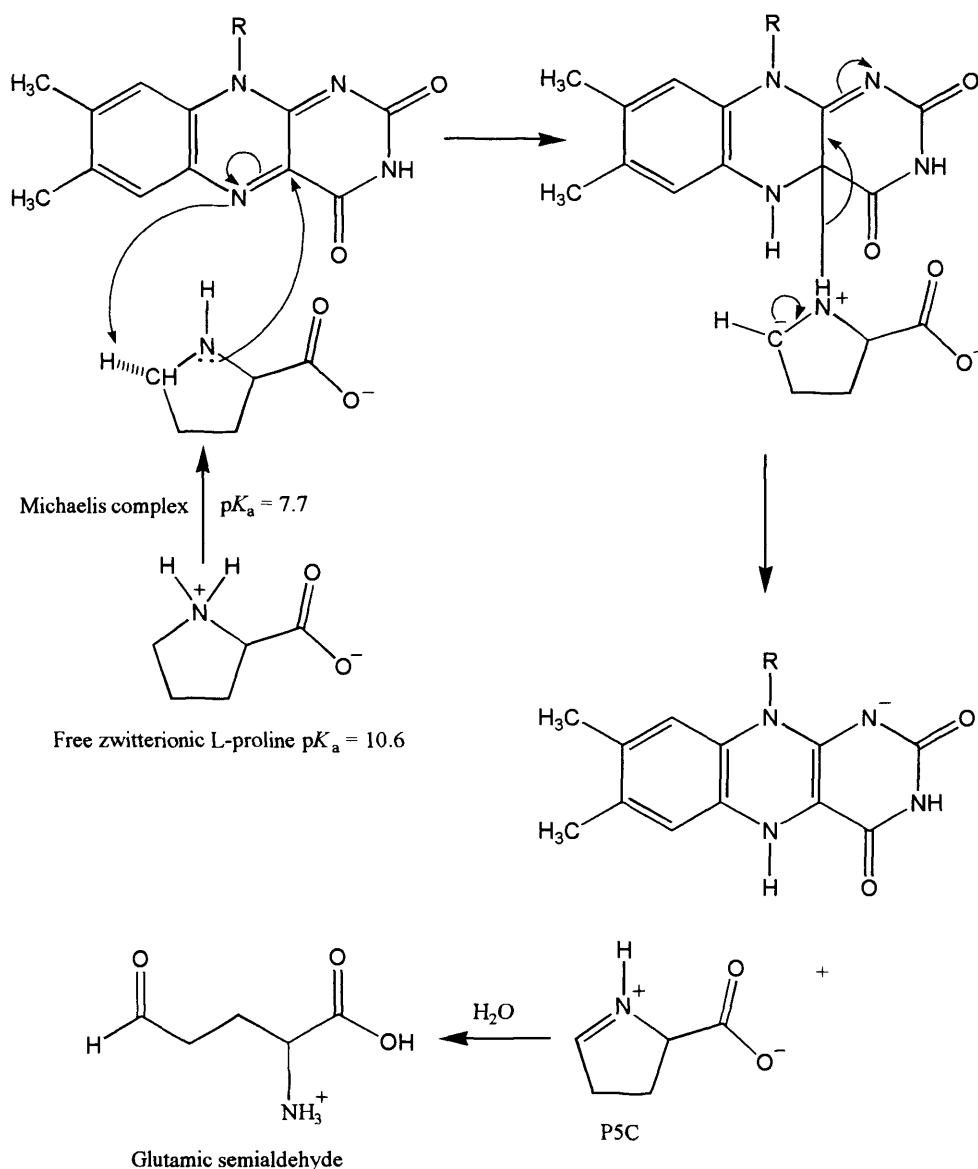
Figure 5. 28. A proposed mechanism for the oxidation of substrate L-proline catalysed by PRODH of *P. furiosus* DSM 3638. The mechanism is analogous to the concerted polar nucleophilic mechanism proposed for the reaction of monoamine oxidase A (Miller and Edmondson, 1999). The stabilised deprotonated form of L-proline substrate in the Michaelis complex ($pK_a = 7.7$) initiates nucleophilic attack at the flavin C4a position forming a 4a-alkylated isoalloxazine ring adduct with concerted transfer of the substrate proton to the basic flavin N5 position ($pK_a \sim 30$) followed by elimination to form the experimentally observed imine product (P5C, figure 4.7) and the reduced flavin cofactor. Labile P5C is non-enzymatically hydrolysed to the open ring γ-glutamic semialdehyde that is subsequently converted to glutamate by the multifunctional PutA of enteric bacteria and by P5CDH, a separate enzyme in eukaryotes.

site residue targeted in these mutagenesis studies (His-225β and Tyr-251β) are essential for catalysis.

A radical based mechanism for the reaction of PRODH cannot be disputed without EPR based analysis, although to date, no tyrosyl radical species has been detectable for the reaction of DMGO and only recently has spectroscopic evidence for the presence of a tyrosyl radical species during the reaction of monoamine oxidase A been presented in the literature (Rigby _et al._, 2005). Additionally, in juxtaposition to His-225β at the active site of PRODH is Tyr-308β (Figure 5.29), the ionisation of this residue cannot be discounted as a potential kinetically influential event and further mutagenesis studies targeting this group may shed more light on the chemistry of the active site and the mechanism of L-proline oxidation utilised by PRODH of _P. furiosus._

5.4. SUMMARY

The X-ray crystal structure of PRODH of _P. furiosus_ has been determined by the molecular replacement method to a resolution of 3.3 Å. The structure as initially indicated from the general self-rotation function analysis is a tetramer of αβ heterodimers (or a heterooctamer) with the heterodimers arranged in _222_ non-crystallographic symmetry (Figure 5.10, A and B). One heterooctamer per unit cell corresponds to an oligomeric molecular mass of ~388.8 KDa. The three-dimensional structure reveals electron density confirming the presence of three cofactors in PRODH; one ATP molecule bound in the Rossmann fold of the α subunit, one molecule of non-covalently bound FAD in the β subunit at the active site for amine oxidation, and one molecule of non-covalent FMN bound atypically at the subunit interface between the Cys-clustered domain of the α subunit and the interface domain of the β subunit. The co-planarity of the flavin cofactor isoalloxazine moieties, in addition to the close proximity and relative orientation of the dimethyl benzene functions of the flavin rings presents a feasible directionality for the electron transfer events during amine substrate oxidation from the FAD to FMN cofactors of PRODH. Electron density symptomatic for the presence of iron in the Cys-clustered domain of the α subunit indulged a plausible means of electron
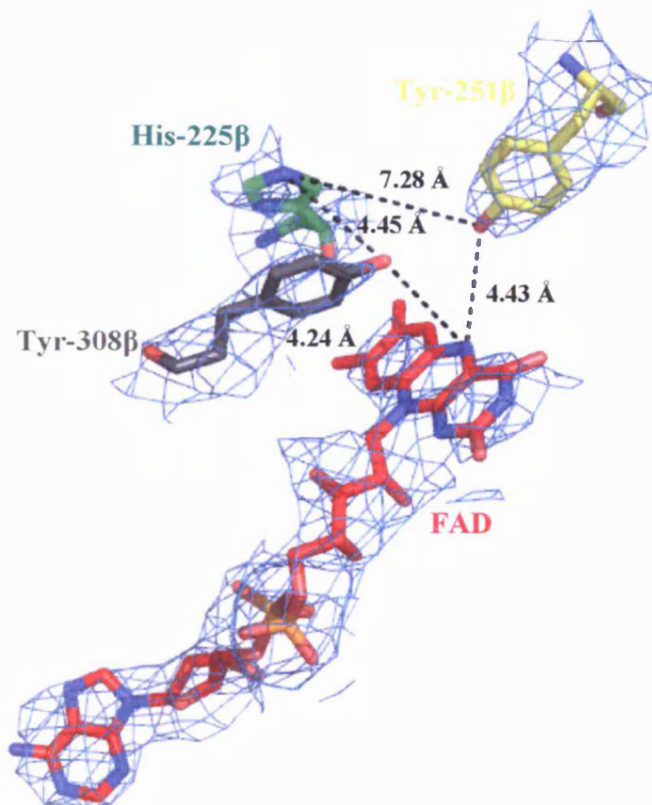
Figure 5. 29. Three-dimensional structure of the FAD cofactor bound in PRODH highlighting the distances between the flavin cofactor and three residues on the *re* face of the FAD isoalloxazine ring moiety. The phenolic hydroxyl group of Tyr-308 (grey stick) is 4.24 Å from the flavin (red stick) N5 atom and is marginally closer to the flavin N5 position than Tyr-251 (yellow stick) targeted for mutagenesis. Additionally, the phenolic hydroxyl group of Tyr-308 is closer to the imidazole ring of His-225 (green stick) targeted for mutagenesis at a distance of 4.45 Å in comparison to the distance between Tyr-251 and His-225 at 7.28 Å. Further mutant studies targeting Tyr-308 in addition to structural studies of substrate-bound PRODH will enable a greater insight into substrate binding and the mechanism of amine oxidation adopted by the enzyme. Electron density for the FAD cofactor and the displayed residues is shown as sky blue mesh and contoured at 2.0 σ. Figure constructed in stick representation using PyMOL v.0.99 (DeLano, 2002; http://www.pymol.org).

transfer from reduced PRODH to the physiological electron acceptor. Extensive screening of candidate electron acceptor molecules, including that of *P. furiosus* 4Fe-4S ferredoxin proved inconclusive and the physiological electron acceptor for PRODH of *P. furiosus* remains to be determined.

Kinetic data from pH-dependence studies with mutant forms of PRODH were consistent with a polar nucleophilic mechanism of substrate amine oxidation, previously proposed for the mechanism of monoamine oxidase A (Miller and Edmondson, 1999) with nucleophilic attack by the substrate nitrogen on the flavin C4a atom resulting in a transient covalent intermediate followed by proton abstraction by the basic flavin N5 atom. This mechanism is consistent with stabilisation of the deprotonated form of substrate with the macroscopic pK_a value of 7.7 for the reaction of wild-type PRODH being assigned to ionisation of L-proline in the Michaelis complex. Kinetic analyses concluded that none of the active site residue targeted in these mutagenesis studies (His-225β and Tyr-251β) are essential for catalysis.

In conclusion, the contrasting kinetic behaviour for both the DMGO and PRODH mutant forms, especially with regard to the Y251F mutant data suggests fundamental mechanistic differences between the two sequence-related proteins. Future studies and data interpretation must therefore be approached with an open mind in the advancement of the understanding of flavoprotein-catalysed amine oxidation, with particular emphasis on the SDH-family of oxidases.

CHAPTER SIX

DISCUSSION AND FUTURE DIRECTION

CHAPTER SIX

DISCUSSION AND FUTURE DIRECTION

6.1   GENERAL SUMMARY

Each results chapter in this thesis (chapters 3-5) is concluded with a short discussion regarding the key experimental findings. This chapter presents a summary of the experimental observations described in this thesis and details future work towards a comprehensive understanding of all the aspects of the L-proline dehydrogenase system from the hyperthermophile *P. furiosus* DSM 3638.

6.2   DISCUSSION

Current theory advocates that hyperthermophilic archaea were amongst the first life-forms to have evolved on Earth (Stetter, 1996). These hyperthermophiles grow optimally at temperatures > 80 °C and as such, pose valuable model systems for scientists towards the understanding of enzyme evolution and the molecular mechanisms of protein thermostability and function at temperatures up to and exceeding 100 °C. Knowledge of the molecular properties of these hyperthermophilic proteins and the chemical reactions they catalyse advances the potential for biotechnological applications (Vieille and Zeikus, 2001). For example, in the field of molecular biology, DNA polymerase enzymes from various hyperthermophilic sources have been isolated for application in the polymerase chain reaction that requires high temperatures (Perler *et al.*, 1996). An understanding of the metabolism of hyperthermophilic organisms will open the door for potential high temperature chemical synthesis applications and also unlock the strategies utilised by these organisms for macromolecular and metabolite thermostability in the harsh environments which they inhabit.

Pyrococcus furiosus DSM 3638 is a hyperthermophilic marine archaea that grows optimally at 100 °C within a pH range of 5-9 by the fermentation of carbohydrates and peptides to organic acids, CO_2 and H_2 (Fiala and Stetter, 1986). This organism is the most extensively characterised hyperthermophile to date. Sugar metabolism by this organism takes the form of a modified non-phosphorylating Entner-Doudoroff pathway (Mukund and Adams, 1991; Schaffer and Schonheit, 1992). The fermentation of peptides is less well understood, but initial hydrolysis by prolidase (Maher *et al.*, 2004) is known to be followed by transamination of the amino acids to 2-keto acid that is subsequently utilised by the acetyl-CoA synthetase isozymes. A variety of ferredoxin:oxidoreductases involved in the catabolism of amino acids have also been isolated from *P. furiosus* and studies have revealed that primary carbon metabolism and energy production in *P. furiosus* is centered on the small iron-sulfur protein ferredoxin (Aono *et al.*, 1989). Availability of the complete genome sequence for *P. furiosus* permitted a search to identify putative flavoprotein amine oxidoreductases with the aim of elucidating key stages in amino acid catabolism. This research was initiated to advance the bigger picture of understanding the nature and regulation of *P. furiosus* metabolism at a systems level.

Chapter three documents the cloning of two open reading frames (ORF's) from the genome of *P. furiosus* DSM 3638. Recombinant protein was overexpressed in *E. coli* strain Rosetta(DE3)pLysS and purified to homogeneity in a three-step scheme (3.13, A). The enzyme was identified spectrophotometrically as a flavoprotein with the UV-visible absorption spectrum highlighting characteristic flavin peaks with absorbance maxima at 367 and 450 nm (Figure 3.13, B). Initial solution studies in the form of high-temperature anaerobic reductive titrations identified the enzymes physiological substrate as L-proline ($t_{1/2}$ = ~105 s^{-1} for spectral bleaching of the oxidised enzyme at 450 nm), with oxidase activity towards the other secondary amine compounds L-pipecolic acid ($t_{1/2}$ = ~110.5 s^{-1}) and sarcosine ($t_{1/2}$ = ~654 s^{-1}; Figure 3.18). Addition of sodium sulfite (50 mM) to purified enzyme did not perturb the flavin UV-visible absorption spectrum, indicating that a flavin-N5-sulfite adduct does not form. This indicated that the enzyme belongs to the dehydrogenase class of flavoproteins, consistent with the slow reoxidation observed

with reduced enzyme upon exposure to air. Together these initial solution studies classified the recombinant enzyme as a hyperthermophilic L-proline dehydrogenase (PRODH). For solution studies, the enzyme was isolated in monoflavinylated form with occupancy of a single redox-active FAD cofactor identified by MALDI-ToF mass spectroscopy (Figure 3.17).

Chapter four builds on the initial steady-state data presented for PRODH and details both temperature dependence and pH-dependence studies of the reaction of PRODH with L-proline substrate in the steady state. Thermodynamic studies revealed that the steady-state reaction of PRODH with the physiological substrate L-proline is extremely temperature dependent as depicted by a large enthalpy of activation $(\Delta H^{\ddagger})$ deduced from Eyring analysis of the raw data (Figure 4.8, B). A greater enthalpy of activation $(\Delta H^{\ddagger} =$ 83.4 $\pm$ 2.9 kJ·mol^{-1}) was determined for the reaction of PRODH in comparison to the corresponding values documented for the flavoprotein tetrameric sarcosine oxidase of *Arthrobacter* sp. 1-IN (Harris *et al.*, 2000) and the quinoproteins methylamine dehydrogenase (MADH) from *Methylophilus methylotrophus* (Basran *et al.*, 1999) and aromatic amine dehydrogenase (AADH) from *Alcaligenes faecalis* (Hothi *et al.*, 2005). Temperature dependence studies with PRODH also highlighted that thermo-inactivation of the enzyme occurs at solution temperatures $\geq$ 100 °C, therefore PRODH of *P. furiosus* is the most thermostable L-proline dehydrogenase described to date.

pH-dependence studies with wild-type recombinant PRODH for the reaction with L-proline illustrated a bell-shaped dependence of k_{cat}/K_m as a function of solution pH yielding macroscopic pK_a values of 7.0 $\pm$ 0.2 and 7.6 $\pm$ 0.2 attributed to residue ionisations in the free enzyme (Figure 4.10, A). The pH-dependence of k_{cat} exhibited simple sigmoidal behaviour with maximum activity realised in the alkaline region (Figure 4.10, B). This dependence is described by a single macroscopic pK_a value of 7.7 $\pm$ 0.1 attributed to the ionisation of L-proline in the Michaelis complex.

The product of PRODH-catalysed L-proline oxidation was identified directly by MALDI-ToF mass spectroscopy as Δ^1-pyrroline-5-carboxylate (P5C; Figure 4.7). The stable

condensation product of the reaction of P5C with *o*-aminobenzaldehyde was identified by electrospray mass spectroscopy (Figure 4.6) and a mechanism for adduct formation was proposed reminiscent of earlier findings regarding the reaction of P5C with pyridoxal phosphate in patients with hyperprolinemia type II (Farrant *et al.*, 2001).

Redox potentiometry experiments over a solution temperature range of 7.5-31 °C demonstrated a 'normal' linear dependence on temperature of the reduction potential of PRODH (Figure 4.14, B). Subsequent thermodynamic analysis of the data gave a standard free energy change $(\Delta G^{\circ\prime})$ = -41.1 kJ·mol^{-1} at 25 °C for the spontaneous reaction. The standard entropy change of the reaction $(\Delta S^{\circ\prime})$ = -290.4 J·mol^{-1}·K^{-1}, and from this the standard enthalpy change of the reaction $(\Delta H^{\circ\prime})$ was calculated as -127.6 kJ·mol^{-1}.

Chapter five describes research efforts that led to the timely elucidation of the X-ray crystal structure of PRODH. The structure resolved at 3.3 Å resolution reveals that the native oligomeric state is a heterooctamer $(\alpha\beta)_4$ with heterodimers $(\alpha\beta)$ arranged in *222* non-crystallographic symmetry (Monaghan *et al.*, 2005). The complete holoenzyme form contains one mol each of FAD, FMN and ATP cofactors per mol of $\alpha\beta$ complex. The active site for amine oxidation is located on the β-subunit where the non-covalently bound FAD cofactor resides and is consistent with the retention of amine oxidase activity observed in the monoflavinylated (FAD-bound) form.

In addition to supplementing current knowledge of *P. furiosus* amino acid metabolism, a priority of this current project was to advance the mechanisms debate concerning amine oxidation by the flavoproteins, a topic that despite concerted research efforts over many years still remains controversial (Scrutton, 2004). With this aim in mind, pH-dependence studies with the H225A, H225Q and Y251F mutant enzymes were initiated (Figure 5.22). In comparison with the earlier pH-dependence data for wild-type PRODH (Chapter four), the mutant secondary plots highlighted a stable pK_a from the sigmoidal dependence of k_{cat} on solution pH. This stable pK_a in the wild-type enzyme (Figure 4.10, B) has been tentatively attributed to the ionisation of L-proline in the Michaelis complex similar to

kinetic observations with the flavoprotein TMADH (Basran *et al.*, 2001a). Mutant data also systematically ruled out the participation of both His-225β and Tyr-251β as catalytic base residues and neither residue is essential for enzyme activity. The kinetics data are consistent with a concerted polar nucleophilic mechanism of amine oxidation initially proposed for MAO-B catalysis (Figure 1.14, B; Miller and Edmondson, 1999) that does not require an active site base residue to facilitate proton abstraction from the amine α-C. However, data are also consistent with Silverman's modified aminyl radical cation mechanism (Lu *et al.*, 2002). Both of these mechanisms consider the flavin itself as the functional active site base with the N5 atom of the flavin isoalloxazine moiety able to abstract the substrate α-proton. To therefore delineate which mechanism is applicable to the catalytic activity of amine oxidation by PRODH, detailed EPR studies must be sought in an effort to detect a potential radical species. This method of investigation has been successful in the detection of a stable tyrosyl radical species in partially reduced MAO-A (Rigby *et al.*, 2005), the first direct evidence for a radical-based mechanism for MAO-A catalysis.

6.3   FUTURE WORK

The midpoint potential for the two-electron reduction of PRODH-bound flavin at a solution temperature of 20 °C is -157 mV. Compared to the reduction potential of the L-proline/P5C couple at the same temperature of -123 mV, this calculates to a $\Delta E^{\circ'}$ of -34 mV, correlating to a thermodynamically unfavourable Gibbs free energy change of +6.56 $kJ \cdot mol^{-1}$. It is not unrealistic that at elevated temperatures, binding of substrate may perturb the midpoint potential of the FAD cofactor (Sablin and Ramsay, 2001), therefore resulting in a thermodynamically favourable potential difference to drive the substrate amine oxidation event. To assess if substrate binding governs the redox poise of the flavin cofactor, future potentiometry measurements must be performed in the presence of the three identified amine substrates: L-proline, L-pipecolic acid and sarcosine.

To further probe the catalytic mechanism of PRODH, X-ray crystallography of PRODH in substrate-bound form will provide valuable structural data concerning the orientation

of substrate in the active site. In addition to these structural investigations, future pH-dependence studies employing stopped flow apparatus with the capacity to withstand high reaction temperatures $\geq$ 60 °C must be performed with wild-type PRODH using both protiated and deuterated substrate. These rapid reaction kinetic investigations will aid in the detection and unequivocal assignment of kinetically influential ionisations in the catalytic reaction of PRODH. Such investigations will also demonstrate if a change in rate limiting step is attributable to the pK_a values calculated from the steady-state experiments documented in chapters four and five.

As stated previously, the first direct evidence for the presence of a stable tyrosyl radical species in partially reduced MAO-A has recently been documented in the literature (Rigby _et al._, 2005). These findings were based on EPR spectroscopy experiments and provided the key missing piece of evidence in support of a single electron transfer mechanism for amine oxidation by MAO-A. Advancement of the aminoalkyl (cation) radical mechanism (Silverman _et al._, 1980) and similar to that proposed previously (Edmondson, 1996) with employment of a tyrosyl radical species has distinguished that the mechanism of amine oxidation by MAO-A is indeed radical-based. Analogous studies utilising EPR spectroscopy with PRODH of _P. furiosus_ must be undertaken in future mechanism investigations in order to resolve whether a polar nucleophilic or radical-based mechanism is prevalent in the hyperthermophilic flavoprotein.

Recently, a second L-proline dehydrogenase has been cloned from the genome of _P. furiosus_ and overexpressed in _E. coli_ strain Rosetta2(DE3)pLysS. This new enzyme, in stark contrast to PRODH characterised in this current project is a heterotetramer ($\alpha\beta\gamma\delta$) with a hydrodynamic molecular weight of ~140 KDa based on light-scattering experiments. An immediate priority for future experimental studies is the functional delineation of the two structurally distinct L-proline dehydrogenases of _P. furiosus_. These future studies are essential in order to decipher the physiological significance of these two isozymic forms. Initial steady-state kinetic experiments with the recently identified heterotetrameric enzyme identified a micromolar K_m for L-proline as substrate. This is in comparison to the millimolar K_m that PRODH possesses for L-proline,

therefore indicating that the enzymes microenvironment *in vivo* with regard to the local cellular levels of L-proline may be functionally significant in regulating the activity levels of these two enzymes.

APPENDIX

APPENDIX

A1.1. SDS-PAGE GEL RUNNING REAGENTS

A1.1.1. 10x RUNNING BUFFER

Tris (30 g, 0.25 M) glycine (144 g, 1.19 M), and SDS (10 g, 1 % w/v) dissolved in 900 ml deionised water and adjusted to pH 8.3 and brought to 1000 ml final volume with deionised water. The solution was stored at ambient temperature.

A1.1.2. 2x SAMPLE LOADING BUFFER

Tris (1.51 g, 0.125 M), SDS (4%), dithiothreitol (2.31 g, 150 mM), glycerol (20%) and Bromophenol Blue (0.01%) was dissolved in deionised water to 90 ml, adjusted to pH 6.8 and brought to a final volume of 100ml with deionised water. The solution was stored at ambient temperature.

A1.1.3. COOMASSIE BLUE R-250 STAIN

5.0 g of Coomassie Brilliant Blue was dissolved into a solution consisting of 500 ml isopropanol (25 % v/v), 200 ml glacial acetic acid (10 % v/v) that was brought up to a final volume of 2 litres with deionised water. The solution was stored at ambient temperature.

A1.1.4. DE-STAIN

Methanol (600 ml, 30 % v/v), glacial acetic acid (200 ml, 10 % v/v) and deionised water (1200 ml) were mixed together giving a final solution volume of 2 litres. The solution was stored at ambient temperature.

A1.2. AGAROSE GEL RUNNING REAGENTS

A1.2.1. 50x TAE BUFFER

Tris base (242 g) was dissolved into 700 ml deionised water and the solution added to 57.1 ml glacial acetic acid and a 100 ml solution of 0.5 M EDTA (pH 8.0). The solution was adjusted to pH 7.2 and brought up to 1 litre final volume with deionised water. The solution was stored at ambient temperature.

A1.2.2. 6x DNA LOADING BUFFER

The loading buffer was made from 10 mM Tris-HCl,pH 7.5 containing 50 mM EDTA, glycerol 10 % v/v and 25 % Bromophenol Blue.

A1.3. CALCULATION OF 'TRUE' K_m FOR AVAILABLE DEPROTONATED SUBSTRATE AT pH 7.5

Using the Henderson-Hasselbalch Equation:

$$pH = pK_a + \log\frac{H^-}{HA} \qquad\longrightarrow\qquad 7.5 = 10.6 + \log\frac{H^-}{HA}$$

$$\log\frac{H^-}{HA} = pH - pK_a \qquad\longrightarrow\qquad \log\frac{H^-}{HA} = -3.1$$

$$\frac{H^-}{HA} = 7.9^{-4} \qquad\longrightarrow\qquad HA = \frac{1}{7.9^{-4}} = 1258.9$$

$$\frac{H^-}{HA} = \frac{1}{1258.9} = \frac{0.079\%}{99.92\%}$$

Apparent K_m for L-proline at 80 °C/pH 7.5 = 30.8 ± 1.1 mM.

$$\frac{0.079\%}{99.92\%} \times 30.8mM = 24.5\mu M$$

A1.4. STABILITY OF FERRICENIUM HEXAFLUOROPHOSPHATE AT 80 °C
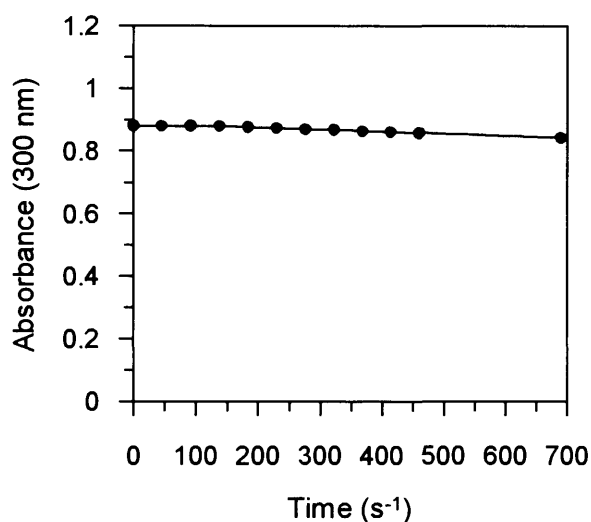
Figure A1. 1. Graph showing the absorbance of artificial electron acceptor ferricenium hexafluorophosphate at a wavelength of 300 nm over a time period of 700 seconds and at a solution temperature of 80 °C. These data indicated that the ferricenium ion (200 µM) is stable at an assay temperature of 80 °C over the relatively short time periods employed for collection of initial velocity readings when assaying PRODH activity (1-5 min^{-1}). Therefore, ferricenium was an appropriate electron acceptor for use in activity assays at the high temperatures required to determine PRODH kinetic behaviour close of the physiological conditions of the source organism *P. furiosus* DSM 3638 (optimal growth temperature = 100 °C).

A1.5.   ALTERNATIVE MECHANISM FOR THE REACTION OF P5C WITH *O*-AMINOBENZALDEHYDE
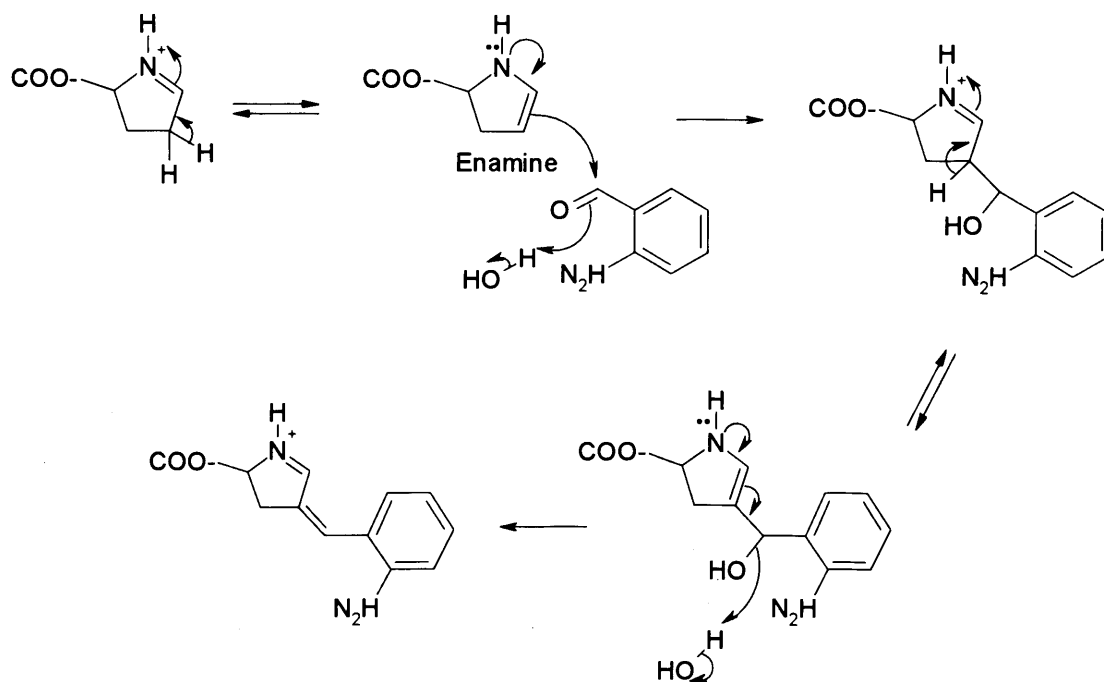
Figure A1. 2.   Reaction scheme describing the reaction of P5C with *o*-aminobenzaldehyde via the enamine. The enamine reacts with *o*-aminobenzaldehyde by nucleophilic attack at the carbonyl function resulting in the formation of a P5C-*o*-aminobenzaldehyde adduct detected by electrospray mass spectroscopy with a single m/ peak of 217 ([M+H]⁺).

A1.6.   CRYSTALLOGENESIS SCREENS

0.3 M Na Acetate, 25 % PEG 2K MME	0.2 M Li$_2$SO$_4$, 25 % PEG 2K MME	0.2 M MgCl$_2$, 25 % PEG 2K MME	0.2 M KBr, 25 % PEG 2K MME	0.2 M KSCN, 25 % PEG 2K MME	0.8 M Na Formate, 25 % PEG 2K MME
0.3 M Na Acetate, 15 % PEG 4K	0.2 M Li$_2$SO$_4$, 15 % PEG 4K	0.2 M MgCl$_2$, 15 % PEG 4K	0.2 M KBr, 15 % PEG 4K	0.2 M KSCN, 15 % PEG 4K	0.8 M Na Formate, 15 % PEG 4K
0.3 M Na Acetate, 10 % PEG 8K + 10 % PEG 1K	0.2 M Li$_2$SO$_4$, 10 % PEG 8K + 10 % PEG 1K	0.2 M MgCl$_2$, 10 % PEG 8K + 10 % PEG 1K	0.2 M KBr, 10 % PEG 8K + 10 % PEG 1K	0.2 M KSCN, 10 % PEG 8K + 10 % PEG 1K	0.8 M Na Formate, 10 % PEG 8K + 10 % PEG 1K
0.3 M Na Acetate, 8 % PEG 20 K + 8 % PEG 550 MME	0.2 M Li$_2$SO$_4$, 8 % PEG 20 K + 8 % PEG 550 MME	0.2 M MgCl$_2$, 8 % PEG 20 K + 8 % PEG 550 MME	0.2 M KBr, 8 % PEG 20 K + 8 % PEG 550 MME	0.2 M KSCN, 8 % PEG 20 K + 8 % PEG 550 MME	0.8 M Na Formate, 8 % PEG 20 K + 8 % PEG 550 MME

Table A1. 1. Table showing the Molecular Dimensions Clear Strategy Screen MD 1-14 Screen I. Protein and the relevant precipitant solution were mixed 1:1 in the crystallisation drop, sealed and incubated at 19 °C with minimal mechanical perturbations. The cell highlighted in yellow indicates the preliminary 'hit' condition in which the initial crystals of purified PRODH expressed from construct pPRODH1 were grown at solution pH 7.5. The cell highlighted in blue indicates the condition in which purified PRODH expressed from construct pPRODH2 were grown at solution pH 7.5.

0.2 M Na Formate, 18 % PEG 2000 MME	0.2 M Na Formate, 18 % PEG 5000 MME	0.2 M Na Formate, 18 % PEG 3000	0.2 M Na Formate, 16 % PEG 6000	0.2 M Na Formate, 14 % PEG 8000	0.2 M Na Formate, 14 % PEG 10,000
0.4 M Na Formate, 20 % PEG 2000 MME	0.4 M Na Formate, 20 % PEG 5000 MME	0.4 M Na Formate, 20 % PEG 3000	0.4 M Na Formate, 18 % PEG 6000	0.4 M Na Formate, 16 % PEG 8000	0.4 M Na Formate, 16 % PEG 10,000
0.6 M Na Formate, 22 % PEG 2000 MME	0.6 M Na Formate, 22 % PEG 5000 MME	0.6 M Na Formate, 22 % PEG 3000	0.6 M Na Formate, 20 % PEG 6000	0.6 M Na Formate, 18 % PEG 8000	0.6 M Na Formate, 18 % PEG 10,000
0.8 M Na Formate, 24 % PEG 2000 MME	0.8 M Na Formate, 24 % PEG 5000 MME	0.8 M Na Formate, 24 % PEG 3000	0.8 M Na Formate, 22 % PEG 6000	0.8 M Na Formate, 20 % PEG 8000	0.8 M Na Formate, 20 % PEG 10,000

Table A1. 2. The secondary crystallisation screen developed to optimise the initial 'hit' conditions where the first crystals of PRODH were observed. The concentration of sodium formate was varied between 0.2-0.8 M and the PEG concentration was varied between 14-24 % (v/v) in conjunction with the nature of the PEG utilised (PEG 2000 MME-PEG 10,000). The cell highlighted in yellow indicates the optimised crystals obtained from this screen at solution pH 8.5.

0.51 M Na Formate	0.51 M NaBr	0.51 M NaCl	0.51 M NaSCN	0.51 M Na Succinate	0.255 M Na$_2$SO$_4$
0.17 M Na$_3$ Citrate	0.51 M LiCl	0.51 M LiSO$_4$	0.51 M KCl	0.51 M MgCl	0.51 M MgSO$_4$
0.51 M MnCl$_2$	0.51 M CH$_2$O$_2$·NH$_3$	0.255 M (NH$_4$)$_2$SO$_4$	0.51 M NH$_4$Cl	0.51 M Ammonium Acetate	0.51 M NH$_4$H$_2$PO$_4$
0.51 M NH$_4$HCO$_3$	0.51 M NH$_4$HPO$_4$	0.51 M Mg Acetate	0.51 M CaCl$_2$	0.51 M Maleic Acid	0.51 M Imidazole

Table A1. 3. Salt screen developed for crytallogenesis trials with PRODH. The trial screened various types of salt present in the mother liquor. PEG 3000 at a concentration of 22 % (v/v) was present in all the precipitant solutions. The screen was performed at solution pH 8.5 buffered by 100 mM Tris-HCl; 19 °C.

0.35 M (NH$_4$)$_2$SO$_4$, 16 % PEG 3000	0.3 M (NH$_4$)$_2$SO$_4$, 16 % PEG 3000	0.25 M (NH$_4$)$_2$SO$_4$, 16 % PEG 3000	0.2 M (NH$_4$)$_2$SO$_4$, 16 % PEG 3000	0.15 M (NH$_4$)$_2$SO$_4$, 16 % PEG 3000	0.1 M (NH$_4$)$_2$SO$_4$, 16 % PEG 3000
0.35 M (NH$_4$)$_2$SO$_4$, 18 % PEG 3000	0.3 M (NH$_4$)$_2$SO$_4$, 18 % PEG 3000	0.25 M (NH$_4$)$_2$SO$_4$, 18 % PEG 3000	0.2 M (NH$_4$)$_2$SO$_4$, 18 % PEG 3000	0.15 M (NH$_4$)$_2$SO$_4$, 18 % PEG 3000	0.1 M (NH$_4$)$_2$SO$_4$, 18 % PEG 3000
0.35 M (NH$_4$)$_2$SO$_4$, 20 % PEG 3000	0.3 M (NH$_4$)$_2$SO$_4$, 20 % PEG 3000	0.25 M (NH$_4$)$_2$SO$_4$, 20 % PEG 3000	0.2 M (NH$_4$)$_2$SO$_4$, 20 % PEG 3000	0.15 M (NH$_4$)$_2$SO$_4$, 20 % PEG 3000	0.1 M (NH$_4$)$_2$SO$_4$, 20 % PEG 3000
0.35 M (NH$_4$)$_2$SO$_4$, 22 % PEG 3000	0.3 M (NH$_4$)$_2$SO$_4$, 22 % PEG 3000	0.25 M (NH$_4$)$_2$SO$_4$, 22 % PEG 3000	0.2 M (NH$_4$)$_2$SO$_4$, 22 % PEG 3000	0.15 M (NH$_4$)$_2$SO$_4$, 22 % PEG 3000	0.1 M (NH$_4$)$_2$SO$_4$, 22 % PEG 3000

Table A1. 4. Ammonium sulphate screen developed for crystallogenesis trials with PRODH. Ammonium sulphate conctration in the mother liquor was varied between 0.1-0.35 M and the concentration of PEG 3000 was also varied between 16-22 % (v/v). The screen was performed at solution pH 8.5 buffered by 100 mM Tris-HCl; 19 °C.

1.5 M (NH₄)SO₄	0.8 M Li₂SO₄	2 M Na Formate	0.5 M KH₂PO₄	25 % PEG 2K MME, 0.2 M Ca Acetate	15 % PEG 4K, 0.2 M Ca Acetate
2.7 M (NH₄)SO₄	1.8 M Li₂SO₄	4 M Na Formate	1.0 M KH₂PO₄	10 % PEG 8K + 10 % PEG 1K, 0.2 M Ca Acetate	8 % PEG 20K + 8 % PEG 550 MME, 0.2 M Ca Acetate
40 % v/v MPD	40 % v/v Butane-diol	20 % PEG 4K, 5 mM CdCl₂	20 % PEG 550 MME, 0.15 M KSCN	20 % PEG 600, 0.15 M KSCN	20 % PEG 1.5K, 0.15 M KSCN
35 % v/v Isopropanol	30 % v/v Jeffamine 600M	20 % PEG 4K, 5 mM NiCl₂	18 % PEG 3350, 0.15 M KSCN	18 % PEG 5K MME, 0.15 M KSCN	15 % PEG 6K, 0.15 M KSCN

Table A1. 5. Table showing the Molecular Dimensions Clear Strategy Screen MD 1-15 Screen II. Protein and the relevant precipitant solution were mixed 1:1 in the crystallisation drop, sealed and incubated at 19 °C with minimal mechanical perturbations.

REFERENCES

Abell, L. M. and Schloss, J. V. (1991) Oxygenase side reactions of acetolactate synthase and other carbanion-forming enzymes. *Biochemistry* **30**, 7883-7887.

Abrahamson, J. L., Baker, L. G., Stephenson, J. T. and Wood, J. M. (1983) Proline dehydrogenase from *Escherichia coli* K12. Properties of the membrane-associated enzyme. *European Journal of Biochemistry* **134**, 77-82.

Adams, M. W. W., Holden, J. F., Menon, A. L., Schut, G. J., Grunden, A. M., Hou, C., Hutchins, A. M., Jenney, F. E. Jnr., Kim, C., Ma, K., Pan, G., Roy, R., Sapra, R., Story, S. V. and Verhagen, M. F. (2001) Key role for sulfur in peptide metabolism and in regulation of three hydrogenases in the hyperthermophilic archaeon *Pyrococcus furiosus*. *Journal of Bacteriology* **183**, 716-724.

Adams, M. W. W., Dailey, H. A., DeLucas, L. J., Lou, M., Prestegard, J. H., Rose, J. P. and Wang, B. C. (2003) The Southeast Collaboratory for Structural Genomics: a high-throughput gene to structure factory. *Accounts of Chemical Research* **36**, 191-198.

Adams, M. W. W. (1992) Novel iron sulfur clusters in metalloenzymes and redox proteins from extremely thermophilic bacteria. *Advances in Inorganic Chemistry* **38**, 341-396.

Adams, M. W. W. (1993) Enzymes and proteins from organisms that grow near and above 100 degrees C. *Annual Review of Microbiology* **47**, 627-658.

Adhin, M. W. and van Duin, J. (1989) Translational regulation of the lysis gene in RNA bacteriophage fr requires a UUG initiation codon. *Molecular & General Genetics* **218**, 137-142.

Adhin, M. W. and van Duin, J. (1990) Scanning model for translational reinitiation in eubacteria. *Journal of Molecular Biology* **213(4)**, 811-818.

Aguilar, C. F., Sanderson, I., Moracci, M., Ciaramella, M., Nucci, R., Rossi, M. and Pearl, L. H. (1997) Crystal structure of the beta-glycosidase from the hyperthermophilic archeon *Sulfolobus solfataricus*: resilience as a key factor in thermostability. *Journal of Molecular Biology* **271**, 789-802.

al-Habori, M. (1995) Microcompartmentation, metabolic channelling and carbohydrate metabolism. *The International Journal of Biochemistry and Cell Biology* **27**, 123-132.

Aloy, P. and Russell, R. B. (2004) Ten thousand interactions for the molecular biologist. *Nature Biotechnology* **22**, 1317-1321.

Aono, S., Bryant, F. O. and Adams, M. W. W. (1989) A novel and remarkably thermostable ferredoxin from the hyperthermophilic archaebacterium *Pyrococcus furiosus*. *Journal of Bacteriology* 171, 3433-3439.

Ashton, N. T., Brown, R. D., Jacobson, F. S. and Walsh, C. T. (1979) Synthesis of 7,8-didemethyl-8-hydroxy-5-deazariboflavin and confirmation of its identity with the deazaisoalloxazine chromophore of *Methanobacterium* redox coenzyme F420. *Journal of the American Chemical Society* 101, 4419-4420.

Auerbach, G., Huber, R., Grattinger, M., Zaiss, K., Schurig, H., Jaenicke, R. and Jacob, U. (1997) Closed structure of phosphoglycerate kinase from *Thermotoga maritima* reveals the catalytic mechanism and determinants of thermal stability. *Structure* 5, 1475-1483.

Baban, B. A., Vinod, M. P., Tanner, J. J. and Becker, D. F. (2004) Probing a hydrogen bond pair and the FAD redox properties in the proline dehydrogenase domain of *Escherichia coli* PutA. *Biochimica et Biophysica Acta* 1701, 49-59.

Backman, K., Ptashne, M. and Gilbert, W. (1976) Construction of plasmids carrying the cI gene of bacteriophage lambda. *Proceedings of the National Academy of Science of the United States of America* 73, 4174-4178.

Backmann, J. and Schäfer, G. (2001) Thermodynamic analysis of hyperthermostable oligomeric proteins. *Methods in Enzymology* 334, 328-342.

Baldwin, T. O. and Ziegler, M. M. (1992) Chapter 16: The biochemistry and molecular biology of bacterial bioluminescence. In *Chemistry and Biochemistry of Flavoenzymes* (volume III) (ed. Müller, F.), pp. 467-530, CRC Press, Inc., Boca Raton, Florida, USA.

Barman, B. G. and Tollin, G. (1972) Flavine-protein interactions in flavoenzymes. Thermodynamics and kinetics of reduction of *Azotobacter* flavodoxin. *Biochemistry* 11, 4755-4759.

Barquera, B., Hase, C. C. and Gennis, R. B. (2001) Expression and mutagenesis of the NqrC subunit of the NQR respiratory Na(+) pump from Vibrio cholerae with covalently attached FMN. *FEBS Letters* 492, 45-49.

Basran, J., Sutcliffe, M. J. and Scrutton, N. S. (1999) Enzymatic H-transfer requires vibration-driven extreme tunneling. *Biochemistry* 38, 3218-3222.

Basran, J., Sutcliffe, M. J. and Scrutton, N. S. (2001a) Deuterium isotope effects during carbon-hydrogen bond cleavage by trimethylamine dehydrogenase. Implications for mechanism and vibrationally assisted hydrogen tunneling in wild-type and mutant enzymes. *The Journal of Biological Chemistry* 276, 24581-24587.

283

Basran, J., Sutcliffe, M. J. and Scrutton, N. S. (2001b) Optimizing the Michaelis complex of trimethylamine dehydrogenase: identification of interactions that perturb the ionization of substrate and facilitate catalysis with trimethylamine base. *The Journal of Biological Chemistry* , 42887-42892.

Basran, J., Bhanji, N., Basran, A., Nietlispach, D., Mistry, S., Meskys, R. and Scrutton, N. S. (2002) Mechanistic aspects of the covalent flavoprotein dimethylglycine oxidase of *Arthrobacter globiformis* studied by stopped-flow spectrophotometry. *Biochemistry* **41**, 4733-4743.

Basran, J., Fullerton, S., Leys, D. and Scrutton, N. S. (2006) On the mechanism of FAD reduction and the role of the active site residues His-225 and Tyr-259 in *Arthrobacter globiformis* dimethylglycine oxidase: analysis of mutant structure and catalytic function. *Biochemistry* In Press.

Bateman, A., Coin, L., Durbin, R., Finn, R. D., Hollich, V., Griffiths-Jones, S., Khanna, A., Marshall, M., Moxon, S., Sonnhammer, E. L., Studholme, D. J., Yeats, C. and Eddy, S. R. (2004) The Pfam protein families database. *Nucleic Acids Research* **32**, D138-141.

Becker, D. F. and Thomas, E. A. (2001) Redox properties of the PutA protein from *Escherichia coli* and the influence of the flavin redox state on PutA-DNA interactions. *Biochemistry* **40**, 4714-4721.

Becker, P., Abu-Reesh, I., Markossian, S., Antranikian, G. and Markl, H. (1997) Determination of the kinetic parameters during continuous cultivation of the lipase producing thermophile *Bacillus* sp IHI-91 on olive oil. *Applied Microbiology and Biotechnology* **48**, 184-190.

Bennett, M. J., Schlunegger, M. P. and Eisenberg, D. (1995) 3D domain swapping: a mechanism for oligomer assembly. *Protein Science* **4**, 2455–2468.

Berezovsky, I. N. and Shakhnovich, E. I. (2005) Physics and evolution of thermophilic adaptation. *Proceedings of the National Academy of Science of the United States of America* **102**, 12742-12747.

Bergfors, T. M. (1999) *Protein Crystallization* International University Line, La Jolla, CA.

Bernal, J. D. and Crowfoot, D. (1934) X-ray photographs of crystalline pepsin. *Nature* **794**, 133-134

Beynon, R. J. and Easterby, J. S. (1996) Buffer Solutions: The Basics. IRL Press at Oxford University Press.

Binda, C., Newton-Vinson, P., Hubalek, F., Edmondson, D. E. and Mattevi, A. (2002) Structure of human monoamine oxidase B, a drug target for the treatment of neurological disorders. *Nature Structural Biology* **9**, 22-26.

Binda, C., Hubalek, F., Li, M., Edmondson, D. E. and Mattevi, A (2004) Crystal structure of human monoamine oxidase B, a drug target enzyme monotopically inserted into the mitochondrial outer membrane. *FEBS Letters* **564**, 225-228.

Blamey, J. M. and Adams, M. W. W. (1993) Purification and characterization of pyruvate ferredoxin oxidoreductase from the hyperthermophilic archaeon *Pyrococcus furiosus*. *Biochimica et Biophysica Acta* **1161**, 19-27.

Böhm, G. and Jaenicke, R. (1994) Relevance of sequence statistics for the properties of extremophilic proteins. *International Journal of Peptide and Protein Research* **43**, 97-106.

Böttcher, B., Scheide, D., Hesterberg, M., Nagel-Steger, L. and Friedrich, T. (2002) A Novel, Enzymatically Active Conformation of the *Escherichia coli* NADH:Ubiquinone Oxidoreductase (Complex I). *The Journal of Biological Chemistry* **277**, 17970-17977.

Bradford, M. M. (1976) A rapid and sensitive method for the quantitation of microgram quantities of protein utilizing the principle of protein-dye binding. *Analytical Biochemistry* **72**, 248-254.

Brandes, L. J., Queen, G. M. and LaBella, F. S. (1998) Potent interaction of histamine and polyamines at microsomal cytochrome P450, nuclei, and chromatin from rat hepatocytes. *Journal of Cellular Biochemistry* **69**, 233-243.

Brandsch, R. and Bichler, V. (1991) Autoflavinylation of apo6-hydroxy-D-nicotine oxidase. *The Journal of Biological Chemistry* **266**, 19056-19062.

Bravo, J. and Aloy, P. (2006) Target selection for complex structural genomics. *Current Opinion in Structural Biology* **16**, 385-92.

Bremer, E. and Kramer, R. (2000) Coping with osmotic challenges: osmoregulation through accumulation and release of compatible solutes in bacteria. In *Bacterial stress response* (ed. Storz, G. and Hengge-Areonis, R.), pp. 79-97. ASM Press, Washington, D.C.

Brereton, P. S., Verhagen, M. F., Zhou, Z. H. and Adams, M. W. W. (1998) Effect of iron-sulfur cluster environment in modulating the thermodynamic properties and biological function of ferredoxin from *Pyrococcus furiosus*. *Biochemistry* **37**, 7351-7362.

Briggs, W. R. and Christie, J. M. (2002) Phototropins 1 and 2: versatile plant blue-light receptors. *Trends in Plant Science* **7**, 204-10.

Briggs, W. R., Christie, J. M., Kineb, E. and Salomon, M. (1999) Phototropin (nph1), a photoreceptor for phototropism, is an FMN-binding chromoprotein. In *Flavins and Flavoproteins* (ed. Ghisla, S., Kroneck, P., Macheroux, P. and Sund, H.), pp. 299-308, Rudolf Weber Agency for Scientific Publications, Berlin.

Brinkmann, U., Mattes, R. E. and Buckel. P. (1989) High-level expression of recombinant genes in *Escherichia coli* is dependent on the availability of the dnaY gene product *Gene* **85**, 109-114.

Brown, L. E. and Hamilton, G. A. (1970) Some model reactions and a general mechanism for flavoenzyme-catalyzed dehydrogenations. *Journal of the American Chemical Society* **92**, 7225-7227.

Brown, E. D. and Wood, J. M. (1992) Redesigned purification yields a fully functional PutA protein dimer from *Escherichia coli*. *The Journal of Biological Chemistry* **267**, 13086-13092.

Brown, E. D. and Wood, J. M. (1993) Conformational change and membrane association of the PutA protein are coincident with reduction of its FAD cofactor by proline. *The Journal of Biological Chemistry* **268**, 8972-8979.

Brown, A. D. (1990) Microbial Water Stress Physiology, Principles and Perspectives. New York: John Wiley & Sons.

Burley, S. K. and Petsko, G. A. (1985) Aromatic-aromatic interaction: a mechanism of protein structure stabilization. *Science* **229**, 23-28.

Byrant, F. O. and Adams, M. W. W. (1989) Characterization of hydrogenase from the hyperthermophilic archaebacterium, *Pyrococcus furiosus*. *The Journal of Biological Chemistry* **264**, 5070-5079.

Byron, C. M., Stankovich, M. T., Hussain, M. and Davidson, V. L. (1989) Unusual redox properties of electron-transfer flavoprotein from *Methylophilus methylotrophus*. *Biochemistry* **28**, 8582-8587.

Calderone, T. L., Stevens, R. D. and Oas, T. G. (1996) High-level Misincorporation of Lysine for Arginine at AGA Codons in a Fusion Protein Expressed in *Escherichia coli*. *Journal of Molecular Biology* **262**, 407-412.

Chakravarti, A. (2002) A compelling genetic hypothesis for a complex disease: PRODH2/DGCR6 variation leads to schizophrenia susceptibility. *Proceedings of the National Academy of Science of the United States of America* **99**, 4755-4756.

Chan, T. W. and Bruice, T. C. (1978) Importance of C4a- and N5-covalent adducts in the flavin oxidation of carbanions. *Biochemistry* **17**, 4784-4793.

Chen, G. F. and Inouye, M. (1990) Suppression of the negative effect of minor arginine codons on gene expression; preferential usage of minor codons within the first 25 codons of the *Escherichia coli* genes. *Nucleic Acids Research* **18**, 1465-1473.

Chen, C. C., Tsuchiya, T., Yamane, Y., Wood, J. M. and Wilson, T. H. Na+ (Li+)-proline cotransport in Escherichia coli. *The Journal of Membrane Biology* **84**, 157–164.

Childs, A. C., Mehta, D. J. and Gerner, E. W. (2003) Polyamine-dependent gene expression. *Cellular and Molecular Life Sciences* **60**, 1394-1406.

Chlumsky, L. J., Zhang, L. and Jorns, M. S. (1995) Sequence analysis of sarcosine oxidase and nearby genes reveals homologies with key enzymes of folate one-carbon metabolism. *The Journal Biological Chemistry* **270**, 18252-18259.

Choi, I.-G., W.-G. Bang, S.-H. Kim, and Y. G. Yu. (1999). Extremely thermostable serine-type protease from *Aquifex pyrophilus*. Molecular cloning, expression, and characterization. *The Journal Biological Chemistry* **274**, 881-888.

Christen, R. P., Nomikos, S. I. and Smith, E. T. (1996) Probing protein electrostatic interactions through temperature/reduction potential profiles. *Journal of Biological Inorganic Chemistry* **1**, 515–522.

Chung, S-T., Tan, R. T. Y. and Suzuki, I. (1971) Glyoxylate carboligase of *Pseudomonas oxalaticus*. A possible structural role for flavine-adenine dinucleotide. *Biochemistry* **10**, 1205-1209.

Cleveland, W. S. (1993) *Visualising Data*. Hobart press, New Jersey.

Cohen, S. S. (1998) *A Guide of Polyamines*, Oxford University Press, New York.

Colibus, L., Li, M., Binda, C., Lustig, A., Edmondson, D. E. and Mattevi, A. (2005) Three-dimensional structure of human monoamine oxidase A (MAO A): relation to the structures of rat MAO A and human MAO B. *Proceedings of the National Academy of Science of the United States of America* **102**, 12684-9.

Cornish-Bowden, A. (1979) *Fundamentals of Enzyme Kinetics*, pp. 82-85, Butterworth, London.

Crowther, R. A. (1972) *The Molecular Replacement Method*, (ed. Rossmann, M. G.) pp. 173-178. New York: Gordon & Breach.

Csonka, L. N. (1989) Physiological and genetic responses of bacteria to osmotic stress. *Microbiological Reviews* **53**, 121-147.
Daff, S. N., Chapman, S. K., Turner, K. L., Holt, R. A., Govindaraj, S., Poulos, T. L. and Munro, A. W. (1997) Redox control of the catalytic cycle of flavocytochrome P-450 BM3. *Biochemistry* **36**, 13816-13823.

Dagley, S. (1987) Lessons from biodegradation. *Annual Review of Microbiology* **41**, 1-23.

Dallmann, H. G. and Dunn, S. D. (1994) Translation through an uncDC mRNA secondary structure governs the level of uncC expression in *Escherichia coli*. *Journal of Bacteriology* **176**, 1242-1250.

Daniel, R. M. and Cowan, D. A. (2000) Biomolecular stability and life at high temperatures. *Cellular and Molecular Life Sciences* **57**, 250-264.

Daniel, R. M. and Danson, M. J. (2001) Assaying activity and assessing thermostability of hyperthermophilic enzymes. *Methods in Enzymology* **334**, 283-293.

Daniel, R. M., Danson, M. J. and Eisenthal, R. (2001) The temperature optima of enzymes: a new perspective on an old phenomenon. *Trends in Biochemical Sciences* **26**, 223-225. Erratum in: *Trends in Biochemical Sciences* **26**, 401.

Danson, M. J. and Hough, D. W. (1998) Structure, function and stability of enzymes from the Archaea. *Trends in Microbiology* **6**, 307-314.

Datta, S., Mori, Y., Takagi, K., Kawaguchi, K., Chen, Z-W., Okajima, T., Kuroda, S., Ikeda, T., Kano, K., Tanizawa, K and Mathews. F. S. (2001) Structure of a quinohemoprotein amine dehydrogenase with an uncommon redox cofactor and highly unusual crosslinking. *Proceedings of the National Academy of Science of the United States of America* **98**, 14268-14273.

Daugas, E., Nochy, D., Ravagnan, L., Loeffler, M., Susin, S. A., Zamzami, N. and Kroemer, G. (2000) Apoptosis-inducing factor (AIF): a ubiquitous mitochondrial oxidoreductase involved in apoptosis. *FEBS Letters* **476**, 118-123.

Davidson, V. L. (2000) Methylamine dehydrogenase. Structure and function of electron transfer complexes. *Sub-cellular Biochemistry* **35**, 119-143.

Day, M. W., Hsu, B. T., Joshua-Tor, L., Park, J. B., Zhou, Z. H., Adams, M. W. W . and Rees, D. C. (1992) X-ray crystal structures of the oxidized and reduced forms of the rubredoxin from the marine hyperthermophilic archaebacterium *Pyrococcus furiosus*. *Protein Science* **1**, 1494-1507.

de Bakker, P. I., Hunenberger, P. H. and McCammon, J. A. (1999) Molecular dynamics simulations of the hyperthermophilic protein sac7d from *Sulfolobus acidocaldarius*: contribution of salt bridges to thermostability. *Journal Molecular Biology* **285**, 1811-30. Decker, K. (1992) How and why are some riboflavin coenzymes covalently attached to proteins? *Journal of nutritional science and vitaminology (Tokyo)*, 40-45.

DeLano, W. L. (2002) The PyMOL User's Manual, DeLano Scientific, San Carlos, CA, USA.

Donald, S. P., Sun, X. Y., Hu, C. A., Yu, J., Mei, J. M., Valle, D. and Phang, J. M. (2001) Proline oxidase, encoded by p53-induced gene-6, catalyzes the generation of proline-dependent reactive oxygen species. *Cancer Research* **61**, 1810-1815.

Drenth, J. (1999) Principles of Protein X-ray Crystallography, 2nd Edition, Springer Verlag, New York.

Duine, J. A. (2001) Cofactor diversity in biological oxidations: implications and applications. *Chemical Record (New York)* **1**, 74-83.

Dutton, P. L. (1978) Redox potentiometry: determination of midpoint potentials of oxidation-reduction components of biological electron-transfer systems. *Methods in Enzymology* **54**, 411-435.

Dym, O. and Eisenberg, D. (2001) Sequence-structure analysis of FAD-containing proteins. *Protein Science* **10**, 1712-1728.

Edmondson, D. E. and De Francisco, R. (1992) Structure, synthesis, and physical properties of covalently bound flavins and 6- and 8-hydroxyflavins. In *Chemistry and biochemistry of flavoenzymes* (volume I) (ed. Muller, F.), pp. 73-103, CRC Press, Inc., Boca Raton, Florida, USA.

Edmondson, D. E. and Ghisla, S. (1999) Flavoenzyme structure and function. Approaches using flavin analogues. *Methods in molecular biology* **131**, 157-179.

Edmondson, D. E., Mattevi, A., Binda, C., Li, M. and Hubalek, F. (2004) Structure and mechanism of monoamine oxidase. *Current Medicinal Chemistry* **11**, 1983-1993.

Edmondson, D. E. (1985) Electron-spin-resonance studies on flavoenzymes. *Biochemical Society Transactions* **13**, 593-600.

Edmondson, D. E. (1995) Aminium cation radical mechanism proposed for monoamine oxidase B catalysis: are there alternatives? *Xenobiotica* **25**, 735-753.

Edmondson, D. (1996) In *Flavins and Flavoproteins* (ed. Stevenson, K., Massey, V. and Williams, C. J.) pp. 23-34, University of Calgary Press, Calgary, Alberta, Canada.

Eichler, J. (2001) Biotechnological uses of archaeal extremozymes. *Biotechnology Advances* **19**, 261-278.

Eirich, L. D., Vogels, G. D. and Wolfe, R. S. (1978) Proposed structure for coenzyme F420 from *Methanobacterium*. *Biochemistry* **17**, 4583-4593.

Elcock, A. H. (1998) The stability of salt bridges at high temperatures: implications for hyperthermophilic proteins. *Journal of Molecular Biology* **284(2)**, 489-502.

Ellis, K. J. and Morrison, J. F. (1982) Buffers of constant ionic strength for studying pH-dependent processes. *Methods in Enzymology* **87**, 405-426.

Emsley, P. and Cowtan, K. (2004) Coot: model-building tools for molecular graphics. *Acta Crystallographica Section D Biological Crystallography* **60**, 2126-2132.

Erdem, S. S., Karahan, O., Yildiz, I. and Yelekci, K. (2006) A computational study on the amine-oxidation mechanism of monoamine oxidase: insight into the polar nucleophilic mechanism. *Organic & Biomolecular Chemistry* **4**, 646-658.

Esposito, C. and Caputo, I. (2005) Mammalian transglutaminases. Identification of substrates as a key to physiological function and physiopathological relevance. *The FEBS Journal* **272**, 615-631.

Ettema, T., van der Oost, J. and Huynen, M. (2001) Modularity in the gain and loss of genes: applications for function prediction. *Trends in Genetics* **17**, 485-487.

Facchiano, A. M., Colonna, G. and Ragone, R. (1998) Helix stabilizing factors and stabilization of thermophilic proteins: an X-ray based study. *Protein Engineering* **11**, 753-760.

Farrant, R. D., Walker, V., Mills, G. A., Mellor, J. M. and Langley, G. J. (2001) Pyridoxal phosphate de-activation by pyrroline-5-carboxylic acid. Increased risk of vitamin B6 deficiency and seizures in hyperprolinemia type II. *The Journal of Biological Chemistry* **276**, 15107-15116.

Felsenstein, J. (1993) PHYLIP (Phylogeny Inference Package) version 3.5c. Distributed by the author. Department of Genetics, University of Washington, Seattle.

Ferry, J. G. and Wolf, R. S. (1977) Nutritional and biochemical characterization of Methanospirillum hungatii. *Applied Environmental Microbiology* **34**, 371-376.

Fiala, G. and Stetter, K. O. (1986) *Pyrococcus furiosus* sp. nov. represents a novel genus of marine heterotrophic archaebacteria growing optimally at 100 °C. *Archives of Microbiology* **145**, 56-61.

Fields, P. A. (2001) Protein function at thermal extremes: balancing stability and flexibility. *Comparative Biochemistry and Physiology, Part A Molecular and Integrative Physiology* **129**, 417-431.

Fischer, E. (1894) Einfluss der configuration auf die wirkung derenzyme. *Berichte der Deutschen Chemischen Gesellschaft* **27**, 2985-2993.

Fraaije, M. W., van den Heuvel, R. H., van Berkel, W. J. and Mattevi, A. (1999) Covalent flavinylation is essential for efficient redox catalysis in vanillyl-alcohol oxidase. *The Journal of Biological Chemistry* **274**, 35514-35520.

Friedman, S. M. (1986) Properties of translational machinery from a sulphur-dependent archaebacterium. *System Applied Microbiology* 7, 325-329.

Frishman, D., Mironov, A., Mewes, H. W. and Gelfand, M. (1998) Combining diverse evidence for gene recognition in completely sequenced bacterial genomes. *Nucleic Acids Research* 26, 2941-2947.

Frishman, D., Mironov, A. and Gelfand, M. (1999) Starts of bacterial genes: estimating the reliability of computer predictions. *Gene* 234, 257-265.

Fuchs, G., Stupperich, E. and Thauer, R. K. (1978) Acetate assimilation and the synthesis of alanine, aspartate and glutamate in *Methanobacterium thermoautotrophicum*. *Archives of Microbiology* 117, 61-66.

Fujiwara, K., Okamura-Ikeda, K. and Motokawa, Y. (1984) Mechanism of the glycine cleavage reaction. Further characterization of the intermediate attached to H-protein and of the reaction catalyzed by T-protein. *The Journal of Biological Chemistry* 259, 10664-10668.

Ghisla, S. and Massey, V. (1989) Mechanisms of flavoprotein-catalyzed reactions. *European Journal of Biochemistry/FEBS* 181, 1-17.

Ghisla, S., Kenney, W. C., Knappe, W. R., McIntire, W. and Singer, T. P. (1980) Chemical synthesis and some properties of 6-substituted flavins. *Biochemistry* 19, 2537-2544.

Goldstein, H. (1959) Classical mechanics. Addison Wesley, London.

Gonzalez, P., Barroso, G. and Labarere, J. (1998) Molecular analysis of the split cox1 gene from the Basidiomycota *Agrocybe aegerita*: relationship of its introns with homologous Ascomycota introns and divergence levels from common ancestral copies. *Gene* 220, 45-53.

Goodenough, P. W. and Jenkins, J. A. (1991) Protein engineering to change thermal stability for food enzymes. *Biochemical Society Transactions* 19, 655-662.

Gorst, C. M., Zhou, Z. H., Ma, K., Teng, Q., Howard, J. B., Adams, M. W. W. and LaMar, G. N. (1995) Participation of the disulfide bridge in the redox cycle of the ferredoxin from the hyperthermophile Pyrococcus furiosus: 1H nuclear magnetic resonance time resolution of the four redox states at ambient temperature. *Biochemistry* 34, 8788-8795.

Graham, S. B., Stephenson, J. T. and Wood, J. M. (1984) Proline dehydrogenase from *Escherichia coli* K12. Reconstitution of a functional membrane association. *The Journal of Biological Chemistry* 259, 2656-2661.

Grissom, C. (1995) Magnetic field effects in biology: a survey of possible mechanisms with emphasis on radical-pair recombination. *Chemical Reviews* **95**, 3-24.

Grogan, D. W. (1998) Hyperthermophiles and the problem of DNA instability. *Molecular Microbiology* **28**, 1043-1049.

Guenther, B. D., Sheppard, C. A., Tran, P., Rozen, R., Matthews, R. G. and Ludwig, M. L. (1999) The structure and properties of methylenetetrahydrofolate reductase from *Escherichia coli* suggest how folate ameliorates human hyperhomocysteinemia. *Nature Structural Biology* **6**, 359-365.

Hagedoorn, P. L., Driessen, M. C., van den Bosch, M., Landa, I. and Hagen, W. R. (1998) Hyperthermophilic redox chemistry: a re-evaluation. *FEBS Letters* **440**, 311-314.

Hannenhalli, S. S., Hayes, W. S., Hatzigeorgiou, A. G. and Fickett, J. W. (1999) Bacterial start site prediction. *Nucleic Acids Research* **27**, 3577-3582.

Harden, A. (1932) *Alcoholic fermentation* (4th Edition). Longmans Green, London.

Harris, R. J., Meskys, R., Sutcliffe, M. J. and Scrutton, N. S. (2000) Kinetic studies of the mechanism of carbon-hydrogen bond breakage by the heterotetrameric sarcosine oxidase of *Arthrobacter* sp. 1-IN. *Biochemistry* **39**, 1189-1198.

Heider, J., Mai, X. and Adams, M. W. W. (1996) Characterization of 2-ketoisovalerate ferredoxin oxidoreductase, a new and reversible coenzyme A-dependent enzyme involved in peptide fermentation by hyperthermophilic archaea. *Journal of Bacteriology* **178**, 780-787.

Hendrickson, W. A., Horton, J. R. and LeMaster, D. M. (1990) Selenomethionyl proteins produced for analysis by multiwavelength anomalous diffraction (MAD): a vehicle for direct determination of three-dimensional structure. *The EMBO Journal* **9**, 1665-1672.

Hill, C. L., Steenkamp, D. J., Holm, R. H. and Singer, T. P. (1977) Identification of the iron-sulfur center in trimethylamine dehydrogenase. *Proceedings of the National Academy of Science of the United States of America* **74**, 547-551.

Hille, R. (2002) Molybdenum and tungsten in biology. *Trends in Biochemical Sciences* **27**, 360-367.

Hoegy, S. and Mariano, P. (1997) Mechanistic and synthetic aspects of amine oxidations promoted by 3-methyl-5-ethyllumiflavinium perchlorate. *Tetrahedron* **53**, 5027-5046.

Hol, W. G., van Duijnen, P. T. and Berendsen, H. J. (1978) The alpha-helix dipole and the properties of proteins. *Nature* **273**, 443-446.

Holm, L. and Sander, C. (1995) Dali: a network tool for protein structure comparison. *Trends in Biochemical Sciences* **20**, 478-480.

Hothi, P., Khadra, K. A., Combe, J. P., Leys, D. and Scrutton, N. S. (2005) Tryptophan tryptophylquinone cofactor biogenesis in the aromatic amine dehydrogenase of *Alcaligenes faecalis*. Cofactor assembly and catalytic properties of recombinant enzyme expressed in Paracoccus denitrificans. *The FEBS Journal* **272**, 5894-5909. Erratum in: *The FEBS Journal* (2006) **273**, 430.

Hu, C. A., Lin, W. W. and Valle, D. (1996) Cloning, characterization, and expression of cDNAs encoding human delta 1-pyrroline-5-carboxylate dehydrogenase. *The Journal of Biological Chemistry* **271**, 9795-9800.

Hua, Z., Wang, H., Chen, D., Chen, Y. and Zhu, D. (1994) Enhancement of expression of human granulocyte-macrophage colony stimulating factor by argU gene product in *Escherichia coli*. *Biochemistry and Molecular Biology International* **32**, 537-43.

Huang, Y., Hager, E. R., Phillips, D. L., Dunn, V. R., Hacker, A., Frydman, B., Kink, J. A., Valasinas, A. L., Reddy, V. K., Marton ,L. J., Casero, R. A. Jr. and Davidson, N. E. (2003) A novel polyamine analog inhibits growth and induces apoptosis in human breast cancer cells. *Clinical Cancer Research* **9**, 2769-2777.

Huang, Y., Keen, J. C., Hager, E., Smith, R., Hacker, A., Frydman, B., Valasinas, A. L., Reddy, V. K., Marton ,L. J., Casero, R. A. Jr. and Davidson, N. E. (2004) Regulation of polyamine analogue cytotoxicity by c-Jun in human MDA-MB-435 cancer cells. *Molecular Cancer Research* **2**, 81-88.

Huang, Y., Pledgie, A., Rubin, E., Marton , L. J., Woster, P. M., Sukumar, S., Casero, R. A. Jr. and Davidson, N. E. (2005) Role of p53/p21(Wafl/Cip1) in the regulation of polyamine analogue-induced growth inhibition and cell death in human breast cancer cells. *Cancer Biology & Therapy* **4**, 1006-1013.

Hudson, R. C., Ruttersmith, L. D. and Daniel, R. M. (1993) Glutamate dehydrogenase from the extremely thermophilic archaebacterial isolate AN1. *Biochimica et biophysica acta* **1202**, 244-250.

Igarashi, K. and Kashiwagi, K. (2000) Polyamines: mysterious modulators of cellular functions. *Biochemical and biophysical research communications* **271**, 559-564.

Ikemura, T. (1985) Codon usage and tRNA content in unicellular and multicellular organisms. *Molecular Biology and Evolution* **2**, 13-34.

Inokuchi, Y., Hirashima, A., Sekine, Y., Janosi, L. and Kaji, A. (2000) Role of ribosome recycling factor (RRF) in translational coupling. *The EMBO Journal* **19**, 3788-3798.

Inoue, H., Nojima, H. and Okayama, H. (1990) High efficiency transformation of *Escherichia coli* with plasmids. *Gene* **96**, 23-28.

Jircitano, A. J., Sommerer, S. O., Shelley, J. J., Westcott, B. L. Jnr. and Suh, I-H. (1994) The self-condensation of a derivative of *o*-aminobenzaldehyde. Structure of the polycyclic bisanhydro trimer of 2-amino-5-bromobenzaldehyde. *Acta Crystallographica* **C50**, 445-447.

Jones, J. B. and Stadtman, T. C. (1980) Reconstitution of a formate-NADP+ oxidoreductase from formate dehydrogenase and a 5-deazaflavin-linked NADP+ reductase isolated from Methanococcus vannielii. *The Journal of Biological Chemistry* **255**, 1049-1053.

Jorns, M. S., Wang, B. and Jordan, S. P. (1987) DNA repair catalyzed by *Escherichia coli* DNA photolyase containing only reduced flavin: elimination of the enzyme's second chromophore by reduction with sodium borohydride. *Biochemistry* **26**, 6810-6816.

Jorns, M. S. (1979) Mechanism of catalysis by the flavoenzyme oxynitrilase. *The Journal of Biological Chemistry* **254**, 12145-12152.

Kalman, S., Mitchell, W., Marathe, R., Lammel, C., Fan, J., Hyman, R. W., Olinger, L., Grimwood, J., Davis, R. W. and Stephens, R. S. (1999) Comparative genomes of Chlamydia pneumoniae and C. trachomatis. *Nature Genetics* **21**, 385-389.

Kawakami, R., Sakuraba, H. and Ohshima, T. (2004) Gene and primary structures of dye-linked L-proline dehydrogenase from the hyperthermophilic archaeon *Thermococcus profundus* show the presence of a novel heterotetrameric amino acid dehydrogenase complex. *Extremophiles* **8**, 99-108.

Kawakami, R., Sakuraba, H., Tsuge, H., Goda, S., Katunuma, N. and Ohshima, T. (2005) A second novel dye-linked L-proline dehydrogenase complex is present in the hyperthermophilic archaeon *Pyrococcus horikoshii* OT-3. *The FEBS Journal* **272**, 4044-4054.

Kawarabayasi. Y., Sawada, M., Horikawa, H., Haikawa, Y., Hino, Y., Yamamoto, S., Sekine, M., Baba, S., Kosugi, H. and Hosoyama, A., Nagai, Y., Sakai, M., Ogura, K., Otsuka, R., Nakazawa, H., Takamiya, M., Ohfuku, Y., Funahashi, T., Tanaka, T., Kudoh, Y., Yamazaki, J., Kushida, N., Oguchi, A., Aoki, K. and Kikuchi, H. (1998) Complete sequence and gene organization of the genome of a hyperthermophilic archaebacterium, *Pyrococcus horikoshii* OT3. *DNA Research* **5**, 55–76.

Kendrew, J. C., Bodo, G., Dintzis, H. M., Parrish, R. G., Wyckoff, H. And Phillips, D. C. (1958) A three-dimensional model of the myoglobin molecule obtained by x-ray analysis. *Nature* **181**, 662-666.

Kengen, S. W., de Bok, F. A., van Loo, N. D., Dijkema, C., Stams, A. J. And de Vos, W. M. (1994) Evidence for the operation of a novel Embden-Meyerhof pathway that involves ADP-dependent kinases during sugar fermentation by *Pyrococcus furiosus*. *The Journal of Biological Chemistry* **269**, 17537-17541.

J. Kim, M. Bogdan and P. S. Mariano, Mechanistic analysis of the 3-methyllumiflavin-promoted oxidative deamination of benzylamine. A potential model for monoamine oxidase catalysis. *Journal of the American Chemical Society* **115**, 10591-10595.

Kim, J., Fuller, J. H., Kuusk, V., Cunane, L., Chen, Z., Mathews, F. S. And McIntire, W. S. (1995) The cytochrome subunit is necessary for covalent FAD attachment to the flavoprotein subunit of p-cresol methylhydroxylase. *The Journal of Biological Chemistry* **270**, 31202-31209.

Kirino, H., Aoki, M., Aoshima, M., Hayashi, Y., Ohba, M., Yamagishi, A., Wakagi, T. And Oshima, T. (1994) Hydrophobic interaction at the subunit interface contributes to the thermostability of 3-isopropylmalate dehydrogenase from an extreme thermophile, *Thermus thermophilus*. *European journal of biochemistry/FEBS* **220**, 275-281.

Klein, A. R., Berk, H., Purwantini, E., Daniels, L. and Thauer, R. K. (1996) Si-face stereospecificity at C5 of coenzyme F420 for F420-dependent glucose-6-phosphate dehydrogenase from *Mycobacterium smegmatis* and F420-dependent alcohol dehydrogenase from *Methanoculleus thermophilicus*. *European journal of biochemistry/FEBS* **239**, 93-97.

Knapp, S., de Vos, W. M., Rice, D. and Ladenstein, R. (1997) Crystal structure of glutamate dehydrogenase from the hyperthermophilic eubacterium *Thermotoga maritima* at 3.0 A resolution. *Journal of Molecular Biology* **267**, 916-932.

Koller, K. B. and Hawkridge, F. M. (1988) The effects of temperature and electrolyte at acidic and alkaline pH on the electron transfer reactions of cytochrome *c* at In_2O_3 electrodes. *Journal of Electroanalytical Chemistry* **239**, 291-306.

Krahe, M., Antyranikian, G. and Märkl, H. (1996) Fermentation of extremophilic microorganisms. *FEMS Microbiology reviews* **18**, 271-285.

Krämer, R. (1994) Sectretion of amino acids by bacteria: physiology and mechanism. *FEMS microbiology reviews* **13**, 75-94.

Krishnan, N. and Becker, D. F. (2005) Characterization of a bifunctional PutA homologue from *Bradyrhizobium japonicum* and identification of an active site residue that modulates proline reduction of the flavin adenine dinucleotide cofactor. *Biochemistry* **44**, 9130-9139.

Kurtz, K. A., Rishavy, M. A., Cleland, W. W. and Fitzpatrick, P. F. (2000) Nitrogen isotope effects as probes of the mechanism of D-amino acid oxidase. *Journal of the American Chemical Society* **122**, 12896–12897.

Lad, C., Williams, N. H. and Wolfenden, R. (2003) The rate of hydrolysis of phosphomonoester dianions and the exceptional catalytic proficiencies of protein and inositol phosphatases. *Proceedings of the National Academy of Science of the United States of America* **100**, 5607-5610.

Laemmli, U. K. (1970) Cleavage of structural proteins during the assembly of the head of bacteriophage T4. *Nature* **227**, 680-685.

Leahy, D. J., Hendrickson, W. A., Aukhil, I. and Erickson, H. P. (1992) Structure of a fibronectin type III domain from tenascin phased by MAD analysis of the selenomethionyl protein. *Science* **258**, 987-991.

Lecompte, O., Ripp. R., Puzos-Barbe, V., Duprat, S., Heilig, R., Dietrich, J., Thierry, J. C. and Poch, O. (2001) Genome evolution at the genus level: comparison of three complete genomes of hyperthermophilic archaea. *Genome Research* **11**, 981-993.

Lee, Y. H., Nadaraia, S., Gu, D., Becker, D. F. and Tanner, J. J. (2003) Structure of the proline dehydrogenase domain of the multifunctional PutA flavoprotein. *Nature Structural Biology* **10**, 109-114.

Legrain, C. M., Demarez, N., Glansdorf, N. and Pierard, A. (1995) Ammonia-dependent synthesis and metabolic channeling of carbamoyl phosphate in the hyperthermophilic archaeon *Pyrococcus furiosus*. *Microbiology* **141**, 1093-1099.

Lehman, T. C., Hale, D. E., Bhala, A. and Thorpe, C. (1990) An acyl-coenzyme A dehydrogenase assay utilizing the ferricenium ion. *Analytical Biochemistry* **186**, 280-284.

Lesage, P., Chiaruttini, C., Graffe, M., Dondon, J., Milet, M. and Springer, M. (1992) Messenger RNA secondary structure and translational coupling in the *Escherichia coli* operon encoding translation initiation factor IF3 and the ribosomal proteins, L35 and L20. *Journal of Molecular Biology* **228**, 366-386.

Lesort, M., Tucholski, J., Miller, M. L. and Johnson, G. V. (2000) Tissue transglutaminase: a possible role in neurodegenerative diseases. *Progress in Neurobiology* **61**, 439-463.

Leveque, J., Foucher, F., Bansard, J. Y., Havouis, R., Grall, J. Y. and Moulinoux, J. P. (2000) Polyamine profiles in tumor, normal tissue of the homologous breast, blood, and urine of breast cancer sufferers. *Breast cancer research and treatment* **60**, 99-105.

Leys, D., Basran, J. and Scrutton, N. S. (2003) Channelling and formation of 'active' formaldehyde in dimethylglycine oxidase. *The EMBO Journal* **22**, 4038-4048.

Li, W. T., Grayling, R. A., Sandman, K., Edmondson, S., Shriver, J. W. and Reeve, J. N. (1998) Thermodynamic stability of archaeal histones. *Biochemistry* **37**, 10563-10572.

Li, M., Hubalek, F., Newton-Vinson, P. and Edmondson, D. E. (2002) High-level expression of human liver monoamine oxidase A in Pichia pastoris: comparison with the enzyme expressed in *Saccharomyces cerevisiae*. *Protein Expression and Purification* **24**, 152-162.

Li, W. F., Zhou, X. X. and Lu, P. (2005) Structural features of thermozymes. *Biotechnology Advances* **23**, 271-281.

Li, M., Binda, C., Mattevi, A. and Edmondson, D. E. (2006) Functional role of the "aromatic cage" in human monoamine oxidase B: structures and catalytic properties of Tyr435 mutant proteins. *Biochemistry* **45**, 4775-4784.

Lim, L. W., Mathews, F. S. and Steenkamp, D. J. (1988) Identification of ADP in the iron-sulfur flavoprotein trimethylamine dehydrogenase. *The Journal Biological Chemistry* **263**, 3075-3080.

Liu, H. Heath, S. C., Sobin, C., Roos, J. L., Galke, B. L., Blundell, M. L., Lenane, M., Robertson, B., Wijsman, E. M., Rapoport, J. L., Gogos, J. A. and Karayiorgou, M. (2002) Genetic variation at the 22q11 PRODH2/DGCR6 locus presents an unusual pattern and increases susceptibility to schizophrenia. *Proceedings of the National Academy of Science of the United States of America* **99**, 3717-3722.

Lowry, O., Oassonneau, J. V. and Rock, M. K. (1961) The stability of pyridine nucleotides. *The Journal of Biological Chemistry* **236**, 2756-2759.

Lu, X., Rodriguez, M., Ji, H. and Silverman, R, B. (2002) Irreversible inactivation of mitochondrial monoamine oxidases. In *Flavins and Flavoproteins* (ed. Chapman, S., Perham, R. and Scrutton, N. S.) pp. 817-830. Rudolf Weber, Berlin.

Ma, J., Yoshimura, M., Yamashita, E., Nayagawa, A., Ito, A. and Tsukihara, T. (2004) Structure of rat monoamine oxidase A and its specific recognitions for substrates and inhibitors. *Journal of Molecular Biology* **338**, 103-114.

Macheroux, P., Bornemann, S., Ghisla, S. and Thorneley, R. N. (1996a) Studies with flavin analogs provide evidence that a protonated reduced FMN is the substrate-induced transient intermediate in the reaction of *Escherichia coli* chorismate synthase. *The Journal of Biological Chemistry* **271**, 25850-25858.

Macheroux, P., Petersen, J., Bornemann, S., Lowe, D. J. and Thorneley, R. N. (1996b) Binding of the oxidized, reduced, and radical flavin species to chorismate synthase. An

investigation by spectrophotometry, fluorimetry, and electron paramagnetic resonance and electron nuclear double resonance spectroscopy. *Biochemistry* **35**, 1643-1652.

Macheroux, P. (1999) UV-visible spectroscopy as a tool to study flavoproteins. *Methods in Molecular Biology* **131**, 1-7.
Maeda-Yorita, K., Russell, G. C., Guest, J. R., Massey, V. and Williams, C. H. Jnr. (1994) Modulation of the oxidation-reduction potential of the flavin in lipoamide dehydrogenase from *Escherichia coli* by alteration of a nearby charged residue, K53R. *Biochemistry* **33**, 6213-6220.

Maeder, D. L., Weiss, R. B., Dunn, D. M., Cherry, J. L., Gonzalez, J. M., DiRuggiero, J. And Robb, F. T. (1999) Divergence of the hyperthermophilic archaea *Pyrococcus furiosus* and *P. horikoshii* inferred from complete genomic sequences. *Genetics* **152**, 1299-1305.

Maher, M. J., Ghosh, M., Grunden, A. M., Menon, A. L., Adams, M. W. W., Freeman, H. C. And Guss, J. M. (2004) Structure of the prolidase from *Pyrococcus furiosus*. *Biochemistry* **43**, 2771-2783.

Mai, X. and Adams, M. W. W. (1994) Indolepyruvate ferredoxin oxidoreductase from the hyperthermophilic archaeon *Pyrococcus furiosus*. A new enzyme involved in peptide fermentation. *The Journal of Biological Chemistry* **269**, 16726-16732.

Manni, A. (1994) The role of polyamines in the hormonal control of breast cancer cell proliferation. *Cancer Treatment and Research* **71**, 209-225.

Manni, A. (2002) Polyamine involvement in breast cancer phenotype. *In Vivo* **16(6)**, 493-500.

Marguet, E. and Forterre, P. (1994) DNA stability at temperatures typical for hyperthermophiles. *Nucleic Acids Research* **22**,1681-1686.

Martins, L. O. and Santos, H. (1995) Accumulation of Mannosylglycerate and Di-myo-Inositol-Phosphate by *Pyrococcus furiosus* in Response to Salinity and Temperature. *Applied Environmental Microbiology* **61**, 3299-3303.

Marton, L. J. and Pegg, A. E. (1995) Polyamines as targets for therapeutic intervention. *Annual Review of Pharmacology and Toxicology* **35**, 55-91.

Masgrau, L., Basran, J., Hothi, P., Sutcliffe, M. J. and Scrutton, N. S. (2004) Hydrogen tunneling in quinoproteins. *Archives of Biochemistry and Biophysics* **28**, -51.

Masgrau, L., Roujeinikova, A., Johannissen, L. O., Hothi, P., Basran, J., Ranaghan, K. E., Mulholland, A. J., Sutcliffe, M. J., Scrutton, N. S. And Leys, D. (2006) Atomic description of an enzyme reaction dominated by proton tunneling. *Science* **312**, 237-241. Erratum in: *Science* (2006) **312**, 1600.

Massant, J. and Glansdorff, N. (2004) Metabolic channelling of carbamoyl phosphate in the hyperthermophilic archaeon *Pyrococcus furiosus*: dynamic enzyme-enzyme interactions involved in the formation of the channelling complex. *Biochemical Society Transactions* **32**, 306-309.

Massey, V. and Hammerich, P. (1980) Active-site probes of flavoproteins. *Biochemical Society Transactions* **8**, 246-257.

Massey, V., Muller, F., Feldberg, R., Schuman, M., Sullivan, P. A., Howell, L. G., Mayhew, S. G., Matthews, R. G. and Foust, G. P. (1969) The reactivity of flavoproteins with sulfite. Possible relevance to the problem of oxygen reactivity. *The Journal of Biological Chemistry* **244**, 3999-4006.

Massey, V. (2000) The chemical and biological versatility of riboflavin. *Biochemical Society Transactions* **28**, 283-296.

Matthews, C. K. and van Holde, K. E. (1996) *Biochemistry* (2nd Edition) Benjamin/Cummings Publishing Company, California, USA.

Matsumura, M., Signor, G. and Matthews, B. W. (1989) Substantial increase of protein stability by multiple disulphide bonds. *Nature* **342**, 291-293.

Mattevi, A., Vanoni, M. A., Todone, F. Rizzi, M., Teplyakov, A., Coda, A., Bolognesi, M. and Curti, B. (1996) Crystal structure of D-amino acid oxidase: a case of active site mirror-image convergent evolution with flavocytochrome b2. *Proceedings of the National Academy of Science of the United States of America* **93**, 7496-7501.

Matthews, B. W. (1968) Solvent content of protein crystals. *Journal of Molecular Biology* **33**, 491-497.

Mayhew, S. G. and Tollin, G. (1992) Chapter 14: General properties of flavodoxins. In *Chemistry and Biochemistry of Flavoenzymes* (volume III) (ed Müller, F.), pp. 389-426, CRC Press, Inc., Boca Raton, Florida, USA.

McPherson, A. (1989) Macromolecular crystals. *Scientific American* **260**, 62-69.

McPherson, A., Luk, T. S., Thompson, B. D., Borisov, A. B., Shiryaev, O. B., Chen, X., Boyer, K. and Rhodes, C. K. (1994) Multiphoton induced x-ray emission from Kr clusters on M-shell (~100 A) and L-shell (~6 A) transitions. *Physical Review Letters* **72**, 1810-1813.

McPherson, A. (2004) Protein crystallization in the structural genomics era. *Journal of Structural and Functional Genomics* **5**, 3-12.

Medina, M. A., Urdiales, J. L., Rodriguez-Caso, C., Ramirez, F. J. and Sanchez-Jimenez, F. (2003) Similar Biochemistry for Different Physiological Missions and Biomedical Applications. *Critical Reviews in Biochemistry and Molecular Biology* **38**, 23–59.

Menzel, R. and Roth, J. (1981) Regulation of genes for proline utilization in *Salmonella typhimurium*: autogenous repression by the *putA* gene product. *Journal of Molecular Biology* **148**, 21-44.

Meskys, R., Harris, R. J., Casaite, V., Basran, J. and Scrutton, N. S. (2001) Organization of the genes involved in dimethylglycine and sarcosine degradation in *Arthrobacter* spp.: implications for glycine betaine catabolism. *European Journal of Biochemistry/FEBS* **268**, 3390-3398.

Messiha, H. L., Munro, A, W., Bruce, N. C., Barsukov, I. and Scrutton, N. S. (2005a) Reaction of morphinone reductase with 2-cyclohexen-1-one and 1-nitrocyclohexene: proton donation, ligand binding, and the role of residues Histidine 186 and Asparagine 189. *The Journal of Biological Chemistry* **280**, 10695-10709.

Messiha, H. L., Bruce, N. C., Sattelle, B. M., Sutcliffe, M. J., Munro, A. W. and Scrutton, N. S. (2005b) Role of active site residues and solvent in proton transfer and the modulation of flavin reduction potential in bacterial morphinone reductase. *The Journal of Biological Chemistry* **280**, 27103-27110.

Mewies, M., McIntire, W. S. and Scrutton, N. S. (1998) Covalent attachment of flavin adenine dinucleotide (FAD) and flavin mononucleotide (FMN) to enzymes: the current state of affairs. *Protein Science* **7**, 7-20.

Mewies, M., Basran, J., Packman, L. C., Hille, R. and Scrutton, N. S. (1997) Involvement of a flavin iminoquinone methide in the formation of 6-hydroxyflavin mononucleotide in trimethylamine dehydrogenase: a rationale for the existence of 8alpha-methyl and C6-linked covalent flavoproteins. *Biochemistry* **36**, 7162-7168.

Mezl, V. A. and Knox, W. E. (1976) Properties and analysis of a stable derivative of pyrroline-5-carboxylic acid for use in metabolic studies. *Analytical Biochemistry* **74**, 430-440.

Mezzetti, M., Maniero, A., Brustolon, M., Giacometti, G. and Brunel, L. (1999) A Tyrosyl Radical in an Irradiated Single Crystal of *N*-Acetyl-L-tyrosine Studied by X-band cw-EPR, High-Frequency EPR, and ENDOR Spectroscopies. *The Journal of Physical Chemistry. A, Molecules, Spectroscopy, Kinetics, Environment & General Theory* **103**, 9636–9643.

Mihalik, S. J., McGuinness, M. and Watkins, P. A. (1991) Purification and characterization of peroxisomal L-pipecolic acid oxidase from monkey liver. *The Journal of Biological Chemistry* **266**, 4822-4830.

Miller, J. R. and Edmondson, D. E. (1999) Structure-activity relationships in the oxidation of para-substituted benzylamine analogues by recombinant human liver monoamine oxidase A. *Biochemistry* **38**, 13670-13683.

Miller, D., Richards, P. L. and Merchant, P. (1995) Magnetic-field effects on submillimeter absorptivity in epitaxial thin films of YBa2Cu3O7. *Physical review. B, Condensed matter* **51**, 8385-8389.

Mofatt, B. A.Studier, F. W. (1987) T7 lysozyme inhibits transcription by T7 RNA polymerase. *Cell* **49**, 221-227.

Monaghan, P. J., Leys, D. and Scrutton, N. S. (2005) Crystallization and preliminary X-ray diffraction analysis of a flavoenzyme amine dehydrogenase/oxidase from *Pyrococcus furiosus* DSM 3638. *Acta crystallographica. Section F, Structural biology and crystallization communications* **61**, 756-758.

Moriyama, H., Onodera, K., Sakurai, M., Tanaka, N., Kirino-Kagawa, H., Oshima, T. and Katsube, Y. (1995) The crystal structures of mutated 3-isopropylmalate dehydrogenase from *Thermus thermophilus* HB8 and their relationship to the thermostability of the enzyme. *Journal of Biochemistry (Tokyo)* **117**, 408-413.

Moser, C. C., Keske, J. M., Warncke, K., Farid, R. S. and Dutton, P. L. (1992) Nature of biological electron transfer. *Nature* **355**, 796-802.

Mrabet, N. T., Van den Broek, A., Van den brande, I., Stanssens, P., Laroche, Y., Lambeir, A. M., Matthijssens, G., Jenkins, J., Chiadmi, M., van Tilbeurgh, H., Rey, F., Janin, J., Quax, W. J., Lasters, I., De Maeyer, M. and Wodak, S. J. (1992) Arginine residues as stabilizing elements in proteins. *Biochemistry* **31**, 2239-2253.

Mukund, S. and Adams, M. W. W. (1991) The novel tungsten-iron-sulfur protein of the hyperthermophilic archaebacterium, *Pyrococcus furiosus*, is an aldehyde ferredoxin oxidoreductase. Evidence for its participation in a unique glycolytic pathway. *The Journal of Biological Chemistry* **266**, 14208-14216.

Mukund, S. and Adams, M. W. W. (1993) Characterization of a novel tungsten-containing formaldehyde ferredoxin oxidoreductase from the hyperthermophilic archaeon, *Thermococcus litoralis*. A role for tungsten in peptide catabolism. *The Journal of Biological Chemistry* **268**, 13592-13600.

Mukund, S. and Adams, M. W. W. (1995) Glyceraldehyde-3-phosphate ferredoxin oxidoreductase, a novel tungsten-containing enzyme with a potential glycolytic role in the hyperthermophilic archaeon *Pyrococcus furiosus*. *The Journal of Biological Chemistry* **270**, 8389-8392.

Müller, U. and Buckel, W. (1995) Activation of (R)-2-hydroxyglutaryl-CoA dehydratase from *Acidaminococcus fermentans. European Journal of Biochemistry/FEBS* **230**, 698-704.

Munro, A. W., Noble, M. A., Robledo, L., Daff, S. N. and Chapman, S. K. (2001) Determination of the redox properties of human NADPH-cytochrome P450 reductase. *Biochemistry* **40**, 1956-1963.

Mure, M., Mills, S. A. Klinman, J. P. (2002) Catalytic mechanism of the topa quinone containing copper amine oxidases. *Biochemistry* **41**, 9269-9278.

Muro-Pastor, A. M., Ostrovsky, P. and Maloy, S. (1997) Regulation of gene expression by repressor localization: biochemical evidence that membrane and DNA binding by the PutA protein are mutually exclusive. *Journal of Bacteriology* **179**, 2788-9127.

Murshudov, G. N., Vagin, A. A. and Dodson, E. J. (1997) Refinement of macromolecular structures by the maximum-likelihood method. *Acta Crystallographica Section D, Biological Crystallography* **53**, 240-255.

Murty, C. V. and Adiga, P. R. (1982) Pregnancy suppression by active immunization against gestation-specific riboflavin carrier protein. *Science* **216**, 191-193.

Narhi, L. O. and Fulco, A. J. (1986) Characterization of a catalytically self-sufficient 119,000-dalton cytochrome P-450 monooxygenase induced by barbiturates in Bacillus megaterium. *The Journal of Biological Chemistry* **261**, 7160-7169.

Navaza, J. (1994) *AMoRe*: an automated package for molecular replacement *Acta Crystallographica Section A* **A50**, 157-163.

Neuhaus, D. and Williamson, M. P. (2000) *The Nuclear Overhauser Effect in Structural and Conformational Analysis* (2nd Edition), John Wiley & Sons.

Newton-Vinson, P., Hubalek, F. and Edmondson, D. E. (2000) High-level expression of human liver monoamine oxidase B in Pichia pastoris. *Protein Expression and Purification* **20**, 334-345.

Okazaki, Y., Furuno, M., Kasukawa, T., Adachi, J., Bono, H., Kondo, S., Nikaido, I., Osato, N., Saito, R., Suzuki, H., Yamanaka, I., Kiyosawa, H., Yagi, K., Tomaru, Y., Hasegawa, Y., Nogami, A., Schonbach, C., Gojobori, T., Baldarelli, R., Hill, D. P., Bult, C., Hume, D. A., Quackenbush, J., Schriml, L. M., Kanapin, A., Matsuda, H., Batalov, S., Beisel, K. W., Blake, J. A., Bradt, D., Brusic, V., Chothia, C., Corbani, L. E., Cousins, S., Dalla, E., Dragani, T. A., Fletcher, C. F., Forrest, A., Frazer, K. S., Gaasterland, T., Gariboldi, M., Gissi, C., Godzik, A., Gough, J., Grimmond, S., Gustincich, S., Hirokawa, N., Jackson, I. J., Jarvis, E. D., Kanai, A., Kawaji, H., Kawasawa, Y., Kedzierski, R. M., King, B. L., Konagaya, A., Kurochkin, I. V., Lee, Y., Lenhard, B., Lyons, P. A., Maglott, D. R., Maltais, L., Marchionni, L., McKenzie, L., Miki, H., Nagashima, T., Numata, K., Okido, T., Pavan, W. J., Pertea, G., Pesole, G., Petrovsky, N., Pillai, R., Pontius, J. U.,

Qi, D., Ramachandran, S., Ravasi, T., Reed, J. C., Reed, D. J., Reid, J., Ring, B. Z., Ringwald, M., Sandelin, A., Schneider, C., Semple, C. A., Setou, M., Shimada, K., Sultana, R., Takenaka, Y., Taylor, M. S., Teasdale, R. D., Tomita, M., Verardo, R., Wagner, L., Wahlestedt, C., Wang, Y., Watanabe, Y., Wells, C., Wilming, L. G., Wynshaw-Boris, A., Yanagisawa, M., Yang, I., Yang, L., Yuan, Z., Zavolan, M., Zhu, Y., Zimmer, A., Carninci, P., Hayatsu, N., Hirozane-Kishikawa, T., Konno, H., Nakamura, M., Sakazume, N., Sato, K., Shiraki, T., Waki, K., Kawai, J., Aizawa, K., Arakawa, T., Fukuda, S., Hara, A., Hashizume, W., Imotani, K., Ishii, Y., Itoh, M., Kagawa, I., Miyazaki, A., Sakai, K., Sasaki, D., Shibata, K., Shinagawa, A., Yasunishi, A., Yoshino, M., Waterston, R., Lander, E. S., Rogers, J., Birney, E. and Hayashizaki, Y. (2002) Analysis of the mouse transcriptome based on functional annotation of 60,770 full-length cDNAs. *Nature* **420**, 563-573.

Ostrovsky, P., de Spicer, O'Brien, K. and Maloy, S. (1991) Regulation of proline utilization in *Salmonella typhimurium*: a membrane-associated dehydrogenase binds DNA in vitro. *Journal of Bacteriology* **173**, 211-219.

Otwinowski, Z. and Minor, W. (1997) Processing of X-ray diffraction data collected in oscillation mode. *Methods in Enzymology* **276**, 307-326.

Owston, P. G. and Shaw, L. S. (1988) Structural investigation of the self-condensation products of o-aminobenzaldehyde, anthranilic acid and related compounds. 1. The TAAB salts $TAABH_2X_2$ [X = picrate (ordered), HSO_4 (disordered) and BF_4 (disordered)]. Hydrogen bonding and the importance of two non-equivalent lone-pair donor sites in the anion for order. *Acta Crystallographica Section B* **B44**, 39-50.

Pace, C. N. (1992) Contribution of the hydrophobic effect to globular protein stability. *Journal of Molecular Biology* **226**(1), 29-35.

Packman,L. C., Mewies, M. and Scrutton, N. S. (1995) The flavinylation reaction of trimethylamine dehydrogenase. Analysis by directed mutagenesis and electrospray mass spectrometry. *The Journal of Biological Chemistry* **270**, 13186-13191.

Palfey, B. A. and Massey, V. (1998) Chapter 29: Flavin-dependent enzymes. In *Comprehensive Biological Catalysis* (volume III) (ed. Sinnott, M.), pp. 84-154, Academic Press Limited, London.

Park, J. B., Fan, C. L., Hoffman, B. M. and Adams, M. W. W. (1991) Potentiometric and electron nuclear double resonance properties of the two spin forms of the [4Fe-4S]+ cluster in the novel ferredoxin from the hyperthermophilic archaebacterium *Pyrococcus furiosus*. *The Journal of Biological Chemistry* **266**, 19351-19356.

Pegg, A. E. (1988) Polyamine metabolism and its importance in neoplastic growth and a target for chemotherapy. *Cancer Research* **48**, 759-774.

Pereira, S. L., Grayling, R. A., Luyrz, R. and Reeve, J. N. (1997) Advances in Protein Chemistry. (ed. Adams, M. W. W.), pp. 12633-12637, Academinc Press, San Diego. Perler, F. B., Kumar, S. and Kong, H. (1996) Thermostable DNA polymerases. *Advances in Protein Chemistry* **48**, 377-435.

Peterson, M. E., Eisenthal, R., Danson, M. J., Spence, A. and Daniel, R. M. (2004) A new intrinsic thermal parameter for enzymes reveals true temperature optima. *The Journal of Biological Chemistry* **279**, 20717-20722. Erratum in: *The Journal of Biological Chemistry* (2005) **280**, 41784.

Petsko, G. A. (2001) Structural basis of thermostability in hyperthermophilic proteins, or "there's more than one way to skin a cat". *Methods in Enzymology* **334**, 469-478.

Phang, J. M., Yeh, G. C. and Scriver, C. R. (1995) Disorders of proline and hydroxyproline metabolism. In *The Metabolic and Molecular Bases of Inherited Disease* (7th Edition) (eds. Scriver, C. R., Beaudet, A. L., Sly, W. S. and Valle, D.), pp. 1125-1146, McGraw-Hill, New York.

Pietila, M., Pirinen, E., Keskitalo, S., Juutinen, S., Pasonen-Seppanen, S., Keinanen, T., Alhonen, L. and Janne, J. (2005) Disturbed keratinocyte differentiation in transgenic mice and organotypic keratinocyte cultures as a result of spermidine/spermine N-acetyltransferase overexpression. *The Journal of investigative dermatology* **124**, 596-601.

Pilato, R. S. and Stiefel, E. I. (1999) Molybdenum and tungsten enzymes. In: *Bioinorganic Catalysis* (2nd Edition) (eds. Reedijk, J. and Buowman, E.), Dekker, pp. 81-152, New York, USA.

Pollegioni, L., Blodig, W. and Ghisla, S. (1997) On the mechanism of D-amino acid oxidase. Structure/linear free energy correlations and deuterium kinetic isotope effects using substituted phenylglycines. *Journal of Biological Chemistry* **272**, 4924–4934.

Pollock, R. J. and Hersh, L. B. (1973) N-methylglutamate synthetase. The use of flavin mononucleotide in oxidative catalysis. *The Journal of Biological Chemistry* **248**, 6724-6733.

Polyak, K., Xia, Y., Zweier, J. L., Kinzler, K. W. and Vogelstein, B. (1997) A model for p53-induced apoptosis. *Nature* **389**, 300-305.

Ramsay, R. R., Upadhyay, A. K., Li, M. and Edmondson, D. E. (2005) Optical and EPR spectroscopic studies on the anionic flavin radical in MAO B and its Y435 mutant forms. In: *Flavins and Flavoproteins* (eds, Nishino, T., Miura, R., Tanokura, M. and Fukui, K.) pp. 137-142, ARchiTect Inc, Tokyo, Japan.

Rees, D. C. (2001) Crystallographic analyses of hyperthermophilic proteins. *Methods in Enzymology* **334**, 423–437.

Renard, M. and Fersht, A. R. (1973) pH dependence of chymotrypsin catalysis. Appendix: substrate binding to dimeric alpha-chymotrypsin studied by x-ray diffraction and the equilibrium method. *Biochemistry* **13**, 1416-1426.

Reuber, B. E., Karl, C., Reimann, S. A., Mihalik, S. J. Dodt, G. (1997) Cloning and functional expression of a mammalian gene for a peroxisomal sarcosine oxidase. *The Journal of Biological Chemistry* **272**, 6766-6776.

Rhodes, G. (1993) *Crystallography Made Crystal Clear*. Academic Press, San Diego.

Rigby, S. E., Hynson, R. M., Ramsay, R. R., Munro, A. W. and Scrutton, N. S. (2005) A stable tyrosyl radical in monoamine oxidase A. *The Journal of Biological Chemistry* **280**, 4627-4631.

Robb, F. T., Maeder, D. L., Brown, J. R., DiRuggiero, J., Stump. M. D., Yeh, R. K., Weiss, R. B. and Dunn, D. M. (2001) Genomic sequence of hyperthermophile, *Pyrococcus furiosus*: implications for physiology and enzymology. *Methods in Enzymology* **330**, 134-157.

Rodriguez-Caso, C., Montanez, R., Cascante, M., Sanchez-Jimenez, F. and Medina, M. A. (2006) Mathematical modeling of polyamine metabolism in mammals. *The Journal of Biological Chemistry* **281**, 21799-21812.

Rohlfs. R. J. and Hille, R. (1994) The reaction of trimethylamine dehydrogenase with diethylmethylamine. *The Journal of Biological Chemistry* **269**, 30869-30879.

Rossmann, M. G. and Blow, D. M. (1962) The detection of sub-units within the crystallographic asymmetric unit. *Acta Crystallographica* **15**, 24-31.

Rossmann, M. G. Moras, D. And Olsen, K. W. (1974) Chemical and biological evolution of nucleotide-binding protein. *Nature* **250**, 194-199.

Rossmann, M. G. (1990) The molecular replacement method. *Acta Crystallographica Section A* **46**, 73-82.

Ruiz-Chica, J., Medina, M. A., Sanchez-Jimenez, F. and Ramirez, F. J. (2001) Fourier transform Raman study of the structural specificities on the interaction between DNA and biogenic polyamines. *Biophysical Journal* **80**, 443-454.

Russell, R. J., Ferguson, J. M., Hough, D. W., Danson, M. J. and Taylor, G. L. (1997) The crystal structure of citrate synthase from the hyperthermophilic archaeon *Pyrococcus furiosus* at 1.9 A resolution. *Biochemistry* **36**, 9983-9994.

Russell, D. H. (1983) Clinical relevance of polyamines. *Critical reviews in clinical laboratory sciences* **18**, 261-311.

Sablin, S. O. and Ramsay, R. R. (2001) Substrates but not inhibitors alter the redox potentials of monoamine oxidases. *Antioxidants & redox signaling* **3**, 723-729.

Sakuraba, H., Takamatsu, Y., Satomura, T., Kawakami, R. and Ohshima, T. (2001) Purification, characterization, and application of a novel dye-linked L-proline dehydrogenase from a hyperthermophilic archaeon, *Thermococcus profundus*. *Applied Environmental Microbiology* **67**, 1470–1475.

Sandman, K., Krzycki, J. A., Dobrinski, B., Lurz, R. and Reeve, J. N. (1990) HMf, a DNA-binding protein isolated from the hyperthermophilic archaeon Methanothermus fervidus, is most closely related to histones. *Proceedings of the National Academy of Science of the United States of America* **87**, 5788-5791.

Sapra, R., Bagramyan, K. and Adams, M. W. W. (2003) A simple energy-conserving system: proton reduction coupled to proton translocation. *Proceedings of the National Academy of Science of the United States of America* **100**, 7545-7550.

Satoh, A., Kim, J-K., Miyahara, I., Devreese, B., Vandenberghe, I., Hacisalihoglu, A., Okajima, T., Kuroda, S., Adachi, O., Duine, J. A., Van Beeumen, J., Tanizawa K. and Hirotsu, K. *The Journal of Biological Chemistry* **277**, 2830–2834.

Scarpulla, R. C. and Soffer, R. L. (1978) Membrane-bound proline dehydrogenase from *Escherichia coli*. *The Journal of Biological chemistry* **253**, 5997-6001.

Schäfer, T. and Schönheit, P. (1991) Pyruvate metabolism of the hyperthermophilic archaebacterium *Pyrococcus furiosus*. *Archives of Microbiology* **155**, 366-377.

Schäfer, T. and Schönheit, P. (1992) Maltose fermentation to acetate CO_2 and H_2 in the anaerobic hyperthermophilic archaeon *Pyrococcus furiosus*: evidence for the operation of a novel sugar fermentation pathway. *Archives of Microbiology* **158**, 188-202.

Schafer, T., and Schonheit, P. (1993) Gluconeogenesis from pyruvate in the hyperthermophilic archaeon *Pyrococcus furiosus*-involvement of reactions of the Embden-Meyerhof pathway. *Archives of Microbiology* **159**, 354-363.

Schenk, P. M., Baumann, S., Mattes, R. and Steinbiss, H. H. (1995) Improved high-level expression system for eukaryotic genes in *Escherichia coli* using T7 RNA polymerase and rare ArgtRNAs. *Biotechniques* **19**, 196-200.

Scherf, U. and Buckel, W. (1993) Purification and properties of an iron-sulfur and FAD-containing 4-hydroxybutyryl-CoA dehydratase/vinylacetyl-CoA delta 3-delta 2-isomerase from Clostridium aminobutyricum. *European Journal of Biochemistry/FEBS* **215**, 421-429.

Schicho, R. N., Snowden, L. J., Mukund, S., Park, J-B., Adams, M. W. W. and Kelly, R. M. (1993) Influence of tungsten on metabolic patterns in *Pyrococcus furiosus*, a hyperthermophilic archaeon. *Archives of Microbiology* **159**, 380-385.

Schut, G. L., Brehm, S. D., Datta, S. and Adams, M. W. W. (2003) Whole-genome DNA microarray analysis of a hyperthermophile and an archaeon: *Pyrococcus furiosus* grown on carbohydrates or peptides. *Journal of Bacteriology* **185**, 3935-3947.

Scrutton, N. S. (1999) Identification of covalent flavoproteins and analysis of the covalent link. *Methods in Molecular Biology* **131**, 181-193.

Scrutton, N. S. (2004) Chemical aspects of amine oxidation by flavoprotein enzymes. *Natural Product Reports* **21**, 722-30. Erratum in: *Natural Product Reports* (2005) **22(2)**, 306.

Scrutton, N. S., Basran, J. and Sutcliffe, M. J. (1999) New insights into enzyme catalysis. Ground state tunnelling driven by protein dynamics. *European Journal of Biochemistry/FEBS* **264**, 666-671.

Seiler, N., Atanossov, C. L. and Raul, F. (1998) Polyamine metabolism as target for cancer chemoprevention. *International journal of oncology* **13**, 993-1006.

Seiler, N. (2005) Pharmacological aspects of cytotoxic polyamine analogs and derivatives for cancer therapy. *Pharmacology and Therapeutics* **107**, 99-119.

Shine, J. and Dalgarno, L. (1974) The 3'-terminal sequence of Escherichia coli 16S ribosomal RNA: complementarity to nonsense triplets and ribosome binding sites. *Proceedings of the National Academy of Science of the United States of America* **71**, 1342-1346.

Silverman, R. B., Hoffman, S. and Catus, I. W. (1980) A mechanism for mitochondrial monoamine oxidase catalyzed amine oxidation. *Journal of the American Chemical Society* **102**, 7126-7128.

Silverman, R. B., Zhou, J. and Eaton, P. (1993) Inactivation of monoamine oxidase by (aminomethyl)cubane. First evidence for an .alpha.-amino radical during enzyme catalysis. *Journal of the American Chemical Society* **115**, 8841-8841.

Silverman, R. B., Lu, X. and Zhou, J. (1994) Monoamine Oxidase B-Catalyzed Oxidation of Cinnamylamine 2,3-Oxide. Further Evidence against a Nucleophilic Mechanism. *Journal of the American Chemical Society* **116**, 11590-11591.

Silverman, R. B. (1992) In : *Advances in Electron Transfer Chemistry* (volume II) (ed. Mariano, P. S.), p. 177, JAI Press Inc, Greenwich.

Silverman, R. B. (1995) Radical Ideas about Monoamine Oxidase. *Accounts of Chemical Research* **28**, 335-342.

Slesarev, A. I., Zaitzev, D. A., Kopylov, V. M., Stetter, K. O. and Kozyavkin, S. A. (1991) DNA topoisomerase III from extremely thermophilic archaebacteria. ATP-independent type I topoisomerase from Desulfurococcus amylolyticus drives extensive unwinding of closed circular DNA at high temperature. *The Journal of Biological Chemistry* **266**, 12321-12328.

Smith, J. L. and Thompson, A. (1998) Reactivity of selenomethionine--dents in the magic bullet? *Structure* **6**, 815-819.

Smith, E. T., Blamey, J. M., Zhou Z. H. and Adams, M. W. W. (1995) A variable-temperature direct electrochemical study of metalloproteins from hyperthermophilic microorganisms involved in hydrogen production from pyruvate. *Biochemistry* **34**, 7161-7169.

Sorensen, M. A., Kurland, C. G. and Pederson, S. (1989) Codon usage determines translation rate in Escherichia coli. *Journal of Molecular Biology* **207**, 365-377.

Stankovich, M. T. (1991) Redox properties of flavins and flavoproteins. In: *Chemistry and Biochemistry of Flavoenzymes* (ed. Muller, F.) pp. 401-425, CRC Press, Boca Raton, USA.

Steenkamp, D. J. and Mallinson, J. (1976) Trimethylamine dehydrogenase from a methylotrophic bacterium. I. Isolation and steady-state kinetics. *Biochimica et Biophysica acta* **429**, 705-719.

Steenkamp, D. J., McIntire, W. And Kenney, W. C. (1978) Structure of the covalently bound coenzyme of trimethylamine dehydrogenase. Evidence for a 6-substituted flavin. *The Journal of Biological Chemistry* **253**, 2818-2824.

Stetter, K. O., Fiala, G., Huber, G., Huber, R. and Segerer, G. (1990) Hyperthermophilic microorganisms. *FEMS Microbiology Reviews* **75**, 117-124.

Stetter, K. O. (1986) Diversity of extremely thermophilic archaebacteria. In: *The Thermophiles, General, Molecular and Applied Microbiology*, (ed, Brock, T. D.) pp. 39-74, John Wiley, New York.

Streitwieser, A., Heathercock, C. H. and Kosower, E. M. (1992) *Introduction to Organic Chemistry*. (Fourth Edition), Macmillan Publishing Company.

Stubbe, J., Nocera, D. G., Yee, C. S. And Chang, M. C. (2003) Radical initiation in the class I ribonucleotide reductase: long-range proton-coupled electron transfer? *Chemical Reviews* **103**, 2167-2201.

Studier, F. W. and Moffatt, B. A. (1986) Use of bacteriophage T7 RNA polymerase to direct selective high-level expression of cloned genes. *Journal of Molecular Biology* **189**, 113-130.

Studier, F. W., Rosenberg, A. H., Dunn, J. J. And Dubendorff, J. W. (1990) Use of T7 RNA polymerase to direct expression of cloned genes. *Methods in Enzymology* **185**, 60-89.

Surber, M. W. and Maloy, S. (1998) The PutA protein of *Salmonella typhimurium* catalyzes the two steps of proline degradation *via* a leaky channel. *Archives of biochemistry and biophysics* **354**, 281-287.

Surber, M. W. and Maloy, S. (1999) Regulation of flavin dehydrogenase compartmentalization: requirements for PutA-membrane association in *Salmonella typhimurium*. *Biochimica et Biophysica Acta* **1421**, 5-18.

Susin, S. A., Lorenzo, H. K., Zamzami, N., Marzo, I., Brenner, C., Larochette, Prevost, M. C., Alzari, P. M. and Kroemer, G. (1999) Mitochondrial release of caspase-2 and -9 during the apoptotic process. *The Journal of Experimental Medicine* **189**, 381-94.

Suvd, D., Fujimoto, Z., Takase, K., Matsumura, M. and Mizuno, H. (2001) Crystal structure of *Bacillus stearothermophilus* alpha-amylase: possible factors determining the thermostability. *Journal of Biochemistry (Tokyo)* **129**, 461-468.

Swartz, P. D. and Ichiye, T. (1996) Temperature dependence of the redox potential of rubredoxin from *Pyrococcus furiosus*: a molecular dynamics study. *Biochemistry* **35**, 13772-13779.

Takagi, H., Takahashi, T., Momose, H., Inouye, M., Maeda, Y., Matsuzawa, H. and Ohta, T. (1990) Enhancement of the thermostability of subtilisin E by introduction of a disulfide bond engineered on the basis of structural comparison with a thermophilic serine protease. *The Journal of Biological Chemistry* **265**, 6874-6878.

Talfournier, F., Munro, A. W., Basran, J., Sutcliffe, M. J., Daff, S., Chapman, S. K. and Scrutton, N. S. (2001) alpha Arg-237 in *Methylophilus methylotrophus* (sp. W3A1) electron-transferring flavoprotein affords approximately 200-millivolt stabilization of the FAD anionic semiquinone and a kinetic block on full reduction to the dihydroquinone. *The Journal of Biological Chemistry* **276**, 20190-20196.

Taniguchi, V. T., Sailasuta-Scott, N., Anson, F. C., and Gray, H. B. (1980) Thermodynamics of metalloprotein electron transfer reactions. *Pure and Applied Chemistry* **52**, 2275-2281.

Tanner, J. J., Hecht, R. M. and Krause, K. L. (1996) Determinants of enzyme thermostability observed in the molecular structure of Thermus aquaticus D-

glyceraldehyde-3-phosphate dehydrogenase at 25 Angstroms Resolution. *Biochemistry* **35**, 2597-2609.

Thoma, R., Hennig, M., Sterner, R. and Kirschner, K. (2000) Structure and function of mutationally generated monomers of dimeric phosphoribosylanthranilate isomerase from *Thermotoga maritima*. *Structure* **8**, 265-76.

Thomazeau, K., Curien G., Thompson, A., Dumas, R. and Biou, V. (2001) MAD on threonine synthase: the phasing power of oxidized selenomethionine. *Acta Crystallographica, Section D Biological Crystallography* **57**, 1337-1340.

Tipton, K. F. (1996) Chapter 4 : Patterns of enzyme inhibition. In *Enzymology LabFax* (ed. Engel, P. C.), pp. 115-174, BIOS Scientific Publishers Limited, Oxford, UK.

Trickey, P., Wagner, M. A., Jorns, M. S. and Mathews, F. S. (1999) Monomeric sarcosine oxidase: structure of a covalently flavinylated amine oxidizing enzyme. *Structure* **7**, 331-45.

Tripathi, G. N. R., and R. H. Schuler. 1984. The resonance Raman spectrum of phenoxyl radical. *Journal of Chemical Physics* **81**, 113-121.

Tse, M.-T. and Schloss, J. V. (1993) The oxygenase reaction of acetolactate synthase *Biochemistry* **32**, 10398-10403.

Tsuge, H., Kawakami, R., Sakuraba, H., Ago, H., Miyano, M., Aki, K., Katunuma, N. and Ohshima, T. (2005) Crystal structure of a novel FAD-, FMN-, and ATP-containing L-proline dehydrogenase complex from *Pyrococcus horikoshii*. *The Journal of Biological Chemistry* **280**, 31045-31049.

Tzeng, S. F., Bryant, M. P. and Wolfe, R. S. (1975a) Factor 420-dependent pyridine nucleotide-linked formate metabolism of *methanobacterium ruminantium*. *Journal of Bacteriology* **121**, 192-196.

Tzeng, S. F., Wolfe, R. S. and Bryant, M. P. (1975b) Factor 420-dependent pyridine nucleotide-linked hydrogenase system of *methanobacterium ruminantium*. *Journal of Bacteriology* **121**, 154-191.

Umhau, S., Pollegioni, L., Molla, G., Diederichs, K., Welte, W., Pilone, M. S. and Ghisla, S. (2000) The x-ray structure of D-amino acid oxidase at very high resolution identifies the chemical mechanism of flavin-dependent substrate dehydrogenation. *Proceedings of the National Academy of Science of the United States of America* **97**, 463-12468

Vagin, A. and Teplyakov, A. (1998) A translation-function approach for heavy-atom location in macromolecular crystallography. *Acta Crystallographica, Section D Biological Crystallography* **54**, 400-402.

Vallon, O. (2000) New sequence motifs in flavoproteins: evidence for common ancestry and tools to predict structure. *Proteins* **38**, 95-114.

Van Berkel, W. J., Eppink, M. H., Middelhoven, W. J., Vervoort, J. and Rietjens, I. M. (1994) Catabolism of 4-hydroxybenzoate in *Candida parapsilosis* proceeds through initial oxidative decarboxylation by a FAD-dependent 4-hydroxybenzoate 1-hydroxylase. *FEMS Microbiology Letters* **121**, 207-215.

Van de Casteele, M., Legrain, C., Desmarez, L., Chen, P. G., Pierard, A. and Glansdorff, N. (1997) Molecular physiology of carbamoylation under extreme conditions: what can we learn from extreme thermophilic microorganisms? *Comparative biochemistry and physiology. Part A, Physiology* **118**, 463-73.

Venci, D., Zhao, G. and Jorns, M. S. (2002) Molecular characterization of NikD, a new flavoenzyme important in the biosynthesis of nikkomycin antibiotics. *Biochemistry* **41**, 15795-15802.

Vieille, C. and Zeikus, G. J. (2001) Hyperthermophilic enzymes : sources, uses, and molecular mechanisms for thermostability. *Microbiology and Molecular Biology Reviews* **65**, 1-43.

Vilchez, S., Manzanera, M. and Ramos, J. L. (2000) Control of expression of divergent Pseudomonas putida put promoters for proline catabolism. *Applied Environmental Microbiology* **66**, 5221-5225.

Vinod, M. P., Bellur, P. and Becker, D. F. (2002) Electrochemical and functional characterization of the proline dehydrogenase domain of the PutA flavoprotein from *Escherichia coli. Biochemistry* **41**, 6525-6532.

Wagner, M. A. and Jorns, M. S. (2000) Monomeric sarcosine oxidase: 2. Kinetic studies with sarcosine, alternate substrates, and a substrate analogue. *Biochemistry* **39**, 8825-8829.

Wagner, M. A., Jorns, M. S. (1997) Folate utilization by monomeric versus heterotetrameric sarcosine oxidases. *Archives of Biochemistry and Biophysics* **342**, 176-181.

Walker, M. C. and Edmondson, D. E. (1994) structure-Activity Relationships in the Oxidation of Benzylamine Analogs by Bovine Liver Mitochondrial Monoamine Oxidase B. *Biochemistry* **33**, 7088-7098.

Wallon, G., Lovett, S. T., Magyar, C., Svingor, A., Szilagyi, A., Zavodszky, P., Ringe, D. and Petsko, G. A. (1997) Sequence and homology model of 3-isopropylmalate dehydrogenase from the psychrotrophic bacterium *Vibrio* sp. I5 suggest reasons for thermal instability. *Protein Engineering* **10**, 665-672.

Walsh, C. T. (1979) Chapter 11: Flavin-dependent dehydrogenases and oxidases. In: *Enzymatic Reaction Mechanisms* (ed. Walsh, C.), pp. 358-405, W. H. Freeman and Company, San Francisco.

Walsh, C., T., (1980) Flavin coenzymes: at the crossroads of biological redox chemistry. *Accounts of Chemical Research* **13**, 148-155.

Wang S. X., Nakamura N., Mure M., Klinman J. P., Sanders-Loehr J. Characterization of the native lysine tyrosylquinone cofactor in lysyl oxidase by Raman spectroscopy. *The Journal of Biological Chemistry* **272**, 28841-28844.

White, T. A. and Tanner, J. J. (2005) Cloning, purification and crystallization of *Thermus thermophilus* proline dehydrogenase. *Acta crystallographica. Section F, Structural biology and crystallization communications* **61**, 737-739.

Wierenga, R. K., Terpstra, P. and Hol, W. G. D. (1986) Prediction of the occurrence of the ADP-binding βαβ-fold in proteins, using an amino acid sequence fingerprint. *Journal of Molecular Biology* **187**, 101-107.

Williamson G. and Edmondson, D. E. (1985) Effect of pH on oxidation-reduction potentials of 8 alpha-N-imidazole-substituted flavins. *Biochemistry* **24**, 7790-7797.

Winkler, A., Hartner, F., Kutchan, T. M., Glieder, A. And Macheroux, P. (2006) Biochemical Evidence That Berberine Bridge Enzyme Belongs to a Novel Family of Flavoproteins Containing a Bi-covalently Attached FAD Cofactor. *The Journal of Biological Chemistry* **281**, 21276-21285.

Wood, J. M., Bremer, E., Csonka, L. N., Kraemer, R., Poolman, B., van der Heide, T. and Smith, L. T. (2001) Osmosensing and osmoregulatory compatible solute accumulation by bacteria. *Comparative biochemistry and physiology. Part A, Molecular & integrative physiology* **130**, 437-460.

Wood, W. B. (1966) Host specificity of DNA produced by *Escherichia coli*: bacterial mutations affecting the restriction and modification of DNA. *Journal of Molecular Biology* **16**, 118-133.

Wood, J. M. (1981) Genetics of L-proline utilization in *Eschericia coli*. *Journal of Bacteriology* **146**, 895-901.

Wood, J. (1987) Membrane association of proline dehydrogenase in *Escherichia coli* is redox dependent. *Proceedings of the National Academy of Science of the United States of America* **84**, 373-377.

Yamazaki, S. and Tsai, L. (1980) Purification and properties of 8-hydroxy-5-deazaflavin-dependent NADP+ reductase from Methanococcus vannielii. *The Journal of Biological Chemistry* **255**, 6462-6465.

Yip, K. S., Stillman, T. J., Britton, K. L., Artymiuk, P. J., Baker, P. J., Sedelnikova, S. E., Engel, P. C., Pasquo, A., Chiaraluce, R., Consalvi, V., Scandurra, R. and Rice, D. W. (1995) The structure of *pyrococcus furiosus* glutamate dehydrogenase reveals a key role for ion-pair networks in maintaining enzyme stability at extreme temperatures. *Structure* **3**, 1147-1158.

Yip, K. S., Britton, K. L., Stillman, T. J., Lebbink, J., de Vos, W. M., Robb, F. T., Vetriani, C., Maeder, D. and Rice, D. W. (1998) Insights into the molecular basis of thermal stability from the analysis of ion-pair networks in the glutamate dehydrogenase family. *European Journal of Biochemistry/FEBS* **255**, 336-346.

Yue, K. T., Bhattacharyya, A. K., Zhelyaskov, V. R. and Edmondson, D. E. (1993) Resonance Raman spectroscopic evidence for an anionic flavin semiquinone in bovine liver monoamine oxidase. *Archives of Biochemistry and Biophysics* **300**, 178-185.

Zanetti, G. and Aliverti, A. (1991) In: *Chemistry and Biochemistry of Flavoenzymes* (volume II) (ed. Muller, F.), pp. 305-315, CRC Press, Boca Raton, Florida.

Zeikus, J. G., Fuchs, G., Kenealy, W. and Thauer, R. K. (1977) Oxidoreductases involved in cell carbon synthesis of *Methanobacterium thermoautotrophicum*. *Journal of Bacteriology* **132**, 604-613.

Zhan, K., (1996) Overexpression of an mRNA dependent on rare codons inhibits protein synthesis and cell growth. *Journal of Bacteriology* **178**, 2926-2933.

Zhang, S., Zubay, G. and Goldman, E. (1991) Low-usage codons in Escherichia coli, yeast, fruit fly and primates. *Gene* **105**, 61-72.

Zhang, W., Zhou, Y. and Becker, D. F. (2004) Regulation of PutA-membrane associations by flavin adenine dinucleotide reduction. *Biochemistry* **43**, 13165-13174.

Zhang, W., Krishnan, N. and Becker, D. F. (2006) Kinetic and thermodynamic analysis of *Bradyrhizobium japonicum* PutA-membrane associations. *Archives of Biochemistry and Biophysics* **445**, 174-183.

Zhao, G. and Jorns, M. S. (2002) Monomeric sarcosine oxidase: evidence for an ionizable group in the E.S complex. *Biochemistry* **41**, 9747-9750.

Zhao, G. and Jorns, M. S. (2005) Ionization of zwitterionic amine substrates bound to monomeric sarcosine oxidase. *Biochemistry* **44**, 16866-16874.

Zhou, Z. and Swenson, R. P. (1995) Electrostatic effects of surface acidic amino acid residues on the oxidation-reduction potentials of the flavodoxin from *Desulfovibrio vulgaris* (Hildenborough). *Biochemistry* **34**, 3183-92.

Zhu, Z. and Becker, D. F. (2003) Flavin redox state triggers conformational changes in the PutA protein from *Escherichia coli*. *Biochemistry* **42**, 5469-5477.

Zhu, W. and Becker, D. F. (2005) Exploring the proline-dependent conformational change in the multifunctional PutA flavoprotein by tryptophan fluorescence spectroscopy. *Biochemistry* **44**, 12297-12306.

Zhu, W., Sandman, K., Lee, G. E., Reeve, J. N. and Summers, M. F. (1998) NMR structure and comparison of the archaeal histone HfoB from the mesophile methanobacterium formicicum with HMfB from the hyperthermophile *methanothermus fervidus*. *Biochemistry* **37**, 10573-10580.